REPUBLIQUE DU CAMEROUN
Paix-Travail-Patrie
****
UNIVERSITE DE YAOUNDE I
****
FACULTE DES SCIENCES
****
DEPARTEMENT DE CHIMIE INORGANIQUE
*****

REPUBLIC OF CAMEROON
Peace-Work-Fatherland
****
UNIVERSITY OF YAOUNDE I
*****
FACULTY OF SCIENCE
****
DEPARTMENT OF INORGANIC CHEMISTRY
*****

POSTGRADUATE SCHOOL OF SCIENCE, TECHNOLOGY AND GEOSCIENCES

CENTRE DE RECHERCHE ET DE FORMATION DOCTORALE EN SCIENCES, TECHNOLOGIES ET GEOSCIENCES

APPLIED PHYSICAL AND ANALYTICAL CHEMISTRY LABORATORY
LABORATOIRE DE CHIMIE PHYSIQUE ET ANALYTIQUE APPLIQUEE

Preparation of Activated Carbons and Activated Carbon-Silver Nanoparticles Composites from *Ricinodendron heudelotti* shells: Adsorption tests of Indigo Carmine and Methyl Orange Dyes from Wastewater and their Anti-Bacterial properties

THESIS

Submitted and Defended in Partial Fulfillment of the Requirements for the Award of the Degree of

Doctor of Philosophy (PhD) of Science in Inorganic Chemistry

Specialty: Inorganic Chemistry

Option: Physical Chemistry

Presented by:

ANKORO Naphtali ODOGU

Registration Number: **09T0013**

M.Sc. Inorganic Chemistry

Supervisor:

KETCHA Joseph MBADCAM, PhD
Professor

Year: 2020

REPUBLIQUE DU CAMEROUN
Paix-Travail-Patrie
****
UNIVERSITE DE YAOUNDE I
****
FACULTE DES SCIENCES
****
DEPARTEMENT DE CHIMIE INORGANIQUE
*****

REPUBLIC OF CAMEROON
Peace-Work-Fatherland
****
UNIVERSITY OF YAOUNDE I
*****
FACULTY OF SCIENCES
****
DEPARTMENT OF INORGANIC CHEMISTRY
*****

ATTESTATION OF PhD/DOCTORATE THESIS CORRECTION OF

Mr. ANKORO Naphtali ODOGU

We the undersigned NDIKONTAR Maurice KOR, Professor (President); SADO KAMDEM Sylvain Leroy, Associate Professor (Examiner) and KETCHA Joseph MBADCAM, Professor (Supervisor); lecturers of the University of Yaoundé I respectively, attest that, this PhD thesis defended on the October 26th, 2020, in the pedagogic Block; hall S01/S02, of the Faculty of Science, University of Yaoundé I by ANKORO Naphtali ODOGU on the topic :

"**Preparation of Activated Carbons and Activated Carbon-Silver Nanoparticle Composites from *Ricinodendron heudelotti* shells: Adsorption tests of Indigo Carmine and Methyl Orange Dyes from wastewater and their Anti-bacterial Properties**",

for the award of a PhD/Doctorate degree in Inorganic Chemistry, has been corrected in conformity with the recommendations of the defense jury

In testimony whereof, this attestation is issued with the privileges thereunto pertaining

Yaoundé, November 23th, 2020

Examiner :

SADO KAMDEM Sylvain Leroy,
Associate Professor

Supervisor :

KETCHA Joseph MBADCAM,
Professor

President :

NDIKONTAR Maurice KOR,
Professor

DEDICATION

This thesis is dedicated to

My lovely daughter NSAMA ANKORO Lydia Beverly.

Let this work serve as an example to help you build your own career in the near future.

ACKNOWLEDGEMENTS

I thank God Almighty the most merciful, for blessing and giving me the knowledge, strength, energy and ability to complete this thesis.

This work has been successful due to the endless contributions of many people. I extend my profound gratitude to the following persons or group of persons who have in one way or the other contributed to the successful completion of this work. In this light. I wish to express my sincere gratitude and appreciation to the following persons:

Prof. KETCHA Joseph MBADCAM for accepting me into his laboratory, his assistance, encouraging words and orientation during my research.

Prof. GHOGOMU Paul MINGO for his valuable contribution to my research efforts.

Prof. NDI Julius NSAMI for his sacrifice and time to tutor and guide me, his corrections, constructive criticisms and recommendations that saw me through the period of this research. I really appreciate him. May God bless him and his family.

I wish to also extend my sincere appreciation to all the Lecturers in the Inorganic Chemistry Department, University of Yaoundé I for their help, encouragements and friendliness over the past few years.

Special thanks to Dr. KOUOTOU Daouda and Dr. BELIBI BELIBI Placide for their availability and services throughout my research work.

Sincere gratitude to Dr. LUNGA Paul KEILAH of the Department of Biochemistry of the University of Yaoundé I for his continuous support, help, cooperation and particularly for the possibility of carrying out anti-bacterial and cytoxicity test not leaving out his corrections of the manuscript.

Sincere appreciation to the Antimicrobial and Biocontrol Agents Unit (AmBcAU), Laboratory for Phytobiochemistry and Medicinal Plants Studies, Department of Biochemistry, Faculty of Science, University of Yaounde´ I for accepting to collaborate with us during the realization of this work.

My seniors in the laboratory: Dr. LEKENE Blaise, Godwin AGBOR TABI, Dr. ESSOMBA Jean, FUMBA Gaston, DAMMI Estelle, Dr. ABEGA Aimé, KOUOH SONE, NDONGO Gervais and Dr. NJOUONKOU Soulémanou for their moral advice.

My mates in the laboratory: ZING ZIND Bertrand and SOBDO Tsopa Michiel Crepin who accompanied me and kept me company throughout my work.

My entire batch for their collaboration in the realization of this work.

I acknowledge my deepest gratitude to my Brothers and Sister: ANKORO Fedelis, ANKORO Grace, ANKORO Isaac, ANKORO Vitalis and their Children for their support and sacrifices.

Special thanks to Mr. NKENYAM Simon Awah and his wife Roseline NKENYAM FOMINYAM for their endless encouragements in the course of this work.

Special and Heartfelt gratitute in memory of my lovely mother ANKORO Lydia NSAMA for for seeing me this far, special care and love throughout my life and career.

Heartfelt thanks to Mrs TCHAKOUTE NGANTCHIA Anine Solange for her support to the success of this work.

Sincere gratitude to Madam NGO ONGLA Berthe Rosalie for her continous support and encouragements throughout this work.

My Friends: FOSSI Roland, LIENOU Jaures, WADJI Yannick and YAMI Theophile for their encouragement, advice and support.

Your name might not have been included here, but I wish to assure you, I highly appreciate your contribution to the success of the realization of this work.

Table of Contents

ABSTRACT

In the course of this present work, two Activated carbons from *Recinodendron heudelotti* shells (RHS) namely H_3PO_4 acid activated carbon (ACP) and $ZnCl_2$ activated carbon (ACZ) were successfully produced using chemical activation with phosphoric acid (H_3PO_4) and zinc chloride ($ZnCl_2$) as activating agents. The preparation of the two samples was modeled through Designing of Experiments (DoE) by using Central Composite Design (CCD). CCD design was used to elucidate the experimental domain both within and without the chosen domain of studies in order to achieve the best overall optimization of the process. This design has been used to develop model equations for activated carbon (AC) preparation by using statistical package Minitab 16 software. The interpretation of effect of main factors and their interactions were carried out and the developed models were validated by conducting experiments at the predicted conditions. The effect of activation temperature (T), activation time (t) and impregnation ratio (R) on iodine number (IN), methylene blue (MB) number and the percentage yield (%Y were studied. The optimum condition of the preparation of the ACP and ACZ samples were found to be 431.821°C, 39.546 min and 0.659 for T, t and R respectively for ACP and 591.506°C. 43.623 min and 1.050 for T, t and R respectively for ACZ. The proximate analysis was used to determine the macronutrients in RHS and was obtained with percentages of moisture content, ash content, volatile matter and fixed carbon to be 5 %, 5 %, 62.57 % and 27 % respectively. X-ray fluorescence result showed that RHS are composed mainly of calcium oxide (CaO) and magnessium oxide (MgO). FTIR analysis showed that hydroxyl, carbonyl, aliphatic carbon, ethers, alcohol, phenol and carboxylic groups present on the surfaces of the RHS and its activated carbons. From the ACP and ACZ samples, two composites samples were prepared by dopping ACP and ACZ with silver nanoparticles (AgNPs). These composites (ACP/AgNP and ACZ/AgNP) were made by successful precipitation loading onto ACP and ACZ with silver nanoparticles of the RHS aqueous extract (RHSNP). As in the case of ACP and ACZ, the two new materials were also characterised by scanning electron microscopy (SEM), Energy dispersive X-ray diffraction (EDX) measurements, Fourier Transform Infra-Red (FTIR) spectroscopy, X-ray diffraction (XRD), particle size measurements by Zeta sizer and specific surface area by BET. The SEM results shows spongy rock-like surface on all adsorbents with the presence of pores. EDX and XRD show the presence of crystalline zincite on ACZ and Ag on theACP/AgNP and ACZ/AgNP. The FTIR spectral for both composite adsorbents presume a composite material while the zeta sizer show that all the samples prepared were in the nano-range. The textural properties of the different materials (RHS, ACP, ACZ, ACP/AgNP and

ACZ/AgNP) show an increase in the specific surface area from the raw precursor (RHS) was found to be 182 m^2/g which increased to 386.613 m^2/g in ACP and 615.400 m^2/g in ACZ after preparation. The composites ACP/AgNP and ACZ/AgNP were found to have lower specific surface area with values of 367.400 m^2/g and 335.100 m^2/g in ACP/AgNP and ACZ/AgNP respectively than their pristine carbons. The antibacterial activities of the four samples, the RHSNP and the RHS extract was done by the Broth microdilution test method on seven different bacteria which are the typhoid-causing *Salmonella Typhi*, food-poisoning *Staphylococcus aureus*, pneumonia-causing *Klebsiella pneumoniae* as well as the diarrheal-manifesting *Escherichia coli* and *Singehla flexneri* species and also on *Salmonella Enteritidis* and *Salmonella Typhimurium*. The extract and ACs showed no antimicrobial activities while the antimicrobial properties were proven to be very interesting for the nanoparticles, ACP/gNP and ACZ/AgNP but higher for the ACZ/AgNP ($7.812 \leq MIC \leq 31.25$ µg/mL). Furthermore, the adsorption capacities of the ACZ and the ACZ/AgNP were investigated using the hazardous Indigo Carmine (IC) and Methyl Orange (MO) dyes. The equilibrium quantities adsorbed using the maximum equilibrium concentration were found to be 177.801 mg/g, 133.407 mg/g, 160.678 mg/g, and 89.181 mg/g for IC adsorption; 178.385 mg/g, 124.204 mg/g, 165.384 mg/g and 120.102 mg/g for MO adsorption on ACP, ACZ, ACP/AgNP and ACZ/AgNP respectively. This gives rise to a percentage decrease of 9.630 % and 33.151 % for IC adsorption; 7.273 % and 3.303 % for MO adsorption from ACP to ACP/AgNP and ACZ to ACZ/AgNP respectively. RHS is therefore a good and promising precursor for the preparation of activated carbon and nanoparticles for bacterial containing water purification and for the treatment of bacterial infections.

Key words: *Recinodendron heudelotti* shells, Activated carbon, Central Composite Design, Silver Nanoparticle, Composite, Adsorption, Antibacterial activity, Cito-toxicity.

RESUME

Dans le cadre de ce travail, deux charbons actifs provenant des coques de *Recinodendron heudelotti*, ont été activés avec succès à H_3PO_4 (ACP) et au $ZnCl_2$ (ACZ). La préparation de ces deux échantillons a été modélisée par la méthodologie des plans d'expériences en utilisant le plan composite centré (PCC). Le PCC a été utilisé pour élucider le domaine expérimental à la fois dans et hors du domaine d'étude choisi, afin de parvenir à la meilleure optimisation globale du processus. Ce plan a été utilisé pour développer des modèles d'équations pour la préparation des charbons actifs en utilisant le logiciel Minitab 16. L'interprétation de l'effet des principaux facteurs et de leurs interactions a été effectuée et les modèles développés ont été validés en menant des expériences dans les conditions prédite. L'effet de la température d'activation (T), du temps d'activation (t) et du ratio d'imprégnation (R) sur l'indice d'iode (IN), l'indice de bleu de méthylène (MB) et le rendement (%Y) a été étudié. Les conditions optimales de préparation des échantillons ACP et ACZ se sont avérées être de 431,821 °C, 39,546 min et 0,659 pour ACP et de 591,506 °C, 43,623 min et 1,050 pour ACZ. L'analyse immédiate a été utilisée pour déterminer les macronutriments dans les coques de *Recinodendron heudelotti* et les teneurs en humidité en cendres, le taux de matières volatiles et de carbone fixe sont respectivement 5%, 5%, 62,57% et 27 %. Les résultats de la fluorescence aux rayons X ont montré que les les coques de *Recinodendron heudelotti* sont principalement composés d'oxyde de calcium (CaO) et d'oxyde de magnésium (MgO). L'analyse infra rouge a montré que des groupes hydroxyle, carbonyle, carbone aliphatique, éthers, alcool, phénol et carboxylique sont présents à la surface des RHS et de leurs charbons actifs. A partir des échantillons ACP et ACZ, deux échantillons composites ont été préparés en dopant les ACP et ACZ avec des nanoparticules d'argent (AgNP). Ces composites (ACP/AgNP et ACZ/AgNP) ont été préparés par précipitation des nanoparticules d'argent à partir de l'extrait aqueux des coques de *Recinodendron heudelotti* sur ACP et ACZ. Comme dans le cas de ACP et de ACZ, les deux nouveaux matériaux ont également été caractérisés par la microscopie électronique à balayage (MEB), la radiographie à dispersion d'énergie (EDX), la spectroscopie infrarouge à transformée de Fourier (IRTF), la diffraction des rayons X (DRX), la taille des particules par le calibreur Zeta et la surface spécifique par la méthode BET. Les résultats de la MEB montrent une surface spongieuse pour ~~sur~~ tous les adsorbants avec la présence de pores. L'EDX et la diffraction des rayons X montrent la présence de la zincite cristalline sur ACZ et, Ag sur ACP/AgNP et ACZ/AgNP. Le spectre IRFTde ACP/AgNP et ACZ/AgNP présume qu'il s'agit des matériaux composites, tandis que analyse de taille par la method ZETA-Sizer montre que tous les

échantillons de matériaux préparés étaient de l'ordre du nanomètre. Les propriétés texturales des différents matériaux (RHS, ACP, ACZ, ACP/AgNP et ACZ/AgNP) montrent une variation de la surface spécifique des differents matériaux. Le précurseur (RHS) présente une valeur de la surface spécifique de 182 m^2/g, tandis que les charbons actifs ont des valeurs de surfaces spécifiques de 386,613 m^2/g pour ACP et de 615,400 m^2/g pour ACZ. Les composites ACP/AgNP et ACZ/AgNP quant à eux ont des surfaces spécifiques plus faibles (367.400 m^2/g et 335.100 m^2/g respectivement) que leurs charbons respectifs. Les activités antibactériennes des quatre échantillons, les nanoparticules d'argent issu de l'extrait des coques *Recinodendron heudelotti* et l'extrait des coques de *Recinodendron heudelotti* ont été réalisées par la méthode de test de microdilution de Broth sur sept bactéries différentes (*Salmonella typhi* causant la typhoïde, *Staphylococcus aureus* empoisonnant les aliments, *Klebsiella pneumoniae*, qui provoque des pneumonies, ainsi que les espèces *Escherichia coli* et *Singehla flexneri*, qui provoquent des diarrhées, et aussi *Salmonella enteritidis*, *Salmonella typhimurium*). L'extrait et les charbons actifs n'ont montré aucune activité antimicrobienne alors que les propriétés antimicrobiennes se sont avérées être très intéressantes pour les nanoparticules, ACP/gNP et ACZ/AgNP mais plus élevées pour les ACZ/AgNP (7.812≤MIC≤ 31,25 µg/ml). En outre, les tests d'adsorption de ACP, ACZ, ACP/AgNP et de ACZ/AgNP ont été réalisés en utilisant les colorants nocifs comme l'Indigo Carmine (IC) et le Methyl Orange (MO). Les quantités adsorbées obtenues au temps d'équilibre se sont avérées être de 177,801 mg/g, 133,407 mg/g, 160,678 mg/g et 89,181 mg/g pour l'adsorption IC; 178,385 mg/g, 124,204 mg/g, 165,384 mg/g et 120,102 mg/g pour l'adsorption MO sur ACP, ACZ, ACP/AgNP et ACZ/AgNP respectivement. Au regard de ces résultats, nous pensons que les coques de *Recinodendron heudelotti* peuvent donc être considérées comme un bon précurseur pour la préparation des charbons actifs et des nanoparticules pour la purification de l'eau contenant des bactéries, ensuite pour le traitement des infections bactériennes.

Mots clés: Coques de *Recinodendron heudelotti*, Charbon actif, Plan composite centré, Nanoparticule d'argent, Composite, Adsorption, Activité antibactérienne, Cito-toxicité.

LIST OF ABBREVIATIONS

AC (s): Activated carbon (s)

ASTM: American Society for Testing and Materials

BAC: Bead activated carbon

BET: Brunauer, Emmet and Teller

BJH: Barret Joyner Halender

D-K-R: Dubinin-Kaganer-Radushkevich

FTIR: Fourier Transform Infrared spectroscopy

GAC: Granulated activated carbon

IC: Indigo Carmine

IN: Iodine Number

MO: Methyl orange

NMR: Nuclear Magnetic Resonance

PAC: Powdered activated carbon

PSD: Pore Size Distribution

%R: Percentage removal

R^2: Correlation coefficient.

R: Impregnation Ratio

RHS: *Ricinodendron heudelotii* shells

SEM: Scanning Electron Microscope

S_{mi} : Microsporous surface area

V_m: Volume for monolayer coverage

W: Pore width

WDFS: Dispersive Fluorescence Spectrometer

XRF: X-Ray Fluorescence

XRD: X-ray Diffraction

MIC: Minimum Inhibitary Concentration

MBH: Minimum Bacteria Concentration

LIST OF TABLES

LIST OF FIGURES

GENERAL INTRODUCTION

Problem definition

During the last two decades water reuse has become a key element in integrated water resources management under water scarcity conditions. In terms of quantity wastewater treatment plant, effluent represents a highly reliable water source but quality aspects prevent high-quality water reuse without advanced water treatment (Elhussien *et al*., 2017). This is basically due to the excess pollution with numerous microbial, organic and inorganic contaminants posing severe health risks (Wang *et al.,* 2015; Ankoro *et al*., 2016). Water reclamation applications such as indirect or even direct potable reuse target therefore at a complete removal of microbial (pathogens), organic, inorganic and trace contaminants to minimise the risk and reach drinking water quality (Vorgelegt, 2011).

The rapid increase in textile industries in the world and the increasing demand for textile, and also the ceramic paper, printing and plastic use large varieties of dyes as their raw materials (Ankoro *et al*., 2016; Harrache *et al*., 2019). Some dyes are used in medicine and biological strain and coloring plastic (Malarvizhi *et al*., 2008; Mohammed and Gemal, 2014). The waste from these industries in one way or the other finally ends up in water, thereby polluting the environment (Sze and McKay, 2008). Unlike other pollutants, dye pollutants especially those with the benzene ring even at low concentrations is visible in water (Min-Shen *et al*., 2003; Ghaedia *et al*., 2013; Li *et al*., 2016) and reduce light penetration in to water, hence causes negative effect on photosynthesis to water plants as they are non-degradable (Gao *et al*., 2016; Maleki *et al*., 2017; Harrache *et al*., 2019).

Furthermore, bacteria, viruses, parasites and fungi have been widely used in food, brewery and many other industries for the production of consumables and also for the production of vaccines. Some of these bacteria, viruses, parasites and fungi are resistant to drugs and hence causes over 700.000 deaths each year. It has been estimated that by 2050, such ‘superbugs’, inured to treatments, could cause up to 10 million deaths annually and cost the global economy of about US$100 trillion (David. 2017). As a matter of facts, Typhoidal *Salmonella enterica* is the leading cause of community-acquired bloodstream infection (Deen *et al.,* 2012), with the greatest burden occurring in Southeast Asia, Latin America and sub-Saharan Africa. Enteric fever (typhoid and paratyphoid fevers) continue to be a significant contributor to global morbidity and mortality with an estimated 17 million illnesses worldwide and approximately 178.000 deaths each year as of 2015 (GBD, 2018).

Waste water containing IC and MO dyes are rich both in colour, organic contents and large amount of suspends solids that are broadly fluctuating pH, high temperature and beside high chemical oxygen demand (Himanshu *et al*., 2010; Sze and McKay, 2012). From the norms of the World Health organization, Indigo Carmine and Methyl Orange dyes at concentration greater than 0.005 mg/L (Miriam *et al*., 2013; Harrache *et al*., 2019) is not acceptable in water while the micro-organisms are not appreciated in normal water no-matter the concentration. Also, water containing bacteria and viruses such as *shigella flexneri, Salmonella typhi* and *Escherichia coli* are known to cause infections such as typhoid fever, joint pains, diarrhea, dysentery etc.

Amoxicillin, ciprofloxacin, ampicillin, azithromycin, ceftriaxone, etc, (Sharma *et al.*, 2016) are amongst the many drugs used to fight bacterial Infections especially those caused by the family of *Salmonella*. But due to many reasons including the extensive and inappropriate use of the same antimicrobials, the increase of immune-compromised patients, delay in diagnosis, and, in some cases, poor hygiene conditions, there have been an increase in multidrug resistant *Salmonella* species (Guimarães *et al.,* 2010) restricting the therapeutic options. In addition, studies have revealed that *Salmonella* serovars has become more resistant to the three first-line classes of antibiotics (chloramphenicol, ampicillin, and co-trimoxazole) (Rahman *et al*., 2014). Moreover, chloramphenicol which for long had been the drug of choice for the treatment of typhoid fever, has been withdrawn from the market due to drawbacks of a high relapse rate, a high rate of continued and chronic carriage, bone marrow toxicity, and high mortality rates (Nauciel and Vildé, 2005). Furthermore, ciprofloxacin which became the alternative option for treating *Salmonella* infections, has recently been reported from a number of countries to encounter resistance (Thanh *et al.,* 2016; Rahman *et al.,* 2014) raising a threat in the treatment of *Salmonella* infections. These setbacks therefore make a great impact on treatment efficacy and increase treatment cost and risk of complications and death (Crump *et al*., 2015; Wong *et al*., 2015).

Therefore, full scale systems apply treatment trains for water reclamation and reuse based on the multi-barrier principle combining several unit processes to remove these unwanted pollutants and microbs to the parts-per-trillion level corresponding to the usual detection limit of the analytical methods is essential. Double membrane processes combining porous membranes with reverse osmosis followed by advanced oxidation represent the state of the art in advanced water treatment for high-quality water reuse (Bixio and Wintgens, 2006; Asano *et al*., 2007, Al-Degs *et al*., 2009). Although very effective for the elimination of the contaminants, the double membrane process is associated with high capital and operating cost, and involves

the use of chlorinated chemicals to suppress membrane fouling (Vorgelegt, 2011). Furthermore, cost-efficient methods for the treatment of reverse osmosis concentrate containing salts, nutrients, disinfection by-products and micropollutants are not yet available (Vorgelegt. 2011). In certain cases, for example, in direct potable reuse, the product water might even require a post-treatment such as re-mineralization (Vorgelegt. 2011). In addition to causing salmonellosis, it has been demonstrated that the entrance of *Salmonella* causes the production of superoxide and nitric oxide which react together to form peroxynitrite, a strong biological oxidant. This consequently increases the levels of reactive oxygen species (Rastaldo *et al.,* 2007). Oxidative stress can be prevented or delayed by using antioxidant agents. However, beside their unavailability, high cost and side effects, frequently used synthetic antioxidants such as Butylated Hydroxyl Anizole (BHA) and Butylated Hydroxyl Toluene (BHT) have been proven to be neurotoxic, hepatotoxic and carcinogenic (Farombi *et al.,* 2000). The above mentioned setbacks in the fight against salmonellosis has motivated scientist to search for alternative sources of antisalmonellal agents not only for treatment of immidiate cases, but to fight against it from the source agent water.

Against this backdrop, activated carbon and most especially activated carbon doped with nanoparticles filtration provides an interesting alternative to reverse osmosis and the number of antibacterial drugs used with a number of advantages associated with low capital and operating cost, effective, eco-friendly, less chemical used and in particular lower rejection of monovalent salts and thus less problematic membrane concentrates. In particular, looking this direction and looking back to history, plants have provided sources of inspiration for the development of medicinal substances and have provided active principles that served as blue prints for synthetic drugs. *Ricinodendron heudelotii* popularly called Ndjansang is a medicinal plant empirically used in the locality of Kumba South West Region of Cameroon for the treatment of typhoid fever, abdominal pains, skin diseases and diarrheae. Most of the parts of the tree from the leaves to the roots have been exploited but to the best of our knowledge, no work has been reported in literature on the valorisation of the nut shells. These shell which could also have interesting properties not only for medicines, but in the treatment of wastewater containing dyes and bacterial.

One of the best and convenient water treatment process is seemed to be adsorption, as it is cheap, easy and simple in operation (Alkhatib *et al*., 2014; Elkady *et al*., 2015). The most popular and commonly used adsorbent in water and wastewater treatment throughout the world is activated carbon (AC) Canteli *et al*., 2014). As standard method for organics, and inorganic

contaminats removal, several projects (Snyder *et al*., 2007; Metzger. 2010; Zwickenpflug *et al.*, 2010; Ndi *et al.*, 2013; Dong *et al*., 2015; Gao *et al*., 2016; Maleki *et al*., 2017) investigated the behaviour and optimisation of activated carbon in effluent treatment. Nanofiltration for the removal of organic micropollutants has also been already employed in large scale projects such as at the Méry-sur-Oise water treatment plant where nanofiltration ensures the safe removal of pesticides from surface water for drinking water production (Beros *et al*., 2003).

AC as adsorbent have relatively high surface area, large porosity, high total pore volume and presence of wide spectrum of functional groups on its surface, which provides a strong affinity for even low concentration organics to attach to itself. Nevertheless, the well-developed internal pore structure of AC with macropores serves as excellent loci for colonization of organisms and support material for bacterial growth (Das *et al.*, 2015; El-Shafey *et al*., 2016). The biofilm layer formations on the AC by the microbes have undesirable effects as the filter may clog up as a result of excessive bacterial growth (Karthik and Radha. 2016).

Nowadays, nanoparticles are used as sorbents for organic and inorganic pollutants removal owning to their high specific surface area and also a large number of unsaturated atoms on their surfaces that can bind readily with most of other atoms. More attention is focused to water treatment with engineered nanoparticles. These nanoparticles can be produced by numerous techniques, including chemical, aerosol, electrochemical, laser irradiation, sonochemical deposition, photochemical reduction and biological techniques (Karthik and Radha, 2016). The biotechnological experimental processes gain importance because of the advantages like safety, cost-effective, sustainable and environmentally friendly processes. These nanoparticles have very attractive properties such as an ordered structure with a high aspect ratio, ultra-light weight, high mechanical strength, electrical and thermal conductivity, and high specific surface area. The properties of nanoparticles differ from those of their corresponding bulk state.

Among the nanoparticles silver nanoparticles (AgNP) are gaining more importance from others because of its antimicrobial and antiviral properties and also use for water purification (Karthik and Radha, 2016; Thomas *et al*., 2018; Al-Ansari *et al*., 2019). The believed mechanism is that AgNPs attach to the surface of cell membrane disturbing the permeability and respiration functions of the cells, which leads to microbial cell death (Thomas *et al*., 2018). Nanocomposite as adsorbent have proven as an efficient adsorbent because of the

increase in their surface-to-volume ratio with the reduction of the size of the adsorbent particles from bulk to nano dimensions.

Ernst (2000) was the first researcher to investigate treatment trains combining nanofiltration and activated carbon for effluent polishing prior to managed aquifer recharge. Using mainly tests at laboratory scale, he identified powdered activated carbon (PAC) and granular activated carbon (GAC) following an 'open' nanofiltration membrane as most efficient and best operable combination (Vincenzo *et al*., 2013). Further biofouling was detected as the main fouling mechanism indirect nanofiltration and it was concluded that porous membranes should serve as a proper pre-treatment, as long as no fouling resistant or back flushable nanofiltration membranes were available. Since then, several treatment trains combining nanofiltration and activated carbon have been investigated. The combination of powdered activated carbon followed by nanofiltration was first applied in land fill leachate treatment (Meier *et al.,* 2002) and later adapted to effluent treatment (Meier and Melin, 2005; Meier, 2008) using capillary nanofiltration membranes (Futselaar *et al*., 2002). Investigating the effect of powdered carbon on nanofiltration, Meier (2008) showed that activated carbon particles have a significant influence on the operability, particularly in terms of membrane abrasion, which occurred at high shear rates above 18.000 s^{-1}. At lower shear rates particle deposition, mainly the small particle fraction, lead to the formation of a cake layer, which reduced the permeate flux and compromised the solute rejection.

The quest for low cost and renewable precursors for the production of activated carbons (Yakout and El-Deen, 2016; Lekene *et al*., 2019) with antibacterial properties still remain a major challenge to researchers since Ernst (2000) as well as Meier (2002) did not investigate his composite material on organic micropollutants. They also failed to carry out a comparative study of the organic and micropollutant removal during the possible process combinations for advanced water treatment. Furthermore, a comparative study of the adsorption capacities and antibacterial studies on the effect of doping activated carbon with AgNP have not yet been exploited given that Karthik and Radha in 2016 only tested the anti-microbial properties but failed to investigate if the material is still a good adsorbent. This is because doping ACs might increases its antibacterial properties and may or may reduce its adsorption properties on organic and inorganic pollutants as a results of the NPs occupying the pores or binding to the active sites needed for surface adsorption. Open questions further exist with regard to the long-term behavior and operability of activated carbon as the previous tests were conducted either in lab- to bench scale or in pilot scale for shorter periods. Therefore, as a contribution to the fight

against dye pollution and diseases causing bacterial in water, we hypothesized that *Ricinodendron heudelotii* shells if well exploited, could be used with safety and with high efficacy in the treatment of wastewate and wastewater containing bacteria. In the present study, silver nanoparticles were biogenically synthesized using extracts from *Ricinodendron heudelotii* shells and the synthesized nanoparticles were incorporated onto activated carbon to produce a nanocomposite. The novelty of this work was therefore based on producing activated carbon composite from novel RHS precursor and biosynthesized AgNPs with high adsorption and interesting antimicrobial properties for wastewater and wastewater containing bacteria purification and drug manufacture.

Ricinodendron heudelotti shells (RHS) is an agricultural waste that is readily available as a by-product of *Ricinodendron heudelotti* processing but requires pretreatment to produce activated carbon for better performance as an adsorbent. The conversion of *Ricinodendron heudelotti* shells into AC using classical methods requires carrying out many experiments and much time is needed. The is because the preparation of activated carbon is influenced by many factors such as temperature, time, impregnation ratio etc. Therefore. it is important to study the effect of these factors on activated carbon production in order to determine the most important ones and their regions of interest (Ahmad *et al*., 2009).

Response Surface Methodology (RSM) is a collection of mathematical and statistical techniques for modeling and analyzing problems in which a response of interest is influenced by several variables. Basically, it had been used in multivariate experimental design, statistical modeling and process optimization. Hence it is a useful tool to study the interactions of two or more factors. RMS usually contains three stages ie design and experiments, response surface modeling through regression and optimization (Ahmad *et al*., 2009; Kundu *et al*., 2015). The optimization process was observed to be important in determining the values of factors for which the response is at maximum. The application of statistical experimental design techniques in the preparation of AC was found to result in reduce process variability combined with the requirement of less resources (time, reagents and experimental work) (Tan et *al*., 2008). The main advantage of RSM is the reduced number of experimental trials needed to evaluate multiple parameters and their interactions.

Objectives of this Research Work

This work aims to valorise RHS for the preparation of ACs by identifying the optimum conditions of AC preparation and AC/AgNP for wastewater purification. As all combinations

involving activated carbon dopped with AgNP filtration can be expected to provide excellent removal of dyes, pathogens and bacterials (micro-organisms) from waste water. The investigation focuses on the removal of Indigo Carmine and methyl Orange compounds from wastewater and the anti-bacterial properties of the two most promising process combinations, PAC, and PAC/AgNPs. It is in the light of this background literature studies that this present research study was designed specifically to:

Optimise the preparation conditions of ACs using the RSM method by evaluating the various operating parameters such as activation temperature, activation time and impregnation ratio for carbon prrepared from RHS,

Obtained optimum conditions for the preparation of PAC and PAC/AgNPs composites,

Study the effect of chemical activation on the development of pore structure of the activated carbon obtained and examine the characteristics of the activated carbon produced (ie elemental analysis, proximate analysis, adsorption capacity, surface functionality and pore size of the prepared activated carbon),

Determine the adsorption capacities of PAC and PAC/AgNP for the removal of Indigo Carmine and methyl Orange dyes and identification of the main governing factors,

Determine the Anti-Bacterial capacities of the PAC and PAC/AgNP and identification of the main governing factors in other to identify the relevant boundary conditions for the employment of activated carbon, such as carbon usage rate, preferred type of carbon, and influence of bulk organics on the micropollutant activities,

Elucidate the fate and removal of Indigo Carmine and Methyl Orange compounds during direct adsorption using activated carbon compared to PAC/AgNPs composite,

Evaluate the Cyto- toxicity of PAC and PAC/AgNP on living organisms to ensure the safety of its used in wastewater treatment or in nanomedicines,

Justification of the research work

Organic, inorganic and microbial pollutants from liquid and gas streams from the different types of local and industrial production is a major problem to developing countries as they lack the necessary equipments for wastewater and wastewater containing bacteria treatments. As a consequence of environmental pollution, the need for activated carbon to comply with environmental regulation will grow at a faster rate due to the growth of industrialization. This

study has therefore been initiated to identify an inexpensive option to remove impurities from drinking water as well as water containing bacteria treatment. In view of the aforementioned limitation, the main goal of this study is to enhance the purification of water via the use of local agricultural waste byproducts to produce a low-tech, chemically activated carbon that could be used in conjunction with existing technologies or as a stand-alone treatment option. It also widens in medical domain as it brings out less expensive green technology which can be used to produce Nano-drugs for water borne diseases like typhoid fever, diarrhoea, dysentery etc. A problem faced by all developing countries which account for more than 25 % of annual death. Thus, unavoidable continuous research has to be carried out on different biomass to develop outstanding quality activated carbon and activated carbon with anti-bacteria properties of different precursors for specific uses and particularly to meet up with the ever-increasing demand for AC.

Scope and outline of the thesis

This research work was carried out at on a laboratory scale. The preparation of activated carbon, AC/AgNPs was developed by a single stage method with RHS shells as the starting material. Two chemical activating agents were used: zinc chloride (Lewis acid), widely used as a strong dehydration agent and phosphoric acid (a strong polyprotic acid), each acting as catalyst to promote cleavage reactions for the targeted materials. This study was centred on the iodine number efficiency, MB number efficiency and % yield of the prepared ACs of different magnitude. The activated carbons, obtained from RHS shells precursor, is designed to improve environmental and hygienic status in principal target, Cameroon where disposal of RHS, water pollution and water quality is a major crisis.

The thesis is divided into three chapters, following the introduction, Chapter one sets the scene and describes the scientific background and regulatory boundary conditions of the study putting the emphasis on the issue of pollution (by dyes) and micro-organisms pollutants (bacteria). Chapter two contain the analysis of the applicability of the prepared materials to remove dyes and organic micro pollutants from wastewater based on experiments in laboratory and pilot-scale. Chapter three round up with results and discussion on the fate of bulk organics in Adsorption both in batch system using ACs and ACs/AgNPs composite processes and the effect of the above adsorbents on bacteria.

Economic and Environmental benefits

This study eventually carried out in laboratory scale could be boosted industrially and the ACs and AC/AgNPs produced will have diverse application. Some shortlisted application includes domains like water purifications **(**CamWater) where it can be used to purify drinking water; in the Brewery industry (Le Brasseries du Cameroun), it can be used in wastewater purification, odour removal etc. In Sosucam, it can be use in heavy (Cu^{2+}, Pb^{2+} , etc.) metal removal, odour and colour removal. In the health domain, it can be used in companies like Biopharmer, Novertis etc for drug production, drugs purification etc while in the cosmetic sector, it can be used in the purification of most essential oils and also in facial beauty and for teeth whitening. It can also be used in agriculture keep soil moisture and prevent the washing away of fertilizers.

CHAPTER I: LITERATURE REVIEW

I.1. Introduction

This chapter details out a review of the precursors, production methods, and industrial applications of activated carbon. Furthermore, it describes the porous structure of activated carbon as well as their surface chemistry including surface functional groups on the carbon materials. It's also bring about some bacterial commonly found in the alimentary canal and in most industrial effluents. The toxicity of some organic colourants is also presented in detailed discussion and their common removal methods.

I.2. Activated Carbon

I.2.1. Role of Activated Carbon

Over the last few decades, adsorption has gained importance as a purification, separation and recovery process on an industrial scale. Activated carbon (AC) is perhaps one of the most widely used adsorbents in industry for environmental applications. Activated carbons are carbons of highly microporous structure with both high internal surface area and porosity, and commercially the most common adsorbents used for the removal of organic and inorganic pollutants from air and water streams (Kundu *et al*., 2015; Fazal-ur-Rehman, 2018). Any cheap material with a high carbon content, low inorganics can be used as a raw material for the production of activated carbon. World demand for virgin activated carbon is forecast to expand by 9 % per annum through 2014 to 1.7 million metric tons (AlOthman *et al*., 2011). Activated carbon demand will benefit from a continuing intensification of the global environmental movement as well as rapid industrialization. In most developing and developed countries, use of AC in pharmaceutical sector offers the strongest growth prospect. Additionally, (Fazal-ur-Rehman, 2018), environmental concerns in developing regions will spur new growth in water treatment applications, which is already the largest single market in developed countries. Besides the necessity of clean drinking water, government environmental regulations that vary by region also impact the demand for AC in this sector significantly (Ramakrishna, 2012).

Recently. carbon has been one of the magnificent elements which have revolutionized material science. From carbon we obtain the best porous absorber (activated carbon) with excellent properties for large spectrum of industrial applications. Activated carbon has been applied by man for over two thousand years. The reason of its application through history is attributable to its unique and versatile properties, which are relatively easy to achieve.

Activated carbon, also widely known as activated charcoal or activated coal Activated carbon is a generic term used for any porous carbonaceous material subjected to controlled thermal treatments, in order to increase the level of porosity. It has a highly developed surface area and rich surface groups (Siti, 2010; Kumar and Jena, 2016). Owing to its high internal surface area and pore volume, activated carbon is a powerful adsorbent (suzane, 2013). The word active is sometimes used in place of activated. Due to such high degree of micro porosity, just 1 gram of activated carbon has a surface area in excess of 500 m^2 (about one tenth the size of an American football field) (Ndi *at al*., 2014), as typically determined by nitrogen gas adsorption. Sufficient activation for useful applications may come solely from the high surface area, though further chemical treatment generally enhances the adsorbing properties of the material.

Activated carbon is most commonly derived from charcoal. It is composed of 87% to 97% carbon but also contains other elements depending on the processing method used and raw material it is derived from (Danish and Ahmad, 2018). Activated carbon's porous structure allows it to adsorb materials from the liquid and gas phase. Its pore volume typically ranges from 0.20 to 0.60 cm^3/g and has been found to be as large as 1 cm^3/g. Its surface area ranges typically from 800 to 1500 m^2/g but has been found to be in excess of 3.000 $m^2/$ g. The surface area contains mostly micropores with pore diameters smaller than 2 nm. These favorable properties make activated carbon a popular adsorbent for many applications (Leimkuehler, 2010**).**

I.2.2. History of activated carbon

The properties of activated carbon were recognized by the Egyptians around 1500 B.C. who used wood char for medical purposes and water treatment. Around 420 BC it was observed that Hippocrates dusted wounds with powdered charcoal to remove their odor (Leimkuehler, 2010; Kundu *et al*., 2015). Ancient Hindu societies purified their water by filtration through charcoal (Siti, 2010; Sivakumav *et al*., 2012). In 1773, the Swedish chemist Karl Wilhelm Scheele was the first to observe adsorption of gases on charcoal. A few years later activated carbons began being used in the sugar industry as a decolorizing agent for syrup. However, commercial activated carbon was first produced in about 1900 for use in the sugar refining industry.

In the early 20^{th} century the first plant to produce activated carbon industrially was built for use in sugar refining industry in Germany. Many other plants emerged in the early 1900's

to make activated carbons primarily for decolourisation (Teh *et al*., 2013). During World War I activated carbon was used in gas masks for protection against hazardous gases and vapors.

Today, activated carbons are used to remove color from pharmaceutical and food products, as air pollution control devices for industrial and automobile exhaust, for chemical purification, in separation/purification of liquid and gases and recovery of solvents, as well as new applications such as a catalyst support (Fazal-ur-Rehman, 2018), super-capacitors, and as electrodes in batteries, 500.000 tons per year of activated carbon are produced globally, 80% of this is used for liquid phase applications, and 20% is used for solid phase applications.

Carbon is the principal constituent of activated carbon and amount up to 85 to 95% of a given sample of activated carbon. The remaining 15 to 20% is composed of other elements such as hydrogen, oxygen, nitrogen, sulphur and phosphorus (Sodeinde, 2012). These hetero-atoms are derived from the source of raw materials or become associated with the carbon during activation or other preparation processes (Ndi,2014).

I.2.3. Structure of activated carbon

Activated carbon in its broadest sense includes a wide range of processed amorphous carbon-based materials. It is not truly an amorphous material but has a microcrystalline structure. Active carbons have a microcrystalline structure that starts to build up during the carbonization process. However, the active carbon microcrystalline structure differs from that of graphite with respect to the interlayer spacing, which is 0.335 nm in the case of graphite and ranges between 0.34 and 0.35 nm in active carbons due to the presence of the heteroatoms.

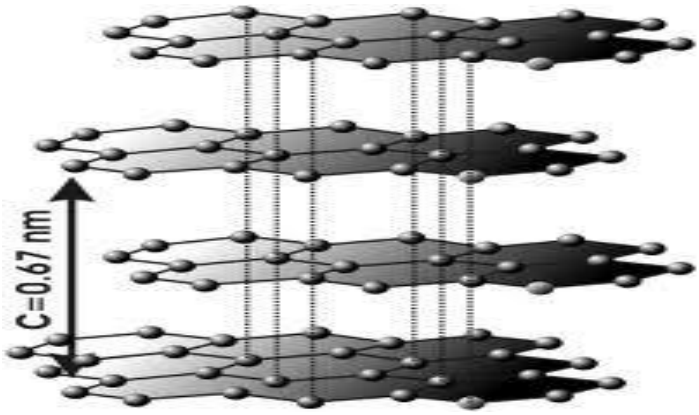

Figure 1: Structure of Activated Carbon

The orientation of the microcrystallite layers is also different, being less ordered in active carbons. Biscoe and Warren proposed the term *turbostratic* for such a structure. This disorder in microcrystallite layers is caused by the presence of heteroatoms such as oxygen and hydrogen, and by the defects such as vacant lattice sites in active carbons (Roop and Meenakshi. 2005). The three-dimensional structure of graphite and the turbostratic structure of active carbons are compared in Figure 2.

…….. (1)

Franklin, on the basis of his x-ray studies, classified active carbons into two types, based on their graphitizing ability. Carbon is converted into graphite when it is burned to 3000 ºC in an inert atmosphere. Activated carbons belong to the second group non graphitizable carbon and are prepared from rich carbon materials that do not pass through a fluid phase during carbonization (Thomas, 2012). The Non graphitizing carbons, during carbonization, develop strong cross-linking between the neighboring randomly oriented elementary crystallites, resulting in the formation of a rigid immobile mass. The charcoals obtained are hard and show a well-developed microporous structure that is preserved even during the subsequent high-temperature treatment. In the case of PVDC (polyvinylidene chloride) charcoal, which is an example of a nongraphitizing carbon, about 65% of the carbon was arranged in graphitic layers of a mean diameter of 16Å. The remaining carbon was highly disordered. 55% of the graphitic layers being grouped in pairs of parallel planes 0.37 nm apart. The average distance between elementary crystallites is approximately 2.5 nm. The PVDC charcoal does not graphitize even at temperatures higher than 3000 °C.

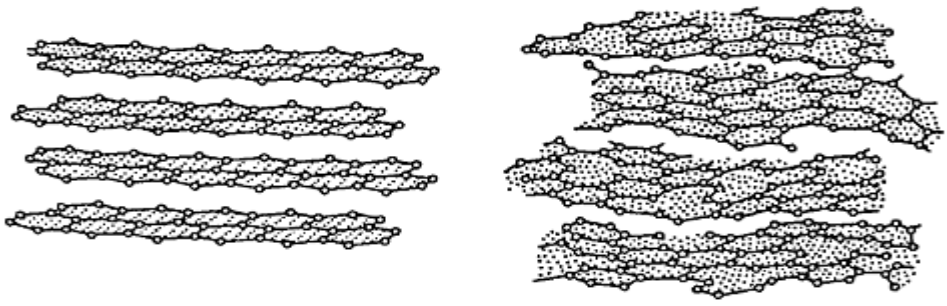

Figure 2: Comparison of three-dimensional crystal lattice of graphite (a) and the turbostratic structure (b) (Roop and Meenakshi, 2005)

The formation of the non-graphitizing structure with strong cross-links is promoted by the presence of associated oxygen or by an insufficiency of hydrogen in the original raw material. In the case of PVC (polyvinyl chloride) charcoal, which is an example of a graphitizing carbon. Franklin observed that the elementary crystallites were mobile and had weak cross-linking from the beginning of the carbonization process (Çiğdem, 2005). The charcoal obtained was weak and had a less-developed porous structure, but the crystallites had a large number of graphitic layers oriented parallel to each other. Franklin observed that. after the elimination of the non-organized carbon, the growth of the crystallites continued, probably by the addition of layers or even groups of layers. The schematic representation of the structures of graphitizing and non-graphitizing active carbons are shown below. The difference in abilities to undergo graphitization results from the difference in the orientation of the crystallites in the two types of carbons.

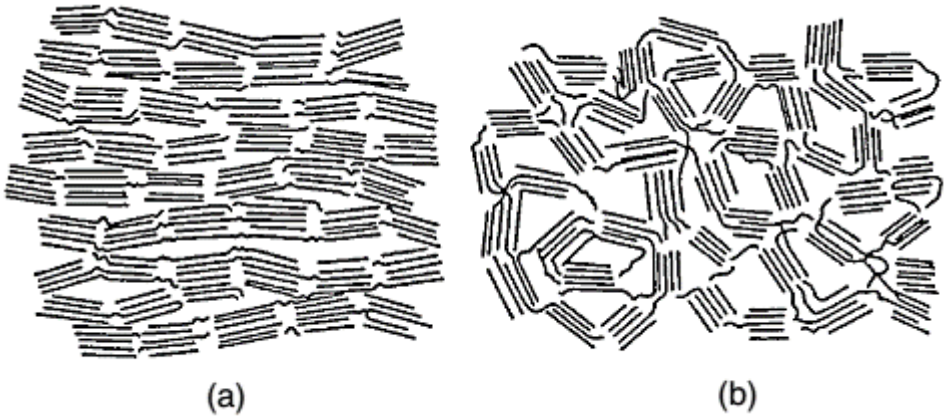

Figure 3: Schematic illustration of the structure of active carbon: (a) easily undergoing graphitization and (b) undergoing graphitization to a small degree (Çiğdem. 2005)

I.2.4. Characteristics of Activated Carbon

Both surface chemistry and pore size distribution (PSD) will affect the ability of activated carbon to adsorb. The type of surface chemical functional groups will determine the interactions of the adsorbate with the activated carbon surface (Kumar and Jena, 2016). PSD on the other hand, will determine how much adsorbate of certain size and shape can access the pore surface. Extensive studies have been done to determine the effects of pore size distribution on adsorption (Nezih, 2004). The pore with the highest adsorption energy is one that has multiple contact points with the adsorbate, and this adsorbate will have a size that is close to

the pore size. It is important that the activated carbon used for water treatment has large amounts of suitable pores for target contaminants.

The International Union of Pure and Applied Chemistry (IUPAC) categorized the size of pores using four different pore widths. Primary micropores have width less than 8 Å, secondary micropores have width of 8-20 Å, mesopores have width of 20-500 Å and macropores have width larger than 500 Å. Most of the surface area available for adsorption is in the micropore size. According to Qin Wei Chow in 2010, Ebie did isotherm experiments with single organic compounds and demonstrated that small halogenated organic compounds adsorbed primarily in pores smaller than 15 Å. They also did experiments with one type of natural organic matter (NOM) and found that NOM adsorbed in the pore size range of 30-100 Å (Chow, 2010). Many studies were also done to better understand the effects of surface chemistry of activated carbon on adsorption. The activated carbon surface is heterogeneous and has several chemical functional groups, most of which contain oxygen. The oxygen functional groups commonly present on the activated carbon surface are carboxylic acid groups, phenolic hydroxyl groups and Quinone carboxyl groups (Boehm, 2002). The presence of these oxygen functional groups increases the surface acidity. The increased acidity causes the surface to become more hydrophilic and to decrease adsorption of hydrophobic organic compounds (Chow, 2010). This decrease in adsorption was accounted by Li *et al*., in their study by the 3 enhanced water adsorptions due to the increase in hydrophilicity of the activated carbon surface (Li *et al*.. 2002).

Besides surface acidity, other surface interactions were also studied. Electrostatic and dispersive interactions on the activated carbon surface were looked at in the work by Radovic *et al*, who showed that modification of the carbon surface will affect adsorption of aromatic compounds. Franz (2000) showed the major mechanisms through which oxygen functional groups affect adsorption are hydrogen bonding, dispersive/repulsive interactions and water adsorption. They also showed that the functional groups of aromatic compounds will affect how target molecules interact with the carbon surface. Activated carbon can therefore be characterized under the based on four primary criteria (Ndi, 2014):

- Total surface area,
- Carbon density,
- Particle size distribution,
- Adsorptive capacity,

I.2.4.1. Total surface area

Total surface area is measured by the adsorption of nitrogen gas onto the carbon and is expressed in square meters of surface area per gram of carbon. Because the gas molecules used to measure adsorption are very small, it should be noted that this measurement of surface area might be misleading when considering the adsorptive capacity of a carbon for large organic macromolecules. Those types of compounds may have adsorption limited by pore size considerations. In fact, the surface area per gram of material ranging from 600 to 1200 m^2/g and as high as 2500 m^2/g have been reported (Li *et al*., 2016).

I.2.4.2 Activated Carbon density

Carbon density is the mass of one milliliter of carbon in air. Bulk density is also sometimes used for carbon as it is for soil, and is expressedin pounds per cubic foot or in kilograms per liter, (Ndi *et al.* 2014).

I.2.4.3. Particle sizes

Particle sizes in carbons are measured using standard U.S. sieve sizes, as for soil constituents. Particle size distributions are important in carbon systems because they influence handling of the activated carbon material. For example, in granular carbon, the particle size affects hydraulic loading and backwash rates for a filter. On the other hand, particle size is often important because of its effect on adsorption rates as well (Ndi *et al*., 2014).

I.2.4.4. Adsorptive capacity

Adsorptive capacity is characterized by the effectiveness of activated carbon in removing a given contaminant (Sathishkumar *et al*., 2012). For comparison, several standard compounds are used for these measurements. For example:

- Iodine number commonly used to describe the carbon's capacity to adsorb low molecular-weight substances. The iodine number indicates the porosity of activated carbon and defined as the milligrams of iodine adsorbed per gram of carbon. The iodine number represents the surface area contributed by the pores larger than 10 Å. Iodine number is commonly used in industry as a rough estimate of surface area of the activated carbon (Li *et al*., 2016).

- Molasses number characterizes a carbon's capacity for more complex compounds. Molasses number represents the surface area contributed by the pores larger than 28 Å.

I.2.5. Production of Activated Carbon

Physical and chemical activation methods are commonly used for production of activated carbon from different precursors (Ramin, 2009).

I.2.5.1 Choice of Precursors

Activated carbons can be produced from most of carbon-containing organic materials, but commercial processes to make activated carbon use precursors, which are either of degraded and coalified plant matter (eg peat, lignite and all ranks of coal) or of the botanical origin (eg wood, coconut shells and nut shells (Ramin, 2009; Sathishkumar *et al*., 2012). These materials have high carbon content and are inexpensive (Ramin, 2009). Coal is commonly used for producing high yields of activated carbon. Materials from botanical origin or in other word, lignocellulosic materials have low inorganic and relatively high volatile content (Kilpimaa *et al*., 2014). The first characteristic results in producing activated carbon with low ash and the second helps to control the production process (Üner *et al*., 2015). In principle. there are two procedures of the activated carbon production: carbonization and activation. Carbonization is a process in which the material is turned into porous carbon structure through pyrolysis or heating. In this process, most of the non-carbon organic matter is decomposed. The combination of carbon atoms-aromatic foliated structure is made with irregular split (Kilpimaa *et al*., 2014). Thus, the split will be developed into a structure with more pores during the process of activation. Activation is used as the steaming or chemical method to remove tar, organic wastes and others. The activation process creates or increases porosity on the activated carbon surface as illustrated in Figure below.

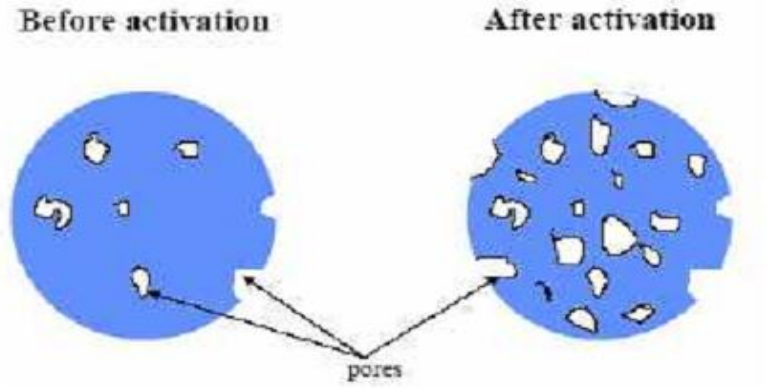

Figure 4: Two-dimensional representation of carbon activation (Ndi, 2014)

Basically, there are 2 different methods in the preparation of activated carbon: single step pyrolysis and two-step pyrolysis. Single step pyrolysis is usually applied in the preparation of activated carbon using chemical activation (Mahmood et al., 2017). However, the one-step method for the production of activated carbon has been developed to reduce the energy expenditure during the process. This method is a feasible alternative to the traditional two-step process for the production of activated carbons by consecutive carbonization of raw material and high temperature activation (900-1000 ºC) of the solid product from carbonization. The mechanism for the process can be visualized as an interaction between the activating agent and the carbon atoms which forms the structure of the intermediate carbonized product (Al-Qodah and Shawabkah, 2008; Ndi, 2014). Production of activated carbon was achieved typically through two routes, physical activation and chemical activation (Ramakrishna, 2012).

I.2.5.2. Physical activation

Physical activation is a two-step process. It involves the carbonization of raw materials followed by activation at elevated temperature in the presence of suitable oxidizing gases such as carbon dioxide, steam, air or their mixtures. Carbonization temperatures ranges between 400 °C to 800 °C, and activation temperature ranges between 800 °C to 1100 °C (Ramakrishna, 2012; Kwaghger *et al.,* 2013). In the physical activation process, the carbonized products develop larger surface areas and porous structures at molecular dimension (Amir, 2012). At this temperature, the rate determining factor is the chemical reaction between the carbon and water vapor or carbon dioxide (Yusufu *et al*., 2012). This reaction takes place at the internal surfaces of the carbon, removing carbon from the pore walls, thereby enlarging them (Mahmood et al., 2017). The activation occurs in two steps. In the first step, the less structured organized carbon is burned out preferentially and the burn-off does not exceed 10 %. This results in the opening of the blocked pores (Li *et al*., 2016). In the second stage, the carbon of the aromatic ring system starts burning, producing active sites and more pores. Activation with carbon dioxide promotes external oxidation and the development of larger pores compared to activation with steam.

I.2.5.3. Chemical activation

Preparation of activated carbon by chemical activation is a single step process in which carbonization and activation is carried out simultaneously. Initially the precursor is mixed with chemical activating agent, which acts as dehydrating agent and oxidant. Chemical activation offers several advantages over physical activation which mainly include (i) lower activation temperature (< 800 ºC) compared to the physical activation temperature (800 – 1100 °C)

(Kumar and Jena, 2016), (ii) single activation step, (iii) higher yields, (iv) better porous characteristics, and (v) shorter activation times (Nowicki *et al*., 2006; Wimonrat *et al.*, 2010). The most commonly used chemical activating agents are H_3PO_4, $ZnCl_2$, and KOH. Zinc chloride ($ZnCl_2$) was used as the first chemical agent for chemical activation, but because of environmental concerns associated with zinc compounds it was displaced by other chemical agents (Yuhui Ma, 2016). The activated carbon produced by $ZnCl_2$ activation are dominantly microporous, but with a significant mesopores which increases by an increase in the impregnation ratio ($ZnCl_2$/precursor). The use of phosphoric acid is increased in industry for either non-carbonized or carbonized raw materials, especially because of the improvement in the process of acid (Li *et al*., 2016). Alkali hydroxide compounds such as KOH and NaOH have been used in order to prepare activated carbons with high specific surface areas, Of the many reagents proposed for chemical activation, the most commonly industrially used, are $ZnCl_2$, H_3PO_4, and KOH (Karacan *et al*., 2007; Üner *et al*., 2015). Also, the effects of this chemical on a single precursor have not been thoroughly investigated in the literature, and the information published is limited, but activated carbon with high specific surface area using $ZnCl_2$ as activating agent has been reported (Mahmood *et al*., 2017).

I.2.6. Porous Structure of the Active Carbon Surface

Active carbons with a random arrangement of microcrystallites and with a strong cross-linking between them have a well-developed porous structure. They have relatively low density (less than 2 gm/cm^3) and a low degree of graphitization. This porous structure formed during the carbonization process is developed further during the activation process, when the spaces between the elementary crystallites are cleared of tar and other carbonaceous material. The activation process enhances the volume and enlarges the diameters of the pores (Danish *et al*., 2018). The structure of the pores and their pore size distribution are largely determined by the nature of the raw material and the history of its carbonization. The activation also removes disorganized carbon, exposing the crystallites to the action of the activating agent and leads to the development of a microporous structure. In the latter phase of the reaction, the widening of existing pores and the formation of large pores by burnout of the walls between the adjacent pores also takes place. This causes an increase in the transitional porosity and macroporosity, resulting in a decrease in the micropore volume. According to Dubinin and Zaverina, a microporous active carbon is produced when the degree of burn-off is less than 50% and a macroporous active carbon when the extent of burn-off is greater than 75%. When the degree

of burn-off is between 50 and 75%, the product has a mixed porous structure and contains all types of pores (Li *et al*., 2016).

Active carbons, in general, have a strongly developed internal surface and they are usually characterized by a poly-disperse capillary structure comprising pores of different sizes and shapes. It is difficult to obtain accurate information on the shape of the pores. Several different methods used to determine the shapes of the pores have indicated ink-bottle shape, capillaries open at both ends or with one end closed, regular slit-shaped, V-shaped, and many other shapes. It may, however, be mentioned that for all practical purposes, the actual shape of the pores is of no consequence (Binti, 2007). Generally, the calculations of the pore radii are made by considering the pores to be ink-bottle shaped or straight and nonintersecting cylindrical capillaries.

Active carbons are associated with pores starting from less than a nanometer to several thousand nanometers. Dubinin proposed a classification of the pores that has now been adopted by the International Union of Pure and Applied Chemistry (IUPAC). This classification is based on their width (w), which represents the distance between the walls of a slit-shaped pore or the radius of a cylindrical pore. The pores are divided into three groups: the micropores, the mesopores (transitional pores), and the macropores.

Micropores have molecular dimensions, the effective radii being less than 2 nm. The adsorption in these pores occurs through volume filling, and there is no capillary condensation taking place. The adsorption energy in these pores is much larger compared to larger mesopores or to the nonporous surface because of the overlapping of adsorption forces from the opposite walls of the micropores (Egila, 2015). They generally have a pore volume of 0.15 to 0.70 cm^3/g. Their specific surface area constitutes about 95% of the total surface area of the active carbon. Dubinin further suggested that for some active carbons, the microporous structure can be subdivided into two overlapping microporous structures involving specific micropores with effective pore radii smaller than 0.6 to 0.7 nm and the super micropores showing radii of 0.7 to 1.6 nm. The micropore structure of active carbons is characterized largely by the adsorption of gases and vapors and, to a smaller extent, by small-angle x-ray scattering technique (Egila, 2015).

Mesopores, also called *transitional pores*, have effective dimensions in the 2 to 50 nm range, and their volume usually varies between 0.1 and 0.2 cm^3/g. The surface area of these pores does not exceed 5% of the total surface area of the carbon. However, by using special

methods, it is possible to prepare activated carbons that have an enhanced mesoporosity, the volume of mesopores attaining a volume of 0.2 to 0.65 cm^3/g and their surface area reaching as high as 200 m^2/g. These pores are characterized by capillary condensation of the adsorbent with the formation of a meniscus of the liquefied adsorbate. The adsorption isotherms show adsorption desorption hysteresis is which stops at a relative vapor pressure of 0.4. Besides contributing significantly to the adsorption of the adsorbate, these pores act as conduits leading the adsorbate molecules to the micropore cavity. These pores are generally characterized by adsorption-desorption isotherms of gases, by mercury porosimetry, and by electron microscopy.

Macropores are not of considerable importance to the process of adsorption in active carbons because their contribution to the surface area of the adsorbate is very small and does not exceed 0.5 m^2/g. They have effective radii larger than 50 nm, and frequently in the 500 to 2000 nm range, with a pore volume between 0.2 and 0.4 cm^3/g. They act as transport channels or high way for the adsorbate into the micro- and mesopores. Macropores are not filled by capillary condensation and are characterized by mercury porosimetry (Worch, 2012).

Thus, the porous structure of active carbons is tri-dispersed, consisting of micro, meso, and macropores, each of these groups of pores plays a specific role in the adsorption process. The micropores constitute a large surface area and micropore volume and, therefore, determine to a considerable extent the adsorption capacity of a given active carbon, provided that the molecular dimensions of the adsorbate are not too large to enter the micropores. Micropores are filled at low relative vapor pressure before the commencement of capillary condensation. The mesopores, on the other hand, are filled at high relative pressures with the occurrence of capillary condensation (Egila, 2015). The macropores enable adsorbate molecules to pass rapidly to smaller pores situated deeper within the particles of active carbons. Thus, according to Dubinin, the pattern of porous structure in active carbons constitutes macropores opening up directly to the external surface, the transitional pores branching off from the macropores, and the micropores in turn branching off from the transitional pores (Sugumaran *et al*., 2012).

It is worthwhile to mention that Dubinin classification of pores in active carbons is not entirely arbitrary because it takes into account differences in the behavior of molecules adsorbed in micro and mesopores. Although adsorption-desorption hysteresis is characteristic of mesopores, it has also been observed in the case of micropores at low relative pressures (Nezih, 2004). This has been attributed to inelastic distortion of some micropores, resulting in

trapping of the adsorbate molecules. Consequently, the accessibility of the micropore system has been found to be increased after a number of adsorption-desorption cycles.

All pores have walls and, therefore, will show two types of surfaces: the internal or microporous surface denoted by *Smi* and the external surface, *Se*. The former represents the walls of the pores and has an area of several hundred square meters per gram of the carbon. It is given by the relationship

$$S_{mi} = \frac{2x10^3\, w}{L} \quad \text{.....(2)}$$

Where S_{mi} is the surface area in m^2/g, *W* is the volume in cm3/g, and *L* is the accessible pore width in nanometers. Because the pore width *L* is very small, the area of the micropores is much larger than the area of mesopores or macropores (Sugumaran *et al*., 2012). The second surface, *Se*, which constitutes the walls of the meso- and macropores as well as the edges and the outer facing aromatic sheets, is small and varies between 10 and 200 m^2/g for many of the active carbons. The difference between *Smi* and *Se* lies in the volume of the adsorption energy, which can be twice as high on the walls of a micropore as on the open surface. This energetic effect decreases rapidly as the pore width increases (Worch, 2012). As the adsorption in micropores takes place at low relative pressures and as the BET approach is unable to interpret the early stages of the adsorption isotherm at low relative vapor pressures, the surface areas of highly micropores carbons obtained using the BET equation are many times unrealistic.

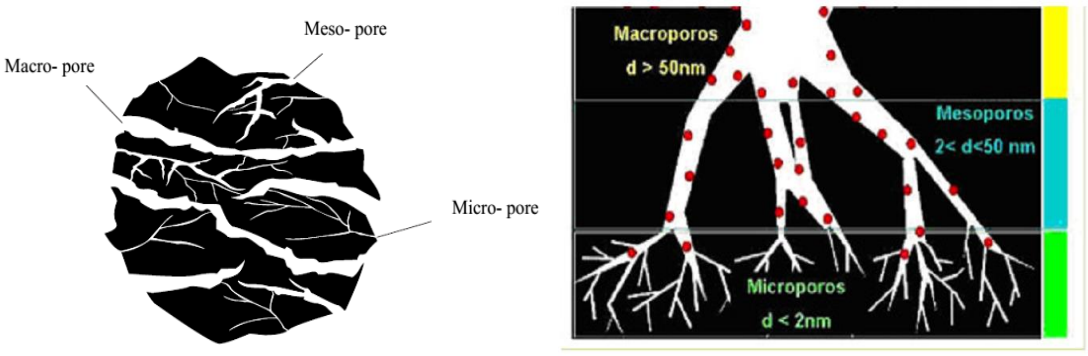

Figure 5: Porous structure of activated carbon

I.2.7. Chemical structure of activated carbon

The selectivity of activated carbons for adsorption is depended upon their surface chemistry, as well as their pore size distribution. Normally, the adsorptive surface of activated carbon is approximately neutral such as that polar and ionic species are less readily adsorbed

than organic molecules (Binti, 2007). Activated carbon can either have surfaces which are acidic, basic or neutral. Figure 6 below gives the various functional groups present on the surface of AC by Mohammad *et al.*, (2010).

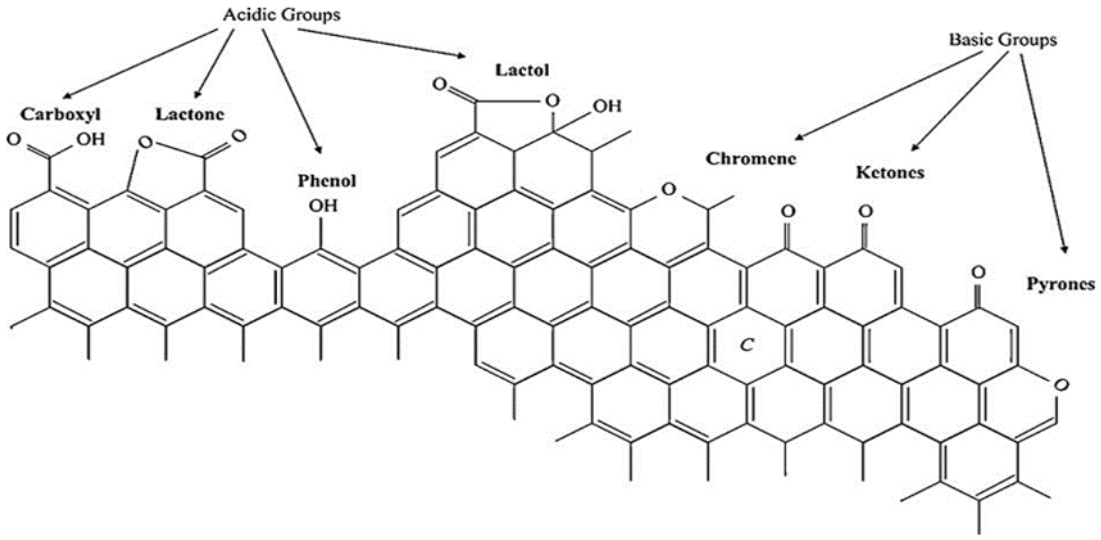

Figure 6: Schematic representation of the main functional group on the surface of activated carbon (Mohammad *et al.*, 2010)

I.2.8. Classification of Activated Carbon

Activated carbons are complex products which are difficult to classify on the basis of their behavior, surface characteristics and other fundamental criteria. However, some broad classification is made for general purpose based on their size, preparation methods porosity and industrial applications (Abdul *et al.*, 2001).

I.2.8.1. Powdered activated carbon

In particulate form as powders or fine granules less than 1.0 mm in size with an average diameter between 0.15 and 0.25 mm. Thus they present a large surface to volume ratio with a small diffusion distance. Activated carbon is defined as the activated carbon particles retained on a 50-mesh sieve (0.297 mm) (Daniel, 2007).

Figure 7: Powder activated carbon

I.2.8.2. Granular activated carbon (GAC)

Granular activated carbon has a relatively larger particle size compared to powdered activated carbon and consequently, presents a smaller external surface. Diffusion of the adsorbate is thus an important factor. These carbons are suitable for absorption of gases and vapors, because they diffuse rapidly. Granulated carbons are used for water treatment, de-odorization and separation of flow system components and are also used in rapid mix basins with a size of greater than 0.297 mm as the minimum GAC size (Micheal, 1999). Granular Activated Carbon (GAC), has mean particle size between 0.6 to 4 mm. It is usually used in continuous processes of both liquid and gas phase applications. GAC has an advantage over PAC, this is because it offers a lower pressure drop along with the fact that it can be regenerated and therefore reused more than once. In addition to the proper micropore size distribution, its high apparent density, high hardness, and a low abrasion index made GAC more suitable over PAC for various applications (Ramakrishna, 2012).

Figure 8: Granular activated carbon

I.2.8.3. Extruded activated carbon (EAC)

Extruded activated carbon combines powdered activated carbon with a binder, which are fused together and extruded into a cylindrical shaped activated carbon block with diameters from 0.8 to 130 mm. These are mainly used for gas phase applications because of their low pressure drop, high mechanical strength and low dust content (Lemaro and Rotich, 2012).

Figure 9: Extruded activated carbon

I.2.8.4. Bead activated carbon (BAC)

Bead activated carbon is made from petroleum pitch and supplied in diameters from approximately 0.35 to 0.80 mm. Similar to EAC; it is also noted for its low pressure drop, high mechanical strength and low dust content, but with a smaller grain size. Its spherical shape makes it preferred for fluidized bed applications such as water filtration (Lemaro and Rotich, 2012).

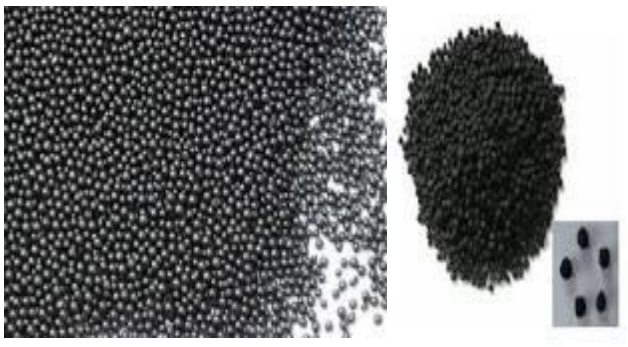

Figure 10: Bead activated carbon

I.2.8.5. Impregnated carbon

Porous carbons containing several types of inorganic impregnate such as iodine, silver, cations such as Al, Mn, Zn, Fe, Li, Ca have also been prepared for specific application in air pollution control especially in museums and galleries (Gh *et al.*, 2010). Due to its antimicrobial and antiseptic properties, silver loaded activated carbon is used as an adsorbent for purification of domestic water. Drinking water can be obtained from natural water by treating the natural water with a mixture of activated carbon and $Al(OH)_3$, a flocculating agent. Impregnated carbons are also used for the adsorption of Hydrogen Sulfide (H_2S) and thiols.

Figure 11: Impregnated carbon

I.2.8.6. Polymer coated carbon

This is a process by which a porous carbon can be coated with a biocompatible polymer to give a smooth and permeable coat without blocking the pores. The resulting carbon is useful for hemoperfusion. Hemoperfusion is a treatment technique in which large volumes of the patient's blood are passed over an adsorbent substance in order to remove toxic substances from the blood (Panahi *et al.*, 2008).

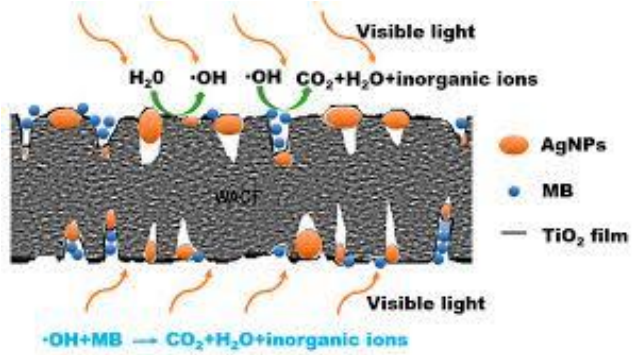

Figure 12: Polymer coated carbon

I.2.8.7. Activated Carbon Fibers

Activated carbon Fibers (ACFs) are carbonized carbons which are subsequently heat treated in an oxidizing atmosphere. ACF began to be developed in 1970 using the precursor viscose rayon which mainly consists of cellulose (Doying, 1966). Later thermoset polymer materials like saran and phenolic resins were used as precursors to produce ACF (Menendez and Martin-Gullon, 2006). A good ACF precursor must be non-graphitic and nongraphitizable carbon fibre which was isotropic in nature. From the end of 1980s, interest is still centered on the production of ACFs from various inexpensive precursors (Derbyshire *et al*., 2001; Foo *et al*., 2002; Nahil and Williams, 2011; Oh and Jang, 2003; Oya et al., 1993; Rosas et al., 2009).

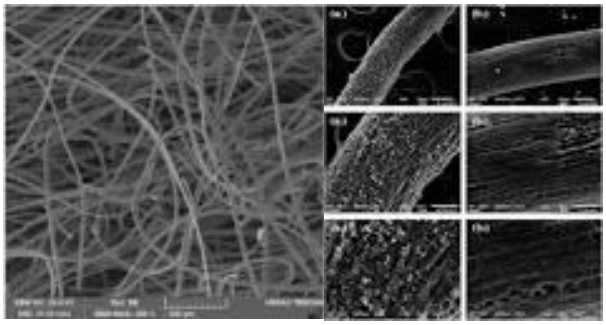

Figure 13: Activated carbon fibers

I.2.9. Uses of Activated Carbon

Activated carbon is widely used in gas purification, decaffeination, gold purification, metal extraction, water purification, medicine, sewage treatment, air filters in gas masks and respirators, filters in compressed air and many other applications. One major industrial application involves use of activated carbon in the metal finishing field. It is very widely employed for purification of electroplating solutions (Wanjun *et al*., 2015; Kumar and Jena, 2016). For example, it is a main purification technique for removing organic impurities from bright nickel-plating solutions. A variety of organic chemicals are added to plating solutions for improving their deposit qualities and for enhancing properties like brightness, smoothness, ductility, etc (Worch, 2012). Due to passage of direct current and electrolytic reactions of anodic oxidation and cathodic reduction, organic additives generate unwanted breakdown products in solution (Wanjun *et al*., 2015). Their excessive build up can adversely affect the plating quality and physical properties of deposited metal. Activated carbon treatment removes such impurities and restores plating performance to the desired level (Hu *et al*., 2011). Other applications include

I.2.9.1. Medical uses

Activated carbon is used to treat poisonings and overdoses following oral ingestion. It is not effective for a number of poisonings including with: strong acids or alkali, iron, lithium, arsenic, methanol, ethanol or ethylene glycol (Danish *et al*., 2018).

I.2.9.2. Analytical chemistry applications

Activated carbon, in 50% w/w combination with celite, is used as stationary phase in low-pressure chromatographic separation of carbohydrates (mono-, di-trisaccharides) using ethanol solutions (5–50%) as mobile phase in analytical or preparative protocols.

I.2.9.3. Environmental applications

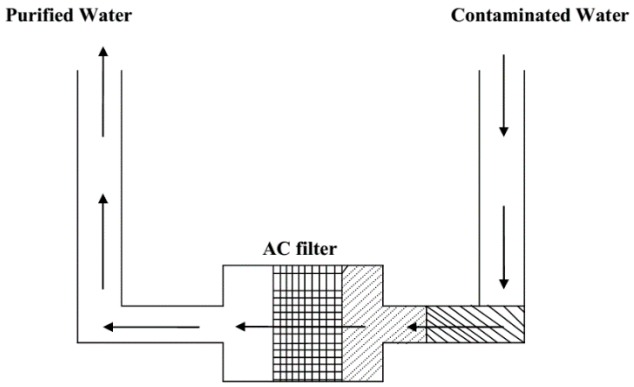

Figure 14: Representation of Activated Carbon in water Filter

Activated carbon is usually used in water filtration systems. In this illustration, the activated carbon is in the fourth level (counted from bottom). Carbon adsorption has numerous applications in removing pollutants from air or water streams both in the field and in industrial processes (Baccar *et al*., 2009; Yusufu *et al*., 2012)such as:

- Spill clean up
- Ground water remediation
- Drinking water filtration
- Air purification
- Volatile organic compounds capture from painting, dry cleaning, gasoline dispensing operations, and other processes (Danish et al., 2018).

I.2.9.4. Fuel storage

Research is being done testing various activated carbons' ability to store natural gas and hydrogen gas. The porous material acts like a sponge for different types of gases. The gas is attracted to the carbon material via Van der Waals forces. Some carbons have been able to achieve bonding energies of 5–10 kJ per mol. The gas may then be desorbed when subjected to higher temperatures and either combusted to do work or in the case of hydrogen gas extracted for use in a hydrogen fuel cell (Thomas, 2012). Gas storage in activated carbons is an appealing gas storage method because the gas can be stored in a low pressure, low mass, low volume environment that would be much more feasible than bulky on-board compression tanks in vehicles. The United States Department of Energy has specified certain goals to be achieved in the area of research and development of nano-porous carbon materials. All of the goals are yet to be satisfied but numerous institutions, including the ALL-CRAFT program, are continuing to conduct work in this promising field (Thomas, 2012).

I.2.9.5. Gas purification

Filters with activated carbon are usually used in compressed air and gas purification to remove oil vapors, odors, and other hydrocarbons from the air. The most common designs use a 1 stage or 2 stage filtration principle in which activated carbon is embedded inside the filter media. Activated carbon is also used in spacesuit Primary Life Support Systems. Activated carbon filters are used to retain radioactive gases from a nuclear boiling water reactor turbine condenser. The air vacuumed from the condenser contains traces of radioactive gases. The large charcoal beds absorb these gases and retain them while they rapidly decay to non-radioactive solid species. The solids are trapped in the charcoal particles, while the filtered air passes through (Kumar and Jena, 2016).

I.2.9.6. Chemical purification

Activated carbon is commonly used to purify solutions containing un-wanted colored impurities such as during a recrystallization procedure in Organic Chemistry.

I.2.9.7. Sound Absorption

Activated carbon can filter air and water. Sound energy is found within air and water and activated carbon can be used to absorb that energy. With its high degree of porosity in each activated carbon granule, sound energy has numerous areas to enter into and be converted to heat. With the energy change to heat, the process of sound absorption occurs. Activated carbon in its granule form can be used to absorb middle and high frequency ranges provided the absorbers design lets air pass through the carbon. Activated carbon can also be used inside of

diaphragmatic absorption technology to increase the rate of absorption within the diaphragmatic absorber (Danish *et al*., 2018).

I.2.9.8. Distilled alcoholic beverage purification

Activated carbon filters can be used to filter vodka and whiskey of organic impurities which can affect color, taste, and odor. Passing organically impure vodka through an activated carbon filter at the proper flow rate will result in vodka with an identical alcohol content and significantly increased organic purity, as judged by odor and taste.

I.2.9.9. Mercury scrubbing

Activated carbon, often impregnated with sulfur or iodine, is widely used to trap mercury emissions from coal-fired power stations, medical incinerators, and from natural gas at the wellhead. This carbon is a specialty product costing more than US$4.00 per kg. However, it is often not recycled (Lemaro and Rotich, 2012).

I.2.9.10. Gold Recovery

Activated carbon acts as a sponge to aurocyanide and other complex ions in solution. Carbon particles which are much larger than the ore particle size can be mixed with the ore and cyanide solution. When this is applied to gold extraction, the gold cyanide complex is adsorbed onto the carbon until it comes to equilibrium with the gold solution. Since the carbon particles are much larger, they can easily be separated from the slurry by screening using a wire mesh. The gold is then reactivated and returned to the circuit (Lemaro and Rotich, 2012).

I.3. Adsorption

I.3.1. Definition of Adsorption

The word "adsorption" was coined in 1881 by a German physicist Heinrich Kayser (1853-1940). In order for a compound to adsorb to a surface, a driving force must exist so that the compound will leave the aqueous phase. Examples of these include hydrophobic forces, electrostatic forces, chemical or Van der Waals forces (Matthew, 2004).

Adsorption is therefore a surface phenomenon where atoms or molecules in a fluid solution (solid or gas) called adsorbate are fixed on a solid surface called adsorbent. In order to better understand the retention capacity of molecules, it is therefore convenient to understand the phenomenon which exists at the molecular level (Fulazzaky, 2011). This phenomenon is called adsorption mechanism. This mechanism depends on the adsorbate-adsorbent interaction and is of two types namely:

-High energy bonds (›80 kJ/mole): Ionic bond or ligand exchange interaction.

-Weak energy bonds (‹80 kJ/mole): dipole-dipole interaction, hydrogen bond, hydrophobic interaction.

Based on these, four principal mechanisms can be distinguished (Moumenine, 2011).

- adsorption by ionic bonds or ions exchange,
- adsorption by hydrogen bond formation,
- adsorption by Van der Waals forces of interaction,
- hydrophobic retention.

Hence molecules interact with surfaces and with forces originating either from the "physical" Van der Waals interaction or from the "chemical" hybridization of their orbitals with those of the atoms of the substrate. Depending on which contribution dominates, adsorption can be divided into two physisorption or chemisorption. These are limiting cases since hybridization is always present at small enough adsorption distances, even for adsorbed rare gases.

I.3.2. Types of adsorption

The adsorption at a surface or interface is largely as a result of binding forces between atoms, molecules and ions of adsorbate and surface. According to the nature of forces involved therefore, adsorption can conveniently be divided into two types: physisorption or physical adsorption and chemisorption or chemical adsorption.

I.3.2.1. Physisorption (Physical adsorption)

When the force of attraction existing between adsorbate and adsorbent are weak Van der Waal forces of attraction, the process is called physical adsorption or physisorption. In physisorption, there is the absence of chemical bonds; the molecule retains its gas phase electronic structure, although some distortion is still possible. The binding energy depends on the polarizability and on the number of atoms involved. Physical Adsorption takes place with formation of multilayer of adsorbate on adsorbent. It has low enthalpy of adsorption that is the enthalpy of adsorption ranges from 20-40 KJ/mol and varies between few meV (light gases) and several eV (large organic molecules). It takes place at low temperature, below the boiling point of the adsorbate. As the temperature increases, the process of Physisorption decreases. The Van der Waals forces of interaction put in place here (Lekene, 2013) are of three types:

Keesom force, which exist between molecules containing permanent dipole moment.

Debye force, which exist between a molecule containing permanent dipole moment and another molecule containing induce dipole moment.

London dispersion force between molecules containing induce dipoles.

I.3.2.2. Chemical adsorption

Chemisorption is a phenomenon characterize by stronger perturbation of the molecular electronic structure with formation of chemical bonds between the adsorbed molecules with the substrate. The energy here is of several eV, Chemisorption is a kind of adsorption which involves a chemical reaction between the surface and the adsorbate. New chemical bonds are generated at the adsorbent surface. The strong interaction between the adsorbate and the substrate surface creates new types of electronic bonds, It has high enthalpy of adsorption and the energy here ranges from 40 to 200 kJ/mol (Aksas, 2012). It can take place at all temperature. When the temperature increases, chemisorption first increases and then decreases. Table I gives some differences between physisorption and chemisorption.

Tableau I: Differences between physical and chemical adsorption (Aksas, 2012)

Parameters	**Physisorption**	**Chemisorption**
Types of bonds	Van der Waals	Chemical bonds
Temperature of process	It decreases with increase in temperature and it is exothermic	Desorption occurs at high temperature and it is exothermic
Individual appearance of molecules	Conservation of molecular structure	Destruction of molecular structure
Desorption	Desorption can easily occur	Desorption cannot easily occur
Kinetics of process	Fast, independent of temperature	Slow
Heat of adsorption	Less than 10 kcal/mole	Higher than 10 kcal/mole
Coverage	Formation of multilayer and monolayer adsorption, weak binding forces and reaction is reversible at low pressure,	Formation of monolayer coverage, a chemical bond has been formed and the reaction is irreversible,

I.3.3. Sorption from solution

Oxide surfaces in aqueous systems adsorb water molecules via strong electrostatic interactions called hydrogen bonds where the proton on water associates with the surface oxygen at the oxide surface. For a solute to chemisorbrd (form an inner-sphere complex) at the aquated oxide surface, the sorbing molecule must displace one of these strongly bound waters, a difficult and energy-intensive interaction. For this reason, the sorption constant (Ksorp) would be expected to be low for neutral organic compounds and high for polar compounds that can compete for charged sites.

When hydrophobic molecules associate with soil organic matter, however, there is no competition with water and the interactions resemble a dissolution reaction into an organic solvent. This requires much less energy and the associated K is much higher.

I.3.4. Factors Determinating Adsorption

I.3.4.1. Surface Area

Surface area is an important parameter to consider when selecting an adsorbent. In an ideal adsorption situation where all other conditions (such as pore size, surface chemistry, and adsorbent-adsorbate interactions) are optimal for contaminant removal the surface area would serve as the limiting factor for the adsorption process. In this case, as the surface area increases, so would the adsorption of the target contaminant (Olushola *et al.*, 2012). The surface area is commonly found using a theory developed by Brunauer, Emmett and Teller (BET) for physical adsorption. While the BET theory is inadequate as a universal equation for physical adsorption, it has been adapted to describe surface area.

I.3.4.2. Pore Size Distribution

Another essential parameter to consider for an absorbent is its pore size distribution (PSD). Pore size distribution is usually expressed as a graphical relationship using pore width (Å) as the independent variable and cumulative pore volume (cc/g) as the dependent variable. Pore widths that fall under 20 Å are considered to be micropores, from 20 to 500 Å are mesopores, and above 500 Å are macropores.

I.3.4.3. pH

When the parameter of pH is discussed in an experiment, commonly it is used as a descriptor to express the ionic conditions of a given aqueous system.

I.3.4.4. Mineral surface properties

Surface charge of an oxide mineral surface in aqueous systems will change with changing pH as a function of the zero-point charge (ZPC) of that mineral. This surface charge creates a surface condition in which there is an uneven charge distribution creating a double-layer of ions. Charged organic solutes may exchange with other counter-ions in the double layer, resulting in physisorption.

I.3.5. Adsorption Isotherms

Two important physicochemical aspects for the evaluation of the adsorption process as a unit operation are the equilibria and the kinetics of the adsorption. Equilibrium studies give the capacity of the adsorbent and quantify the adsorption process (Keith *et al*., 2000). The equilibrium relationship between adsorbent and adsorbate are described by adsorption isotherm, usually the ratio between the quantity adsorbed and that remaining in solution at a fixed temperature at equilibrium.

I.3.5.1. The Langmuir Isotherm

Irving Langmuir an American chemist who was awarded the Nobel Prize for Chemistry in 1932 for 'his discoveries and researches in the realm of surface chemistry', developed a relationship between the amount of gas adsorbed on a surface and the pressure of that gas (Thuan *et al*., 2016). Such equations are now referred to as the Langmuir adsorption isotherms, a theoretical adsorption isotherm in the ideal case (Villota et al., 2017). The Langmuir adsorption isotherm is often used for adsorption of a solute from a liquid solution (Ketcha *et al*.,2012). The Langmuir adsorption isotherm is perhaps the best known of all isotherms describing adsorption and its nonlinear form is often expressed as (Li *et al*., 2011):

$$Q_e = \frac{Q_m K C_e}{1+KC_e} \quad \text{..... (3)}$$

where:

Q_e (mg of adsorbate per g of adsorbent) is the adsorption density at the equilibrium solute concentration C_e.

C_e is the equilibrium concentration of adsorbate in solution (mg/L)

Q_m (mg of solute adsorbed per g of adsorbent) is the maximum adsorption capacity corresponding to complete monolayer coverage. K is the Langmuir constant related to energy

of the adsorption (L of adsorbate per mg of adsorbent) (Babayemi, 2016). Equation 3 can be rearranged to the following linear form:

$$\frac{C_e}{Q_e} = \frac{1}{Q_m K} + \frac{C_e}{Q_m} \quad \text{..... (4)}$$

The linear form can be used for linearization of experimental data by plotting C_e/Q_e against C_e. The Langmuir constants Q_m and K can be evaluated from the slope and intercept of the linear equation.

This is the simplest physically possible isotherm. It is based on three assumptions:

1. Adsorption cannot proceed beyond monolayer coverage.

2. All surface sites are equivalent and can accommodate at most one adsorbed atom.

3. The ability of a molecule to adsorb at a given site is independent of the occupation of neighbouring sites.

I.3.5.2. Freundlich Adsorption Isotherm

Herbert Max Finley Freundlich, a German physical chemist presented an empirical adsorption isotherm for non-ideal system in 1906. The Freundlich isotherm is the earliest known relationship describing the adsorption equation and is often expressed as (Goel *et al*., 2005; Villota et al., 2017):

$$Q_e = K_f C_e^{1/n} \text{.....} \quad \text{(5)}$$

where:

Q_e is the quantity of solute adsorbed at equilibrium (adsorption density: mg of adsorbate per g of adsorbent).

C_e is the concentration of adsorbate at equilibrium.

K_f and n are the empirical constants dependent on several factors and n is greater than one.

This equation is conveniently used in linear form by taking the logarithmic of both sides to give equation 6:

$$\ln Q_e = \ln K_f + \frac{1}{n} \ln C_e \quad \text{.....(6)}$$

A plot of lnQ_e against lnC_e yielding a straight line indicates the confirmation of the Freundlich isotherm for adsorption. The constants can be determined from the slope and the intercept (Thuan *et al*., 2016; Ketcha *et al*.,2012).

I.3.5.3. Tempkin Isotherm

This isotherm contains a factor that explicitly taking into the account of adsorbent–adsorbate interactions. By ignoring the extremely low and large value of concentrations, the model assumes that heat of adsorption (function of temperature) of all molecules in the layer would decrease linearly rather than the logarithmic with coverage (Dada *et al.*, 2012). As implied in the equation, its derivation is characterized by a uniform distribution of binding energies (up to some maximum binding energy) was carried out by plotting the quantity sorbed Q_e against lnCe and the constants were determined from the slope and intercept. The model is given by equation 7 (Babayemi, 2016; Ketcha *et al*.,2009):

$$\frac{Q_e}{Q_m} = \frac{RTln(A_T C_e)}{b_T} \quad \text{.....(7)}$$

Linearising equation 7 gives:

$$Q_e = BlnK_T + BlnC_e \quad \text{..... (8)}$$

where.

$B = RT/b_T$: constant related to heat of sorption (J/mol)

R: universal gas constant

T: absolute temperature

b_T: Tempkin isotherm constant (J/mol)

K_T: Tempkin isotherm equilibrium binding constant (L/mg)

I.3.5.4. Dubinin –Kaganer-Radushkevich isotherm model

Dubinin–Kaganer-Radushkevich isotherm is generally applied to express the adsorption mechanism with a Gaussian energy distribution onto a heterogeneous surface (Dada *et al.*, 2012). The model has often successfully fitted high solute activities and the intermediate range of concentrations data well.

$$Q_e = Q_m \exp(-A\varepsilon^2) \quad \text{..... (9)}$$

where.

$\varepsilon = RTln\,(1 + {}^{1}/_{C_e})$……..(10)

Q_e: amount of adsorbate in the adsorbent at equilibrium (mg/g);

Q_m : theoretical isotherm saturation capacity (mg/g);

ß : Dubinin–Kaganer-Radushkevich isotherm constant (mol /kJ)

ε :Dubinin–Kaganer-Radushkevich isotherm constant.

The approach was usually applied to distinguish the physical and chemical adsorption of metal ions with its mean free energy. E per molecule of adsorbate (for removing a molecule from its location in the sorption space to the infinity) can be computed by the relationship (Dada *et al.*, 2012).

I.3.5.5. The BET Isotherm

In the Langmuir model, it was assumed that adsorption could only occur on the unoccupied substrate adsorption sites. We will now remove this restriction. If the initial adsorbed layer can act as a substrate for further adsorption, then, instead of the isotherm levelling off to some saturated value at high pressures, it can be expected to rise indefinitely. The most widely used isotherm dealing with multilayer adsorption was derived by Stephen Brunauer, Paul Emmett and Edward Teller and is called the BET isotherm.

$Q_e = \frac{CZ}{(1-C)[-1(1-C)Z]}$ …….……..…… (11)

where:

$Z = \frac{P}{P^*}$ …… …… .....(12)

In this expression P* is the saturation pressure of the gas, Q_e is the quantity of solute adsorbed at equilibrium and c is the BET constant.

I.3.6. General Adsorption Isotherms

Adsorption is usually described through isotherms, which is, the amount of adsorbate on the adsorbent as a function of its pressure (if gas) or concentration (if liquid) at constant temperature. The quantity adsorbed is nearly always normalized by the mass of the adsorbent to allow comparison of different material

In this light, the different types of adsorption isotherm observed during the adsorption of gases by solid is the outcome of the forces of attraction between the individual molecules of gas and the atoms or ions composing the solid (Nkwaju, 2013). IUPAC has therefore classified in the case of gases the different types of possible isotherms as shown in Figure 15.

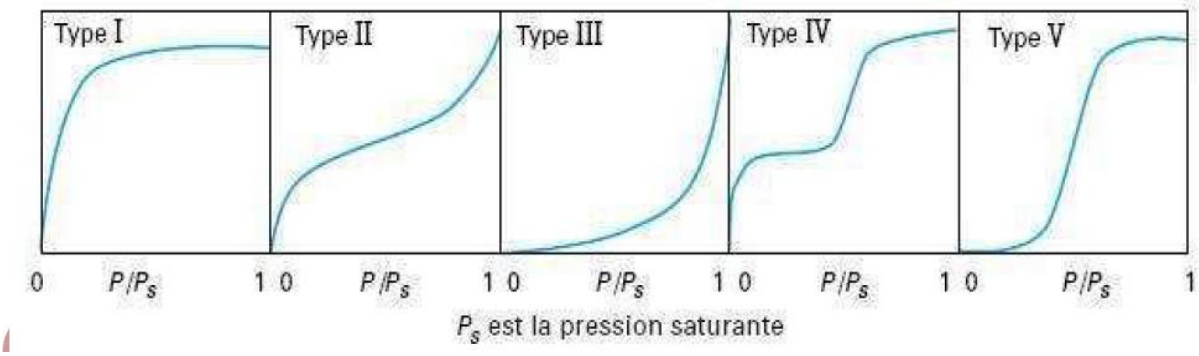

Figure 15: **Brunauer's five Types of Adsorption Isotherms**

From the types of isotherms obtain we can draw qualitative conclusions of the types of interaction between the adsorbate and the adsorbent (Worch, 2012).

The type I isotherms are characteristics of monolayer adsorption or it correspond to filling of micro pores with saturation when the dispose volume is completely filled. This corresponds to characteristics adsorption on micro porous activated carbon and zeolite.

The type II isotherms correspond to a muti-layer adsorption. However, type II isotherm can also correspond to the sum of the isotherm I + II (filling of micro pores followed by an external surface adsorption).

The type III isotherms reflect the absence of attraction between the adsorbate and the adsorbent; and the adsorbate-adsorbate interaction is very strong. Such cases are seen in the adsorption of water on hydrophobic surfaces.

The type IV isotherms result from the combination of type I (strong but limited adsorption) and of type V. This is the case of water on oxygen reach carbon.

The type V isotherms also reflect interaction between the adsorbate. Furthermore, the hysteresis in the course of desorption reflect the presence of mesopores in which the vapors condense to form meniscus of strong graph.

The type VI isotherms are characteristics of multilayer adsorption on a non-porous uniform surface; this isotherm presents characteristics bidimensional condensation movement.

I.3.7. Adsorption Kinetics

The adsorption onto or into adsorbent surfaces with respect to time is known as adsorption kinetics. The batch studies play a significant role in designing and evolution for the performance of adsorption kinetics. Adsorption is a time- dependent process, and to determine the rate of adsorption is highly important in the design and evaluation of adsorbent in removing pollutants from wastewater. The kinetic study of adsorption process provides information on the adsorption mechanism on the transfer of solute on the liquid phase to the solid phase. The kinetic adsorption constants can be used to optimize the residence condition (Mona and Amina, 2012). The kinetics model depends on the nature and complexity of the adsorbent material (Lekene, 2013). The adsorption kinetics may be determined by following main stages.

External diffusion: Diffusion of molecules from the bulk phase towards the interface space.

Internal diffusion: Diffusion of molecules inside the pores.

Surface diffusion: Diffusion of molecules in the surface phase.

Adsorption/desorption elementary processes.

The kinetics models which exist are based on:

a) Composition of medium: Here the speed of adsorption at any instant t is determined by the standard deviation between the state of the system at that instant and its state at equilibrium.

b) Diffusion: With diffusion the speed of adsorption is determined by the molecular diffusion of the substances.

Chemical kinetics is the study of the rates and mechanism of chemical reactions. The study of adsorption kinetics describes the resistance to solute transfer from the solution up to the boundary layer at the solid-liquid interface to the pore water and then to the solid. The solute uptake rate and evidently this rate controls the residence time of adsorbate at the solid-solution interface. The transfer of adsorbate through the fluid to the surface of the adsorbent consists of a number of stages which depend on hydrodynamic characteristics of the system (type of apparatus, rate), physical constants of the adsorbent (especially the diffusion coefficient) and the chemical nature of the adsorbent (Worch, 2012).

It is well known that adsorption kinetics is mainly controlled by the following steps;

- Solute molecules transfer from the solution to the boundary film;

- Solute molecules transfer from the film to the surface of the sorbent (external diffusion);

- Diffusion from the surface to intra-particle sites and

- Interaction of solute molecules with the available sites on the internal surface.

The first one is bulk diffusion, the second is external mass transfer resistance and the third is intra-particle mass transfer resistance.

The evolution of the adsorption process can be followed by measuring the number of particles adsorbed per unit time. Many kinetic models have been proposed for the adsorption of solutes on solids. They include amongst others the Lagergren's pseudo-first-order kinetic model, pseudo-second order model, the Elovich model, mass transfer and intraparticle diffusion models.

I.3.7.1. Medium composition base Model

I.3.7.1.1. Pseudo-First order kinetic Model

The pseudo-first order kinetic model is the earliest known in describing adsorption rate based on the adsorption capacity (Mona and Amina, 2012). The pseudo-first order equation of Lagergren is generally express as in equation 13 (Tagne *et al*., 2013).

$$\frac{dQ_t}{dt} = K_1(Q_e - Q_t) \quad \text{..... (13)}$$

where Q_e and Q_t are the sorption capacity at equilibrium and at time t and k_1 is the rate constant of pseudo-first order sorption ($Lmin^{-1}$).

Integrating equation (13) at t = 0 and at t = t; $Q_t = 0$ and $Q_t = Q_t$ gives:

$$\ln\frac{(Q_e - Q_t)}{Q_e} = K_1 t \quad \text{.....(14)}$$

Or

$$\ln C_t = K_1 t + \ln C_o \quad \text{.....(15)}$$

I.3.7.1.2. Pseudo-second order kinetic model

The Pseudo-second order kinetic model considers the rate-limiting step as the formation of a chemisorptive bond involving the sharing or the exchange of electron between the sorbate

and the sorbent (Samarghandi *et al.*, 2009; Dina Joy *et al*., 2012; Fumba *et al*., 2014). The Pseudo-second order rate equation is express as (Angus *et al*., 2012):

$$\frac{dQ_t}{dt} = K_2(Q_e - Q_t)^2 \quad \text{(16)}$$

where K_2 is the pseudo-second order rate coefficient ($g.mg^{-1}.min^{-1}$)

Integrating equation (16) at t = 0 and at t = t; $Q_t = 0$ and $Q_t = Q_t$ gives: the following equation is obtained.

$$\frac{t}{Q_e} = \frac{1}{K_2 Q_e^2} + \frac{t}{Q_e} \quad \text{(17)}$$

I.3.7.2. Model based on molecular diffusion

I.3.7.2.1. Intra-particle diffusion model

The intra-particle model is based on the theory proposed by Weber and Morris and is used to identify the diffusion mechanism of sorbent and the sorbate (Mona *et al*., 2012). This take place in stage: the first stage is the instantaneous adsorption or external surface adsorption of the adsorbate on the surface of the adsorbent (Ghasemi et al., 2015; Thuan *et al*., 2016). The second stage is the gradual adsorption stage where intra-particle diffusion into the inner layer takes place and is the rate limiting stage (Anagho *et al*., 2013). According to this theory;

$$Q_t = K_{id} t^{0.5} + C \quad \text{(18)}$$

Where:

K_{id} is the intra-particle diffusion constant

C = constant which an idea about the thickness of the boundary.

I.3.7.2.2. Elovich model

This model is used to describe kinetic adsorption on heterogeneous surfaces (Gaston *et al*., 2014; Anagho *et al*., 2013). It is generally represented by eqation 19:

$$\frac{dQ}{dt} = \alpha e^{-\beta Q_t} \quad \text{(19)}$$

Linearizing equation 19 using the $\alpha\beta >> t$, $Q_t = 0$ to t = 0, $Q_t = Q_t$ at t = t, gives:

$$Q_t = \frac{1}{\beta}\ln(\alpha\beta) + \frac{1}{\beta} lnt \quad \text{(20)}$$

Where:

α: speed of adsorption ($mg.g^{-1}.min^{-1}$)

β: desorption Constant ($g.mg^{-1}$).

I.3.8. Methodology of theoretical modelling application

I.3.8.1. Lineal and Non-linear forms of modelling application

To explore novel adsorbents in accessing an ideal adsorption system, it is essential to establish the most proper adsorption equilibrium correlation and kinetic correlation. It is crucial for reliable prediction of adsorption parameters and quantitative comparison of adsorbent behavior for different adsorbent systems or experimental conditions (Hossain *et al.*, 2013). In the perspective, equilibrium relationships, generally known as adsorption isotherms, describe how pollutants interact with the adsorbent materials, and thus are critical for optimization of the adsorption mechanism pathways, expression of the surface properties and capacities of adsorbents, and effective design of the adsorption systems. Similarly, the kinetics parameters, generally adsorption time and pattern of metals onto biosorbents are known from the fitness of kinetic parameters (Hossain *et al.*, 2013). In the past, linear least-squares method was widely used by transforming the equation into a conventional linear form to calculate or predict the isotherms/kinetics parameters or the most fitted models. Principally, the models are subjected to their goodness of fit to the experimental data with the magnitude of coefficients of determination that close to unity (Ngako *et al*., 2019). On the other hand, a significant limitation related to the linearized form of isotherm/kinetics equation has recently been pointed out, which produces a vast amount of different outcomes, implicitly alter the error structure, violates the error variance and normality assumptions of standard least squares leading to the bias of the adsorption data (Asuquo and Alastair, 2016). Due to the inherent bias resulting from linearization, alternative isotherm parameter sets were determined by non-linear regression. This provides a mathematically rigorous method for determining the isotherm parameters using the original form of the isotherm equation (He, 2013)

The introduction of computers into research makes it straight forward to fit data with simple functions such a linear regression, but it is more difficult and complicated to fit data with non-linear functions. Most of the programs (e.g. MATLAB, C^{++}, Microcal Origin, Sigma Plot or Graph Pad Prism) require special mathematical knowledge to use and provides different options such as capability of fitting user-input functions to data (Hossain *et al.*, 2013). In addition, these programs are expensive and significantly excess cost for simply fitting the data with non-linear functions. Additionally, these programmes cannot easily manipulate the data and tend to display data, graphs, results, and analysis in multiple windows, which can lead to confusion and figures are not useable for article publication (Hossain *et al.*, 2013).

An alternative method is to use Microsoft Excel to fit non-linear functions. An advantage of this method is that Excel is probably included in the computer package as part of Microsoft office, and thus no additional cost is required (Fylstra *et al*., 1998). Spreadsheet programmes are among the most commonly used software, and most researchers have experience with them. Excel offers a friendly user interface, flexible data manipulation, built-in mathematical functions and instantaneous graphing of data. It contains a function, named SOLVER, which is ideally suited to fitting data with non-linear functions via an iterative algorithm, which minimizes the sum of the squared difference between experimental data and predicted data. The methodology of theoretical modelling by non-linear regression is based on using the SOLVER function of Excel as well as to compare the predicted parameters to the experimental data of the different isotherm and kinetic models.

I.3.8.2. Error Functions for Goodness of fit

Goodness of fit is an essentially important parameter that estimates how well the curve (i.e. the prediction) pronounces the experimental data. Generally, least squares method is used to measure of the goodness of fit. It is based on the theory that the scale of the difference between the experimental data points and the prediction curve is a good measure of how well the curve fits the data. For the purposes the least squares fit method will be demonstrated by linear regression where 'independent' and 'dependent' variables are used.

In the past, non-linear data would be changed into a linear form and consequently analysed by the least squares fit method. This analysis could yield inaccurate measurements and predictions of the data and may alter the experimental error or alter the relationship between the 'independent' and 'dependent' variables (Hossain *et al.*, 2013). It is presumed that this method is erroneous and old fashioned which should not be operated. For data not describable by a linear function, it is crucial to apply a protocol that will fit a non-linear function to the data. A suitable method for this procedure is called iterative nonlinear least squares fitting. This process will fulfill the same goal as used for linear regression, i.e. minimizing the value of the sum of squared of the difference between data and prediction. However, it is still different from linear regression in a way that it is an iterative process based on algorithm. Initial parameters are estimates based on previous experience of the data and on a sensible guess based on knowledge of the function used to fit the data. The following parameters are measured and judged the goodness of fit:

(i) The sum of squares (SS)

The best fit of the data is judged by the sum of squares (*SS*) and the smallest value for the sum of squares (*SS*) is the best fitted data of the model. This is described by the function (see table below). The first iteration calculates the *SS* value based on the initial parameters and the second iteration involves varying the parameter values by a small amount and recalculates the SS. This process is repeated several times until a smallest possible value of *SS* is achieved.

(ii) The coefficient of determination (R^2)

The coefficient of determination, R^2, is practical as it gives the proportion of the variance of one variable that is predictable from the other variable. It is a measure that allows verifying how certain one can be in making predictions from a certain model. The coefficient of determination is such that $0 < R^2 < 1$, and denotes the strength of the linear association between 'experimental data, $q_{e.exp}$'and 'prediction data, $q_{e.model}$'. The coefficient of determination represents the percent of the experimental data that is the closest to the line of best fit/prediction. The models fitness is signified by the coefficient of determination (R^2) and the following expression is used to determine the R^2.

(iii) Residual root mean square error (*RMSE*) and the chi-square test ($\chi 2$)

Non-linear error functions such as the residual root mean square error (RMSE) and the chi-square test ($\chi 2$) are used to judge the equilibrium model with the optimal magnitude. The standard equations are as shown in Table II.

In this work, the R^2, *RMSE* and the $\chi 2$ coupleed with the other constant of the respective model was used toevaluate the goodness of each model on the adsorptionprocess. The small values of *RMSE* and $\chi 2$ indicate the better model fitting and the similarity of model with the experimental data respectively. The different error function used are regrouped in Table II.

Table II: The Different Error Functions for Goodness of fit

Different Error Functions	Related Equation
The sum of squares (*SS*)	$SS = \sum_{i=1}^{n} [q_{exp} - q_{model}]^2$
coefficient of determination (R^2)	$R^2 = 1 - \frac{\sum_{n=1}^{n} (q_{e.exp.n} - q_{e.model.n})^2}{\sum_{n=1}^{n} (q_{e.exp.n} - \overline{q_{e.exp.n}})^2}$
Residual root mean square error (*RMSE*)	$RMSE = \sqrt{\frac{1}{n-1} \sum_{n=1}^{n} (q_{e.exp.n} - q_{e.model.n})^2}$
Chi-square test ($\chi 2$)	$\chi^2 = \sum_{n=1}^{n} \frac{(q_{e.exp.n} - q_{e.model.n})^2}{q_{e.exp.n}}$

where, $q_{e.exp}$ is the equilibrium sorption capacity found from the batch experiment, $q_{e.model}$ is the prediction from the isotherm model for corresponding to Ce and n is the number of observations.

I.4. Indigo Carmine

I.4.1. Generalities and Uses of Indigo Carmine dye (IC)

Indigo is one of the oldest known dyes that were used for dyeing and printing since ancient times. The natural indigo has been obtained from a variety of plant sources, such as *Indigofera* tinctorial (Africa, Asia, East India and South America), *Indigofera suffructiosa (*South and Central America), *Polygonum tinctorium* (China, Korea, and Japan) *and Isatis tinctorial* (Woad) (Europe) (Naparat, 2010**).**

The history is studied by the original historical sources, included the patent literature. The lawyer Johann Christian Barth (around 1700 to 1759) at Großenhain in Saxony. Germany, discovered a blue dye by treating natural indigo with concentrated sulphuric acid in 1743. He named it 'Sächsisch Blau' after his native region. For this invention he received the title Kurfürstlich-Sächsischer Bergrat (Counselor) in 1746 (Harrache *et al*., 2019). In 1754 it was renamed indigo carmine. Other synonyms and obsolete names are indigo extract, intense blue, Murabba, Saxe blue, Saxon blue, Chymick and chemick blue. In the last quarter of the 18th

century and the first half of the 19th century the use as a dye is often mentioned in dye books. A new episode for indigo carmine starts with the discovery and industrial production of synthetic indigo in the last decades of the 19th century (Naparat, 2010**)**. German patents from 1890 till 1903 prove that it was produced and even in sample books from one German dye factory, dated 1922, indigo carmine was used for dyeing wool, silk and leather. Indigo carmine is still used as a colorant for food, pharmaceuticals, and cosmetics (Keijzer et al., 2015; Ngulube *et al*., 2017).

Indigo carmine (IC) is one of the oldest dyes that are still involved in many industrial purposes especially in dyeing of clothes (blue jeans), other blue denim, and also as coloring agent in confectionery, food, beverages (Ramesh and Sreenivasa, 2015; Harrache *et al*., 2019). It has also been used as additive in pharmaceutical tablets medical diagnostic as it also serves as a diagnostic aid (eg in renal function tests), an oxidation -reduction indicator in analytical tests, and a micro stain in biology (Ramesh and Sreenivasa, 2015; Harrache *et al*., 2019). The dyestuff is dissolved in water to which alum and cream of tartar might be added and wool is dyed at boiling temperature. The properties of indigo carmine are poor: the fastness to light compared to indigo is much reduced and the color changes from blue to green to yellowish. Also, the fastness to washing is low; it is soluble in water (Keijzer et al., 2015; Ngulube *et al*., 2017).

Indigo carmine or 5,5'-indigodisulfonic acid sodium salt, also known as Indigotine or Food Blue 1 is a derivative of indigo and also a pH indicator with the chemical formula $C_{16}H_8N_2Na_2O_8S_2$ and has the commercial number E132 given by Sumalatha *et al*., (2014).

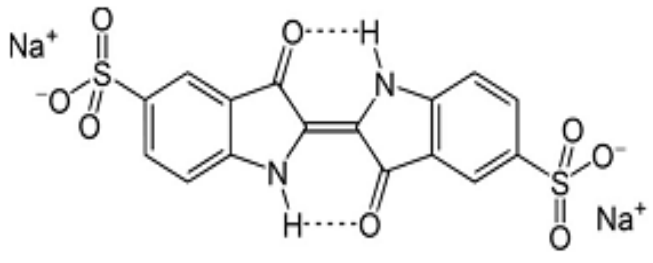

Figure16: Structure of Indigo Carmine

Table III gives some physic-chemical properties of indigo carmine.

Table III: Physic-chemical properties of indigo (Sumalatha et al., 2014)

Properties of Indigo Carmine dye	
Parameters	**Values**
Molecular formula	$C_{16}H_8N_2Na_2O_8S_2$
Molar mass	466.36 ± 0.001 g/mol
Apparence	Purple solid
Melting point	>300 °C
Solubility in water	10 g/L (25 °C)

I.4.2. Negative effect of Indigo Carmine (IC)

According to the United Nations Educational, Scientific and Cultural Organization standards, the World Health Organization has established that, indigo carmine at a concentration above 0.005 mg/L is not acceptable in water (Ankoro *et al*., 2016; Harrache *et al*., 2019). IC is not only a nuisance for the aquatic life, but also for the humans. It is considered as a highly toxic class of IC and its touch can cause skin and eye irritation for humans (Ankoro *et al*., 2016; Harrache *et al*., 2019). It can also produce permanent damage to the cornea and conjunctiva. Consumption of the dye can also be fatal because it is inherently carcinogenic and can lead to a reproduction, development, neurotoxicity and acute toxicity (Ahmed et al., 2017). It has also been established that it causes tumor formation at the application site. Mild effects on hypertension, cardiovascular system and respiration have also been reported. Wastewater containing IC dyes is rich in color and organic content and a large number of suspended solids whose pH, temperature and chemical oxygen demand (COD) vary considerably (Sánchez-Rodríguez et al., 2015; Ahmed et al., 2017).

I.5. Methyl Orange (MO)

I.5.1. Generalities and Uses of Methyl Orange (MO)

Methyl Orange is a water-soluble azo dye, which is widely used in the textile, printing, paper manufacturing, pharmaceutical, food industries and also in research laboratories (Middea *et al*., 2017). In the Analytical Chemistry Laboratories, it is mainly used as an acid base indicator due to its ability to function as weak acid as the aqueous solution of the dye has a pH value of approximately 6.5 (5 g/L, H_2O, 20 °C) (Mittal *et al*., 2007). Because it changes colour at the pH of a mid-strength acid, it is usually used in titrations for acids (Angus *et al*., 2012).

Unlike a universal indicator, methyl orange does not have a full spectrum of colour change, but has a sharper end point. In a solution becoming less acidic, methyl orange moves from red to orange and finally to yellow with the reverse occurring for a solution increasing in acidity. The entire colour change occurs in acidic conditions (Chakkrit and Songsak, 2013; Middea *et al*., 2017). Microbial succession and intestinal enzyme activities in the developing rat has also been studied for the Methyl Orange and the dye is found to increase their nitro reductase and azo reductase activities significantly with the appearance of anaerobes in the large intestine.

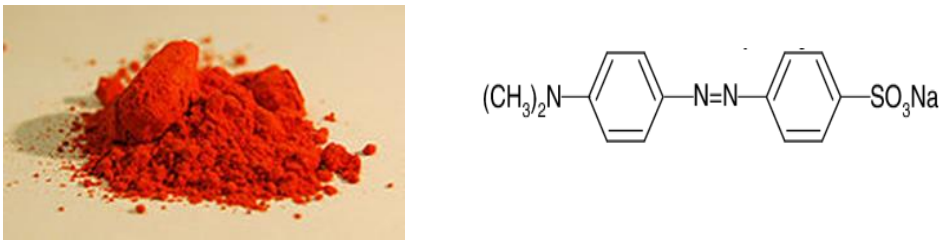

Figure17: MO powder and Structure of Methyl Orange

Table IV present some physico-chemical properties of methyl orange dye.

Table IV: Physic-chemical properties of Methyl Orange (Middea *et al*., 2017)**.**

Properties	
Parameters	**Values**
Molecular formula	$C_{14}H_{14}N_3NaO_3S$
Molar mass	327.33 ± 0.001 g/mol
Apparence	Orange solid
Density	1.28 g/cm^3, solid
Melting point	>300 °C (572 °F; 573 K) not precisely defined
Solubility in water	0.5 g/100 mL (20 °C) soluble in hot water

I.5.2. Negative effect of MO

Azo dyes are well known carcinogenic organic substances (Khan *et al*., 2016). Like many other dyes of its class Methyl Orange on inadvertently entering the body through ingestion, metabolizes into aromatic amines by intestinal microorganisms. Reductive enzymes in the liver can also catalyze the reductive cleavage of the azo linkage to produce aromatic amines and can even lead to intestinal cancer (Mittal *et al*., 2007). The toxic nature of the dye

is still not quantified much but its high content in living systems can prove to be harmful (Khan *et al*., 2016). Methyl orange on inadvertently entering the body through ingestion, metabolites into aromatic amines by intestinal microorganisms. Reductive enzymes in the liver can also catalyze the azo, linkage to produce aromatic amines and can even lead to intestinal cancer (Alzaydien, 2015; Khan et al., 2016).

I.6. Overview on Bacteria

I.6.1. Definition of Bacteria

Bacteria are microscopic single-celled organisms, typically 0.5 to 5 µm long, that lack a nuclear membrane (prokaryotic) and organelles like mitochondria, are metabolically active and divides mostly by binary fission (Schulz and Jorgensen, 2001; Berg *et al*., 2002). There are thousands of different kinds of bacteria, and they live in various environments all over the world. Some bacteria live in the bodies of humans, animals and in plants and can be pathogenic or not to these organisms. Others however live in the soil, water, and air (Fredrickson *et al*., 2004). Bacteria were among the first life forms to appear on earth and the worldwide bacterial biomass exceeds that of all plants and animals on earth (Hogan, 2011). However, the majority of bacteria have not yet been characterised. They come in many different sizes and shapes (Figure 19) determined by the bacterial cell wall and cytoskeleton (Cabeen and Jacobs-Wagner, 2005). The generic cell structure of a bacterium is shown in Figure 18.

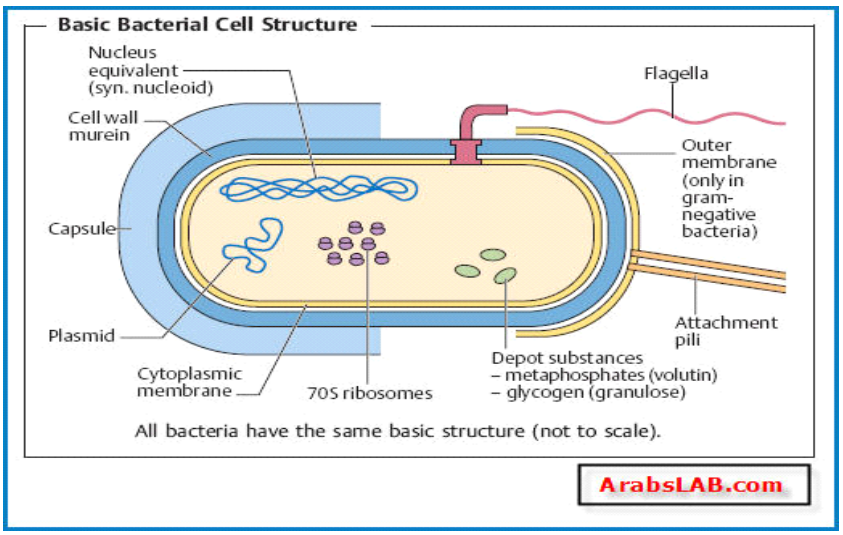

Figure 18: Bacteria cell structure (Rastaldo *et al*., 2007)

I.6.2. Classification of bacteria

They are most commonly classified based on their morphology or shape (Dusenbery, 2009). The three basic shapes are;

- Spherical (cocci): They may be single bacterium, or they may occur in pairs, chains or clusters of bacteria, depending on the bacterium and environmental conditions (Pommerville, 2013). Among the more common cocci are *Staphylococcus aureus and Neisseria meningitidis*.
- Spiral-shaped: They can be further categorized depending in part on how much spiraling they show (Taro and Kathleen, 2007). As such, we have;
- Vibrio: They are comma-shaped bacteria, appearing like curved rods. They typically live in aquatic environments. An example is *Vibrio cholerae* that causes cholera.
- Spirillum: Is another subgroup of bacteria with a more rigid, corkscrew-like spiral shape. *Campylobacter jejuni* is a common example.
- Spirochete: They are long, thin and flexible corkscrew-shaped bacteria. Two well-known spirochetes that cause disease in humans are *Treponema pallidum* and *Borrelia burgdorferi*.
- Rod shaped (Bacilli): they are bacteria that look like little sausages, occurring singly or in linked chains. Here, we commonly find *Escherichia coli*, normally living in the intestinal tract and *Salmonella* causing salmonellosis, etc.

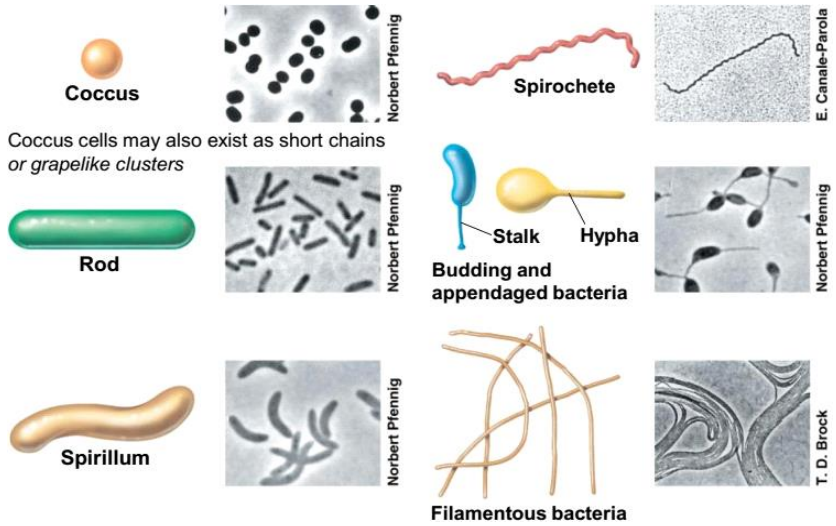

Figure 19: Representative cell morphology of bacteria

Bacteria can also be divided into two major groups, called Gram positive and Gram negative. The original distinction between Gram positive and Gram-negative was based on a special staining procedure, the Gram stain, but differences in cell wall structure (Figure 20) are at the base of these differences in the Gram staining reaction (Richard *et al.*, 2006)

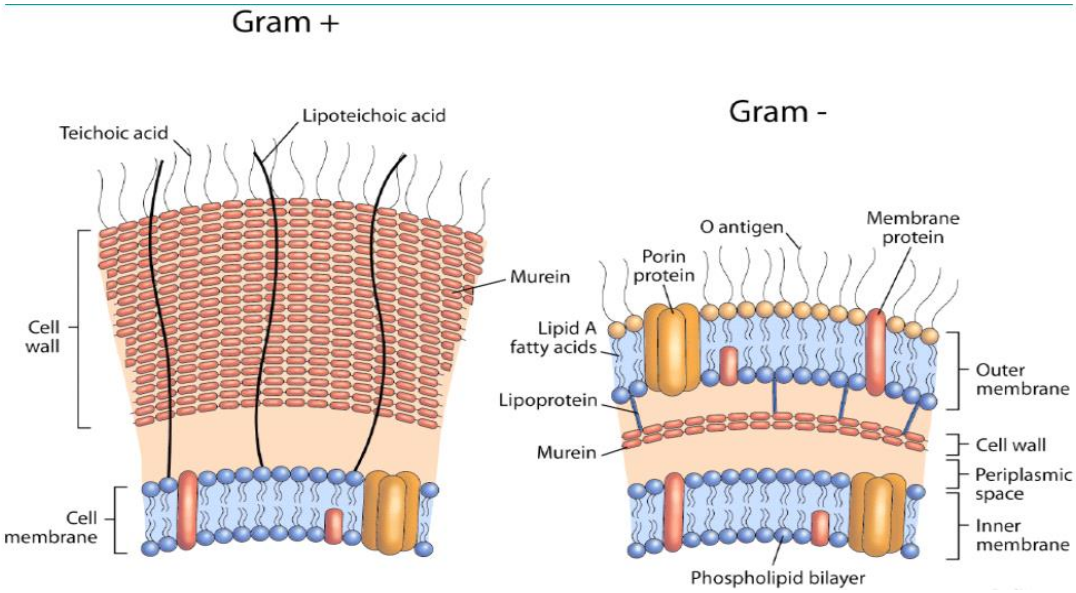

Figure 20: Architecture of bacterial cell wall (Richard *et al*., 2003)

I.6.3. Generalities on *Salmonella*

The family *Salmonella* is a rod-shaped (bacillus), flagellated, facultative anaerobic, Gram-negative bacterium of the Enterobacteriaceae family (Crump *et al.*, 2015). They are 2–5 µm long by 0.5–1.5 µm wide. The serovars of this genus, which is estimated to have diverged from *Escherichia coli* approximately 100 to 150 million years ago (Doolittle *et al*., 1996), are considered resilient microorganisms that readily adapt to extreme environmental conditions. The optimum temperature for growth is in the range of 35 – 37 ˚C but some can grow at temperatures as high as 54 ˚C and as low as 2 ˚C (Gray and Fedorka-Cray, 2002). Also, growth pH range from 4 - 9 with the optimum being 6.5 - 7.5. In addition, *Salmonella* has adapted to colonise many different niches. For example, *Salmonella* can be found as both commensal and pathogen in warm and cold blooded animals and is capable of surviving free in the environment (Djague, 2019). The genus is placed under two species each of which contains multiple serotypes.

- ***Salmonella enterica*** – is a diverse bacterial species that remains a common cause of infectious disease in humans and animals throughout the world (Popoff *et al.*, 2004). The species contains six subspecies, with 99.5% of all isolated strains belonging to *S. enterica* subspecies *enterica* (known as subspecies I). Isolated mainly from warm blooded animals (Fabien *et al.*, 2016). The remaining subspecies and *S. bongori* are mainly isolated from cold-blooded animals and account for less than 1% of clinical isolates (Pui *et al*., 2011). Further classification is based on differences in genomic phylogeny, of which individual serovars are distinguished by antigenic, serologic and biochemical tests (fermentation of glucose, negative

urease reaction, lysine decarboxylase, negative indole test, negative Voges-Proskauer (VP) reaction, H_2S production, and fermentation of lactose) (Djague**,** 2019). While almost 2600 serovars and more than 50 serogroups have been described so far, only a few of these are pathogenic to humans and animals (Fabien *et al.,* 2016).

- ***Salmonella bongori****:*

With one subspecies, contains about 20 serotypes. Historically, salmonellae have been clinically categorized as typhoidal and non-typhoidal based on host preference and disease manifestations in humans (okoro *et al.,* 2012). The former category includes the human host-restricted *S. enterica serovars typhi, paratyphi A, paratyphi B* and certain strains of *S. paratyphoi C* that cause typhoid and paratyphoid fevers, referred collectively as enteric fevers (Gal-Mor *et al.,* 2014), while ubiquitous non-typhoidal Salmonellae (NTS) such as *S. enterica serovar typhimurium* and *S. enterica serovar enteritidis* have a broader host range and predominantly causes self-limiting gastroenteritis in animals and humans (Langridge *et al.,* 2009).

I.6.4. Sources and Modes of Transmission of *Salmonella*

Salmonella bacteria are widely distributed in domestic and wild animals. Transmission is generally via the faecal-oral route, by either the consumption of contaminated food or water person-to-person contact, or from direct contact with infected animals (Djague, 2019). Approximately 10% of patients recovering from this infection excrete *Salmonella* in the stool for three months (Zige *et al*., 2013). *Salmonella* may be spread through poor hygiene habits and public sanitation conditions, and sometimes also by flying insects feeding on faeces (Zige *et al*., 2013).

I.6.5. Mechanism of infection and Pathogenesis

The ability to cross the intestinal barrier constitute a crucial step for infection establishment and sets typhoidal *Salmonella serovars* apart from non-typhoidal - *Salmonella serovars* (limited to gastroenteritis) (Keestra-Gounder *et al.,* 2015). After the ingestion of contaminated food or water, *Salmonella* colonizes the distal ileum and proximal colon (Lönnermark *et al.,* 2015) by triggering their own phagocytosis, using a sophisticated array of effector proteins that are injected into the host cell cytoplasm through a type III secretion apparatus. The translocated effector proteins effectively allow the bacteria to “hijack” many essential intracellular processes and induce a massive reorganization of the host actin cytoskeleton, resulting in intense membrane ruffling and internalization of the bacteria.

Internalized bacteria remain enclosed in a membrane-bound vacuole, referred to as the *Salmonella*-containing vacuole (SCV), which it modifies to prevent its maturation into, or fusion with lysosomal compartments. This invasion process is referred to as a Trigger mechanism (Djague, 2019). Typhoidal *Salmonella* and NTS cause different clinical syndromes, suggesting they cause disease by different mechanisms (Gal-Mor *et al.,* 2014). NTS invades the intestinal epithelium and triggers a massive neutrophil influx in the intestine, resulting in inflammatory diarrhoea. Typhoidal strains, in contrast, evade the gut mucosal immune response and progress to a systemic infection with initial colonisation of the submucosal lymphoid tissues and then liver, spleen and bone marrow where it may result in the development of other human diseases like gallbladder cancer (Gunn *et al.,* 2014).

I.6.6. *Klebsiella pneumoniae*

Ventilator-associated pneumonia (VAP) is defined as nosocomial pneumonia occurring in a patient after 48 h of mechanical ventilation. The occurrence rate of VAP is reportedly 9–27 %, and mortality reaches 20 - 50 %. Common causative pathogens of VAP include gram-negative bacteria such as Pseudomonas aeruginosa, *Klebsiella pneumoniae*, and Escherichia coli and gram positive bacteria such as Staphylococcus aureus (Guo *et al.,* 2016). K. pneumoniaeis a common pathogen responsible for both community-acquired and nosocomial infections. It also causes miscellaneous infections such as meningitis, septicemia, purulent abscesses, and pneumonia. Previous investigations have implicated K. pneumoniaein 7–12 % of nosocomial pneumonia in intensive care units in the United States

I.6.7. *Staphylococcus aureus*

Food born diseases (FBD) are defined by the WHO as ‘diseases of infectious or toxic nature caused by, or thought to be caused by the consumption of food and water’ (Le Loir *et al.,* 2003) Staphylococcus aureus is a bacterium that causes staphylococcal food poisoning, a form of gastro enteritis with rapid onset of symptoms. *S. aureus* is commonly found in the environment (soil, water and air) and is also found in the nose and on the skin of humans. It is a Gram-positve, non-spore forming spherical bacterium that belongs to the Staphylococcus genus. The Staphylococcus genus is subdivided into 32 species and subspecies. *S. aureus* produces staphylococcal enterotoxin (SE) and is responsible for almost all staphylococcal food poisoning (FDA, 2012).

- **Symptoms of disease**

Staphylococcal food poisoning symptoms generally have a rapid onset, appearing around 3 hours after ingestion (range 1–6 hours) (ECDC and EFSA, 2017). Common symptoms include nausea, vomiting, abdominal cramps and diarrhoea. Individuals may not demonstrate all the symptoms associated with the illness (Stewart, 2003). In severe cases, Head ache, muscle cramping and transient changes in blood pressure and pulse rate may occur. Recovery is usually between 1–3 days (ECDC, 2016). Fatalities are rare (0.03% for the general public) but are occasionally reported in young children and the elderly (4.4% fatality rate). S. aureus can cause various non-food related health issues such as skin inflammations (eg boils and styes), mastitis, respiratory infections, wound sepsis and toxic shock syndrome (ECDC and EFSA, 2017).

I.6.8. Shigella flexneri

Shigella flexneri is a Gram-negative facultatively intracellular pathogen responsible for bacillary dysentery in humans. More than one million deaths occur yearly due to infections with Shigella and the victims are mostly children of the developing world. The pathogenesis of Shigella centres on the ability of this organism to invade the colonic epithelium where it induces severe mucosal in£ammation. Infection with Shigella spp. is a serious cause of morbidity and mortality especially in children of the developing world. Recently, the World Health Organization estimated that 1.1 million deaths per year are attributed to shigellosi (Philpott et al., 2000). There are four species of Shigella that cause these infections, with *S. flexneri* and, to a lesser extent, *S. sonnei*, accounting for most of the endemic disease. Epidemic disease is usually due to *S. dysenteriae*, which displays the same invasive capacity as the other species but in addition, secretes a potent cytotoxin, *Shiga toxin*, that can cause haemolytic uraemic syndrome (CDCP, 2007). Shigellosis is highly infectious, with ingestion of as few as 100 organisms resulting in disease, and is transmitted by person-to-person contact or indirectly through contaminated food or water. Shigellosis produces a spectrum of clinical outcomes ranging from watery diarrhoea to classic dysentery characterized by fever, violent intestinal cramps and discharge of mucopurulent and bloody stools (CDCP, 2007).

- **Symptoms of Shigella Infection**

People who are sick with Shigella usually start experiencing symptoms 1 to 2 days after putting something in their mouth or swallowing something that has come into contact with the bacteria. Symptoms of shigellosis may include: diarrhea (sometimes bloody), fever, stomach pain, Feeling the need to pass stool [poop] even when the bowels are empty.

I.7. Methodology of Experimental Design

I.7.1. Definition and Fundamentals of DOE

The methodology of experimental design is a process of conception, planification and analyses of experiments to meet specified objectives (Lekene *et al.*, 2019). Planning an experiment properly is very important in order to ensure that the right type of data and a sufficient sample size and power are available to answer the research questions of interest as clearly and efficiently as possible.

I.7.1.1. Design of Experiments (DOE)

Design of Experiments (DOE) refers to the process of planning, designing, and analyzing the experiment so that valid and objective conclusions can be drawn effectively and efficiently. A process is a transformation of inputs into outputs and sometimes, an output can also be referred as response (Babayemi, 2016). In performing a designed experiment, changes to the input variables (or factors) are to be made intentionally to observe the corresponding change in the response. Some of the inputs or factors can be controlled fairly easily and some of them are hard or expensive to control at standard conditions (Lekene *et al.*, 2019). The general model of a process or system was shown in figure 21 below.

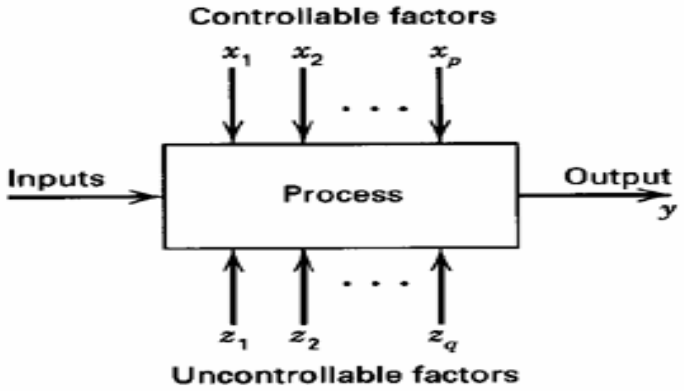

Figure 21: General model of a process or system

The easily controllable variables, represented by Xi, have a key role to play in the process characterization. The uncontrollable variables, represented by Z's, are difficult to control during the experiment. These both controllable and uncontrollable factors are responsible for the variability in the response of the system. The fundamental strategy of DOE is to determine the optimal settings of controllable factors (X's) to minimize the effects of uncontrollable factors (Zi) on the response. There are other ways that we can categorize factors:

I.7.1.2. Objectives of DOE

The response surface designs are types of designs for fitting response surface (Thuan *et al*., 2016). Therefore, the objective of studying RSM can be accomplish by

(1) Understanding the topography of the response surface (local maximum, local minimum, ridge lines), and

(2) Finding the region where the optimal response occurs, the goal is to move rapidly and efficiently along a path to get to a maximum or a minimum response so that the response is optimized (Villota *et al.,* 2017).

I.7.1.3. Purpose of Experimentation

Designed experiments have many potentials uses in improving processes and products, including:

- **Comparing Alternatives.** In the case of our AC preparation example, we might want to compare the results from two different types of activating agent. If it turned out that the effect of the different activation agents is not significant, we could select the lowest-cost activating agent. If activating agents are significant, then we are going to select the best one for the desing. The experiment(s) should allow us to make an informed decision that evaluates both quality and cost (Goupy and Creighton, 2006).
- Identifying the Significant Inputs (Factors) Affecting an Output (Response) - separating the vital few from the trivial many. We might ask a question: "What are the significant factors beyond activation temperature, activation time and impregnation ratio?"
- Achieving an Optimal Process Output (Response), "What are the necessary factors, and what are the levels of those factors, to achieve the exact quality and quantity of activated carbon?
- Reducing Variability, "Can the recipe be changed so it is more likely to always come out the same?"
- Minimizing or Targeting an Output (Response), "How can the activated carbon with high IN, MB number, % Yield and high surface area be prepared are very low temperature, low activation time and low impregnation ratio?"
- Improving process or product "Robustness" - fitness for use under varying conditions, "Can the factors and their levels (recipe) be modified so that AC will have the same characteristics or nearly the same no matter what type of furnace is used?" (Douglas, 1997).
- Balancing Tradeoffs when there are multiple Critical to Quality Characteristics (CTQC's) that require optimization, "How do you produce the activated carbon with good

characteristics (high IN, MB number, % Yield and high surface area) at the lowest activation temperature and shortest activation time?"

I.7.1.4. Steps used in DOE

Designing an Experiment means performing the following steps (Douglas, 1997):

1. Define the problem and the questions to be addressed.
2. Define the population of interest.
3. Determine the need for sampling.
4. Define the experimental design.

Write Down Research Problem and Questions Before data collection begins, specific questions that the researcher plans to examine must be clearly identified. In addition, a researcher should identify the sources of variability in the experimental conditions (Douglas, 1997). One of the main goals of a designed experiment is to partition the effects of the sources of variability into distinct components in order to examine specific questions of interest (Kundu et al., 2015). The objective of designed experiments is to improve the precision of the results in order to examine the research hypotheses.

I.7.2. Terms used in Design of Experiments (DOE)

I.7.2.1. Factors or Independent Variables

A- Experimental vs Classification Factors

i) Experimental Factors - these are factors that you can specify (and set the levels) and then assign at random as the treatment to the experimental units. Examples would be temperature, level of an additive fertilizer amount per acre, etc (Goupy and Creighton, 2006).

ii) Classification Factors - can't be changed or assigned, these come as labels on the experimental units. The age and sex of the participants are classification factors which can't be changed or randomly assigned. But you can select individuals from these groups randomly (Goupy and Creighton, 2006).

B- Quantitative vs Qualitative Factors

i) Quantitative Factors - you can assign any specified level of a quantitative factor. Examples: percent or pH level of a chemical.

ii) Qualitative Factors - have categories which are different types. Examples might be species of a plant or animal, a brand in the marketing field, gender, - these are not ordered or continuous but are arranged perhaps in sets (Douglas, 1997).

I.7.2.2. Levels or settings of each factor in the study

These are values given to a factor to quantify it response. Examples include the oven temperature and Impregnation ration, carbonisation time, heating speed and flow rate are usually chosen for evaluation.

I.7.2.3. Naturelle and Coded Variables

Natural variables are variables defined algebraically to quantify different or diverse factors. They usually have magnitude and units. On the other hand, coded variables are values obtained from the transformation of Natural variables with units to dimensionless variables without units (Villota *et al.,* 2017). The transformation of Natural variables to coded variables is generally very important because natural variables usually have different units which make their compariation very impossible (Kouotou, 2014). This transformation therefore permits the experimenter to compare the interaction of these variables since they will all become dimensionless. The transformation of natural variables (U_{ij}) to coded variables (X_{ij}) without units is given by (Adewumi *et al*., 2005; Ahmad *et al.*, 2009):

$$\boldsymbol{Xij} = \frac{(\boldsymbol{Uij} - \boldsymbol{Uj}^{\circ})}{\boldsymbol{\Delta Uj}} \quad \text{.....(21)}$$

where:

X_{ij}: value of the coded variable j of experiment i

U_{ij}: value natural variable j of experiment i

$U_j°$: value of natural variable j at the center of the experimentators domain, it usually corresponds $X_j=0$

ΔU_j: distance chosen between two points of the natural variable j.

I.7.2.4. Domaine of variation of factors

The domaine of variation of a factor is an assembly of values which can represent the factor in the lower and the upper limits. The experimental study of a factor is generally limited to domaine of variation chosen by the experimenter. This usually done by chosen experimental limits that is the lower limit usually denoted as (- 1) and the upper limits of the factor denoted as (+1) (Villota *et al.,* 2017) (see Table V).

Table V: Example of Experimental domaine

Coded variables	Factors	Levels	
		-1	+1
X_1	Temperature (°C)	500	700
X_2	Activation time (mins)	60	120
X_3	Impregnation ration	1	2

I.7.2.5. Experimental Matrice and Experimental plan

An experiment is usually defined by an assembly of experimental condition. For each experiment, the level and limits of each natural and coded variable are determined. An experimental matrix is therefore a mathematical object which present in coded form the complete number of experiments to be carried out. It usually consists of a table comprises of N rows (corresponding to the number of experiments to be carried out) and K columns (corresponding to the number of variables to be studied) (Qui *et al*., 2014; Nouri *et al*., 2015). On the other hand, an experimental plan is the transformation of the experimental matrix from coded variables to natural variables with units (Kouotou *et al*., 2013). It is therefore a table comprises of the different experimental data in their respective units which is directly applicable to the experimenter. Just like the experimental matrix, experimental plan also consist of a table comprises of N rows (corresponding to the number of experiments to be carried out) and K columns (corresponding to the number of variables to be studied) (Gratuito *et al*., 2008)

Table VI : Experimental Matrice and Experimental plan

N° of experiments	Experimental Matrice			Experimental plan		
	X_1	X_2	X_3	Temp (°C)	Time (mins)	Ratio
1	-	-	-	500	60	1
2	+	-	-	700	60	1
3	-	+	-	500	120	1
4	+	+	-	700	120	1
5	-	-	+	500	60	2
6	+	-	+	700	60	2
7	-	+	+	500	120	2
8	+	+	+	700	120	2

I.7.2.6. Response, or output of the experiment

Responses or output (eg IN, MB number, %Yield, Quantity adsorbed, % adsorbed, etc) are usually measurable outcomes potentially influenced by the factors and their respective levels. Experimenters often desire to avoid optimizing the process for one response at the expense of another. For this reason, important outcomes are measured and analyzed to determine the factors and their settings that will provide the best overall outcome for the critical-to-quality characteristics - both measurable variables and assessable attributes (Thuan et al., 2016).

$$Y = \tau + e \qquad (22)$$

I.7.3. Mathematical Modeling

Mathematical Modeling of DOE is a mathematical function which expresses the awaited responses as a function of the independent variables (factors) of the experimental domain. It is usually dynamic/provisional that is permits to predict the responses at any given instant of the experimental domain that is permits the quantification (determine the magnitude) of the effects of the chosen factors on the response studied (points out which factor is more significant that the others) (N’guessan, 2010; Kundu et al., 2015). In this light, many mathematical models have been postulated such as: polynomial, exponential and logarithmic models to give an estimate of the best response studied by the experimentator in the experimental domain (Babayemi, 2016). These models are developed with the aim of respondings to the experimentators desire such as:

- Maximium efficiency

- A minimum number of experiments (N) or at least a number of experiments equall to the number of coefficients to be determined

In this regard, the second order poly nomial model is mostly used to satify the experimentator's desire. This model is developed using the Taylo's series as represented by equation 23 (Essa *et al*., 2013; Gratuito *et al*., 2008)):

$$Y = a_o + \sum_i a_i X_i + \sum_i \sum_j a_{ij} X_i X_j + \sum_i \sum_j \sum_n a_{ijk} X_i X_j X_k + \ldots \quad (23)$$

$1 \leq i \leq k \quad 1 \leq i \leq j \leq n \quad 1 \leq i \leq j \leq k \leq n$

and can be written in the form $Y = \Gamma + \mathcal{E}$

Where:

Y: Experimental Response of the model as a function of the factors

Γ: Theoreticl Response of the model as a function of the factors

Ɛ: Experimental errors of the measured quantities

X_i: variable of factor i which can take values of +1 or-1

a_o : Mean value of the response in the experimental domain

a_i: Coefficient which measures the effects of factors i

a_{ij}: Coefficient which measures the effects of first order entre between factors i and j

a_{ijk}: Coefficient which measures the effects of first second order between factors i, j and k

n: number of factors studied.

I.7.4. Central Composite Designs (CCD)

Central Composite design is a response surface design which apart from the 3 level factors has axial or star point. The axial or star point usually denoted as (α) increases the number of levels to 5 levels thereby giving the experimental design flexibility. Its advantages over Box-Behnken is that it allows the experimental designer to know what effect the factors had on response if the experimental designer goes beyond or below the chosen levels of factors (Mahmood *et al*., 2017). The CCD method was selected as experimental design which is suitable for fitting a quadratic surface with a minimum number of experiments (Kundu *et al*., 2015). It also helps to optimize the effective process parameters as well as to analyze the interaction between these parameters. However, in Central Composite Design the minimum numbers of factors it can accommodate is two (ie numerical or continuous factors). CCD consists of three operations namely, 2^n factorial runs, 2n axial runs and nC center runs (Babayemi, 2016; Mahmood *et al*., 2017). The independent variables studied were activation temperature (X1), activation time (X2) and impregnation ratio (X3). These three variables with

their respective ranges were selected based on the literature and preliminary studies and the number of experiments is calculated from the equation (Thuan et al., 2016).

$$\mathbf{N = 2^n + 2\times n + n_c} \quad \text{..... (24)}$$

Where **N** is the number of runs, **n** is the number of factors (indipendent variables), $\mathbf{n_c}$ is the number of centre points the designer desire.

The independent variables are coded as -1 and +1which represent the eight factorial points at their low and high levels respectively. The six axial points are located at (±α, 0, 0); (0, ±α, 0); (0, 0, ±α) (Ahmad *et al.*, 2009). The replicates are located at the center (0, 0, 0) and are run to examine the experimental error and the reproducibility of the data. α is the distance of axial point from center which makes the design rotatable and had fixed value depending on the number of independent variables (Ahmad *et al.*, 2009). This value of rotatability α, which depends on the number of parameters in the experiment, was obtained from the equation 25.

$$\boldsymbol{\alpha} = (2^{\boldsymbol{n}})^{\frac{1}{4}} \quad \text{..... (25)}$$

Where: n is the number of factors. To get value for the axial point, we apply this equation.

Axial point = mean of both the upper or lower level ± α (range between the upper and lower level divided by 2). Hence it can be given mathematically as:

$$\text{Axial point} = \overline{\boldsymbol{X}} \pm \alpha \quad \text{..... (26)}$$

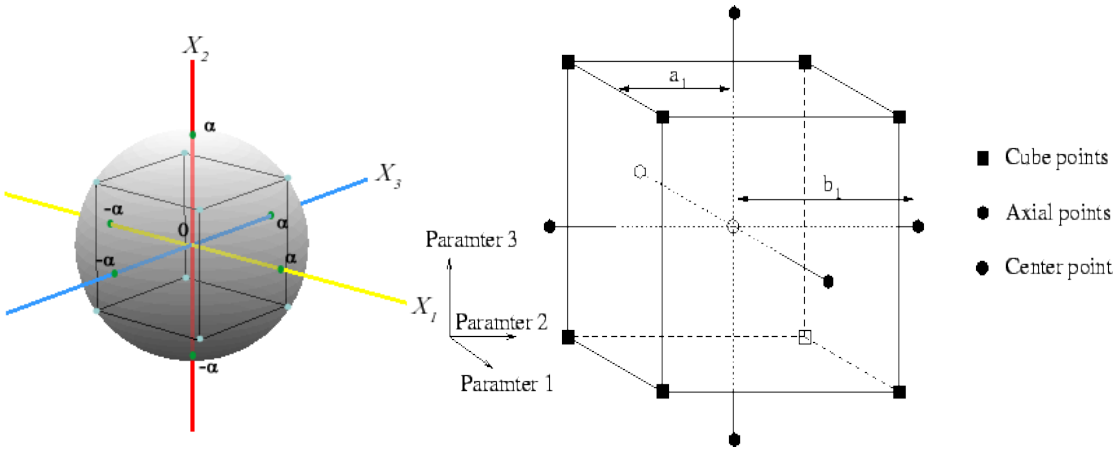

Figure 22: Central Composite Designe (CCD) box

The responses (Y = IN, MB and %Yield) considered in the preparation of the ACs (equation 26) are used to develop an empirical model that correlated the response to the preparation variables using a second-degree polynomial equation as expressed in equation 23.

I.8. *Ricinodendron heudelotti*

Ricinodendron heudelotti is a fast-growing tree, which produces edible seeds, traditionally used in many countries of Africa. It is called the ndjanssang tree and belongs to the family Euphorbiaceae (Maeva *et al*., 2015). The Euphorbiaceae is the largest family of the order Euphorbiales. The family contains over 300 genera and maybe over 7000 species. Not surprisingly, with so many species, many of them are of economic importance (Kristina, 1997). They include rubber (Hevea), cassava (Manihot esculenta Crantz.), tung oil treeand related species (Aleurites), castor bean (Ricinus communisL.), purging nut (Jatropha spathulata Müll-Arg.), and purging croton (Croton tigliumL.), all of which have been domesticated (Parys, 2012). These latter include many medicinal plants, such as species of Euphorbia Hura, Pedilant husand Phyllanthus and species for multipurpose uses. eg several species of Jatropha and Schinziophyton rautanenii Schinz. Ricinodendron heudelotti is one of the most traded none-timbered forestry products (Kristina, 1997).

1.8.1. The family Euphorbiaceae and its divisions

1.8.1.1. Description of the flowers and fruit

Flowers are usually small or very small, unisexual, monoecious or dioecious, and usually regular. The perianth is occasionally absent in one or both sexes, simple, valvate or imbricate, calycine, rarely petaloid; or double, both outer and inner calycine and imbricate, or the inner petaloid and imbricate; rarely subvalvate, longer or shorter than the outer (Assanvo *et al*., 2015). Stamens are one to indefinite, free or united in various ways; filaments are free or connate; anthers are 2-(rarely 3 – 4)-celled; cells are usually parallel, adnate to the connective throughout, or free except at base or apex; erect, divaricated or suspended, rarely superposed; dehiscence is usually longitudinal, and rarely porous (Parys, 2012). A rudimentary ovary may be present in male flowers. Females are flowers with sessile ovary, rarely shortly stipate. Gynoecium is usually tripartite (occasionally 2 or 4), with axile placentae and 3 loculi. Styles are usually as many as and continuous with the carpels, free or less connate, usually 2-lobed, with the inner face usually stigmatic. Ovules are similar throughout the family and are a characteristic feature: there are 1 or 2 in each loculus, they are pendulous from the inner angle, and the funicle is often thickened. Fruits are usually capsular with 2-valved cocci separating from a persistent axis; or indehiscent and drupaceous, 1–3-celled; or 1, 2, or 3 connate nuts (Kristina, 1997).

1.8.1.2. Description of ndjanssang

Ndjanssang is a large deciduous, fast-growing tree averaging 20–30 m in height but being able to reach 50 m. The trunk averages 1.5–2.7 m diameter. The trunk is straight but the base is thicker due to short buttresses with big running roots (Vivien and Faure, 1985). Young trees have whorled branches, which arch upwards. The broad, spreading crown is candela bra-like, and broken branches can commonly be seen in the crown (Parys, 2012). Branches are often stubby and contorted. Branches are densely brown, hairy when young, and about 1 cm thick. The slash bark is red, densely mottled with scattered pits; the smooth bark is bright grey, becoming scale-like with age. The wood is white or pale yellow, darkening on exposure, and is very soft (Vivien and Faure, 1985).

a) Leaves

The leaves are alternate and each leaf is divided into leaflets arranged digitately. The leaflets are elliptic from 10 to 20 cm long and 3 to 12 cm broad at the middle, with bases lengthily attenuated at the top of the petiole (Kristina, 1997). Leaflet tips are acute and acuminate. In young leaves, the leaflets may be sessile or sub-sessile, or united at the base, so that the lamina is simply digitately lobed, with 3 to 6 lobes, sometimes 7. There are generally (10 –)12 to 15(–16) pairs of side veins per leaflet. Leaf margins possess small glands, as regular small projections. Young leaflets are covered with very fine spangled hairs, which can disappear when adult (Parys, 2012).

b) Fruits

Fruiting occurs in September and October. The fruit is an indehiscent yellow-green capsule somewhat plum-like 3.5 to 5 cm long and 2.5 to 4 cm wide (Ngo Mpeck *et al*., 2003), and is generally spherical, with 1, 2 or 3 seeded lobes (Ngo Mpeck *et al*., 2003). They weigh 19–47 g, and have a hard indehiscent, thin shell, although some fruits have been reported to be self-cracking (Ngo Mpeck *et al*., 2003). The fruits smell of over-ripe apples. Young fruit is covered with fine hairs on the outer green skin; this turns brown on maturity.

c) Seeds

Each seed is reddish brown-black and usually consists of a testa with a yellow kernel inside. Inside the fruit shell is a soft spongy pulp layer making up about 20% of the fresh fruit, 10% being the fruit skin. Seeds make up the rest (Maeva *et al*., 2015). Five different types of seed numbers are known: single-seeded fruit with an aborted lobe; two-seeded fruit with two lobes; thre eseeded fruit with three lobes; single-seeded fruit; and two- seeded fruit with unequally developed lobes (Fondoun *et al*., 1999).

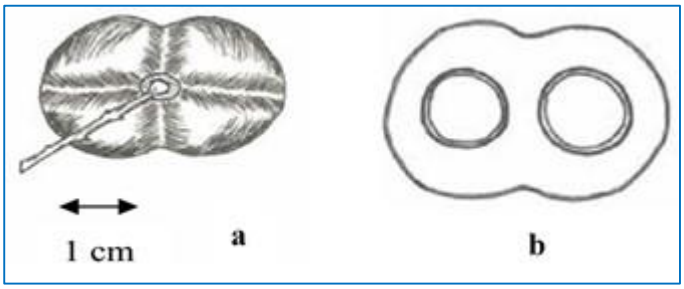

Figure 23: Mature fruits of Ndjansang (2-seeded lobes): a-Whole fruit, b- Vertical section through mature fruits to show seed arrangement.

1.8.1.3. Common names

In English the species is referred to as African nut tree, African wood-oil nut tree, Zambezi almond or Zambezi corkwood, but its promotion in Cameroon is leading to the adoption of the Bakweri name, ndjansanga. However, in Southern Africa the common name is more frequently mongongo or manketti, which can refer to *R. heudelotii* **(**CIFOR**. 2008)**.

Table VII : Local names of *R. heudelotii* in Cameroon

Ethnic groups	Local name
Bakweri	Ndjansanga
Banka	Njansang
Bassa	Njansang
Bibaya	Gobo
Bobilis	Ezol
Boulou	Ezezang
Douala	Nyansang
Ewondo	Ezezang
Ntumu	Ezang
Maka	Zouol

1.8.1.4. Distribution of the genus

The genus is endemic to tropical Africa (Kristina, 1997). The area where it is endemic is shown in Figure 24 ndjansang occurs throughout this area.

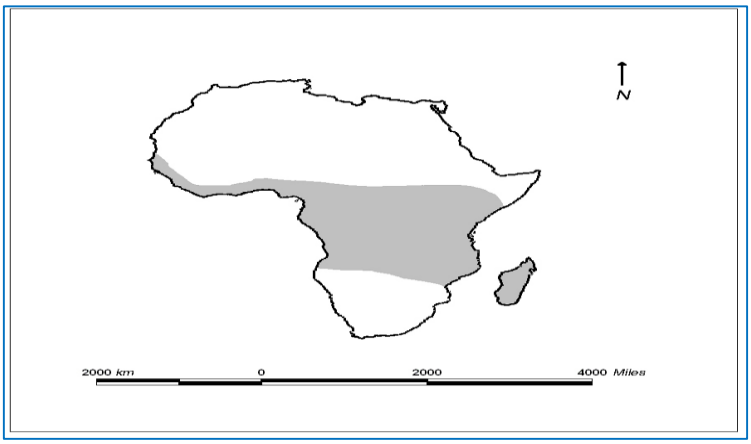

Figure 24: Geographcal Distribution of ndjansang (RH)

1.8.1.5. Distribution of ndjansang

The species is found in central, western and southern Africa in Senegal, Guinea Conakry, Sierra Leone, Liberia, Ivory Coast, Ghana, Benin, Nigeria, Fernando Po, Cameroon, Central African Republic, Sudan, Gabon, Congo, Democratic Republic of the Congo, Uganda, Kenya, Angola, Zambia, Tanzania and Madagascar (Assanvo *et al*., 2015).

1.8.1.6. Distribution in anthropogenic areas

Bush fallows, cacao (Theobroma cacao) plantations, home gardens and crop fields are common habitats of the species (Fondoun *et al.*, 1999), where it is used as a soil fertility improving species. This means the species is an incipient domesticate with great potential for further utilisation.

1.8.2. Production Areas

Despite the fact that ndjanssang is undomesticated, gathering, transportation and marketing systems have developed in several areas of tropical Africa. However, the system developed in Cameroon dominates all others (Caspa et al., 2018).

1.8.2.1. The Cameroon production to consumption system

The humid forest zone of Cameroon is the main production area of ndjansang, and it is traded to neighboring countries Central African Republic, Gabon, Equatorial Guinea and

Nigeria (Assanvo *et al*., 2015), areas of Central Africa, and also to Europe (Sunderland and Obama, 1999; Tabuna, 1999). In 1995, a survey of markets showed that 35,952 kg of ndjansang kernels were marketed in the humid forest zone of Cameroon, for a total value of 43,432,200 CFA, about (Assanvo *et al*., 2015). In Manyu Division more than 66% of farmers have trees on their farms (31% on cacao farms and 33.6% on arable fields), whereas in Lekie Division 90% of farmers have trees on their farms (60% on cacao farms and 81.5% on arable farms).

1.8.2.2. Minor production areas

Ndjansang kernels are also gathered in the rest of the humid forest zone of Cameroon and there is also local traditional gathering scattered through other parts of the distribution of the species.

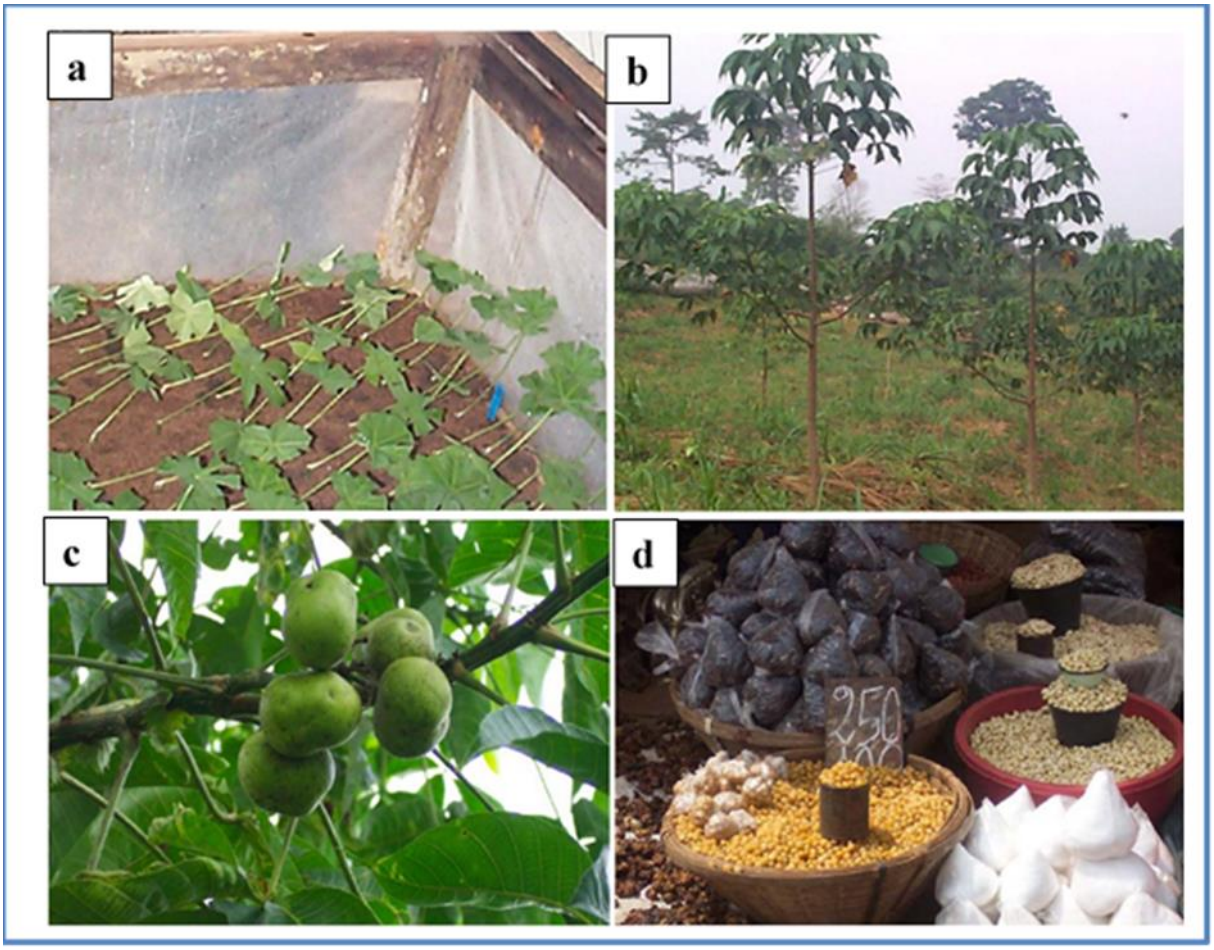

Figure 25: a) Ndjansang cuttings in a non-mist propagator. b) Planting out Ndjansang trees in Cameroon, c) Fruits of Ndjansang and d) Ndjansang kernels for sale at Mfoundi market, Yaoundé, Cameroon (Tchoundjeu and Atangana, 2006; CIFOR, 2008)

1.8.3. Properties of Njansang

1.8.3.1. Seed

The physio-chemical properties of dry kernels, defatted kernels and oil extracted from kernels have been studied in recent years in Cameroon and Nigeria. A summary of properties of dry kernels is provided in Table VII (Maeva et al., 2015; Assanvo et al., 2015) is reported on a wider range of chemical properties and this data is included in Table VIII.

Table VIII: Chemical composition of kernels (Tchoundjeu and Atangana, 2006)

Constiuent	**Amount (%)**
Water	3.1 ± 0.8
Fatty acid	47.4 – 55.3
Crude protein	24.3 -65.2
Total carbohydrates	5.6 – 9.3
Digestible carbohydrates	5.6 – 9.3
Crude fibres	8.9 -9.3
Ash	10.5 -17.8
Nitrogen	8.6 ± 0 .9
Dry extracts	97.8
pH	7.84

It appears that kernels are rich in crude protein, oils and also fibres. In relation to the lipids, tocopherol content is 0.45 ± 0.63 – 2.38 ± 0.12 mg / 100 g; α-tocopherol is a lipid soluble antioxidant (Ketaona *et al*., 2013).

1.8.3.2. Wood

Ndjansang wood is white, grey or pale yellow and darkens on exposure. The sapwood, not differentiated from heartwood, is the same colour. It is very soft and weakly resistant to chipping and shocks (Babweteera and Brown, 2010). The grain is straight, without luster, and its texture is somewhat coarse. The wood saws and works easily, and nails without splitting, but it is liable to decay and termite attack. It has disseminated pores and its ring limits are absent or not distinct. The fresh density varies between 0.7 and 0.9 g/cm^3 and dry density (at 12% humidity) between 0.25 and 0.4 g/cm^3 **(**Tchoundjeu and Atangana, 2006). The shrinkage from

green to oven dry is 2% (radial), 4.8% (tangential) and 7.6% (volumetric). The basic specific gravity varies between 0.2–0.4 c/cm^3.

1.8.4. Uses

Surveys of the use made by farmers of ndjansang have been reported by (Assanvo et al., 2015) and show that the highest priority use is for food, followed by medicinal use, cultural and soil fertility improvement.

1.8.4.1. Fruit and food products

The seed kernels constitute the edible part of the fruits. The kernels make up 31–33% of the seeds, which in turn make up a little over two-thirds of the indehiscent fruit capsule. The kernel is often referred to as the 'nut meat'. When seeds are extracted the pulp and shell are normally discarded. The kernels are usually dried for use as a flavouring agent in food dishes in West and Central Africa (Yirankinyuki et al., 2018). If oil is extracted, this is used in cooking whilst it is fresh. Tests on the properties. especially the iodine value, show that the oil is good for cooking purposes **(**CIFOR, 2008**)**. The paste of ground kernels is sometimes used as a thickening agent for soups and stews and incorporated in to baby cereals and cakes, due to their high oil retention capacity (Leakey, 1999**).** Stews made with kernel extracts are reported to have a good taste and can substitute for the use of peanuts **(**CIFOR, 2008). The paste is obtained by crushing dried, ground kernels with stones. Seeds may also be pounded to powder for use in making porridge in times of food shortage. Fruit pulp is not yet used commonly in human diets across the geographic distribution of ndjansang. The pulp, however, is dried for use as flavouring (Yirankinyuki *et al*., 2018).

1.8.4.2. Medicinal uses

a) Bark

The bark of the roots, bole and branches is used medicinally (CE-FAO, 1999). Local preparations take many forms but are usually decoctions or other liquid extracts. Bark is variously used to treat leprosy, elephantiasis, gonorrhea, dysentery, diarrhea, coughs, hernia, rheumatism, abscesses, rickets and smallpox (Andel, 2006) in West and Central Africa. It is also used in southern Cameroon to cure yellow fever, anemia, skin diseases, malaria, stomach pain, headache, toothache, worms; to provide easy child delivery (although in certain doses it can be an abortifacient); and as an aphrodisiac (Alison, 2007).

b) Seed

The seed, seed shell and latex contain a resin, which along with the oil is used in West Africa as a remedy for gonorrhoea and diarrhea (Yirankinyuki *et al*., 2018).

c) Leaves

A decoction of leaves is used for fevers. The pulp of the leaves is used against mycoses, and to treat abscesses in Senegal (Andel, 2006).

d) Sap

The sap of the plant is used for eye infections and decoctions of leaves are used as a febrifuge. The latter is also used in cases of dysentery, oedema and female sterility (Olasehinde *et al.*, 2016).

e) Roots

The roots are used as aphrodisiacs in Ivory Coast; seed husks and latex of the plant are used in West Africa to cure gonorrhoea and diarrhea (Olasehinde *et al.*, 2016).

1.8.4.3. Socio-cultural aspects

Dried seeds of ndjanssang are used in the southern Cameroon for a popular game called 'songho', in Sierra Leone for rattles for bundu dances, and in Nigeria the Ibo people use them in a game called 'okwe'. Its wood is used for drum manufacture for traditional dances **(**CIFOR**,** 2008). In Democratic Republic of the Congo, the wood is used for making drums, which are said to be very sonorous, and in southern Nigeria, Gabon and Angola, it is carved to make the whole or the resonant parts of musical instruments (Manirakiza, 2007).

1.8.4.4. Agroforestry and land use

Ndjansang trees are found in diverse land use systems such as fallow land, home gardens, natural and semi-natural forests, plantations and food crop fields (Ndumbe *et al*., 2018). The majority are to be found in plantations and arable fields. Trials to better incorporate ndjansang into food crop systems are in progress at ICRAF-West Africa in Cameroon. The rate of destruction of the rainforest for shifting cultivation in Central Africa is estimated at 60% **(**Egbe et al., 2012**)**. Ricinodendron heudelotii was identified as a priority species for domestication under ICRAF's Humid Lowlands of West Africa (HULWA) project, which includes assessing farmers' and users' needs, assessing the species currently grown, and ranking

the importance of tree products according to food and nutritional security, market value and potential value **(**Egbe et al., 2012**)**. In southern Cameroon, ndjansang is commonly used as a soil- fertility-improving tree (Tchoundjeu and Atangana, 2006) as well as a shade tree in cacao plantations.

1.8.4.5. Industrial uses

The oil obtained from dried kernels could be used for soap and varnish making The iodine and saponification values also point to the potential of the oil in paint and for cosmetic use. The oil is thick and pale yellow. Wood ash of the tree is locally used in soap making. Fibres of the tree are suitable for paper pulp **(**Tchoundjeu and Atangana, 2006).

1.8.4.6. Other uses

At the present time industrial applications are only possibilities. Due to its low resistance. ndjansang wood is very little used in carving and furniture making. Nonetheless, currently the wood is used to manufacture boxes and crates, plywood, coffins, rafts, and fishing floats. It is considered to be a good balsa substitute **(**Egbe *et al*., 2012**)**. The wood is also used for fuel, poles and rough planks. It is also used in Uganda by Semliki and Unyoro forest dwellers for making the doors of their huts. It is carved into fetish masks, spoons, ladles, plates, platters, bowls, dippers and stools. The sawdust is suitable for use in sun helmets (Ndumbe *et al*., 2018)**,** and is used for filling lifebelts.

1.8.5. Agronomy

Research is ongoing on agronomy and most efforts have been focused on propagation techniques. Numerous aspects of husbandry such as spacing, pruning, nutrition and irrigation are yet to be investigated. Trials on intercropping and transplanting are in process at ICRAF-West Africa, and this chapter relies heavily on Cameroonian experiences (Manirakiza, 2007).

1.8.6. Harvesting

Ndjanssang trees start bearing fruit at 8 to 10 years of age. Flowering is somewhat negatively influenced at low altitudes (Caspa et al., 2018). The extraction of the seed kernels is time consuming due to the seed shells. Normally farmers allow the fruits to fall from the trees, gather them into piles, and leave them to rot. Once rotten, the seeds can be extracted by washing and boiling, and are then put into cold water and left for 24 hours. They are then subjected to

further boiling to crack the seed shells, enabling the kernels to be extracted using a knife. The kernels are then dried. Most of this work is done by women (Manirakiza, 2007).

1.8.7. Post-harvest handling

This is limited to transport from production areas to markets. There is no special packaging: jute bags or polythene bags are used. At the market, amounts are measured out by volume (Cosyns et al., 2013).

1.8.8. Production

Trees bear fruit usually once in a 2–3-year period, but some can fruit each year. Kernel yield varies between provenances and 100 fruit weight ranges from 165–275 g. An individual tree can produce up to 900 fruits in a fruiting year. Domestication is in the early stages, so production per tree and yield per unit area have not yet been established (Caspa *et al*., 2018).

1.8.9. Storage

Most traditional methods of storing kernels are based on avoiding excess humidity, such as by sun drying and storing them in a dry place. In the humid forest zone of Cameroon, the following are recorded: sun-dried kernels in bags (the most practised method), sun-dried kernels in a calabash, kernels dried on the fire place and bagged, sun-dried kernels in baskets, sun-dried kernels in a closed cooking pot, complete seeds previously washed and boiled, kernels dried on the fire place and put in tins, sun-dried kernels in closed demijohns and fresh kernels in plastic bags (Caspa *et al*., 2018). The storage places reported by farmers range from bamboo racks hung over fireplacesto hanging from the ceiling. These traditional methods of storage are adequate for 1–2 years. Stored kernels need protecting from rodents (Manirakiza, 2007).

1.8.10. Processing

A very limited amount of local seed oil extraction is carried out. More scientific extraction has been worked out (Ndumbe *et al*., 2018). The γ-tocopherol content results in the oil being stable and prevents it from becoming rancid very quickly.

1.8.11. Marketing and Trade

Ndjansang fruits are mainly harvested from the wild. Since plantations are in their infancy, it is difficult to consider the economics of production. Most trees are scattered in different land use systems in the humid tropics of Africa, mainly fallows, cacao farms, food crop fields, home gardens and forest, or in fairly substantial groves in parts of southern Africa

(Caspa *et al*., 2018). Quantities and values of traded seeds are not recorded in local official statistics. Nonetheless, ndjansang is one of the most traded non-timber forest products (NTFP) in the humid forest zone of Cameroon **(**Tchoundjeu and Atangana, 2006) and prices of kernels have been recorded in Libreville and even in specialised shops in France and Belgium selling NTFPs from Central Africa. Quantities and amounts traded in the humid forest zone of Cameroon from January to July 1995 by 271 traders from 31 markets were estimated at 35.952 kg for a value of 66,000 Euros. However, the absence of any institutional framework, as well as the poor organisation of market networks of NTFPs, is the main constraint in assessing the trade (Ndumbe *et al*., 2018). In Cameroon, kernels are mainly sold in piles or in cups and the prices vary according to periods of abundance and scarcity, as well as the sizes of the piles and cups (Caspa *et al*., 2018). For instance, piles in Yaoundé markets cost 50 to 100 CFA francs according to the sizes of piles in periods of abundance, and these prices go up in periods of scarcity. Cups cost 150 to 300 CFA francs, according to their sizes, in periods of abundance, and prices go up to 200 to 400 and more in periods of scarcity. The markets for ndjansang kernels vary with their proximity to the urban centres **(**Tchoundjeu and Atangana, 2006; Caspa *et al*., 2018). The net marketing margin in the Littoral province of Cameroon is 35-40% (Ndoye *et al*., 1998), twice that of the Centre province, due to the poorer supply in Littoral province. In addition, fish is plentiful in Littoral province and ndjansang is eaten as a flavouring with fish dishes.

I.9. NANOPARTICLES

I.9.1. Generalities on nanoparticles

Nanoparticles are particles with diameters between 1 and 100 nanometres in size and are made up of carbon, metal, metal oxides or organic matter **(**Hasan S, 2015). Nanoparticles exhibit a unique physical, chemical and biological properties at nanoscale compared to their respective particles at higher scales. These phenomena are due to a relatively larger surface area to the volume, increased reactivity or stability in a chemical process, enhanced mechanical strength, etc. (Hasan S, 2015) thereby leading to its use in various applications.

Nanoparticles vary in dimensions, to shapes and sizes apart from their material (Cho *et al*., 2013). A nanoparticle can be either a zero dimensional where the length, breadth and height is fixed at a single point for example nano dots, one dimensional where it can possess only one parameter for example graphene, two dimensional where it has length and breadth for example carbon nanotubes or three dimensional where it has all the parameters such as length, breadth

and height for example silver or gold nanoparticles. Nanoparticles are of different shape, size and structure. They may be spherical, cylindrical, tubular, conical, hollow core, spiral, flat, etc. or irregular and differ from 1 nm to 100 nm in size. The surface can be uniform or irregular with surface variations. Some nanoparticles are crystalline or amorphous with single or multi crystal solids either loose or agglomerated (Machado *et al.,* 2015).

Numerous synthesis methods are either being developed or improved to enhance the properties and reduce the production costs. Some methods are modified to achieve process specific nanoparticles to increase their optical, mechanical, physical and chemical properties (Cho *et al*., 2013).

The nanoparticles are generally classified into the organic, inorganic and carbon based

I.9.1.1. Organic nanoparticles

Dendrimers, micelles, liposomes and ferritin, etc. are commonly known organic nanoparticles or polymers. These nanoparticles are biodegradable, non-toxic, and are sensitive to thermal and electromagnetic radiation such as heat and light (Tiwari et al, 2008). These unique characteristics makes them an ideal choice for drug delivery. The organic nanoparticles are thus most widely used in the biomedical field for example drug delivery system as they are efficient and also can be injected on specific parts of the body that is also known as targeted drug delivery.

I.9.1.2. Inorganic nanoparticles

Inorganic nanoparticles are particles that are made up of metal and metal oxide. Metal based nanoparticles are synthesized from metals to nanometric sizes either by destructive or constructive methods. Almost all metals can be synthesized into their nanoparticles (Salavatiniasari *et al*., 2008) distinctive properties such sizes as low as 10 to 100nm, surface characteristics like high surface area to volume ratio, pore size, surface charge and surface charge density, crystalline and amorphous structures, shapes like spherical and cylindrical and colour, reactivity and sensitivity to environmental factors such as air, moisture, heat and sunlight etc. The metal oxide based nanoparticles are synthesized to modify the properties of their respective metal based nanoparticles, for example nanoparticles of iron (Fe) instantly oxidises to iron oxide (Fe2O3) in the presence of oxygen at room temperature that increases its reactivity compared to iron nanoparticles. Metal oxide nanoparticles are synthesised mainly due to their increased reactivity and efficiency (Tai *et al*., 2007).

I.9.1.3. Carbon based

Nanoparticles made completely of carbon are knows as carbon based (Rahmaniyan et al 2015). They can be classified into fullerenes, graphene, carbon nano tubes (CNT), carbon nanofibers and carbon black and sometimes activated carbon in nano

Nanomaterials are the leading requirement of the rapidly developing field of nanomedicine, bionanotechnology. Nanoparticles are being utilized as therapeutic tools in infections, against microbes thus understanding the properties of nanoparticles and their effect on microbes is essential to clinical application. Among noble metal nanoparticles, silver nanoparticles have received considerable attention owing to their attractive physicochemical properties. They are said to be stable and have disinfectant and antibacterial properties (Hulteen *et al.,* 1999).

I.9.2 Silver Nanoparticles

The biological applications of silver nanoparticles have been effective in combating many dreadful diseases, especially those caused by multi-drug resistant pathogens (Rahmaniyan *et al.*, 2015). In addition, silver nanoparticles have been reported to possess antibacterial, anti-fungal, as well as anti-cancer properties (Veerasamy *et al*., 2011). Previous studies have shown that they are not cytotoxic to humans, and are effective against fungi, viruses, and bacteria at low concentrations, with minimal or no side effects (Yu *et al.,* 2012).

The antibacterial property of silver has been knowns for centuries. These nanoparticles have attracted great interest in their development as potential antibacterial drugs (Hsiao *et al*., 2006), which has also been reported that many biophysical interactions occur between silver nanoparticles and bacteria including biosorption, nanoparticles decomposition and cellular uptake, with effects bacterial cell membrane damage and toxicity (Priester *et al*., 2009; Brayner, *et al*., 2006). Silver has been used as a water disinfectant and has shown effectiveness against planktonic bacteria (Silvestry-Rodriguez, *et al.,* 2007). Silver has gained this efficacy through its binding to disulfide or sulfhydryl groups present in the cell wall proteins (Feng *et al*., 2000). Silver has also been shown to bind DNA in the nucleus thus causing cell death. Many methods are available for synthesis of Ag NPs which include physical, chemical and biological synthesis. Among these methods, the biological means of synthesis gained good-attention compared to other two methods due to low cost, simple, environmentally friendly and efficient substitute for the mass production of nanoparticles (Firdhouse and Lalitha. 2015). In biological methods, Ag NPs are synthesized via using fungus (Mukherjee *et al.,* 2001) microbes (Saklani *et al.,* 2012)

and plants (Govindarajan *et al.,* 2016*).* Compared to the fungus and microbes, plants are promising source for nanoparticles production. The advantages of the plant-mediated synthesis of nanoparticles include cost efficient, large-scale production and require low maintenance (Govindarajan *et al.,* 2016). Important point of using plants in nanoparticles production instead of fungus or bacteria is the lack of pathogenicity (Pantidos and Horsfall, 2014)..

In this study *Ricinodendron heudelotti* shells extract were used for the synthesis of silver nanoparticles which were then doped with activated carbon from this same plant source and evaluated for its adsorption, antibacterial and cytotoxicity properties.

CHAPTER II: MATERIALS AND EXPERIMENTAL PROCEDURE

II.1. Introduction

This chapter presents the materials used in this work to achieve our aim, the experimental procedure for the preparation of the adsorbents and the adsorbate and also the methods used for the physico-chemical characterization.

II.2. Materials and Chemicals

II.2.1. Materials

Table IX gives the different materials used to carry out this work:

Table IX: Materials used in the course of this work

Equipment	**Mark**
Furnaces	Carbolite furnaces (OSI)
Oven	Blue pard
Electronic balance of precision 0.001	Kern (PC)
pH meter	Golden-Mettler U. S. A.
Magnetic agitator	Horse shoe IKA
Stop watch	/
Filter paper	Whatman 05 of density 64 g/m^3
UV-visible spectrometer	ANLAGE 260
Petsch pulveridette grinder	/
Multipurpose flask shaker	TT12F Techmel and Techmel USA

II.2.2. Chemicals used for the realization of this work

Laboratory grade reagents supplied by Merck and Fluka, were used without further purification for the preparation of synthetic aqueous solutions. The summary of these reagents are listed in Table X:

Table X: List of chemicals

Product name	Chemical formulae	Appearance	Purity	Source
Indigo Carmine	$C_{16}H_8N_2Na_2O_8S_2$	Purple solid	85%	Merck
Methyl Orange	$C_{14}H_{14}N_3NaO_3S$	Orange solid	100%	Merck
Hydrochloric acid	HCl	Colorless liquid	33%	Fluka
Zinc Chloride	$ZnCl_2$	Colorless liquid	pure	Merck
Phosphuric acid	H_3PO_4	Colorless liquid	85%	Fluka
Sodium hydroxide	NaOH	White solid	99%	Fluka
Iodine	I_2	Black solid	Pure	Merck
Methylene Blue	$C_{16}H_{18}ClN_3S$	Solid	pure	Merck
Sodium thiosulphate	$Na_2S_2O_3$	solid	Pure	Fluka
Starch	Pure	White	Pure	Merck
Silver nitrate	$AgNO_3$	solide	Pure	Merck

II.3. Proximate analysis of the RDH shells

The RHS were washed. dried and crushed ionto verious merch sizes of X<0.75 mm, 0.70 mm<X<0.8 mm, 0.8 mm<X<1.6 mm and X>1.6 mm (where X = RHS). The proximate analysis of a material is used to determine the distribution of products obtained when the sample is heated under specific conditions. It is defined by ASTM D2866-94 (Ndi *et al.*, 2014); and separates the products into four groups :

- **Moisture content :** Water content present in the sample

- **Volatile matter content :** Gases and vapours driven from the sample during the heating process

- **Fixed carbon content :** Nonvolatile fraction of sample (basically the carbon content of the sample)

- **Ash content :** Inorganic residue remaining after combustion (inertmatter present in the sample)

To determine the four products on heating, the sample must be subjected to specific conditions for each test.

II.3.1. Moisture Content

Activated carbon is generally priced on a moisture-free basis, although occasionally some moisture content is permissible, eg 3, 8, 10 %. Unless packaged in airtight containers, some activated carbons when stored under humid conditions will adsorbe considerable moisture over a period of a month They may adsorb as much as 25 to 30 % moisture and still appear dry. For many purposes, this moisture content does not affect the adsorptive power, but obviously it dilutes the carbon. Therefore, an additional weight of moist carbon is needed to provide the required dry weight. The percentage of moisture content (% M) is given by equation 27:

$$Moisture = \frac{m_i - m_f}{m_i} x\ 100 \ldots\ldots\ldots\ldots\ldots\ldots\ldots\ldots\ldots\ldots\ldots\ldots\ldots (27)$$

Where m_i and m_f are the masses of the precursor before and after heating.

II.3.2. Ash content

Ash level reflects the purity of the carbon. The ash content of activated carbon is a measure of the mineral content (Ca, Mg, Si, Fe, salts, etc.) left in the carbon after the manufacturing process. The inorganic mineral might result from the base of the precursor or some elements which were chemically bounded to the organic matter during treatment. *Ash content can lead to* increased hydrophilicity and can have catalytic effects, causing restructuring process during regeneration of used activated carbon. The inorganic material contained in activated carbon is measured as ash content, generally in the range between 2 and 10 %. To determine the ash content, a weighed quantity (in grams, of powdered carbon, or granular carbon) is placed in a crucible and heated in a furnace until the carbon has been completely burned. The temperature should be below 600˚C to minimize volatilization of inorganic constituents and also to leave the ash in a suitable condition for further examination. The ash content can be calculated by using equation 28:

$$Ash\ content = \frac{m_{Ash}}{m_i} x\ 100 \ldots \ldots \ldots \ldots \ldots \ldots \ldots \ldots \ldots \ldots \ldots \ldots \ldots (28)$$

Where m_{Ash} and m_f are the masses of the precursor before and after heating.

II.3.3. Volatile matter content

The volatile matter content is obtain by heating 10 g of the RHS sample between a temperature range of about 900 °C - 950 °C in a closed crucible for a time varying between 7 to 8 minutes ; the weight before and after heating is then used. Then by using the same drying and weighing method, the volatile matter could also be calculated using equation 29:

$$Volatile\ matter\ content = \frac{m_i - m_f}{m_i} x\ 100 \ldots \ldots \ldots \ldots \ldots \ldots \ldots \ldots (29)$$

Where m_i and m_f are the masses of the precursor before and after heating. A larger weight loss of the substance implies greater volatile matter content.

II.3.4. Fixed carbon content

The fixed carbon content is determined by subtracting the sum of percentage compositions of moisture content, volatile content, and ash content from 100. The value obtained is the amount of fixed carbon present in the sample expressed in percentage.

$$Fixed\ carbon\ content = 100 - (\%a + \%b + \%c) \ldots \ldots \ldots \ldots \ldots \ldots \ldots (30)$$

Where **a** is the humidity content, **b** is Volatile matter content and **c** is the ash content respectively.

II.4. Preparation and Characterization of Activated Carbon derived from RHS

II.4.1. Active preparation of RHS, AC based H_3PO_4 and AC based $ZnCl_2$

The work had as main aim the valorization of RH shells in the production of ACs by identifying the optimum conditions of activated carbon preparation and activated carbon doped with AgNP for wastewater reclamation/purification. The chemical activation method was used with phosphoric acid and zinc chloride as activating agents.

II.4.1.1. Preparation of RHS precursor

The shells of RH were collected after the fruits had fallen, rotten and the nuts processed to obtained the eadible part in the village of Etam II of the Tombe sub-division of the South West Region of Cameroon. These shells were transported to the Physical and Theoretical

Chemistry Laboratory, Faculty of Sciences of the University of Yaoundé I. Here they were washed several times with tap water, rinsed with distilled water to remove dirt and then sun-dried. The dried shells were mechanically crushed using a Retsch Pulverisette grinder, then sieved for various mesh sizes of X<0.75 mm, 0.70mm<X<0.8 mm, 0.8 mm<X<1.6 mm and X>1.6 mm.

II.4.1.2. Impregnation process

10 g of the crushed dried RH shells were impregnated with the solution of an activating agent ($ZnCl_2$ or H_3PO_4) in a desired impregnation ratio (R) of RHS. Each mixture was left for 60 min at room temperature, so that reagents are fully absorbed into the RHS. The impregnated RHS were dried at 110 °C for 24 hours in an oven. The dried impregnated RHS were cooled in a desiccator for 60 min and the dried sample was carbonised at the required temperature using a Carbolite Furnace. The activated carbons obtained were washed with distilled water till neutral pH for the sample activated with phosphoric acid while the sample activated with Zinc Chloride was tested for Chloride ions using Silver nitrate solution until no precipitate of AgCl was obtained. A summary of the experimental protocol is shown in Figure 26.

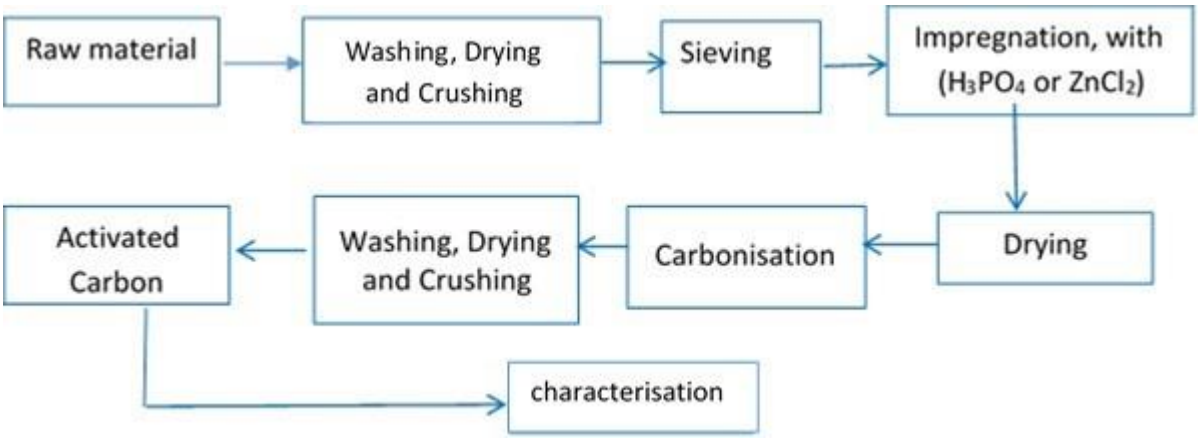

Figure 26: Procedure followed during the one step process for the production of activated carbon from RHS

II.4.1.3. Optimising the preparation condition of the Activated Carbons

a) Experimental Design and Statistical Analysis

As an important subject in the statistical design of experiments, the Response Surface Methodology (RSM) is a collection of mathematical and statistical techniques useful for the modeling and analysis of problems in which a response of interest is influenced by several variables and the objective is to optimize this response (Nuran, 2014). When treatments are

from a continuous range of values, then a Response Surface Methodology is useful for developing, improving, and optimizing the response variable (Nuran, 2014). In this case, Response surface methodology (RSM) was used to fit the independent variables to the response variables Iodine number, Methylene Blue number and % Yield. A central composite design (CCD) was used with 3 factors, namely, carbonisation temperatures (500–700 °C), activation time (1 - 2 hrs) and impregnation ratio (1:1, 1 :2 and 2:1). The design variables in this study with actual and coded levels are shown in Table XI.

Table XI: Designing of Experimental Matrix

Variables (factors)	Code	Unit	Coded variable Levels				
			-α	**-1**	**0**	**+1**	**+α**
Carbonisation Temperation	X_1	°C	431.821	500	600	700	768.179
Carbonisation time	X_2	Minutes	39.546	60	90	120	140.454
Impregnation Ratio	X_3	/	0.659	1	1.5	2	2.341

The designed matrix of all the factors in coded and reall values for all the Experimental runs are shown in Table XII.

Table XII: Experimental matrix and Experimental plan (CCD design matrix with coded and real values

Standard Run	Coded values			Real values		
	X_1	X_2	X_3	X_1 (°C)	X_2 (mins)	X_3
1	-1	-1	-1	500	60	1
2	1	-1	-1	700	60	1
3	-1	1	-1	500	120	1
4	1	1	-1	700	120	1
5	-1	-1	1	500	60	2
6	1	-1	1	700	60	2
7	-1	1	1	500	120	2
8	1	1	1	700	120	2
9	-1.682	0	0	431.821	90	1.5
10	1.682	0	0	768.179	90	1.5
11	0	-1.682	0	600	39.546	1.5
12	0	1.682	0	600	140.454	1.5
13	0	0	-1.682	600	90	0.659
14	0	0	1.682	600	90	2.341
15	0	0	0	600	90	1.5
16	0	0	0	600	90	1.5
17	0	0	0	600	90	1.5
18	0	0	0	600	90	1.5
19	0	0	0	600	90	1.5
20	0	0	0	600	90	1.5

The statistical package Minitab 16 was used for statistical analysis of the results. The experimental design was composed of 20 experiments including 12 full factorial design points, 6-star points, and 6-centre points. The significant terms in different models were found by analysis of variance (ANOVA) for each response. Significance was judged by determining the probability level that the *F* (Fisher variation ratio) statistic calculated from the data is less than 5%. Numerical optimization technique of the package Minitab 16 was used for simultaneous optimization of the multiple responses. The desired goals for response were chosen. All the independent variables were kept within range while the responses were maximized. The graphs of the corresponding results, contour plot (2- dimensional grahp) and surface Responds graphs (3-dimensiol graph) was drawn using SigmaPlot 11 software (Systat. Software Inc.). That's not

withstanding, to obtain the different activated carbons with the desired characteristics (large specific surface area, high micro and meso pores capacity, not leaving out a high % yield; the required awaited responses are Iodine number (IN), Methylene Blue number (MB) and % Yield of the activated carbon. The responses are coded and together with their respective unites are given in Table XIII.

Table XIII: Responses studied

Response	Coded Value	Unites
Iodine Number	Y1	mg/g
Methylene Blue number	Y2	mg/g
% Yield	Y3	%

II.4.2. Preparation of Silver nanoparticle loaded activated carbon (An escalated nanocomposite with antimicrobial property)

II.4.2.1. Synthesis of AgNP

5 g of the powder raw RHS was mixed with 200 mL of distilled water and stirred using a magnetic stirer for 30 min and filtered. In 100 mL of 1 mM, 2 mM and 3 mM silver nitrate ($AgNO_3$) solution, 100 mL of supernatant sample was added slowly and was observed for colour change. The particles resulting from the reduction of $AgNO_3$ are called as AgNP. This method is reffered to as Green Synthesis.

II.4.2.2. Preparation of Nanocomposite

The AgNP was loaded on AC by means of simple agitation. 5 g of AC was taken and added to result AgNPs solution. It was mixed vigorously by continuous stirring for 1 h at 150 rpm using IKA LABORTECHNIK argitator. The nanocomposite product was obtained by drying the AgNP loaded activated carbon (AgNP-AC) powder in an oven at a temperature of 110 ºC as proposed by (Karthik and Radha, 2016) with some modifications.

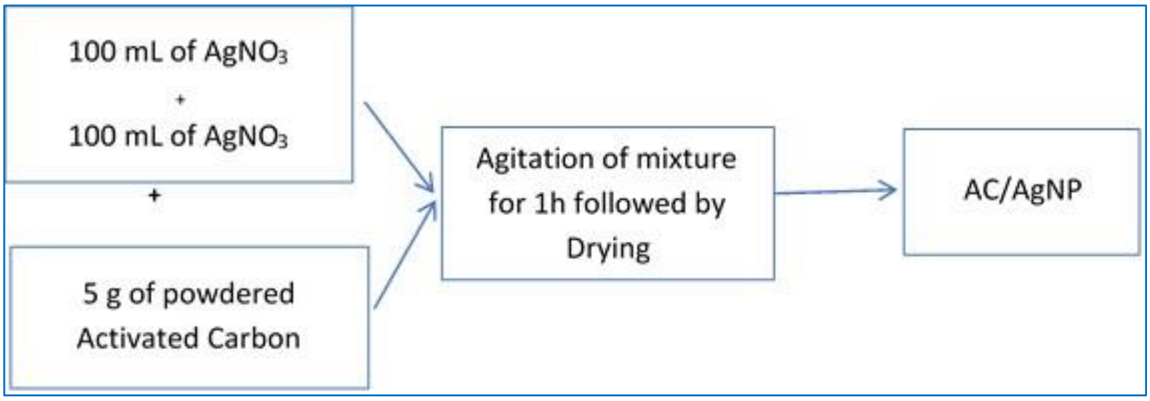

Figure 27: Flow diagram for the preparation of AC/AgNP

II.4.3. Iodine number (IN)

The iodine number is a relative indicator of the porosity in an activated carbon (Ndi *et al*., 2014). It is a measure of the micropore contents of the activated carbon (up to 2 nm). The iodine number is defined as the amount in milligrams of iodine adsorbed by 1.0 g of activated carbon when the iodine concentration is 0.02 N. The iodine number is accepted as the most fundamental parameter used to characterize activated carbon performance. The different reactive used to determine the iodine number are regrouped in Table X.

- Standardization of iodine solution

10 mL of 0.02 N iodine solutions were pipetted into a conical flask; 2-3 drops of starch solutions were added. The pale-yellow color of iodine solution turned blue-black and was titrated with 0.005 N sodium thiosulphate solutions till it became colourless (Ndi *et al*., 2014).

- Iodine Number determination

0.1g of AC(s) was weighed accurately into a dry screw caped conical flask, 30 mL of 0.02 N iodine solutions were added. The content was magnetically stirred for 3 hours and filtered. The filtrate was collected in a dry flask and 10 mL of the filtrate was titrated against sodium thiosulphate solution using starch as indicator till the blue color of the solution turns courless (Lekene *et al* ., 2019). The equation of the reaction is:

$$2Na_2S_2O_{3\,(aq)} + I_2 \longrightarrow Na_2S_4O_{6\,(aq)} + 2NaI \quad (31)$$

Knowing that the final concentration of I_2 can be used to determine the quantity of Iodine number adsorbed by the relation (Nasehir *et al*., 2010):

$Q = \frac{(Co-Ce).V}{M_{PAC}}$ ..... (32)

II.4.4. Methylene blue adsorption

II.4.4.1. Preparation of Solutions

Laboratory grade methylene blue (MB), a cationic dye having molecular formula of $C_{16}H_{18}N_3SCl$ supplied in powder form by Merck, was used without further purification for the preparation of synthetic aqueous solution to determine the methylene blue number which gives an idea of the mesopore (2 – 50 nm) (Lekene *et al.*, 2019) quantity present on the surface of the activated carbons. A stock solution of methylene blue of concentration 500 ppm (500 mg/L) was prepared by dissolving (0.5000 ± 0.0001) g of methylene blue in a 1000 mL volumetric flask, agitated by using a magnetic stirrer for a period of 30 mins and completed with distilled water up to the mark. This solution was again stirred with a magnetic stirrer for two hours to obtain homogeneity. Solutions of which was used concentrations were obtained by dilution to obtained the titration curve for the Experiments. The batch experiments of the adsorption studies were conducted at room temperature (25 °C) in a 250 mL screw-capped conical flask. For each run, 0.1 g of the activated carbon was weighed and placed in a screw-capped conical flask containing 100 mL solution of methylene blue of concentration 100 ppm. The suspensions were stirred for 3 hours, using a Multy-pourpose Shaker. After agitation, the suspensions were filtered using Whattman N°1 filter paper. The concentration of the filtrate was determined by measuring the absorbance using a UV-visible spectrophotometer at the maximum absorption wavelength of 660 nm. The quantity adsorbed by a unit mass of an adsorbent at equilibrium (Q_e) the percentage (%R) adsorbed was calculated using the relations 32 and 33 respectively.

$$Q_e = \frac{(C_o - C_e).V}{m} \quad \text{..... (33)}$$

$$\%P = \frac{(C_o - C_e)}{C_o} x100 \quad \text{..... (34)}$$

Where: C_o and C_e are the initial and equilibrium concentrations (mg/L) of the adsorbate, V (L) the volume of the adsorbate solution agitated and m (g) the mass of the adsorbent used.

II.4.4.2. Percentage Yield of the Activated Carbon

The % yield of the activated carbons was calculated after the impregnated RHS were carbonised, washed to neutral pH (case of carbon activated with H_3PO_4 acid) or nill production of AgCl precipated (case of carbon activated with $ZnCl_2$ acid) using equation 35.

$$\% \, Yield = \frac{mass\,(g) of\ dried\ activated\ carbon}{mass\,(g) of\ raw\ material} \, x \, 100 \ldots\ldots (35)$$

II.5. Methods of Characterization of RHS, AC and AC/AgNP materials

Activated carbons are strongly heterogeneous due to the existence of different sizes of pores including micropores, mesopores and macropores. In addition, the surface heterogeneity of activated carbons is often significant because of various oxygen and other groups present on the surface. Surface and structural properties of the activated carbons can be studied directly by employing various techniques like electron microscopy, X-ray analysis and various spectroscopic methods. In addition, these properties can be investigated by indirect methods such as gas adsorption and thermal analyses. To characterize the RHS, its ACs and its AC/AgNPs composite, analysis such as : infrared spectroscopy (IR), determination of iodine number and specific surface area by BET method, bacterial inhibition and toxicity test were carried out (Westerhoff, 2006).

II.5.1. Scanning electron microscope analysis (SEM)

A scanning electron microscope (SEM) is a type of electron microscope that images a sample by scanning it with a high-energy beam of electrons in a raster scan pattern. The electrons interact with the atoms that make up the sample producing signals that contain information about the sample's surface topography, composition, and other properties such as electrical conductivity. The types of signals produced by SEM include secondary electrons, back-scattered electrons (BSE), characteristic X-rays, light (cathode luminescence), specimen current and transmitted electrons. The the RHS, its ACs and AC/AgNPs samples from their different methods of preparation that had high iodine number were chosen for SEM analysis. The samples were scattered and coated with gold to study the surface morphology and to verify the porosity.

II.5.2. Thermal Gravimetric Analysis (TGA)

Thermal analysis refers a range of techniques, involving measurement of physical and chemical changes of material with increasing temperature. Thermal Gravimetric Analysis (TGA) is one of the most common tests used to characterise materials, which provides information on the dynamics of the thermal process such as degradation temperature, maximum volatile releasing rate and its corresponding temperature. In this work, The Thermogravimetric analyzer (TGA) used in the analysis of theRHS sample was the LINSEIS STA PT-1000 instrument. The thermogravimetry of RHS was carried out by placing accurately weighted

2.000 ±0.001 mg of ground RHS into alumina micro-crucibles. The results from thermal analysis could slightly change with changing the particle size of sample therefore, samples were all crushed and sieved through a 75 µm mesh for this analysis. The crucible was placed on one side of the thermo-balance hang-down, along with an inert empty reference alumina crucible on the other hang-down, and then subjected to heating up to 1000 °C. Heating was conducted under constant flow of nitrogen (57 mL/min). The instrument can provide dynamic thermogravimetric curves through its computer software, which plots weigh loss versus temperature or Thermogravimetry (TG) curves. The Derivative Thermogravimetry (DTG) plots are the first derivatives of the original TG curve, which indicates the critical points with the highest decomposition rate within the term of each thermal event. However, the nature of the reaction cannot be determined by only using the DTG curves. The instrument is also able to simultaneously measure the heat flow into the sample, as well as providing data on enthalpy changes, known as Differential Scanning Calorimetry (DSC) or heat flow curves (Mateke, 2010**;** Suzan, 2013). The TGA and DSC curves were subsequently produced using the recorded using the Universal Analysis 2000 software.

II.5.3. Infrared spectroscopy (IR)

Infrared spectroscopy carried in the analytical chemistry of the University of Yaoundé I was used to determine the surface functional groups present on the surface of the adsorbents. The IR spectra of catalysts were obtained using diffuse reflectance infrared Fourier transform spectroscopy (DRIFTS). The activated carbon samples from each preparation method that had high iodine number were chosen for analysis using FT-IR spectroscopy to study the surface chemistry of carbon samples. 0.01 g of the undiluted activated carbons sample, in the powdered form (after grinding), were scanned and recorded using a spectroscope (Spectrum GX, PerkinElmer (see Appendix Figure C-6) by 256 scans at a resolution of 4 cm-1and in the wave number range of 4000 - 400 cm-1. Before each measurement, the instrumentwas run with empty sample holder to establish the background, which was then automatically subtracted from the sample spectrumd (Ramine, 2009; Ríos-Hurtado *et al*., 2016). The resulting information's are recorded in a spectrogram by the computer.

II.5.4. BET for measurement of specific surface area

BET surface area and pore structure analysis using nitrogen adsorption isotherms BET (Brunauer, Emmett, and Teller) surface area and pore structure of precursors and activated carbons were determined by an automated gas adsorption analyzer, ASAP 2020 (Micromeritics,

Instruments Inc., GA USA). After degassing of samples at 300 °C to a vacuum of 550 μmHg, nitrogen adsorption-desorption isotherms at -196 °C were measured by this equipment. The BET surface area was calculated by using the BET equation. For each analysis ~ 0.2 g of sample was used. The accuracy of measurements performed by this equipment was ± 5 %. The micropore size distribution was determined using two methods; density functional theory, and Horvath Kawazoe (HK) method (Westerhoff et al., 2006; Ramin, 2009). The mesopore size distribution was measured by density functional theory. The general equation is given by relation 36.

$$\frac{P_o}{V(P_o-P)} = \frac{1}{V_m C} + \frac{C-1}{V_m C} \cdot \frac{P}{P_o} \quad \text{(36)}$$

Where:

V: volume of the vapor adsorbed per gram of the solid at pressure P

P_o: saturated vapor pressure adsorbed at constant temperature

V_m: Volume of vapor required to fill a monolayer surface of the adsorbent

C: Characteristics solid –gas constant value

The linearized form permits us to calculate C and V_m. For known monolayer volume, the specific surface area can be calculated using t equation 37:

$$S_g = \frac{V_m.N.A_m}{22.414\ m} \quad \text{(37)}$$

Where:

N: Avogadro's number,

V_m: monolayer volume occupied by gas molecule (Nitrogen),

m: mass of sample

Am: area occupied by one molecule.

II.5.5. X-Ray Fluorescence (XRF)

XRF is a ND technique used for chemical analysis of materials. An X-ray source is used to irradiate the specimen and to cause the elements in the specimen to emit (or fluoresce) their characteristic X - rays. A detection system (wavelength dispersive) is used to measure the peaks of the emitted X -rays for qual /quant measurements of the elements and their amounts. The techniques were extended in the 1970's to analyze thin films. XRF is routinely used for the simultaneous determination of elemental composition and film thickness. Analyzing Crystals used: LiF (200), (220), graphite (002), W/Si, W/C, V/C, Ni/C.

II.5.6. X-ray diffraction (XRD)

XRD patterns of RH shell samples were recorded on a Phillips PW1450/70 diffractometer equipped with a PW1390 channel control goniometer supply, argon filled proportional counter used as a detector was linked to a PW1373 rate meter and channel analyzer. CuKα 0.15418 nm radiation was generated using a Phillips PW1730 X-ray generator operated at 40 kV and 30 mA. 0.5 g of the Powdered samples were pressed into pellets on a hydraulic press (25 kN) before XRD measurements (appendix Figure C-5). The graph of intensity against the angle of diffraction and different pics if present was determine using the Bragg's law (equation 38) (Das, 2014).

$n\lambda = 2d_{hkl}\sin\Theta$ ……..... (38)

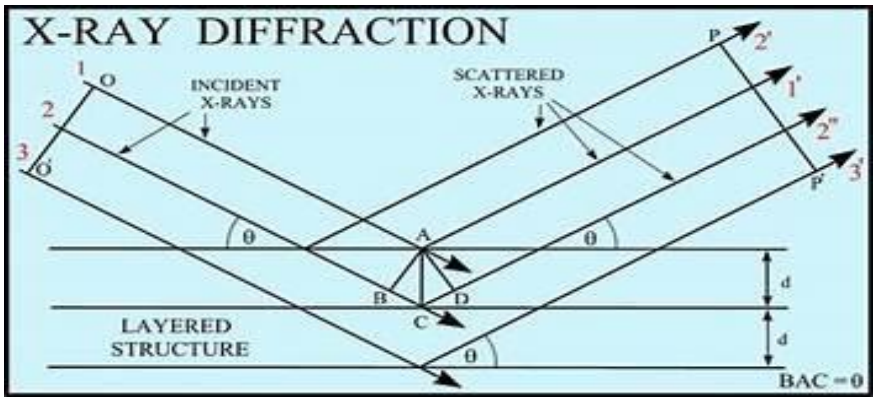

Figure 28: Analytical method of XRD Analysis

II.5.7. Particle size determination

Carbon samples were crushed and sieved in the size less than 75 µm and 0.04-0.05 g of each sample was added into 5 mL of methanol. Suspensions which have different pH values to determine zeta potential and isoelectric points of activated carbons. Samples were stabilized 24 h for sedimentation of particles. After 24 hours, equilibrium pH of each sample was recorded and zeta potential of samples was measured by using MALVERN Zetasizer Nano ZS90 at 25 °C. Samples of the suspensions were collected with plastic syringes and injected into the electrophoresis cell. Measurements were duplicated and averages of the results were used. Equilibrium graphs of particle size vs intensities were plotted. The particle size value determined using the mean average size of the different sizers obtained.

II.5.8. Determination of point of zero charge (pHpzc)

The pH point of zero charge determination of the activated carbons were carried out by adding 0.1 g of carbon to 40 mL solution of 0.1 M NaCl whose initial pH had been measured and adjusted with 0.1 M NaOH and 0.1M HCl varying between 3-11. The containers were sealed and placed on an agitator for 72 hours after which the pH was measured. The pHpzc occurs if there is no change in the pH after contact with adsorbent. This was done as recorded by (Ndi *et a*l., 2014; Lekene *et al*., 2019) with some modifications.

II.5.9. Determination of oxygen containing functional groups determination

The Boehm titration method is the most used for this analysis. It is based on the selective neutralisation of oxygen containing functional groups. 0.1 g of the activated carbon was added to a separate 40 mL solution of $NaHCO_3$(0.1 M), Na_2CO_3 (0.1 M) and NaOH (0.1 M) for acidic groups and 0.1 M HCl for basic groups, respectively, at room temperature under agitation for 48 hours. Subsequently, the aqueous solutions were back-titrated with HCl (0.1 M) in the presence of methyl orange and phenolphthalein indicators for acidic groups and NaOH (0.1 M) in the presence of phenolphthalein indicator for basic groups (Kouotou *et al*., 2013). The number and type of acidic sites were calculated by considering that NaOH neutralizes carboxylic, lactonic and phenolic groups, Na_2CO_3 neutralizes carboxylic and lactonic groups and that $NaHCO_3$ neutralizes only carboxylic groups. Carboxylic groups were therefore quantified by direct titration with NaHCO3 (Ndi *et al*., 2014). The difference between the groups titrated with Na_2CO_3 and those titrated with $NaHCO_3$was assumed to be lactones and the difference between the groups titrated with NaOH and those titrated with Na_2CO_3 was assumed to be phenol. In order to neutralize basic groups, the remaining HCl in the solution was back-titrated with 0.1 M NaOH. Neutralization points were known using pH indicators of phenolphthalein solution for titration of strong base and strong acid, methyl orange solution for weak base with strong acid (Ndi *et al*., 2014).

II.6. Experimental Procedure

II.6.1. Influential study of some Parameters

A fixed mass of the different adsorbents was introduced in a reactor together with a fixed volume of the IC or MO solution (appendix B: figure B-1 and B-2). The system was then put under magnetic agitation for a known time interval. The quantity of the adsorbate adsorbed in milligram per gram was calculated by using the formula:

$Q_e = \frac{(C_o - C_e).V}{m}$ ……..... (39)

Where.

C_o and C_e are the initial and equilibrium concentrations (mg/L) of the adsorbate, V (L) the volume of the adsorbate solution agitated and m the mass of the adsorbent used.

The percentage adsorbed is calculated using the formula:

$\%P = \frac{(C_o - C_t)}{C_o} x\ 100$…… (40)

II.6.1.1. Influence of pH

Using a fixed volume of 20 mL of the solution (IC and MO respectively) and a mass of 0.01 g, the pH was varied from 2 - 11 for the respective materials. After agitation for a fixed interval of time, the solutions were filtered and titrated using UV-visible spectrometer where the pH of maximum adsorption was chosen for the subsequence experiment.

II.6.1.2. Influence of agitation time (contact time)

Using a fixed volume of 20 mL of solution of IC and MO, a mass of 0.01 g and the maximum pH of the respective dye adsorption, the agitation time was varied between 0 – 60 min and after agitation, the solutions were filtered and titrated using UV-visible spectrometer where the time of maximum adsorption was chosen for the subsequence experiment.

II.6.1.3. Influence of adsorbent mass

Using six conical flasks each with a fixed volume of 20 mL of solution of IC and MO dyes, the maximum time or contact time and the pH_{max} where pH_{max} is the pH with maximum dye adsorption, the mass of the adsorbent was varied between 0.01 – 0.06 g, and after agitation, the solutions were filtered and titrated using UV-visible spectrometer where the mass for maximum adsorption was chosen for the subsequence experiment.

II.6.1.4- Influence of the initial concentration

With the pH_{max}, contact time and the fixed mass of the adsorbent, the concentrations of the standard solutions were varied as 50, 60, 70, 80, 90 and 100 mg/L. After agitation, the solutions were filtered and titrated using UV-visible spectrometer.

II.6.2. Antibacterial and Anti-toxicity test of RHS, ACs and AC/AgNPs

II.6.2. 1. *In vitro* anti-bacterial assay

A- Preliminary screening of plants extracts

- **Procedure**

During this process, 96 µL of Muller Hinton broth were aseptically introduced into the wells of a 96-well micro-plate. Four 4 µL of each sample, initially prepared at 100 mg/mL in 100% DMSO were added into the wells followed by 100 µL of standardized bacterial suspension (1.5 $x10^6$ CFU/mL) to obtain final volumes of 200 µL. The tests were performed simultaneously for negative control (MHB + bacteria) and sterility control (MHB alone). Ciprofloxacin was used as the positive control and prepared at 5 µg/mL. The test was performed in triplicate and the plate was incubated at 37 °C for 24 h. After this time, samples that were active on at least one of the tested bacteria, revealed by the necked eyes and with Resazurin were selected in order to determine the MIC.

II.6.2. 2. Determination of minimum Inhibition Concentration (MIC) for the samples

The MIC were determined by the broth micro-dilution method, using an Resazurin based assay as previously described by Lunga *et al*., 2014.

- **Principle**

The principle of the method is based on the reduction of blue or purple colour of Resazurin (7-Hydroxy-3H-phenoxazin-3-one-10-oxide) by bacterial dehydrogenase to an insoluble pink colour Resorufin (7-Hydroxy-3H-phenoxazin-3-one), in metabolically active cells (viable cells).

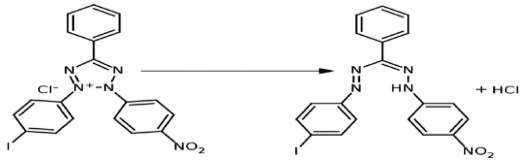

…….... (41)

INT **Formazan**

- **Procedure**

Initially, 196 µL of Muller Hinton broth (MHB) were introduced into the wells of the first line and 100 µL in the remaining wells. Four microliters (4 µL) of each extract, initially prepared at 100 mg/mL in 100% DMSO were added into the wells of the first line. Serial two-fold dilutions

of the test samples were made up to the sixth well. One hundred microliters (100 µL) of standardized bacterial suspension (1.5 x10^6 CFU/mL) was introduced into the wells to obtain final volumes of 200 µL. MHB and the bacteria constituted the negative control while the sterility control contained MHB alone. Ciprofloxacin was used as the positive control

The final concentration ranged from 1000 to 1.95 µg/mL for the extracts and from 5 to 0.01 µg/mL for the positive control. The final concentration of DMSO was ≤ 1% and preliminary test with it did not inhibit bacterial growth. The plates were incubated overnight at 37 °C for 24 hours. After this time, 50 µL of 0.15 mg/mL of Resazurin were added in the wells and incubated at 37 °C for 30 min. The MIC was considered as the lowest concentration where no visible colour change was observed after 30 min.

a **b**

Figure 29: Anti-bacteria test in Wells containing MHB and bacteria before (a) and after (b)

II.6.2.3. In vitro cytotoxicity evaluation of RHS, RHS/AgNPs, ACP, ACZ, ACP/AgNP and ACZ/AgNP

This test was performed on Vero cells (ATCC CRL 1586) using the colorimetric MTT(3-(4,5-dimethythiazol-2-yl)-2,5-diphenyl tetrazolium bromide) method described by Mosmann in 1983 (Mosmann *et al*., 1983).

- **Principle**

The principle of the method used is based on the ability of cells to survive in a medium containing the antimicrobial substance (activated charcoal). The viability of the cells is determined by evaluating the reduction of the yellow colour MTT (3-(4, 5-Dimethylthiazol-2-yl)-2,5-diphenyltetrazolium bromide) by mitochondrial succinate dehydrogenase to purple

crystalline formazan in metabolically active cells (viable cells). The amount of formazan produced is directly proportional to the number of living cells (Mosmann *et al.*, 1983). This reaction takes place in the presence of reduced NADH which is oxidized by MTT.

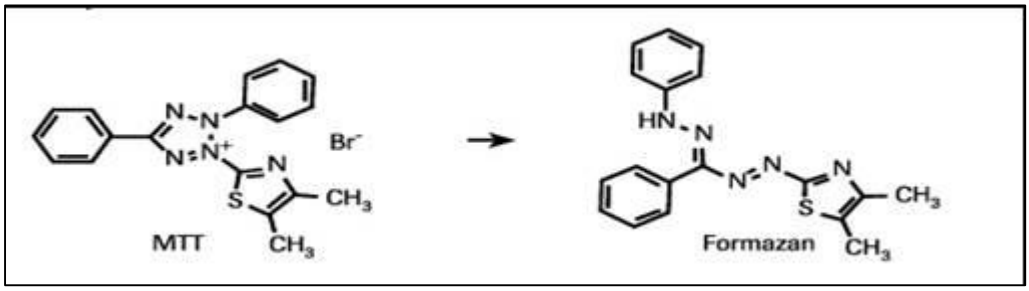

……(42)

II.6.2.4. Preparation of Dulbecco's modification of eagle medium (DMEM)

1% of the antibiotics penicillin/streptomycin and 10% FBS was prepared. In a 500 mL volumetric flask containing 890 mL of an incomplete culture medium. 10 mL of the antibiotic and 100 mL of FBS (inactivated in a water bath at 56°C for 30 min) was added to supplement the culture medium and obtain a final volume of 1000 mL. The resulting mixture was well homogenized, filtered using a 0.22 µm filter, and conserved at 4°C for further use.

II.6.2.5. In vitro culture of Vero cells

The cells were cultured using the following procedure; The Vero cell stock was removed from -80 °C. Once removed, the vial was quickly thawed by gently swirling in a 37 °C water bath, making sure that the cap of the vial is kept out of the water to reduce the risk of contamination. The Vero cell suspension from the vial was then transferred into a 15 mL conical tube containing 10 mL of DMEM (supplemented with 10% FBS). The cell suspension was centrifuged at 1800 g for 5 min at room temperature after which the supernatant will be discarded and the pellet (Vero cells) resuspended in 10ml of the culture medium. The Vero cell suspension was transferred into a 50 cm^2 tissue culture flask (T-flask) with vented cap and incubated in a humidified 37 °C incubator with 5% CO_2. The cells were monitored daily while changing the media every 3 days till cells reach a > 90% confluence. To prepare the inoculum, cultured cells were harvested by trypsinization in a tissue culture flask, centrifugate at 1800 turns/min for 5 min. After this time, the supernatant was discarded and the pellet resuspended in a 50 mL vial using 1 mL of DMEM, 20 µL of the suspension was added to 20 µL of trypan blue and incubated for 1 minute. After this time, the cellular density was determined using the Neubauer counting chamber and a light microscope (Lunga *et al.*, 2014).

- **Preparation of intermediate solution of activated charcoal**

This was done on 96 well microplates. For this, 196 µl of DMEM was introduced in the wells (A1 to G1) while the rest contained 100 µL of the medium, 4 µL of the ACs and composites (100 mg/mL) was pipetted and added into the wells (A1 to G1). Serial two-fold dilutions were performed from column 1 to 6 to obtain concentrations of (2000 µg/mL to 62.5 µg/mL). The wells of row H served as sterility control. The microplates were then sealed and incubated at 4 °C for further experiments.

- **Preparation of test plates**

The test was performed in triplicate on 96 well microplates as previously described. For this, 100 µL of cell suspension was introduced into the wells of the plates to a final charge of $1x10^4$ cells/well and incubated for 4 h under standard conditions (a humidified atmosphere, 5% CO_2 incubator at 37 ^{0}C (memmert). After this time, the medium was removed and replaced with 96 µL of a fresh medium, 4 µL of each diluted charcoal was added in the wells. The plates were again incubated for 24 h under standard conditions. Wells H1 to H4 was serve as positive control (containing 100 µL of 0.2 % DMSO), wells H5 to H8 as negative control (containing 100 µL of 10 % DMSO), wells H9 to H12 as sterility control and were made of 100 µL culture medium. The charcoal concentration varied as previously (2000 µg/ml to 62.5 µg/ml). After this time, 20 µL of a solution of MTT (5 mg/mL in PBS) was added into each well and then incubated again for an additional 4 hours until purple precipitates of formazan were observed. The medium together with MTT was aspirated off the wells, then 100 µL of DMSO was added to solubilize the formed formazan. The optical density of the formed formazan was measured at 570 nm using a micro-titer plate reader Infinite $_{M200}$ (TECAN). From the values of the optical densities, the percentage cell viability (CV) was calculated manually using the formula:

$$\% \, cell \, survival = \frac{(A_t - A_b)}{(A_c - A_b)} x \, 100 \quad \ldots\ldots\ldots\ldots\ldots\ldots\ldots\ldots\ldots\ldots(43)$$

Where : At = Absorbance of Test.
Ab= Absorbance of Blank (Media).
Ac= Absorbance of control (cells)
% cell inhibition = 100 − % cell survival

A dose-response curve (of CV against Concentration of the extracts) was plotted using graph pad prism software, so as to determine the concentration that kills 50% of the Vero cells (IC_{50}).

CHAPTER III : RESULTS AND DISCUSION

This present chapter elucidate the acheivement of the last chapter. Firstly it higlight the optimum conditions for the preparation of ACs by the REM using the CCD matrix with H3PO4 and $ZnCl_2$ as activating agent. Effect of various preparation parameters like impregnation, carbonisation temperature and holding time on size, surface morphology of the porous characteristics of ACs were determine by estimating the IN number and MB number of the prepared ACs. It also permits to understand the characterisation used to estimate suitability of the proces used in the preparation of the composites. Various other characterisations such as SEM-EDX, XRD, FTIR, Zeta sizer, UV and N_2 gas adsorption-desorption isotherms were carried out to be acquainted with other properties of ACs, composites and the AgNPs. For a realistic performance evaluation of the prepared materials. The last part of this chapter continues with the fate (application) of the adsorbents on adsorption process of IC and MO dyes including the mechanisms involved. In the second phase of the application, it concludes its elucidation on anti-microbial activities and toxicities of the material with its main fucus on the mechanisms involved.

III.1. Characterisation of precursor (RHS)

It was thought that it will be interesting to point out the nature and characteristics of RHS as starting material for the production of activated carbon in comparison with commercial precursors like coal, lignite, peat, and coke which are fast runnig out of rich as starting marterials.

III.1.1. Influence of Size and Steps on the Production of Activated Carbon from RHS

Sizes of 0.70 mm‹X‹0.8 mm and 0.8 mm‹X‹1.6 mm (Where X = RHS) each were carbonized using both the one step and two step chemical activation using 50 % H_3PO_4 acid to better understand the size of the precursor and stages of carbonization for the production of the Activated carbon. The experimental results results are shown in the Table XIV:

Table XIV: Iodine number of different sizes of RH shells and Steps of production of AC

	Step(s) used	Size of RHS		
		0.70 mm ‹X‹0.8 mm	0.8 mm‹X‹1.6 mm	1.6 mm‹X‹ 3.4mm
IN (mg/g)	One step	491.122	**586.301**	473.437
	Two step	582.484	**605.337**	513.435

X: Size of RHS

Form Table XIV, it can be concluded that, the Iodine number increases with increase in precursor size and further drops as the sizes continuous to increase in both cases. It can also be seen that the Iodine number for the Two-Step process is higher than that of the One-Step process with an increase of 91.367 mg/g, 19.036 mg/g and 39.999 mg/g for the sizes of 0.70 mm ‹X‹0.8 mm. 0.8 mm‹X‹1.6 mm and 1.6 mm ‹ X ‹ 3.4 mm respectively. From the above results, considering the high cost of production using the two-step process it can therefore be concluded that, the best size of precursor to be use is 0.8 mm ‹ X ‹ 1.6 mm of the one-step process since its Iodine number difference is very small.

III.1.2. Proximate Analysis of RHS precursor

The proximate analysis is carried out in order to have an idea on the moisture, volatile matter, ash and fixed carbon contents of the precursor material. In the process, 10.00 g of the raw precursor was used for each analysis and it should also be noted that each of the separate experiments were done in triplicates. The proximate analysis for the determination of the volatile matter, ash content, moisture content and fixed carbon content was examined (see data in appendix A, Table A-1 page 219) and plotted in Figure 30:

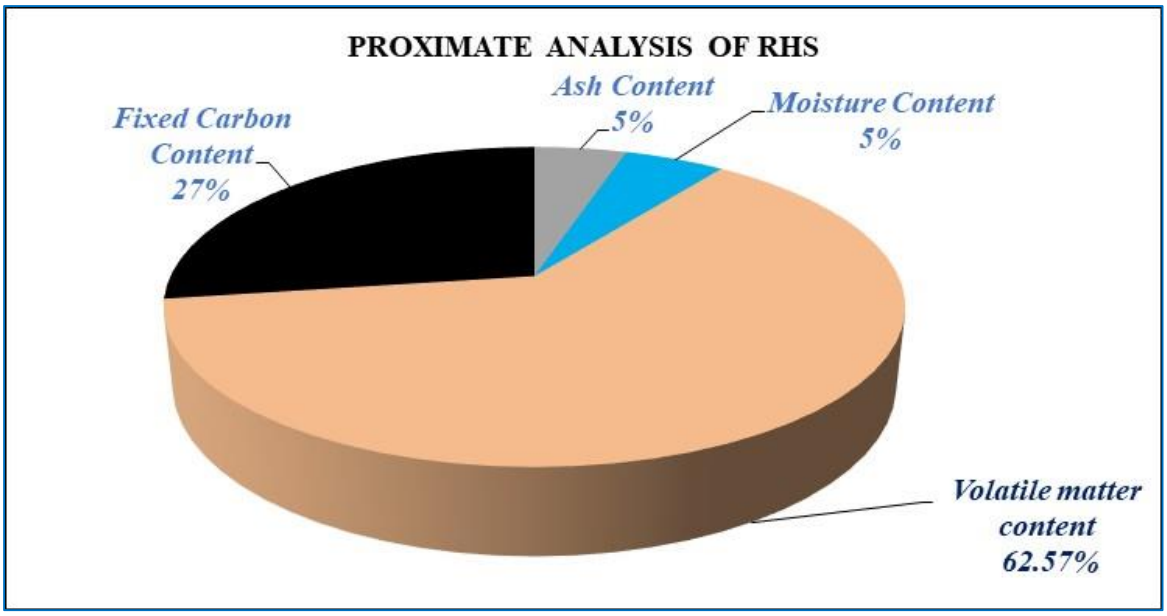

Figure 30: Proximate Analysis of RHS

Proximate analysis an indicator of the quality of a raw material for activated carbon production. The lower the ash content of the raw material, the better its activated carbon. In the present work, RHS precursor had ash content lower than 4.883 % with volatile matter content of 62.571% and fixed carbon content of 27.266 %. Similar results were obtained by Lekene and co-workers in 2019 during the preparation and characterization of activated carbons from *Cucumerupsi mannii Naudin* by chemical activation. It is therefore most probable that RHS are good and promissing precursor for activated carbon production.

III.1.3. Fourier Transformed Infra-Red Spectroscopy

The surface chemistry of the of the raw RHS was materialised using the FTIR spectroscopy. Figure 32 shows the different functional groups present on the RHS.

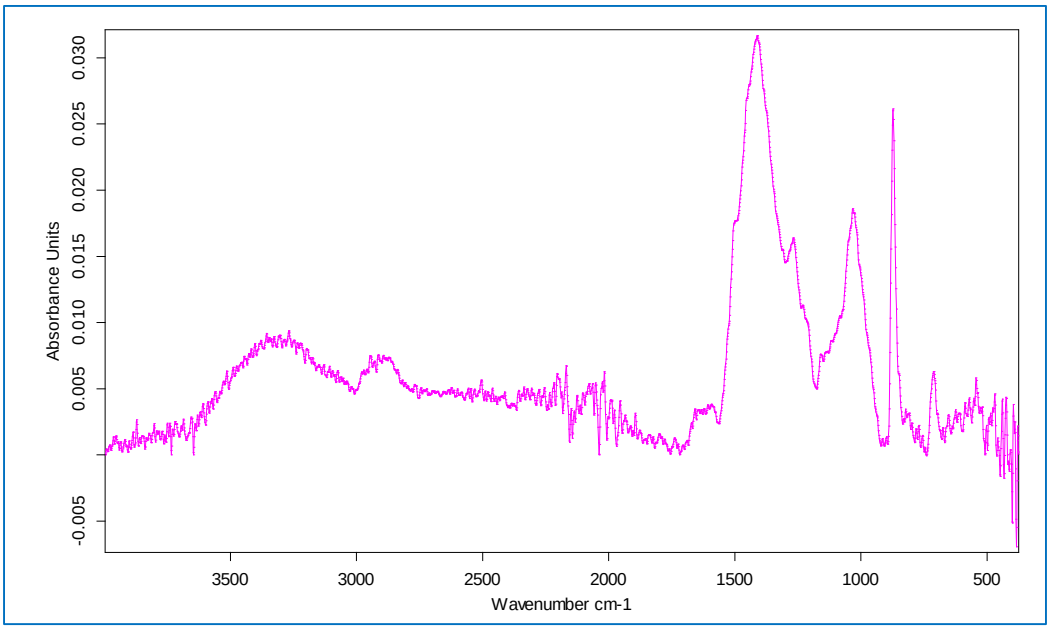

Figure 31: Fourier Transform Infra-Red Spectroscopy of RHS

From Figure 31, a summary of the vibration bans and their respective functional groups of the RHS for maximum visibility and clear interpretation are grouped in Table XV.

Table XV: Table of Vibration frequencies bands with their corresponding functional groups

Material	Adsorption frequency (cm^{-1})	Functional group
RHS	3300	-OH (alcohol, phenol)
	2990	- CH_2 (Asymmetric stretching)
		- CH_3 (symmetric stretching)
	1500-1650	-C=C (monosubstituted alkene)
		- C=O (Ketone or Aldehyde)
	1000-1500	-CH_2 and CH_3 (deformation)
		═CH_2 (plane and out of plane deformation)
	500-950	-C-O (secondary alcohol)
		-C-H (deformation)
		-C-X (Halogeno-Alkanes)

The FTIR results shows a large portion of organics, corfirming the high volatile matter as shown in Figure 30.

III.1.4. Thermal Gravimetric Analysis of RHS

Thermal gravimetric analysis was carried out in order to invstigate the physical and chemical changes of the RHS with increasing temperature. It also helps to study the dynamics of the thermal process such as degradation temperature, maximum volatile releasing rate and its corresponding temperature. Figure 32 illustrates the thermogravimetric profile of the raw precursor.

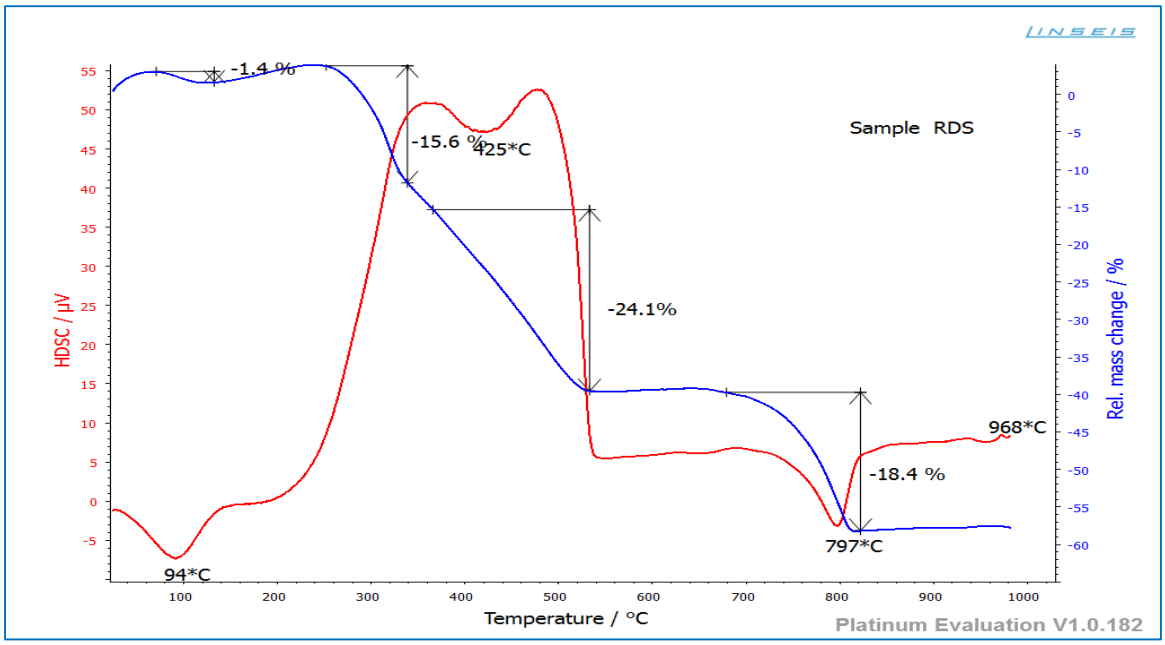

Figure 32: Thermal gravimetric analysis of RHS

From the Figure 32, the pyrolysis of RHS from the result above shows four principal thermo-gravimetric accidents. The first thermal accident takes place around 94 °C which is as a result of loss of free water on the surface of the biomass and with a weight loss of 1.4 % and the processed is endothermic as seen on the DSC graph. Hence the departure of the moisture content takes away latent heat leading to a drop-in temperature. The second thermal accident is around 379 °C, resulting to a loss of 15.6 ¨% by weight of the biomass. This loss of weight is because of the degradation of Hemicellulose and the processed produces heat hence exothermic (Yang *et al.*, 2006; Dias-Júnior *et al.*, 2019).

The third thermal accident is around 425 °C giving a 24.1% lost in weight. The thermal accidents from 379-425 °C usually conveys to the main weight loss for all Biomass fuels and is followed by a slow and continuous weight loss. The former step is due to the primary devolatilization, whereas the latter is attributed to the degradation of heavier chemical structures in the solid matrix, which can also be produced during the previous thermal devolatilization. This stage is due to the degradation of Cellulose (Elyounssi *et al*., 2012) and the beginning of lignin.

The fourth weight lost from 520 to 797 °C. This range of temperature denotes the decomposition of a specific component. Such temperature in these conditions is typical of the complete degradation of lignin and also degradation of carbonates (of calcium carbonate) present in the sample (Biagini *et al*., 2006). This last two steps are also exothermic hence the zone where carbonization is efficient. Above 797 °C, all the Lignin's structure (carbon skeleton) must have been destroyed to produce ash and calcium oxide as remains. Hence the zone of temperature of 500-700 °C was chosen for activated carbon preparation

III.1.5. X-ray Diffraction Measurement of the RHS

XRD analysis was carried out in order to investigate the crystallinity of the raw material. Figure 33 shows the XRD plot of RHS.

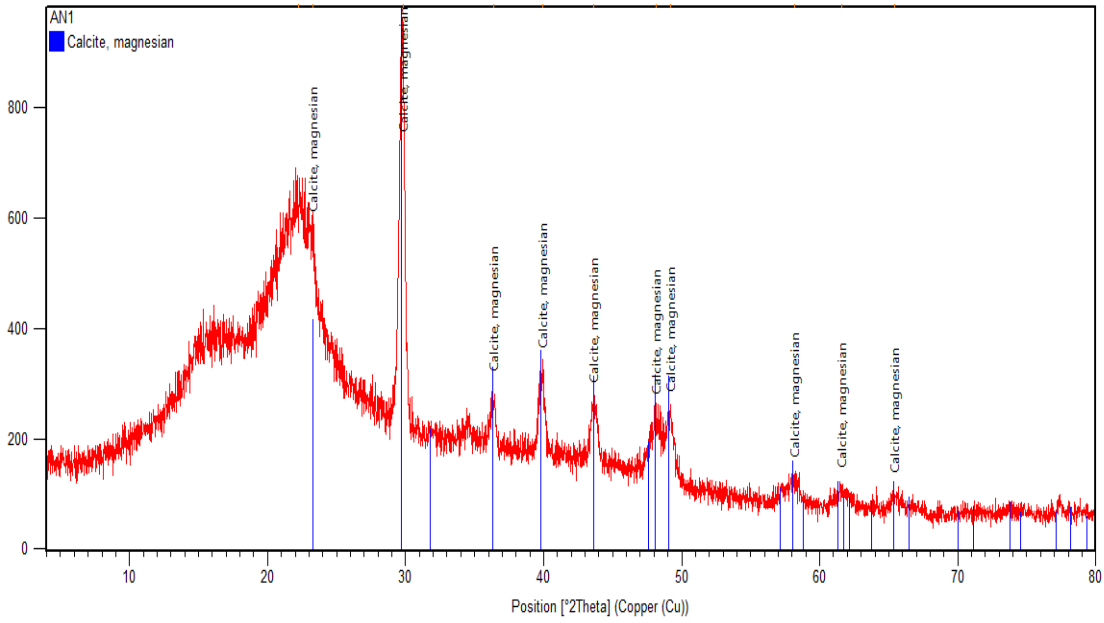

Figure 33: X-ray diffraction of RHS

Figure 33 shows the X-ray diffractogram of RHS. The RHS sample was found to contain a s strong diffraction peak at 29.965 °C and a series of weak diffraction peaks at 23.486°, 36.582°, 40.173°, 43.937°, 48.490°, 49.489°, 58.617° and 65.742° respectively was observed in figure 24 above. This value corresponds to reference code number 96-900-0575 (d_{hkl} = 5.40) and is attributed to the calcite. Furthermore, from the above diffractogram, it can be seen that the material contained both the amorphous and crystalline phase from 2θ values between 0 to 80 degrees but it can be seen that the amorphous part occupies the lion share of the diffractogram. This implies that the material contains a greater degree of non-arrangement in the molecular chain. The few peaks of crystallinity have been depicted to be either calcite (amorphous) or magnesia. However, decisive acid test shows the presence of calcium carbonate and magnesium carbonate. Also, the presence of calcium carbonate is a greater advantage because of its high porogenic nature arose from its decomposition to produce carbon dioxide which will create and developed more pores on it eschew to the exterior.

III.1.6. Scanning Electron microscope (SEM) of RHS

The morphology of raw hazelnut shells was investigated through scanning electron microscope (SEM) images, of which an image at x1000 is shown in Figure 34.

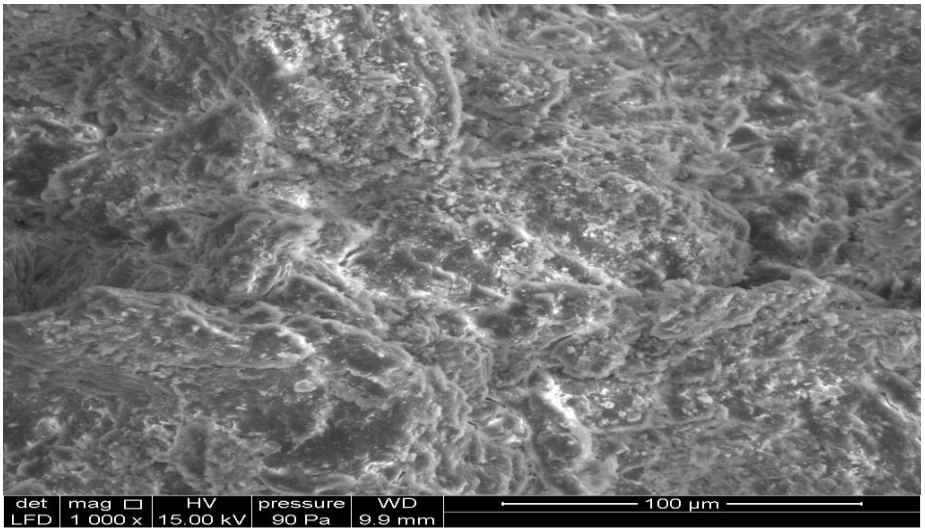

Figure 34: Scanning Electron Micrograph of RHS

The Scanning electron microscope was use to get the actual microscopic image of the RHS. The above photograph obtain with 1000 x magnification shows a compact structure with an infinitely little or no pores on the surface of the RHS. This smooth and compacted structure

is as a result of the crystalline calcium carbonate or magnesium carbonate present in the precursor material.

III.1.7. X-Ray Fluorescence Analysis of RHS prcursor

The Flouresence analysis was done to obtaine the mineral composition of RHS and the analytical results for the mineral analysis of RHS are shown in the Figure 35.

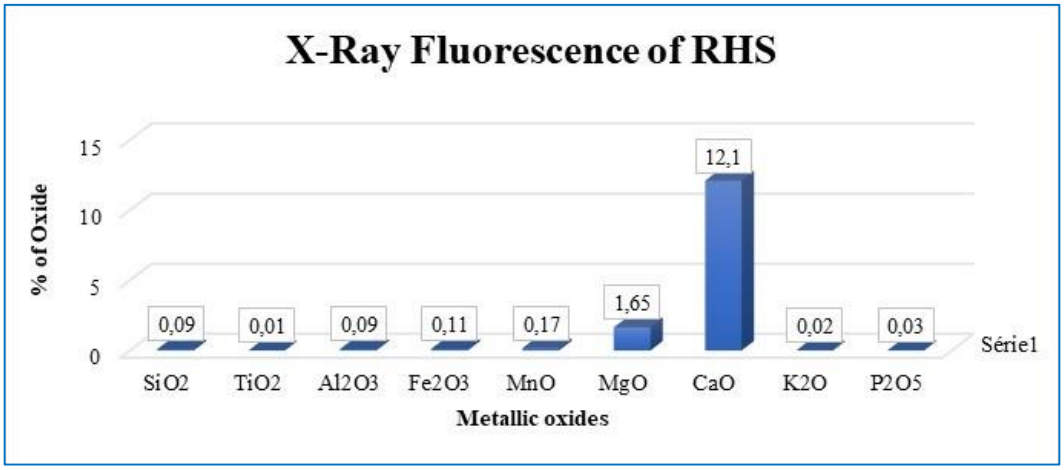

Figure 35: Graph of X-Ray Flouresence of RHS

From Figure 35, it can be seen that RHS are rich in calcium oxide (CaO) with percentage composition of 12.1 % followed by magnesium oxide with percentage composition of 1.65 %. The oxides of SiO, TiO, Al_2O_3, Fe_2O_3, MnO, K_2O and P_2O_5 are found in traces in the said material (appendix A, Table A-2, page 219). This implies that the main metallic oxides found in RHS is CaO. This further confirms the results of XRD which shows crystalline pics corresponding to calcite or magnesium carbonate. The sum of the percentages of metallic oxides being less than 20% indicates once more the high quantities of carbonaceous compounds which further puts in to evidence the large amorphous section on the XRD graph. Hence a good precursor for AC production.

III.1.8. Total Carbon Analysis of RHS

The total carbon content present in the raw material was obtain by the total carbon analysis using the aj-Multi analyser N/C 2100 S, multiWin 4.09 of serial number N5-772/O. The results obtain are shown in Figure 36.

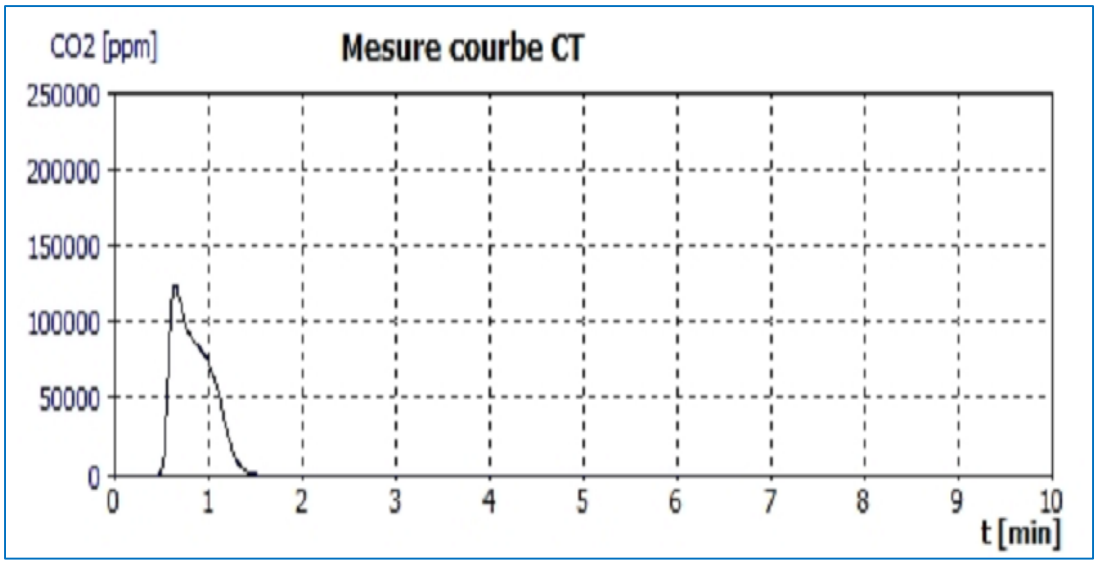

Figure 36: Measurement of total carbon present in RHS

From Figure 36, 150 mg of powdered RHS was subjected for analysis using the above analyzer. The carbon dioxide obtained was passed through lime water and the quantity of carbon present was subsequently calculated. The results show that the material contains about 73.59 % of carbon in grams per kilogram of the total raw RHS material. These high values imply that RHS is good and promising precursor for the preparation of activated carbon.

III.1.9. Porous Characteristics of RHS precursor

The determination of the pore size distribution (PSD) is an important aspect of characterization of micro-porous adsorbents. Various techniques exist for evaluating PSD of a micro-porous material such as the measurement of saturated amounts of probe molecules of various sizes, and by measurement of a single adsorption isotherm of gases at subcritical temperatures. In this work BET method was used to determine the surface area while the Barret Joyner Halender (BJH) adsorption desorption method was used o determine the pore volume and pore diameter. The N_2 adsorption-desorption isotherms of RHS are shown in Figure 37.

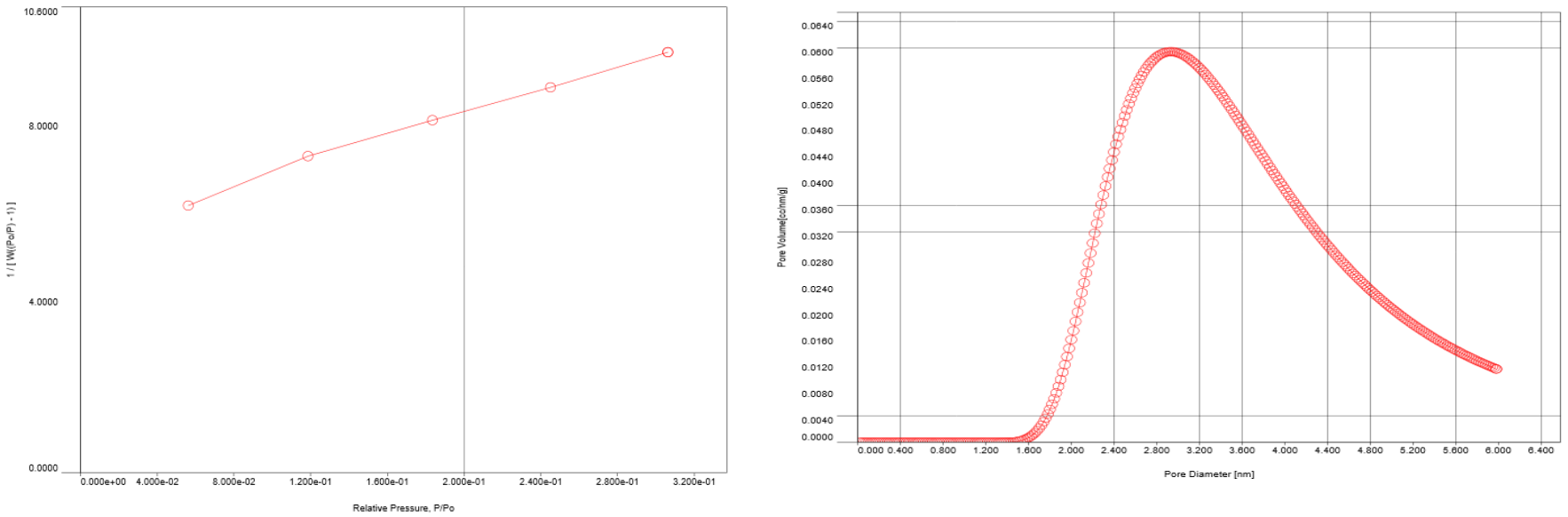

Figure 37: BET adsorption isotherm and Dubinin-Astakhov (DA) pore size distribution for RHS

Table XVI: Summary Report of micromeritics analysis of RHS

Sample	Surface Area (m^2/g)						Pore volume (cc/g)			Pore (nm)		
	Single Point BET	Multipoint Point BET	Langmuir surface area	BJH Cum. Adsorption surface area	t-method external surface area	DR Method micropore area	BJH Cum. adsorption pore volume	DH Cum. adsorption surface area	DR method micropore area	DA method adsorption pore diameter	BJH Cum. adsorption pore diameter	DR method adsorption pore diameter
RHS	111.4	182.5	1050	205.3	182.5	196.5	10.10	10.33	698.4	2.94	2.133	6.243

From Table XVI, it can be seen that the specific surface area of the RHS from the BET method is 182.50 m2/g. Also, the Langmuir surface ares and that of the BJH are higher than those of the the BET. This difference in surface area and quantity absorbed can be explained by the fact that, during adsorption, the ratio of the number of the adsorption particles with adsorption sites are less in multiple layer adsorption than in a single phase (monolayer) coverage. The total external surface area for the t-plote method is equal to that of the BET while that of DR is slightly higher than of BET. The BJH cumulative pore volume and DA pore diarmeter (Figure 37) are 10.10 cc/g et 2.94 nm respectively. The pore diameter for BJH and DA are approximately equal hence shows that RHS is rich in micropores and mesopores from IUPAC classification. Lekene et al., 2019 observed similar results.

III.2. Optimisation of the preparation of activated carbons

III.2.1. Optimisation of the preparation condition of H_3PO_4 Activated carbon

After planification and modelisation, the experimented and predicted values obtained from the activated carbon based H_3PO_4 are given in Table XVI.

Table XVII: Experimental and Predicted Responses for the production of ACP

Exp. No	Variables			Y1 (IN)		Y2 (MB)		Y3 (Yield)	
	X1	X2	X3	Exp.	Pred.	Exp.	Pred.	Exp.	Pred.
1	500.00	60.00	1.00	**605.73**	**615.24**	**99.46**	**98.95**	52.00	52.89
2	700.00	60.00	1.00	537.38	541.17	96.34	94.13	50.00	49.41
3	500.00	120.00	1.00	599.63	593.75	99.46	98.15	51.00	52.29
4	700.00	120.00	1.00	567.76	567.78	98.83	95.20	47.00	46.31
5	500.00	60.00	2.00	518.39	526.10	88.38	88.84	55.00	56.32
6	700.00	60.00	2.00	461.42	475.03	**62.32**	**60.46**	50.00	49.34
7	500.00	120.00	2.00	531.68	535.62	89.91	88.95	53.00	54.22
8	700.00	120.00	2.00	534.43	532.66	65.11	62.45	**45.00**	**44.75**
9	431.82	90.00	1.50	563.96	558.60	98.50	98.35	**61.00**	**58.50**
10	768.18	90.00	1.50	499.40	493.82	67.37	72.00	46.00	47.61
11	600.00	39.55	1.50	582.95	566.09	86.81	87.73	52.00	51.74
12	600.00	140.45	1.50	590.54	596.47	85.17	88.73	48.00	47.37
13	600.00	90.00	0.66	592.44	591.75	99.26	102.29	49.00	48.77
14	600.00	90.00	2.34	**497.50**	**487.26**	64.79	66.24	51.00	50.34
15	600.00	90.00	1.50	550.36	558.52	86.05	85.89	52.00	51.19
16	600.00	90.00	1.50	558.26	558.52	86.01	85.89	51.00	51.19
17	600.00	90.00	1.50	552.57	558.52	86.02	85.89	51.00	51.19
18	600.00	90.00	1.50	558.26	558.52	86.00	85.89	52.00	51.19
19	600.00	90.00	1.50	565.86	558.52	86.00	85.89	51.00	51.19
20	600.00	90.00	1.50	563.96	558.52	86.02	85.89	50.00	51.19

The complete design matrix with the values of both the response obtained from the experimental works and the predicted values are given in Table XVII. Runs 15-20 at the center point were used to determine the experimental error. From the table above, it can be seen that the IN for the ACP varies from 497.50 and 605.24 mg/g, the value for MB number varies between 62.32 and 99.46 mg/g, while the % Yield varies also between 45.00 and 61.00 %. Nevertheless, higher capacities of iodine and methylene blue adsorption was observed at lower

temperature (experiment n^o 1 for both I_2/ACP and MB/ACP). On the contrary the highest % yield came from lower temperature (experiment n^o 9 for ACP). This high IN and MB number corresponds to activating temperature of 500 °C, activation time of 60 minutes with an impregnation ration of 1 :1. That's not withstanding, lower adsorption of iodine (IN) was observed at a temperature of 600 °C, activation time of 90 minutes and a corresponding impregnation ratio of 2.34 whereas the highest % yield corresponds to activating temperature of 431.82 °C, activation time of 90 minutes and an impregnation ration of 1.5. It can also be seen that for all the cases, the Experimental results and the theoretical results are in conformity. For instance, looking at the highest values of IN, MB and % Yield. the difference between the theoretical and the experimental results are 1.55%, 0.51 and 4.10% respectively.

Using the experimental results, the regression model equations (second-order polynomial) relating the preparation of ACP and process parameters were developed and are given in equations 43, 44 and 45 for IN, MB number and %Yield respectively. Apart from the linear effect of the preparation parameters, the RSM also gives an insight into the quadratic and interaction effects of the parameters. These analyses were done by means of Fisher's 'F' test and student '*T*' test. The student '*T*' test was used to determine the significance of the regression coefficients of the parameters. The *P* values were also used as a tool to check the significance of each of the interaction among the variables which in turn may also be used to indicate the patterns of the interactions among the variables. Generally, the larger the magnitude of *T* and the smaller the value of *P*, the more significant is the corresponding coefficient term (Ravikumar *et al*., 2006).

The estimated regression coefficient, *t* and *P* values for all the linear, quadratic and interaction effects of the parameters are given in Tables XVIII, XIX and XX for IN, MB number and %Yield for the preparation of ACP respectively.

III.2.1.1. Estimated regression coefficient for the responses studied

The individual runs of experimental design shown in Table XVI are conducted by using ACP and the responses were measured. A linear regression model was fitted for the experimental data using least square technique. The model coefficients, effects and standard error of the factors and interactions for the estimated regression coefficient, *T* and *P* values for all the linear, quadratic and interaction effects of the parameters are given in for IN, MB number and %Yield for the preparation of ACP respectively are shown in Tables XVII, XVIII and XIX.

Table XVIII: Estimated regression coefficient of model terms and their effects on the response for IN (ACP)

Factor/Term	DF	Coef	SE Coef	T	P-value
Constant	/	558.532	4.225	132.198	0.000**
X_1	1	-19.259	2.803	-6.870	0.000**
X_2	1	9.032	2.803	3.222	0.009**
X_3	1	-31.065	2.803	-11.082	0.000**
X_1X_1	1	-11.425	2.729	-4.187	0.002**
X_2X_2	1	8.044	2.729	2.948	0.015**
X_3X_3	1	-6.725	2.729	-2.465	0.033**
X_1X_2	1	12.026	3.662	3.284	0.008**
X1X3	1	5.752	3.662	1.571	0.147
X_2X_3	1	7.754	3.662	2.117	0.060*

DF: degrees of freedom, **: significant, *: slightly significant

Table XIX: Estimated regression coefficient of model terms and their effects on the response for MB (ACP)

Factor/Term	DF	Coef	SE Coef	*T*-value	*P*-value
Constant	/	85.8879	1.1402	75.329	0.000**
X_1	1	-7.8327	0.7556	-10.354	0.000**
X_2	1	0.2969	0.7556	0.392	0.703
X_3	1	-10.7164	0.7556	-14.166	0.000**
X_1X_1	1	-0.2518	0.7364	-0.342	0.739
X_2X_2	1	0.8292	0.7364	1.126	0.286
X_3X_3	1	-0.5732	0.7364	-0.778	0.454
X_1X_2	1	0.4695	0.9884	0.475	0.645
X1X3	1	-5.8895	0.9884	-5.959	0.000**
X_2X_3	1	0.2290	0.9884	0.232	0.821

DF : degrees of freedom, **: significant, *: slightly significant

Table XX: Estimated regression coefficient of model terms and their effects on the response for %Yield (ACP)

Factor/Term	Coef	SE Coef	*T*-value	*P*-value
Constant	51.1922	0.5715	89.58	0 .000**
X_1	-3.2384	0.3792	-8.541	0.000**
X_2	-1.298	0.3792	-3.423	0.007**
X_3	0.466	0.3792	1.229	0.247
X_1X_1	0.6579	0.3691	1.782	0.105*
X_2X_2	-0.5795	0.3691	-1.570	0.147
X_3X_3	-0.5795	0.3691	-1.57	0.147
X_1X_2	-0.625	0.4954	-1.262	0.236
X1X3	-0.875	0.4954	-1.766	0.108*
X_2X_3	-0.375	0.4954	-0.757	0.467

DF : degrees of freedom, **: significant, *: slightly significant

The model coefficients are obtained by dividing the effects by two *P* value is the probability value that is used to determine the effects in the model that are statistically significant. Factors having *P* value less than 0.05 are considered to be statistically significant for a 95 % confidence level.

In the case of IN it was observed that the coefficients for the linear effect of all the factors temperature, time and ratio (*P*= 0.000, 0.009 and 0.000) for the preparation of ACP were highly significant, the quadratic effects were also significant (*P* = 0.002, 0.015 and 0.008) while only the X_1X_2 interaction was significant with *P* value = 0.008, X_1X_3 was insignificant with *P* value = 0.147, and X_2X_3 interaction was slightly significant (*P* = 0.060). With respect to Estimated regression coefficient of model terms and their effects on the response for MB (ACP), only the coefficients for the linear effect of the factors temperature and ratio (*P*= 0.000 and 0.000) for the preparation of ACP were highly significant, none of the quadratic effects were significant (*P* = 0.739, 0.286 and 0.454) while only the X_1X_3 interaction was significant with *P* value = 0.000 as X_1X_2 and X_2X_3 were insignificant with *P* values of 0.645 and 0.821 respectively. Looking at the estimated regression coefficient of model terms and their effects on the response for %Yield (ACP), it can be seen that, the coefficients for the linear effect of

all the factors temperature, time and ratio (P = 0.000, 0.000 and 0.007) for the preparation of ACP were highly significant, none of the quadratic effects of interaction effects were significant with P = 0.105, 0.147 and 0.147; and P = 0.236, 0.108 and 0.467 respectively. The significance of these interaction (those with p values < 0.05), would have been lost if the preparation of the ACP was carried out under conventional or classical methods. The resultant model is represented as:

$$Y_1 = 558.823 - 19.259X_1 + 9.032X_2 - 31.065X_3 - 11.425X_1X_1 + 8.044X_2X_2 - 6.725\,X_3X_3 + 12.026X_1X_2 + 5.752X_1X_3 + 7.754X_2X_3 \quad \ldots\ldots (44)$$

$$Y_2 = 85.8879 - 7.8327X_1 + 0.2969X_2 - 10.7164X_3 - 0.2518X_1X_1 + 0.8292X_2X_2 - 0.5732\,X_3X_3 + 0.4697X_1X_2 - 5.8895X_1X_3 + 0.2290X_2X_3 \quad \ldots\ldots (45)$$

$$Y_3 = 51.1922 - 3.2384X_1 - 1.2980X_2 + 0.4660X_3 + 0.6579X_1X_1 - 0.5795X_2X_2 - 0.5795\,X_3X_3 - 0.6250X_1X_2 - 0.8750X_1X_3 - 0.3750X_2X_3 \quad \ldots\ldots (46)$$

The three model equations (44, 45 and 46) were optimized using statistical package Minitab 16. The optimal values of the process parameters were first obtained in coded units and then converted to uncoded units using equation 22. The statistical significance of ratio of mean square variation due to regression and mean square residual error was tested using analysis of variance (ANOVA). After estimating the main effects, the effect of interactions was determined by performing the analysis of variance (ANOVA). Sum of squares (SS) of each factor quantifies its importance in the process and as the value of SS increases, the significance of the corresponding factor in the process also increases. The ANOVA results for the production of ACP are presented in Tables XXI, XXII and XXIII.

III.2.1.2. Analysis of Variance (ANOVA) Results for the production of ACP

Tables XXI, XXII and XXIII presents the results analysis of variance (ANOVA) for IN, MB number and %Yield respectively for the preparation of ACP.

Table XXI: Analysis of Variance (ANOVA) results for IN for ACP

Source	DF	Seq SS	Adj SS	Adj MS	F-value	P-value
Regression	9	24973.200	24973.200	2774.800	25.860	0.000**
Linear	3	19358.600	19358.600	6452.900	60.130	0.000**
Temp	1	5065.400	5065.400	5065.400	47.20	0.000**
Time	1	1114.100	1114.100	1114.100	10.380	0.009**
Ratio	1	13179.100	13179.100	13179.100	122.810	0.000**
Square	3	3712.000	3712.000	1237.300	11.530	0.001**
Temp*Temp	1	1955.500	1881.000	1881.000	17.530	0.002**
Time*Time	1	1104.700	932.600	932.600	8.690	0.015**
Ratio*Ratio	1	651.800	651.800	651.800	6.070	0.033**
Interaction	3	1902.600	1902.600	634.200	5.910	0.014**
Temp*Time	1	1157.000	1157.000	1157.000	10.780	0.008**
Temp*Ratio	1	264.700	264.700	264.700	2.470	0.147
Time*Ratio	1	480.9	480.9	480.9	4.48	0.06**
Residual Error	10	1073.1	1073.1	107.3		
Lack-of-Fit	5	888.1	888.1	177.6	4.8	0.055*
Pure Error	5	185	185	37		
Total	19	26046.3				

DF : degrees of freedom, **: significant, *: slightly significant

Table XXII: Analysis of Variance (ANOVA) results for MB for ACP

Source	DF	Seq SS	Adj SS	Adj MS	F-value	P-value
Regression	9	2704.400	2704.400	300.490	38.450	0.000**
Linear	3	2407.450	2407.450	802.480	102.680	0.000**
Temp	1	837.870	837.870	837.870	107.210	0.000**
Time	1	1.200	1.200	1.200	0.150	0.703
Ratio	1	1568.380	1568.380	1568.380	200.680	0.000**
Square	3	17.270	17.270	5.760	0.740	0.554
Temp*Temp	1	1.110	0.910	0.910	0.120	0.739
Time*Time	1	11.430	9.910	9.910	1.270	0.286
Ratio*Ratio	1	4.730	4.730	4.730	0.610	0.454
Interaction	3	279.670	279.670	93.220	11.930	0.001**
Temp*Time	1	1.760	1.760	1.760	0.230	0.645
Temp*Ratio	1	277.490	277.490	277.490	35.510	0.000**
Time*Ratio	1	0.420	0.420	0.420	0.050	0.821
Residual Error	10	78.150	78.150	7.820		
Lack-of-Fit	5	78.150	78.150	15.63	52072.25	0.000**
Pure Error	5	0.000	0.000	0.000		
Total	19	2782.550				

DF : degrees of freedom, **: significant, *: slightly significant

Table XXIII: Analysis of Variance (ANOVA) results for % Yield for ACP

Source	DF	Seq SS	Adj SS	Adj MS	F	P
Regression	9	196.917	196.917	21.880	11.140	0.000**
Linear	3	169.202	169.202	56.401	28.730	0.000**
Temp	1	143.226	143.226	143.226	72.950	0.000**
Time	1	23.011	23.011	23.011	11.720	0.007**
Ratio	1	2.965	2.965	2.965	1.510	0.247
Square	3	17.340	17.340	5.780	2.940	0.085*
Temp*Temp	1	8.534	6.238	6.238	3.180	0.105*
Time*Time	1	3.966	4.840	4.840	2.470	0.147
Ratio*Ratio	1	4.840	4.840	4.840	2.470	0.147
Interaction	3	10.375	10.375	3.458	1.760	0.218
Temp*Time	1	3.125	3.125	3.125	1.590	0.236
Temp*Ratio	1	6.125	6.125	6.125	3.120	0.108*
Time*Ratio	1	1.125	1.125	1.125	0.570	0.467
Residual Error	10	19.633	19.633	1.963		
Lack-of-Fit	5	16.800	16.800	3.360	5.930	0.037**
Pure Error	5	2.833	2.833	0.567		
Total	19	216.550				

DF : degrees of freedom, **: significant, *: slightly significant

ANOVA is a statistical technique that subdivides the total variation in a set of data into component parts associated with specific source of variation for the purpose of testing hypotheses on the parameters of the model (Ravikumar *et al*., 2006). According to the ANOVA Tables XXI, XXII and XXIII, the $F_{statistic}$ values for all regressions be it IN, MB number or %Yield was very higher. The large value of *F* indicates that most of the variations in the response can be explained by the regression equation. Also, the associated *P* value is used to

estimated whether $F_{statistic}$ is large enough to indicate statistical significance (Ravikumar *et al*., 2006). In the case of IN and MB number, the impregnation ratio was found to have the greatest effect on these two responses, with the highest *F* value of 122.81 and 200.68 respectively while for %Yield, the activation temperature was found to have the highest effect with *F* value of 72.95. Nevertheless, a *P* value lower than 0.05 indicates that the model is considered to be statistically significant, *P* values between 0.05 and 0.10 are considered to be statistically less significant while those with P values greater than 0.100 are considered not significant.

The *P* values for all the overall regression models (for IN, MB number or %Yield) were lower than 0.05. This indicate that at least one of the terms in the different regression equations have a significant correlation with the response variables (Y_1, Y_2 and Y_3). The ANOVA tables of the different responses showed for each term for residual error, which measures the amount of variation in the response data unexplained by the model. The absence of the term for residual error in the different responses implies that the form of the model chosen to explain the relationship between the factors and the different responses is perfect. The analysis of variance (ANOVA) for the preparation of ACP indicates that the second-order polynomial model equations 44, 45 and 46 were highly significant and adequate to represent the actual relationship between the responses (IN, MB number and %Yield) and variables with very small *P* values (0.000 for each response) and a high correlation coefficient of determination (R^2 = 0.9588, 0.9719 and 0.9093 for IN, MB number and %Yield respectively).

This implies that 95.88 %, 97.19% and 90.93 % of the sample variation for IN, MB number and % yield respectively for the preparation of ACP are explained by the independent variables and this also means that the model did not explain only 4.12%, 2.81% and 9.07% of the sample variation for IN, MB number and %Yield respectively for ACP preparation. It also indicates that 95.88 %, 97.19% and 90.93 % of the total variation for IN, MB number and % yield respectively for the preparation of ACP was attributed to the experimental variable studied. The standard deviation of the three models (IN, MB number and % yield) were respectively 10.359, 2.7956 and 1.4012 for equation 44, 45 and 46 above which implies the experimental results are in close agreement with the predicted once.

III.2.1.3. Normal Probability Plot for the optimisation ACP preparation

The normal probability plot indicates whether the residuals follow a normal distribution, in which case the points will follow a straight line. The normality of the data can be checked by plotting a normal probability plot of the residuals. If the data points fall fairly close to the

straight line, then the data are normally distributed (Gonzàlez *et al.*, 2014). The statistical analysis of the data in terms of the standardized residual was conducted to verify the normality of the data. The normal probability plot of the residuals results of ACP is shown in Figure 38. The data points fairly close to the straight line indicate that the experiments came from a normally distributed population.

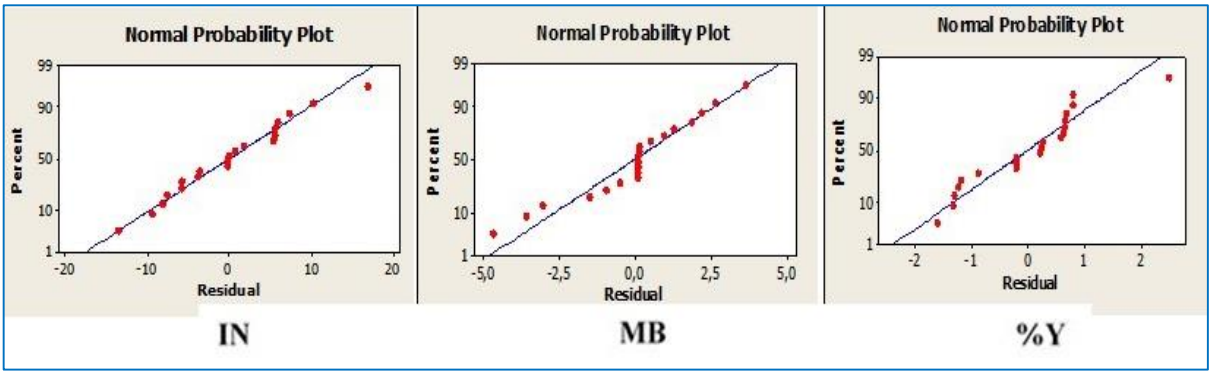

Figure 38: Normal probability plots for IN, MB and %Yield on ACP preparation

Then R^2 values of the different normal probability plot for the different responses (IN, MB number and % Yield) are summarized in the Table XXIV.

Table XXIV: Correlation coefficients of Responses for the preparation of ACP

Responses	**Y_1**	**Y_2**	**Y_3**
R^2	0.9588	0.9719	0.9093
R^2-Adjusted	0.9217	0.9466	0.8277

From Table XXIV, the R^2 values for the responses Y_1, Y_2 and Y_3 are respectively 0.9588, 0.9719 and 0.9093 while their respective R^2-Adjusted are 0.9217, 0.9466 and 0.8277. This implies that 95.88, 97.19 and 90.93 % of the theoretical value of IN, MB number and % yield respectively are closed to their experimental value. The more R^2 draws closer to unity the more the theoretical values are closer to the experimental value. This also an indication of good correlation between the experimental and the predicted values for the responses obtained from these three models and hence implies the results are reproducible. According to Lekene *et al*., 2019, for an optimisation model to be valid, it R^2-adjusted values most be ≥ 0.8. In this work, the R^2-adjusted are all greater than 0.8 for a confidence limit of 95% implying that the results are satisfactory with its respective optimisation equations and hence are in accordance with other authors in literation.

III.2.1.4. Interaction Effects

The Response surface graphs and contour plots of interaction of factors are shown in Figures 39 and 40 were chosen from the table of ANOVA regression coefficient for the responses studied. Compared to the effects of main factors, the effect of interaction of factors on the response are chosen based on the *P*-values from the ANOVA results, 5% was chosen as the minimum magnitude for any interaction to have an effect on the response. Any factor or interaction whose value is higher than 10 %, that factor or interaction was considered to have a negligible effect on the results under study. Factors or interactions whose *P*-values are less than 5 % are consider to be significant while those with P-values are found between 5 % and 10 % are regarded to be less significant.

i) Iodine Number measurement for ACP preparation

From the Table XX1, compared to the effects of main factors, the effect of interaction of factors on the response was studied and the interaction effects that are considered to be significant in the case of ACP production are the quadratic factors of X_1X_1, X_2X_2, X_3X_3 and only X_1X_2 interaction has a significant effect on the results (Y_1). The figure below shows the Surface response plots (3-Dimensional) (a) and contour plots (2-Dimensional) (b) of the respective interactions whose p-value have significant effects on the Iodine number measurement.

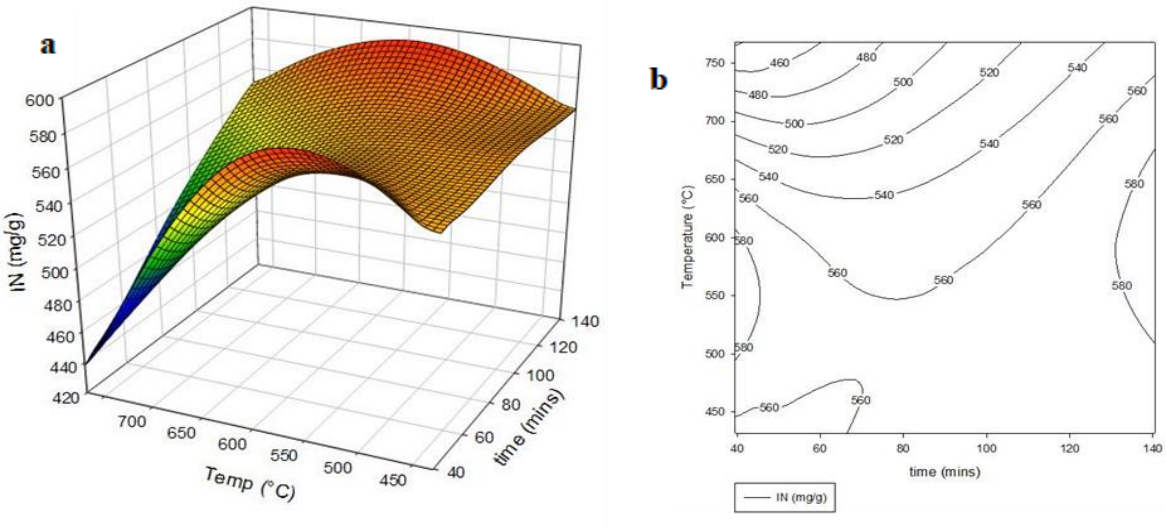

Figure 39: Surface Responds plot (a) and contour plot on IN number : Effect of variation of Temperature and time on the preparation of ACP

From Figure 39, it can be observed that, IN increases as the carbonization temperature and time increases up to a temperature of 600 °C and a resident time of 120 min. This is because as the temperature increases the amount of volatile matter eliminated increases favourising the development of micropores on the surface of the activated carbon up to a temperature of 600 °C. This can also perhaps be as a result of the fact that an increase in activation time and slight decrease in temperature (below 700 °C) leads to formation of micropores in the prepared ACP as the high temperature and longer activation time favours the Diels-Alder reaction which leads to rapid aromatization. This therefore develops the formation of the carbon skeleton. Further increase in temperatures greater than 600 °C, decreases slowly the IN and this is probably because, at temperatures greater than 600 °C, there is destruction of the carbon skeleton and the micropores hence turning them into larger pores which reduces the adsorption of iodine and hence decreases the IN. Similar observation was achieved be Aber *et al*. 2009.

Also, IN increases at higher temperatures with a lower resident time and decreases as the temperature increases and the resident time increases. This is due to the fact that higher temperature and lower resident time is just sufficient to eliminate the volatile matter and produce micro-pores. IN also increases at longer resident time but with lower temperature. This may be due to the fact that at lower temperature a longer resident time is sufficient for complete removal of organic/volatile matter for the development of micropores. IN decreases at longer or extended resident time and may be as a result of the breaking down of the micropore walls turning them into mesopores and macropores.

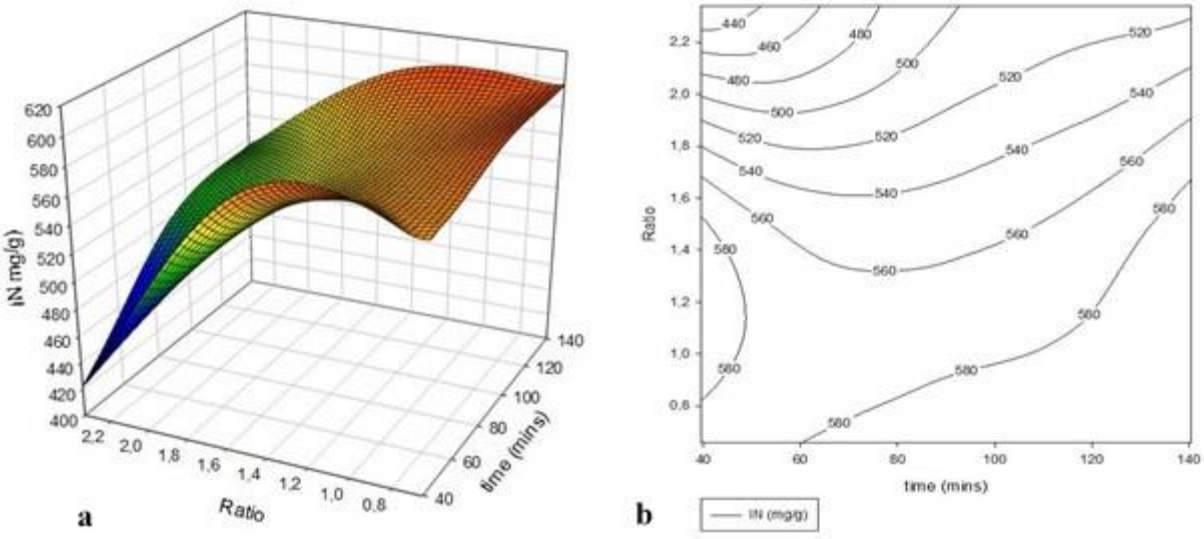

Figure 40: Surface Responds plot (a) and contour plot on IN number : Effect of variation of time and ratio on the preparation of ACP

As can be seen from Figure 40, IN increases with increase in activation time up to a resident time of 140 mins and decrease in IR. The increase in IN at longer activation time may be as a results of continous removal of volatile matter from the material. This therefore favours the developement of micropores hence increasing IN. It is also observed that as the activation time becomes longer at higher IR, the IN decreases. This might result from the breaking down of the walls of the micropores hence converting the micropores to mesopore as the activation time increases. The decrease in IN as the IR inreseases may certainly be resulting from the crumbling of the char skeleton as the activating agent concentration increases.

ii) Methylene Blue Number measurement for ACP

From Table XXII, compared to the effects of main factors (except the factor X_1), the effect of interaction of factors on the response was studied and the interaction effects that are considered to be significant in the case of ACP production is only X_1X_3 interaction has a significant effect on the results (Y_2). The contour plot (2-Dimensional) and Surface response plots (3-Dimensional) of the interaction X_1X_3 whose p-value have significant effect on the methylene blue number measurement are shown in Figure 41.

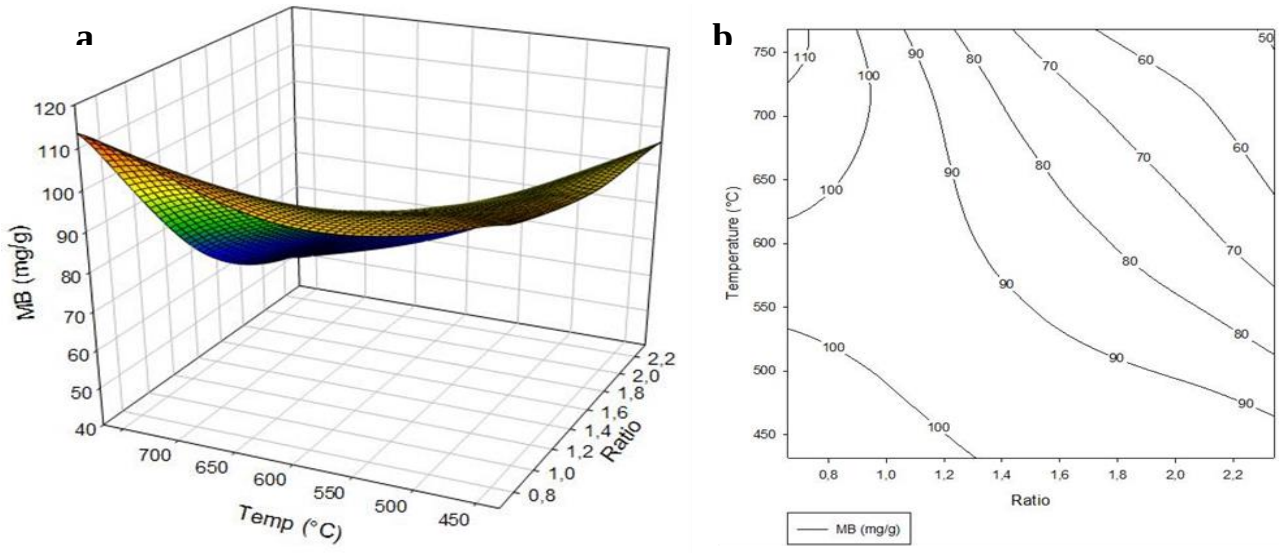

Figure 41: Surface Responds plot (a) and contour plot onMB number : Effect of variation of Temperature and Ratio on the preparation of ACP

The results of Figure 41 shows that MB number increases as the temperature increases and decrease in impregnation ratio. This is as a result of pore widening at higher temperatures. It decreases at higher temperature and higher impregnation ration due to destruction of the carbon skeleton by the high temperature and excess activating agent. Nevertheless, MB

increases with increase in impregnation ratio probably as a result of increase in the formation of mesopores which are more effective in adsorption. Also, MB number increases at lower temperature and high impregnation ratio. This may be attributed to the fact that lower temperature is just sufficient enough for the excess activating agent to produce more pores and consequently widen the existing pores of the activated carbon resulting to an increase in MB number. Kundu *et al*., observed similar situation. The higher MB number at higher impregnation ratio can be explain by the fact that the activating agent (H_3PO_4) reacts with the carbonate present in the biomass to produce CO_2 gas which on escaping at high temperatures favours the development and widening of pores. The proposed equation of the reaction can be represented as follows

$$2H_3\,PO_{4(aq)} + \quad 3CO^{2-}_{3(aq)} \rightarrow\ 2PO^{3-}_{4(aq)} +\ 3H_2\,O_{(l)} + 3CO_{2\,(g)} \ldots\ldots\ldots\ldots\ldots (47)$$

It can also be observed that further increase in activation temperature and impregnation ratio decreases the MB capacity. This may probably be as a result from excess dehydration by the activating agent and destruction of the mesopore walls turning them into larger macropores and probably destroying the carbon skeleton which reduces the adsorption capacity of MB.

iii) Percentage Yield (%Yield) measurement for ACP

From the Table XXIII, compared to the effects of main factors, the effect of interaction of factors on the response was studied and the interaction effects X_2X_3 are considered have slight significance on the %Yield in the case of ACP production. This implies that none of the interaction between factors (quadratic) any impact on the % Yield while only the X_2X_3 interaction within factors have an impact on the % Yield of the activated carbon activated with phosphoric acid. That's notwithstanding, it can be seen from the ANOVA table using the main factors that temperature has the highest effect on %Yield followed by the activation time. From the regression equation it can also be seen that temperature factor has an antagonistic effect with %Yield while time and ratio have synergic effect with %Yield with impregnation ratio having the highest synergic effect with magnitude of 20.636 meaning an increase in impregnation ratio increases the yield of ACP. The two variables were found to have significant effects on the activated carbon yield and also antagonistic interactions occurred between activation temperature and impregnation ratio. This behavior was attributed to the fact that, the reaction of lignocellulosic compounds with phosphoric acid begins as soon as the components are mixed. The acid first attacks hemicellulose and lignin because cellulose is more resistant to acid hydrolysis (Kouotou *et al*., 2013). At this stage, the acid will hydrolyse glycosidic linkages

in lignocellulosic and cleave aryl ether bond in lignin. These reactions are accompanied by further chemical transformations that include dehydration, degradation and condensation. As the temperature increase, the aromatic condensation reactions also take place among the adjacent molecules, which resulted in the evolution of gaseous products (CO_2, H_2O, CH_4, etc) from aromatic structure of the carbonised char leading to decrease in yield of the carbon. This observation is consistent with other authors (Kouotou *et al*., 2013).

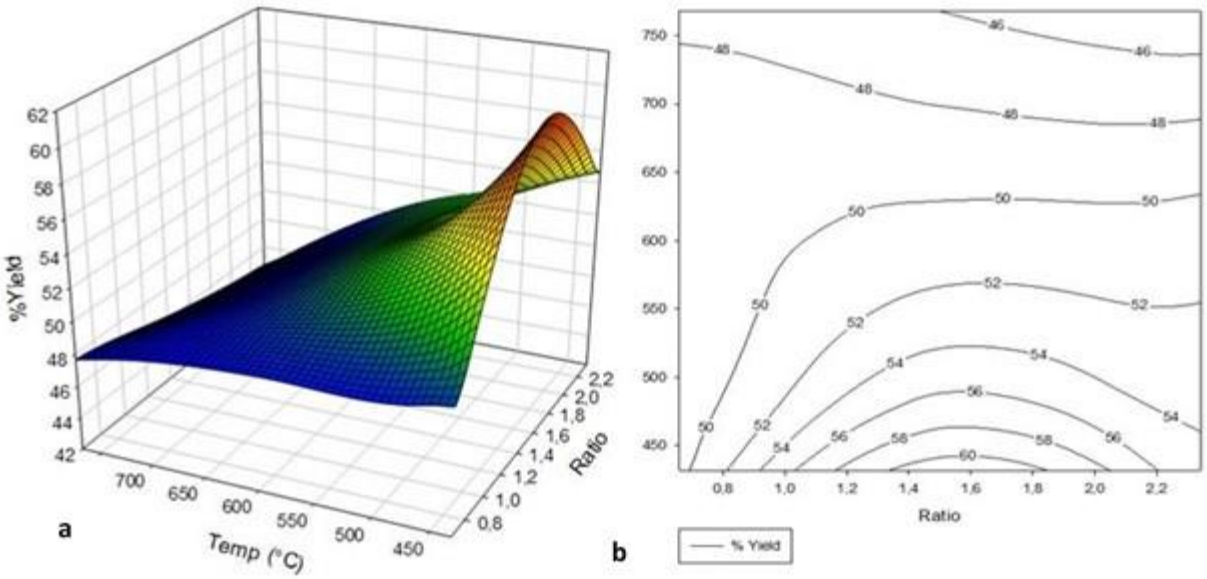

Figure 42: Surface Responds plot (a) and contour plot on %Yield number : Effect of variation of Temperature and Ratio on the preparation of ACP

Figure 42 presents the results of %Yield as a function of temperature and impregnation ratio. It is observed that the %Yield of the activated carbon indecreases at higher temperature and increases at lower temperature while in the case of the impregnation ratio, %Yield increase as the IR is increased. The decrease in %Yield at higher temperature is as a result of destruction of the carbon skeleton by the high temperation.

III.2.1.5. Validation Experiments of Response Optimisation of ACP preparation

In order to verify the optimization results, an experiment was performed under predicted conditions by the developed model. The model predicted a series of solutions as shown in Table XXV.

Table XXV: Predicted values of factors and responses to be tested

Sugested solution (s)	Factors			Predicted Response			Composite Desirability
	Temp(X_1)	Time (X_2)	Ratio(X_3)	IN (Y_1)	MB(Y_2)	%Yield (Y_3)	
L. S. (1)	431.821	39.546	0.659	671.598	101.914	51.317	1.000
L. S. (2)	431.822	140.454	0.659	590.089	98.961	52.608	0.965
L. S. (3)	768.179	140.454	0.659	560.800	108.587	43.129	0.575
L. S. (4)	768.179	39.5462	0.659	506.252	106.228	48.910	0.382
L. S. (5)	633.049	39.5462	0.957	589.706	98.358	49.523	0.934
L. S. (6)	431.821	139.090	1.917	533.756	99.000	57.245	0.696
L. S. (7)	431.844	39.5462	2.149	519.040	99.000	59.631	0.575
L. S. (8)	768.179	135.418	0.659	553.762	108.025	43.729	0.585
L. S. (9)	768.179	137.049	0.659	555.992	108.202	43.538	0.583
G. S.	431.821	39.5462	0.659	671.598	101.914	51.317	1.000

LS(1…9): Local solution number 1 to 9, GS: General solution

The tested experiments were chosen based on the cost (temperature, time, ratio), the response(s) awaited (IN, MB, %Yield) and most importantly on the desirability of the solution to give the required reponse. In this regard, LS n^o 5 and the GS was chosen for the verification test. The results of the test are given in Table XXVI.

Table XXVI: Theoretical and Experimental results for the validation prediction on ACP production

Experiment	Response	Theoretical results	Experimental results	% Difference
LS (5)	IN (mg/g)	589.706	599.626	1.654
	MB (mg/g)	98.358	99.375	1.023
	%Yield	49.523	51.720	4.567
GS	IN (mg/g)	671.598	685.287	1.998
	MB (mg/g)	101.914	98.876	2.981
	%Yield	51.317	53.660	4.366

LS(5): Local solution number 5, GS: General solution

From Table XXVI, all the experimental values obtained at these conditions are closely in agreement with the result obtained from the model and hence validated the findings optimization of the model. For further analysis and continuation of this work, only the ACP obtained from the general solution (GS) was used. This is not only due to it added advantage of high IN, MB and % Yield, but also due to its low preparation cost in the laboratory and industrial scale (Low temperature, small activation time).

III.2.2. Optimisation of the preparation condition of $ZnCl_2$ Activated carbon

After planification and modelisation. the experimented and predicted values obtained from the activated carbon based $ZnCl_2$ are given in Table XXVII.

Table XXVII: Experimental and Predicted Responses for ACZ production

Exp.	Variables			Y1 (IN)		Y2 (MB)		Y3 (Yield)	
No	X1	X2	X3	Exp.	Pred.	Exp.	Pred.	Exp.	Pred.
1	500.00	60.00	1.00	565.90	559.14	97.87	96.81	53.00	53.42
2	700.00	60.00	1.00	**655.77**	651.77	98.94	98.54	50.00	49.51
3	500.00	120.00	1.00	594.33	587.89	95.55	94.67	46.00	48.10
4	700.00	120.00	1.00	650.30	643.56	**99.08**	98.82	38.00	39.19
5	500.00	60.00	2.00	553.53	556.40	94.34	93.58	59.00	58.64
6	700.00	60.00	2.00	563.23	565.79	97.18	97.04	50.00	48.72
7	500.00	120.00	2.00	600.64	600.76	93.18	92.55	51.00	52.31
8	700.00	120.00	2.00	570.30	573.18	98.41	98.44	**37.00**	37.40
9	431.82	90.00	1.50	**552.57**	556.77	**88.38**	89.87	**61.00**	59.33
10	768.18	90.00	1.50	610.19	611.47	96.32	96.27	43.00	43.50
11	600.00	39.55	1.50	584.54	585.85	98.50	99.40	52.00	53.41
12	600.00	140.45	1.50	612.06	616.24	98.24	98.78	42.00	39.42
13	600.00	90.00	0.66	613.97	626.33	97.45	98.49	48.00	46.48
14	600.00	90.00	2.34	571.74	564.86	95.05	95.45	49.00	49.35
15	600.00	90.00	1.50	613.97	614.60	97.56	97.53	51.00	51.37
16	600.00	90.00	1.50	614.35	614.60	97.55	97.53	50.00	51.37
17	600.00	90.00	1.50	613.97	614.60	97.56	97.53	51.00	51.37
18	600.00	90.00	1.50	615.97	614.60	97.99	97.53	53.00	51.37
19	600.00	90.00	1.50	615.97	614.60	97.34	97.53	52.00	51.37
20	600.00	90.00	1.50	614.35	614.60	97.40	97.53	51.00	51.37

From Table XXVII, it can be seen that the IN for the ACZ varied 497.50 and 605.24 mg/g, the value for MB number varies been 62.32 and 99.46 mg/g, while the % Yield varies also between 45.00 and 61.00 %. Nevertheless, higher capacities of iodine and methylene blue adsorption was observed at lower temperature (experiment n^o 1 for both I_2/ACZ and MB/ACZ). On the contrary the highest % yield came from lower temperature (experiment n^o 9 for ACZ). This high IN and MB number corresponds to activating temperature of 500 °C, activation time of 60 minutes with an impregnation ration of 1 :1. That notwithstanding, lower adsorption of IN was observed at a temperature of 600 °C, activation time of 90 min and a correspondent impregnation ratio of 2.34 whereas the highest % yield corresponds to activating temperature

of 431.82 °C, activation time of 90 min and an impregnation ration of 1.5. It can also be seen that for all the cases, the Experimental results and the theoretical results are in conformity. For instance, looking at the highest values of IN, MB and % Yield, the difference between the theoretical and the experimental results are 1.55%, 0.51 and 4.10% respectively.

III.2.2.1. Estimated regression coefficient for the responses studied for ACZ

The individual runs of the experimental design shown in Table XXVII are conducted by using ACZ and the responses measured. A linear regression model was fitted for the experimental data using least square technique. The model coefficients, effects and standard error of the factors and interactions for the estimated regression, *T* and *P* values for all the linear, quadratic and interaction effects of the parameters are given in for IN, MB number and %Yield for the preparation of ACZ respectivelyare are shown in Tables XXVIII, XXIX and XXX.

Table XXVIII: Estimated regression coefficient of model terms and their effects on the response for IN (ACZ)

Factor/Term	DF	Coef	SE Coef	T	P-value
Constant	/	614.601	2.628	233.848	0.000**
X_1	1	16.264	1.744	9.327	0.000**
X_2	1	9.037	1.744	5.183	0.000**
X_3	1	-18.277	1.744	-10.481	0.000**
X_1X_1	1	-10.778	1.697	-6.349	0.000**
X_2X_2	1	-4.793	1.697	-2.823	0.018**
X_3X_3	1	-6.72	1.697	-3.959	0.003**
X_1X_2	1	-9.243	2.278	-4.057	0.002**
X_1X_3	1	-20.81	2.278	-9.134	0.000**
X_2X_3	1	3.901	2.278	1.712	0.118

DF : degrees of freedom, **: significant, *: slightly significant

Table XXIX: Estimated regression coefficient of model terms and their effects on the response for MB (ACZ)

Factor/Term	DF	Coef	SE Coef	T	P-value
Constant	/	97.526	0.364	268.219	0.000**
X_1	1	1.904	0.241	7.894	0.000**
X_2	1	-0.186	0.241	-0.772	0.458
X_3	1	-0.904	0.241	-3.749	0.004**
X_1X_1	1	-1.575	0.235	-6.706	0.000**
X_2X_2	1	0.553	0.235	2.356	0.040**
X_3X_3	1	-0.197	0.235	-0.839	0.421
X_1X_2	1	0.606	0.315	1.921	0.084*
X_1X_3	1	0.432	0.315	1.372	0.200
X_2X_3	1	0.279	0.315	0.886	0.396

DF : degrees of freedom, **: significant, *: slightly significant

Table XXX: Estimated regression coefficient of model terms and their effects on the response for %Yield on ACZ preparation

Factor/Term	Coef	SE Coef	T-value	P-value
Constant	51.367	0.699	73.455	0.000**
X_1	-4.706	0.464	-10.143	0.000**
X_2	-4.160	0.464	-8.967	0.000**
X_3	0.855	0.464	1.844	0.095*
X_1X_1	0.017	0.452	0.038	0.970
X_2X_2	-1.751	0.452	-3.876	0.003**
X_3X_3	-1.220	0.452	-2.702	0.022**
X_1X_2	-1.250	0.606	-2.062	0.066*
X_1X_3	-1.500	0.606	-2.474	0.033**
X_2X_3	-0.250	0.606	-0.412	0.689

DF: degrees of freedom, **: significant, *: slightly significant

Same as in the case of ACP, model coefficients are obtained by dividing the effects by two. *P*-value is the probability value that is used to determine the effects in the model that are

statistically significant in the case of ACZ. Factors having *P*-value less than 0.05 are considered to be statistically significant for a 95% confidence limit, slightly significant between 0.05 and 0.10 and insignificant above 0.10 (Tan *et al*., 2008).

In the case of IN, it was observed that the coefficients for the linear effect of all the factors temperature, time and ratio (with all having values of *P*= 0.000) for the preparation of ACZ were highly significant, including the quadratic effects which were also highly significant (*P* = 0.000, 0.018 and 0.003). With respect to interactions between factors, the X_1X_2 and X_1X_3 interactions were the most significant with *P* values of 0.002 and 0.000 respectively, while X_2X_3 interaction was insignificant (*P* = 0.118). With respect to Estimated regression coefficient of model terms and their effects on the response for MB (ACZ), the coefficients for the linear effect of the factors Temperature and ratio (*P*= 0.000 and 0.004) for the preparation of ACZ were the most significant as X_2 (time with *P* = 0.458) was insignificant. The X_1X_1 and X_2X_2 quadratic effects were also significant with *P* values of 0.000 and 0.040 respectively. None of the interaction effects were significant (*P* = 0.084, 0.200 and 0.396) for respectively X_1X_2, X_2X_3 and X_1X_3 interactions. Looking at the estimated regression coefficient of model terms and their effects on the response for %Yield (ACZ), it can be seen that, the coefficients for the linear effect of the temperature and time factors (*P*= 0.000 and 0.000) given that ratio factor was insignificant (*P* = 0.095) for the preparation of ACZ. The quadratic effects of X_2X_2 and X_3X_3 *P* values of 0.003 and 0.022 were significant whereas the X_1X_1 quadratic effect (*P* = 0.970) was insignificant. In the case of factors interaction during the preparation, only the X_1X_3 (*P* = 0.033) was significant as X_1X_2 was slightly significant and X_2X_3 were insignificant interactions (*P* values of 0.066 and 0.689 respectively). Judging from the *P* value of X_1X_2 of 0.066, this interaction may be seen as slightly significant as it if closer to 0.05. The significance of these interaction (those with *P* values < 0.05), would have been lost if the preparation of the ACZ was carried out under conventional or classical methods. The resulting model can be represented using the second order polynomial model as:

$$Y_1 = 614.601 + 116.264X_1 + 9.037X_2 - 18.277X_3 - 10.778X_1X_1 - 4.793X_2X_2 - 6.720\,X_3X_3 - 9.243X_1X_2 - 20.810X_1X_3 + 3.901X_2X_3 \quad \ldots\ldots\ldots\ldots\ldots\ldots\ldots\ldots\ldots\ldots\ldots\ldots\ldots\ldots\ldots (48)$$

$$Y_2 = 97.5263 + 1.9044X_1 - 0.1862X_2 - 0.9043X_3 - 1.5749X_1X_1 + 0.5534X_2X_2 - 0.1971\,X_3X_3 + 0.6056X_1X_2 + 0.4324X_1X_3 + 0.2794X_2X_3 \quad \ldots\ldots\ldots\ldots\ldots\ldots\ldots (49)$$

$$Y_3 = 51.3668 - 4.7062X_1 - 4.1604X_2 + 0.8554X_3 + 0.0172X_1X_1 - 1.7505X_2X_2 - 1.2202\,X_3X_3 - 1.2500X_1X_2 - 1.5000X_1X_3 - 0.2500X_2X_3 \quad \ldots\ldots\ldots\ldots\ldots\ldots\ldots (50)$$

After estimating the main effects, the effect of interactions was determined by performing the analysis of variance (ANOVA). Sum of squares (SS) of each factor quantifies its importance in the process and as the value of SS increases, the significance of the corresponding factor in the process also increases. The ANOVA results for the production of ACZ were presented in Tables XXXI, XXXII and XXXIII.

III.2.2.2. Analysis of Variance (ANOVA) results for the preparation of ACZ

After estimating the main effects, the effect of interactions were determined by performing the analysis of variance (ANOVA). Sum of squares (SS) of each factor quantifies its importance in the process and as the value of SS increases, the significance of the corresponding factor in the process also increases. The ANOVA results for the IN, MB number and %Yield measurements for ACZ are presented in Tables XXXI, XXXII and XXXIII respectively.

Table XXXI: Analysis of Variance (ANOVA) results for IN for ACZ

Source	DF	Seq SS	Adj SS	Adj MS	F-value	P-value
Regression	9	15849.600	15849.600	1761.060	42.410	0.000**
Linear	3	9289.800	9289.800	3096.610	74.570	0.000**
Temp	1	3612.500	3612.500	3612.470	86.990	0.000**
Time	1	1115.300	1115.300	1115.330	26.860	0.000**
Ratio	1	4562.000	4562.000	4562.030	109.860	0.000**
Square	3	2289.900	2289.900	763.300	18.380	0.000**
Temp*Temp	1	1391.500	1674.000	1673.950	40.310	0.000**
Time*Time	1	247.700	331.000	331.010	7.970	0.018**
Ratio*Ratio	1	650.700	650.700	650.720	15.670	0.003**
Interaction	3	4269.800	4269.800	1423.270	34.270	0.000**
Temp*Time	1	683.400	683.400	683.430	16.460	0.002**
Temp*Ratio	1	3464.600	3464.600	3464.620	83.430	0.000**
Time*Ratio	1	121.800	121.800	121.770	2.930	0.118
Residual Error	10	415.300	415.300	41.530		
Lack-of-Fit	5	410.700	410.700	82.150	91.020	0.000**
Pure Error	5	4.500	4.500	0.900		
Total	19	16264.800				

DF : degrees of freedom, **: significant, *: slightly significant

Table XXXII: Analysis of Variance (ANOVA) results for MB for ACZ

Source	DF	Seq SS	Adj SS	Adj MS	F-value	P-value
Regression	9	109.464	109.464	12.163	15.300	0.000**
Linear	3	61.174	61.174	20.391	25.660	0.000**
Temp	1	49.532	49.532	49.532	62.320	0.000**
Time	1	0.473	0.473	0.474	0.600	0.458
Ratio	1	11.169	11.169	11.168	14.050	0.004**
Square	3	43.235	43.235	14.412	18.130	0.000**
Temp*Temp	1	37.898	35.743	35.743	44.970	0.000**
Time*Time	1	4.777	4.413	4.4123	5.550	0.040**
Ratio*Ratio	1	0.560	0.560	0.560	0.700	0.421
Interaction	3	5.054	5.054	1.685	2.120	0.161
Temp*Time	1	2.934	2.934	2.934	3.690	0.084*
Temp*Ratio	1	1.496	1.496	1.496	1.880	0.200
Time*Ratio	1	0.624	0.624	0.624	0.790	0.396
Residual Error	10	7.948	7.948	0.795		
Lack-of-Fit	5	7.692	7.692	1.538	30.020	0.001**
Pure Error	5	0.256	0.256	0.051		
Total	19	117.412				

DF : degrees of freedom, **: significant, *: slightly significant

Table XXXIII: Analysis of Variance (ANOVA) results for % Yield for ACZ

Source	DF	Seq SS	Adj SS	Adj MS	F	P
Regression	9	641.151	641.151	71.239	24.230	0.000**
Linear	3	548.857	548.857	182.952	62.230	0.000**
Temp	1	302.480	302.480	302.480	102.890	0.000**
Time	1	236.385	236.385	236.385	80.410	0.000**
Ratio	1	9.992	9.992	9.992	3.400	0.095*
Square	3	61.294	61.294	20.431	6.950	0.008**
Temp*Temp	1	1.197	0.004	0.004	0.000	0.970
Time*Time	1	38.641	44.161	44.161	15.020	0.003**
Ratio*Ratio	1	21.457	21.457	21.457	7.300	0.022**
Interaction	3	31.00	31.000	10.333	3.510	0.057*
Temp*Time	1	12.500	12.500	12.500	4.250	0.066*
Temp*Ratio	1	18.00	18.000	18.000	6.120	0.033**
Time*Ratio	1	0.500	0.500	0.500	0.170	0.689
Residual Error	10	29.399	29.399	2.940		
Lack-of-Fit	5	24.065	24.065	4.813	4.510	0.062*
Pure Error	5	5.333	5.333	1.067		
Total	19	670.550				

DF : degrees of freedom, **: significant, *: slightly significant

According to the ANOVA Table XXXI, XXXII and XXXIII, the $F_{statistic}$ values for all regressions be it IN, MB number or %Yield were higher. The large the value of *F* indicates that most of the variations in the response can be explained by the regression equation. Also, the associated *P* value is used to estimate whether $F_{statistic}$ is large enough to indicate statistical significance (Ahmad and Alrozi, 2010; Lekene *et al.*, 2019). In the case of IN, the impregnation ratio was found to have the greatest effect on this response, with the highest *F* value of 109.86. This factor was closely followed by temperature whose *F* value is 86.99. This implies that temperature and impregnation ratio were have dominate effect interms of the linear factors (Tan *et al.*, 2008). In terms of interaction, X_1X_1 was dominant with *F* value of 40.31 and for the interaction, X_1X_3 was dominate with *F* value of 83.43. Looking at the MB number, temperature (X_1) had the highest effect *F* value of 62.32 in terms of linear factors whereas X_1X_1 had the

highest effect in terms of quadratic interaction. With respect to %Yield, activation temperature had the highest effect (F= 102.89) and was closely followed by activation time (F = 80.01) in terms of linear effect given that impregnation ration was no significant. Nevertheless, a P value lower than 0.05 indicates that the model is considered to be statistically significant.

The P values for all the for the overall regression models (that for IN, MB number or %Yield) were lower than 0.05. This indicate that at least one of the terms in the different regression equations have a significant correlation of 0.000 with the response variables (Y_1, Y_2 and Y_3). The ANOVA tables of the different responses also show for each a term for residual error, which measures the amount of variation in the respond data unexplained by the model. The absence of the term for residual error in the different responses implies that the form of the model chosen to explain the relationship between the factors and the different responses are correct. The analysis of variance (ANOVA) for the preparation of ACZ indicates that the second-order polynomial model equations 48, 49 and 50 above were highly significant and adequate to represent the actual relationship between the responses (IN, MB number and %Yield) and variables with very small P values (0.000 for each response) and a high correlation coefficient of determination (R^2 = 0.9745, 0.9323 and 0.9562 for IN, MB number and %Yield respectively).

This implies that 97.45 %, 93.23% and 95.62 % of the sample variation for IN, MB number and % yield respectively for the preparation of ACZ are explained by the independent variables and this also means that the model did not explain only 2.55%, 6.77% and 4.38% of the sample variation for IN, MB number and %Yield respectively for ACZ preparation (Zhang *et al*., 2011). It also indicates that 97.45 %, 93.23% and 95.62 % of the total variation for IN, MB number and % yield respectively for the preparation of ACZ was attributed to the experimental variable studied. The standard deviation of the three models (IN, MB number and % yield) were respectively 6.4408, 0.891526 and 1.71460 for equations 48, 49 and 50 which implies the experimental results are in close agreement with the predicted once.

III.2.2.3. Normal Probability Plot for ACZ preparation

The normal probability plot indicates whether the residuals follow a normal distribution, in which case the points will follow a straight line. The normality of the data can be checked by plotting a normal probability plot of the residuals. If the data points fall fairly close to the straight line, then the data are normally distributed (Antony, 2003). The statistical analysis of the data in terms of the standardized residual was conducted to verify the normality of the data.

The normal probability plot of the residuals of ACZ is shown in Figure 43. The data points fairly close to the straight line indicate that the experiments came from a normally distributed population.

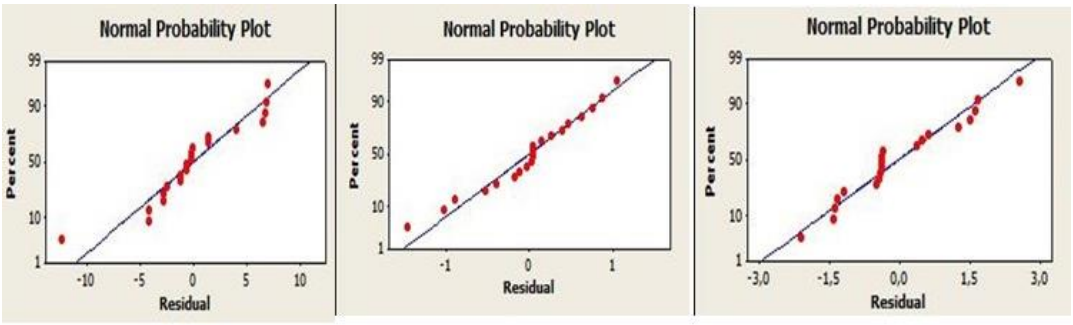

Figure 43: Normal probability plots for IN, MB and %Yield on ACZ preparation

Then R^2 values of the different normal probability plot for the different responses (IN, MB number and % Yield are summarized in Table XXXIV.

Table XXXIV: Correlation coefficients of Responses for the preparation of ACZ

Responses	**Y_1**	**Y_2**	**Y_3**
R^2	0.9745	0.9323	0.9562
R^2-Adjusted	0.9515	0.8714	0.9167

From the Table XXXIV, the correlation coefficient (R^2) values for the responses Y_1, Y_2 and Y_3 are respectively 0.9588, 0.9719 and 0.9093 while their respective R^2-Adjusted are 0.9217, 0.9466 and 0.8277. This implies that 95.88, 97.19 and 90.93 % of the theoretical value of IN, MB number and % Yield respectively are closed to their experimental value. This also indicate that there was a good agreement between the experimental and the predicted values for the responses obtained from these three models and that the results can be reproducible. This also implies that the experiments are carried out under good conditions are that the results can be reproducible. According to Lekene *et al*., 2019, for an optimisation model to be valid, it R^2-adjusted values most be ≥ 0.8. In this work, the R^2-adjusted are all greater than 0.8 for a confidence limit of 95% implying that the results are a satisfactory with its respective optimisation equations and are in accordance to with other authors in literation.

III.2.2.4. Interaction effects for the surface response optimisation of ACZ preparation

The Response surface graphs and contour plots of interaction of factors are shown in Figures 35 and 36; and were chosen from the table of Estimated regression coefficient for the responses studied. Compared to the effects of main factors, the effect of interaction of factors on the response are chosen based on the p-values from the ANOVA results. 5% was chosen as the minimum magnitude for any interaction to have an effect on the response. Any factor or interaction whose value is higher than 10%, that factor or interaction was considered to have a negligible effect on the results under study.

i) Iodine Number (IN) measurement for ACZ preparation

From Table XXXI, apart from the effects of main factors, the effect of interaction of factors on the response was studied and the interaction effects that are considered to be significant in the case of ACZ production are the quadratic factors of X_1X_1, X_2X_2, X_3X_3 and the interaction/interactive effects of X_1X_2 and X_1X_3 interactions, that have significant effects on the results (Y_1). The figure below shows the Surface response plots (3-Dimensional) (a) and contour plots (2-Dimensional) (b) of the respective interactions whose *P*-value have significant effects on the Iodine number measurement.

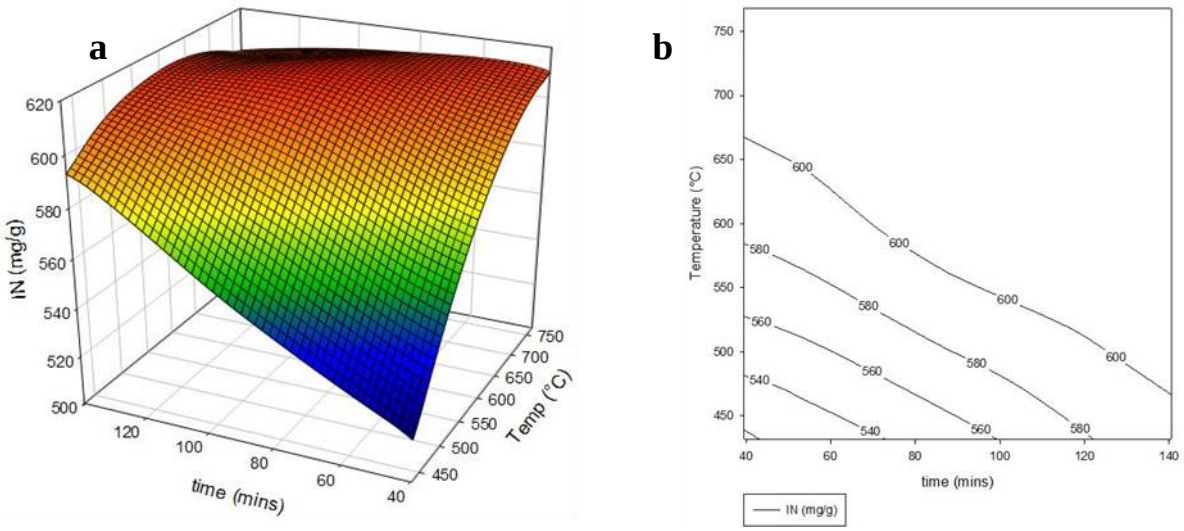

Figure 44 : Surface Responds plot (a) and contour plot on IN: Effect of variation of Temperature and time on the preparation of ACZ

With respect to Figure 44, it can be observed that, IN increases as the carbonisation temperature and time increases up to a temperature of 650 °C and a resident time of 120 mins. This can be attributed to the fact that as the temperature increases the amount of volatile matter eliminated increases favorising the development of micropores on the surface of the activated

carbon up to a temperature of 650 °C. This can also be perhaps as a result of an increases in activation and formation of micropores in the prepared ACZ. Further increase in temperatures that is greater than 600 °C, the IN decreases slowly and this is probably be because, at temperatures greater than 600 °C, there is destruction of the carbon skeleton and the micropores hence turning them into larger pores which reduces the adsorption of iodine and hence decreases the IN. Also, IN increases at higher temperatures with a lower resident time and decreases as the temperature increases and the resident time increases. This is due to the fact that higher temperature and lower resident time is just sufficient to eliminate the volatile matter and produce micro-pores. IN also increases at longer resident time but with lower temperature. This may be due to the fact that at lower temperature a longer resident time is sufficient for complete removal/elimination of organic/volatile matter for the development of micropores. IN decreases at longer or extended resident time and may be as a result of the breaking/collapsing down of the micropore walls turning them into mesopores and macropores.

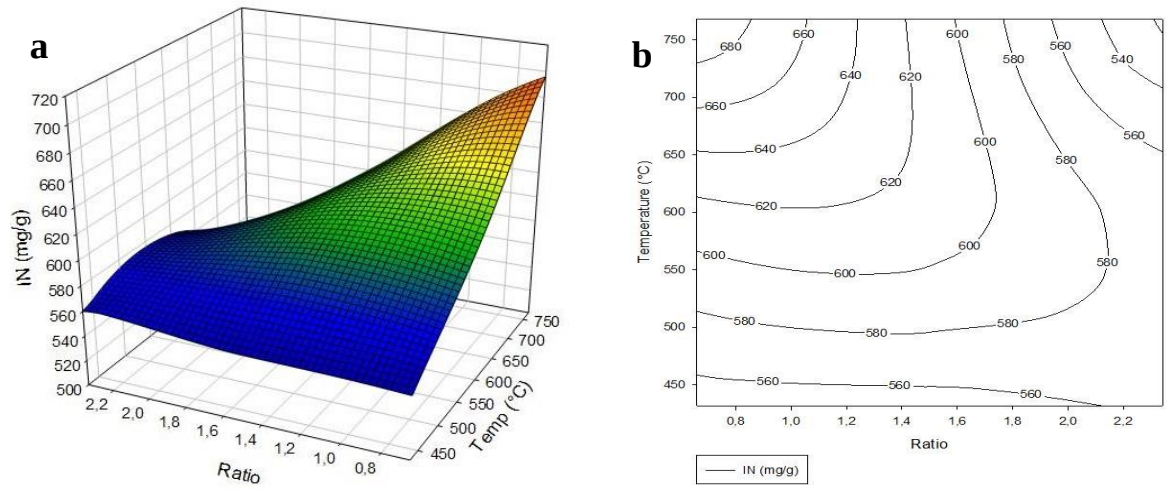

Figure 45 : Surface Responds plot (a) and contour plot on IN: Effect of variation of Temperature and Ratio on the preparation of ACZ

Looking at Figure 45, IN increases as carbonisation temperature increases from 450 °C to 750 °C and impregnation ratio decreases from 2.2 to 0.8, IN value of increases to 680 mg/g. IN increases at high temperature due to elimination of organic/volatile matter from the biomass, restructuration of the carbon skeleton and the fact that the decomposition of $CaCO_3$ to produce CO_2 gas favors the production of micropores on the activated carbon. This implies that activated temperature had a synergic effect with IN while impregnation ratio has an antagonistic effect with IN adsorption. The decrease in IN at lower temperature may be due lower rate of volatile matter elimination while the decrease in IN at higher impregnation ratio

may attributed to destruction of the skeleton by the excess activating agent. It is also observed that at higher temperature and impregnation ratio, IN decreases drastically due to destruction and widening of the micropore walls of the carbon ACZ by the high temperature and excess activating agent.

The proposed equation for the action of the activating agent (ZnCl2) on the precursor was thought to start principally with the carbonate as demonstrated as follows:

$$ZnCl_2 \quad + \quad CaCO_3 \longrightarrow CaCl_2 + ZnCO_3 \quad \text{.....(51)}$$

After activation, the $ZnCO_3$ could decomposed to produced zincite, liberating CO_2 as proposed in the equation below.

$$ZnCO_{3_{(s)}} \quad \longrightarrow \quad ZnO_{(s)} + CO_{2_{(g)}} \text{.....(52)}$$

It is belived that the CO_2 generated could develop more pores (increase the porosity) of the AC.

ii) Methylene Blue Number (MB) measurement for ACZ preparation

From Table XXXII, compared to the effects of main factors (except the factor X_2 which is not significant), the effect of interaction of factors on the response was studied and the interaction effects that are considered to be significant in the case of ACZ production are the quadratic factors of X_1X_1, X_2X_2 (except the factor X_3X_3 which is not significant). The interaction effects that are considered have no significance on the MB number in the case of ACZ production. This implies that none of the interaction between factors (quadratic) nor within factors have any impact on the % Yield of the activated carbon activated with zinc chloride. Nevertheless, it can be seen from the ANOVA table using the main factors that, temperature has the highest synergic effect on MB number adsorption while time and ratio both have antagonist effect of MB adsorption.

Figure 46 presents the results of responds surface and the contour plots of Methylene blue adsorption as a function of time and temperature.

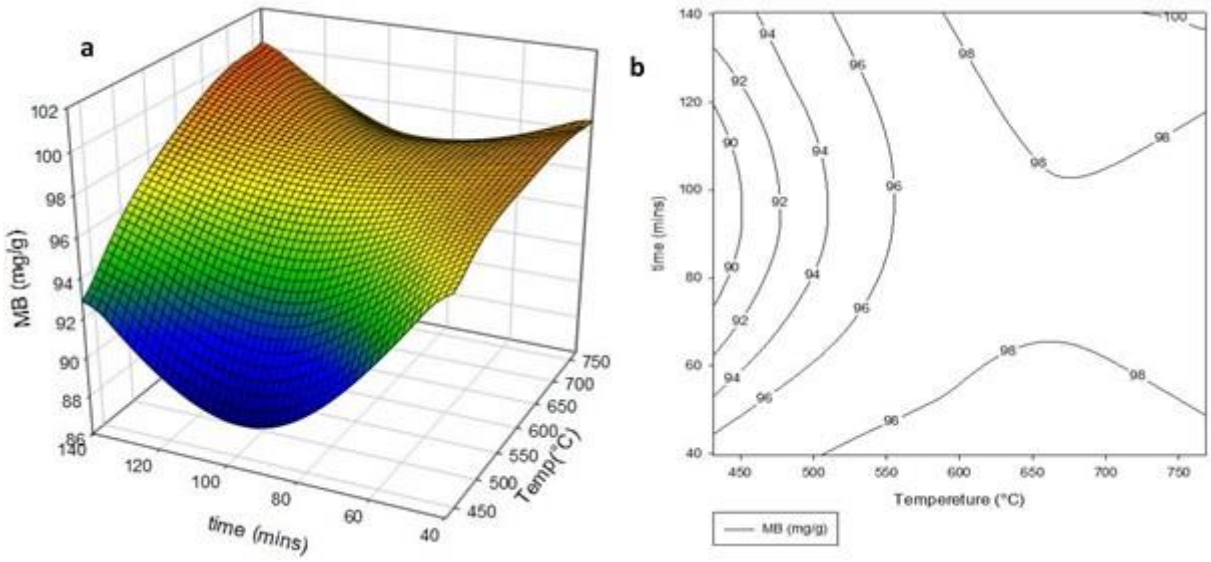

Figure 46 : Surface Responds plot (a) and contour plot on MB number : Effect of variation of Temperature and time on the preparation of ACZ

From Figure 46, MB number increases with increase in activation time and carbonisation temperature. This is as a result of pore enlargement resulting from the high carbonisation temperature and longer activation time. This leads to widening of the micropore wall to form mesopores hence increasing the quantity of MB adsorbed. MB number decreases at lower carbonisation temperature. This might result from decrease in the rate of volatilisation of the volatile matter and condensate gases which condenses and blocks the some of the pores. The high MB number at high temperature and longer activation time can also be explained by the fact that the activating agent ($ZnCl_2$) reacts with the carbonate present in the biomass and decomposes at high temperature to produce CO_2 gas as shown by equation 51 and 52. The CO_2gas produce on escaping at high speed widens the pores hence increasing the MB number.

iii) Percentage yield (%Yield) measurement for ACZ preparation

From Table XXXIII, compared to the effects of main factors (except the factor X_1), the effect of interaction of factors on the response was studied and the interaction effects that are considered to be significant in the case of ACZ production is only X_1X_3 interaction has a significant effect on the results (Y_3) (*P*-value less than 0.05) while X_1X_2 interaction was only slightly significant (*P*-value between 0.05 and 0.10).

Figure 48 shows the contour plot (2-Dimensional) and Surface response plots (3-Dimensional) of the interaction X_1X_3 on the %Yield.

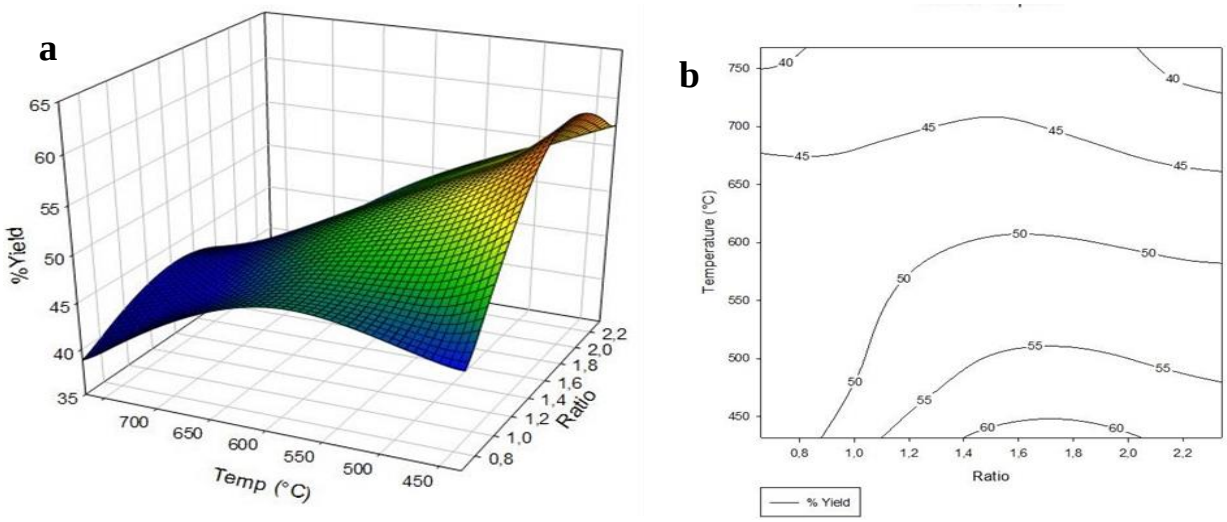

Figure 47: Surface Responds plot (a) and contour plot on % Yield : Effect of variation of Temperature and Ratio on the preparation of ACZ

The graphs of Figure 47 shows that, as the temperature increases, the %Yield of the ACZ decreases and increases as the carbonisation temperature decreases. This implies that an increase in activating temperature from 430 °C to 750 °C and an increase in impregnation ratio from 0.8 to 2.2, % Yield reduces. This may be attributed to a remarkable degradation of the microstructure of the ACZ. Such degradation conducted to relatively important mass losses. This mass effect becomes more and more noticeable as the temperature increases resulting to a progressive decrease in the global yield of the process. The activation temperature therefore has a negative effect on carbon yield (ANOVA table of %Yield). Also, as the %yield increases as the impregnation ratio increases and carbonisation temperature decreases. The response surface shows a curvature indicating that the interaction effect between activation temperature and impregnation ratio on the yield is pronounced. The two variables were found to have significant effects on the activated carbon yield and also antagonistic interactions occurred between activation temperature and impregnation ratio. This behavior was attributed to the fact that, the reaction of lignocellulosic compounds with phosphoric acid begins as soon as the components are mixed. The acid first attacks hemicellulose and lignin because cellulose is more resistant to acid hydrolysis (Kouotou *et al*., 2013). At this stage, the acid will hydrolyse glyosidic linkages in lignocellulosic and cleave aryl ether bond in lignin. These reactions are accompanied by further chemical transformations that include dehydration, degradation and condensation. As the temperature increase, the aromatic condensation reactions also take place among the adjacent molecules, which resulted in the evolution of gaseous products (CO_2, H_2O, CH_4, etc) from aromatic structure of the carbonised char leading to decrease in yield of the carbon. This

observation is consistent with other authors (Kouotou *et al*., 2013). According to the polynomial equation, the impregnation ratio is another critical parameter that affects the activated carbon yield.

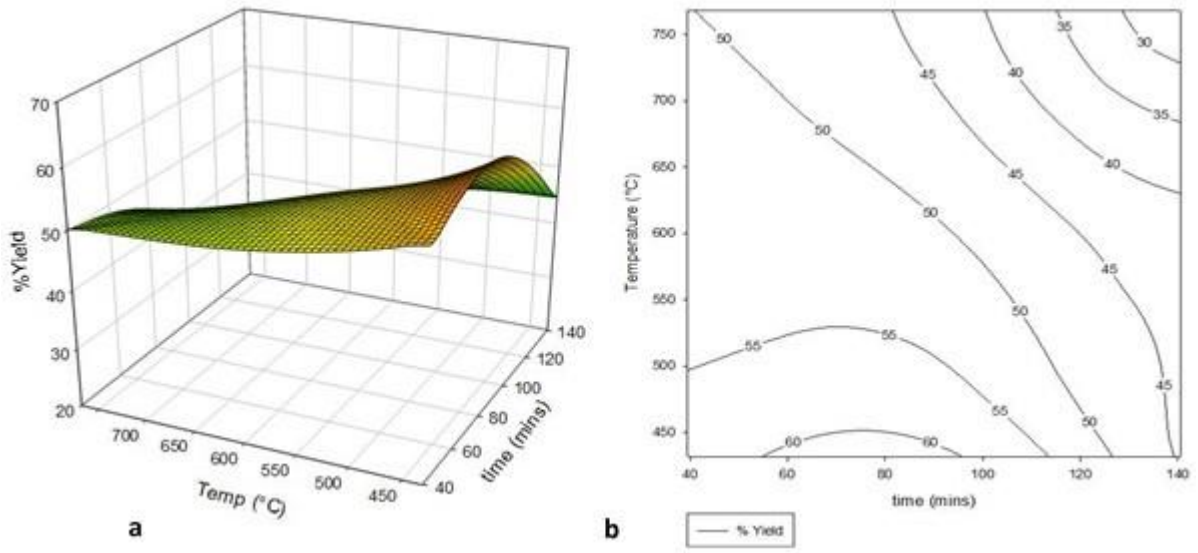

Figure 48: Surface Responds plot (a) and contour plot on % Yield : Effect of variation of Temperature and time on the preparation of ACZ

Figure 48 presents the results of %Yield as a function of temperature and time. It is observed that when the carbonisation temperature and activation time increases, the %Yield decreases and increases at lower carbonisation temperature and activation time. The decrease in %Yield at higher temperature and longer activation time might be as a result of destruction of the carbon skeleton by the high temperation.

III.2.2.5. Validation Experiments of Response Optimisation for ACZ preparation

In order to verify the optimization results, an experiment was performed under predicted conditions by the developed model. The model predicted a series of solutions for ACZ as shown on the Table XXXV.

Table XXXV: Predicted values of factors and responses to be tested

Sugested solution (s)	Factors			Predicted Response			Composite Desirability
	Temp(X_1)	Time (X_2)	Ratio(X_3)	IN (Y_1)	MB(Y_2)	%Yield (Y_3)	
L. S. (1)	591.506	43.623	1.050	601.352	100.119	51.629	1.000
L. S. (2)	744.142	39.546	1.375	622.595	97.585	49.840	0.9604
L. S. (3)	431.821	140.454	2.341	604.703	86.897	52.441	0.514
L. S. (4)	530.275	52.038	0.755	568.803	98.975	50.000	0.882
L. S. (5)	537.118	39.546	1.250	565.785	99.000	53.639	0.867
L. S. (6)	464.312	58.710	0.659	516.057	96.136	49.699	0.498
L. S. (7)	758.674	39.547	1.673	588.413	96.584	48.797	0.863
L. S. (8)	729.541	110.220	1.212	635.723	98.030	40.927	0.442
L. S. (9)	536.982	113.445	2.341	586.199	93.426	49.883	0.800
G. S.	591.506	43.623	1.050	601.352	100.119	51.629	1.000

LS(1…9): Local solution number 1 to 9, GS: General solution

The tested experiments were chosen based on the cost (temperature, time, ratio), the awaited response(s) (IN, MB, %Yield) and most importantly on the desirability of the solution to give the required response. In this regard, LS n^o 2 and the GS was chosen for the verification test. The results of the test are given in the Table XXXVI.

Table XXXVI: Theoretical and Experimental results for the validation prediction on ACP production

Experiment	Response	Theoretical results	Experimental results	% Difference
LS (2)	IN (mg/g)	622.595	628.180	0.889
	MB (mg/g)	97.585	98.375	0.803
	%Yield	49.840	50.200	0.717
GS	IN (mg/g)	601.352	609.144	1.279
	MB (mg/g)	100.119	98.358	1.759
	%Yield	51.629	52.730	2.088

LS(2): Local solution number 2, GS: General solution

From Table XXXVI, all the experimental value obtained at these conditions are closely in agreement with the result obtained from the model and hence validated the findings of the optimization as the difference between the theoretical and experimental results were all less than 5%. For further analysis and continuation of this work, only the ACZ obtained from the GS was used. This is not only due to it added advantage of high IN, MB and % Yield, but also due to its low cost of production in the laboratory and industrial scale (Low temperature, small activation time).

III.3. IN and MB number Characterization of Preparation of Silver nanoparticle loaded activated carbon nanocomposite

The different nanocoposite materials prepared were characterised using IN and MB number with the aim of increasing their respective antibacterial properties witout destroying their respective adsorption properties. The results obtained (see ata in appendix A, Table A-3, page 219) are shown in Figure 49.

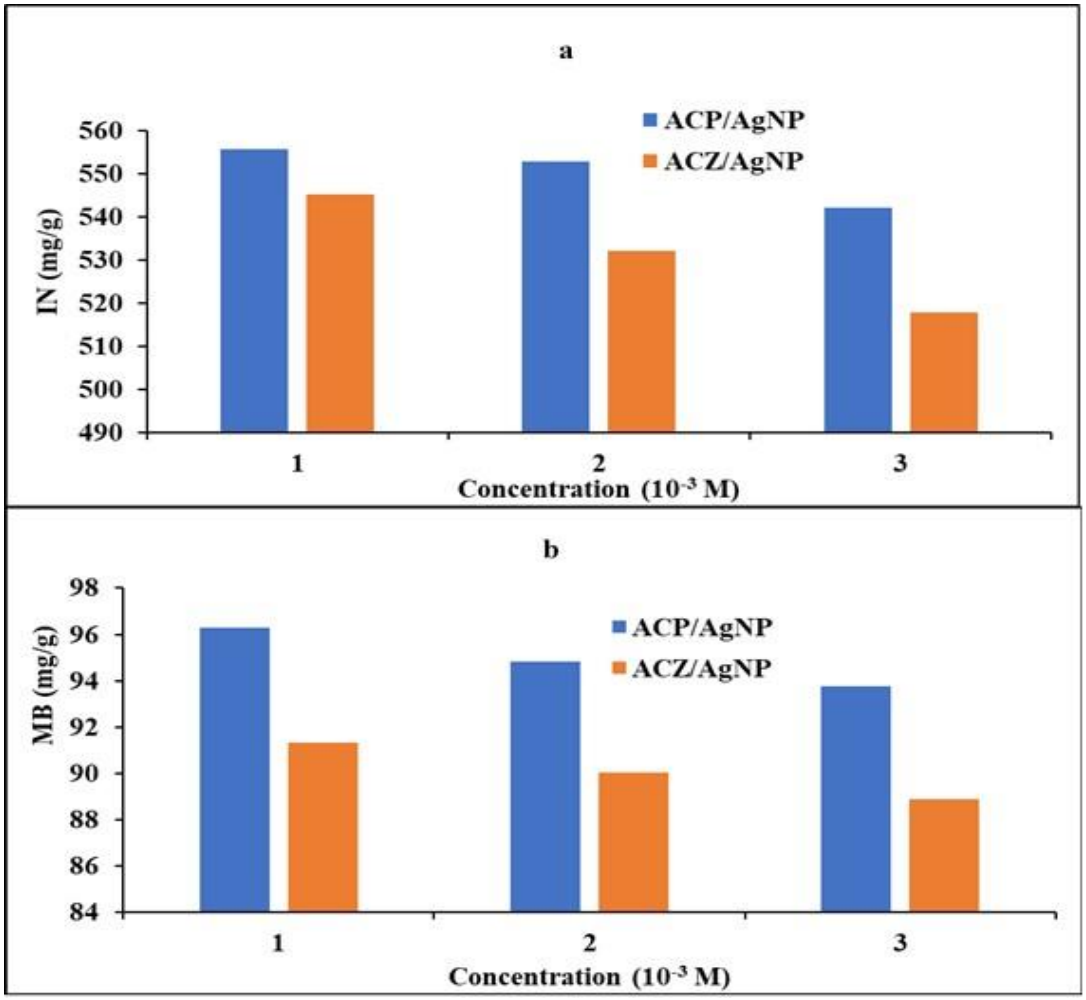

Figure 49: Graphs of IN (a) and MB number (b) test on ACP/AgNP and ACZ/AgNP

From Figure 49, it can be seen that there was a sharp drop followed by a gradual decrease both IN and MB number for the two carbons (ACP/AgNP and ACZ/AgNP) as the concentration of the $AgNO_3$ used in the preparation of the nanoparticles increases. This might be due to the fact that as the concentration of solution increases, more of the nanoparticles are formed and subsequently precipitated on the surface of the activated carbons (ACP and ACZ) to form the ACP/AgNP and ACZ/AgNP materials. The continuous precipitation may of the AgNPs on the surface of the ACs may result in the nanoparticles occupying the micro and meso pores of the activated carbons leading to a decrease in the quantities of Iodine and methylene blue adsorbed hence decreasing the IN and MB number respectively. Furthermore, the percentage decrease of the doped carbons from the original carbons was 8.238 % and 16.835 (for IN); 3.177% and 7.827% (for MB number) for ACP/AgNP and ACZ/AgNP respectively. It was also observed that the percentage decrease in the case on ACZ/AgNP is twice that of ACP/AgNP. This indicates that more of the micro pores were blocked in the case of ACZ/AgNP than in the case of ACP/AgNP. Nevertheless, the percentage decrease in both case was less than 20%

confirming the aim of this doping process which was to precipitate AgNPs on the surface of the activated carbons (to increase it antibacterial properties) without destroying its adsorption capacity (IN and MB number respectively).

III.4. Characterisation of the Prepared ACs and the composites

III.4.1. Determination of oxygen containing functional groups ACP, ACZ, ACP/AgNP and ACZ/AgNP

The Bohem titration method was used to quantify the different functional groups present on the activated carbons and their respective composites. Figure 57 presents the results carried out on ACP, ACZ, ACP/AgNP and ACZ/AgNP.

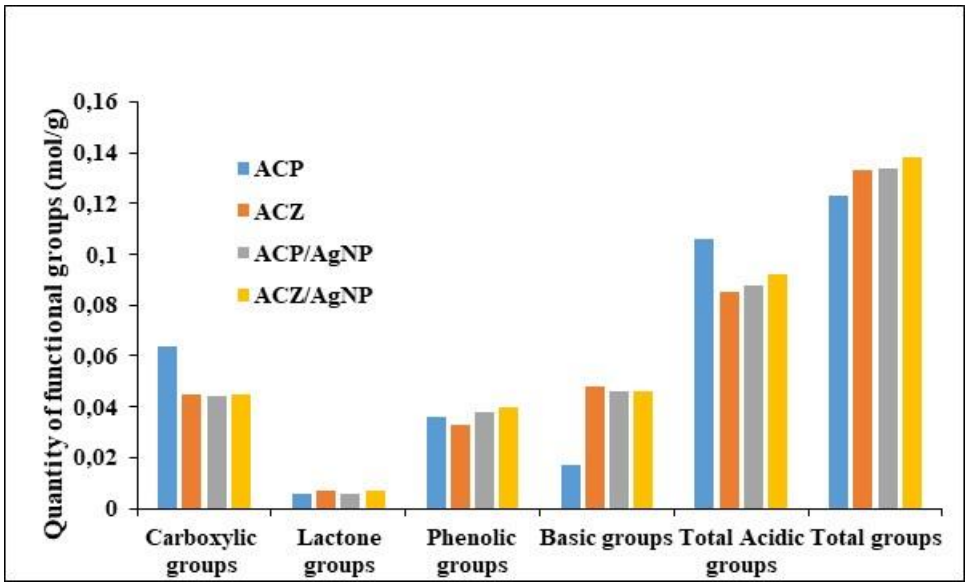

Figure 50: Concentrations of surface functional groups on ACP, ACZ, ACP/AgNP and ACZ/AgNP

From Figure 50, it can be seen all the adsorbents (ACP, ACZ, ACP/AgNP and ACZ/AgNP) all contains significant amount of acidic groups such carboxylic, lactone and phenolic groups with the ACP adsorbent shaving the highest quantity of the carboxilic groups and the lowest quantity of basic groups. This can be seen from it low value of pHzpc of the ACP adsorbent which is 4.0. It can be seen that after doping with AgNPs, most of the carboxylic groups of the ACP were neutralised to form ACP/AgNP hence justifies why the pHzpc move from 4.0 to 7.6 given a drift of 3.6 units. In the case of ACZ and ACZ/AgNP, the neutralisation was not significant hence the pHzpc drift from ACZ (pHzpc = 7.7) to ACZ/AgNP (pHzpc = 7.9) was only 0.2 unit.

III.4.2. UV–Vis Analysis of $AgNO_3$, RHS extract and AgNP

The reduction of the pure Ag+ ions was monitored by measuring the UV-Vis spectrum of the reaction medium. The UV-Vis spectral analysis was conducted using a UV-Vis spectrophotometer between 300 and 1100 nm. Figure 51 presents the analytical results obtained for the RHS extract, the silver nitrate solution and the silver nanoparticles.

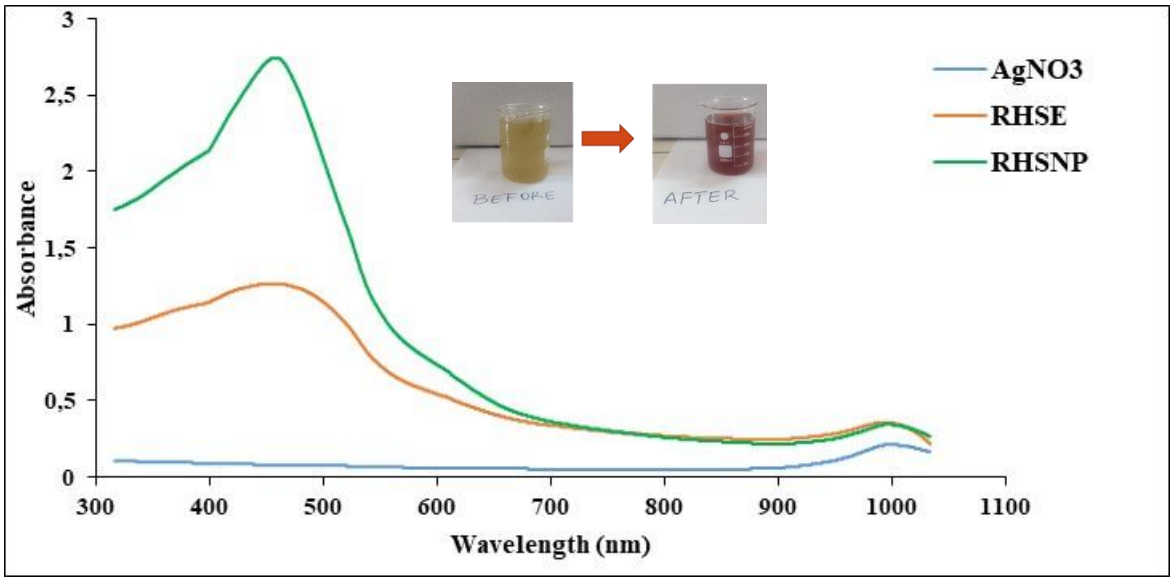

Figure 51: UV–Vis analysis of *Ricinodendron Heudelotti* shell extract, pure $AgNO_3$ and synthesized Ag NPs

The *Ricinodendron Heudelotti* shell extract was slowly introduce in the $AgNO_3$ solution. Initially it was observed that the orange-clear solution was rapidly changed into dark brown indicating the formation of AgNPs. No colour change was observed for the $AgNO_3$ solution in the absence of shell extract and equally, no colour change was seen for the shell extract in the absence of the $AgNO_3$ solution. Based on the visual observation, it was confirmed that the colour change was due to the reduction of Ag^+ into Ag^0 (Al-Ansari *et al.*, 2019). Furthermore, the optical UV–Vis analysis of *Ricinodendron Heudelotti* shell extract, Ag NO_3 solution and the synthesized AgNPs in aqueous solution was monitored by recording the absorption spectra at a wavelength range of 300-1050 nm and are shown in Figure 51. The shell presents a dome shape of the shell extract around 500-950 which is attributed to CO_3^{2-} ions and Ag NO_3 solution does not showed any absorbance peak in that region. For the AgNPs, a strong and sharp peak was observed at 453 nm which explains the surface plasmon resonance (SPR)

phenomenon (Thomas *et al*., 2018; Al-Ansari *et al*., 2019) that confirmed the synthesis of AgNPs attributed to spherical nanoparticles of phenol. Past studies suggested that a SPR peak located between 410 and 460 nm has been observed for AgNPs and might be attributed to spherical nanoparticles phenol (Al-Ansari *et al*., 2019). All the three solutions showed weak dome band around 900-1000 nm. The band at 1043 nm were assigned for N-H and C-N (amines) stretch vibration of the proteins respectively. The band at 1377 nm exemplifies the N-O symmetry stretching typical of the nitro compound. The band at 1240 nm corresponds to C-N stretching of amines. These functional groups have role in stability/capping of AgNP as reported in many studies.

III.4.3. Determination of the pH of point of zero charge (pH_{PZC})

The point of zero charge (PZC) of the ACP, ACZ, ACP/AgNP and ACZ/AgNP samples were also studied in this series of pH experiments. The pHpzc of an adsorbent refers to the pH level at which the surface of the adsorbent has zero net charge or the point at which the quantity of the acidic groups is equals that of the basic groups. The pHpzc of the carbonaceous materials in this work were determined using the solid addition/ pH drift method. This method involves preparing a series of solutions of NaCl of concentration 0.1 N with a range of known pH values. 0.1 g of the respective ACs and their Composites were added to each flask and the suspensions were agitated for 3 hours and allowed for 48 hours to reach equilibrium. The pH of the supernatant was recorded and the differences between final and initial pH values (ΔpH) were plotted against the corresponding initial pH values (pHi) (see appendix A, Table A-3, page 219). Figure 52 shows the plot of ΔpH against pHi in order to determine pH_{PZC}. The poin at which the curves cut the pH axis is taking as the pH_{PZC} of the respective materials.

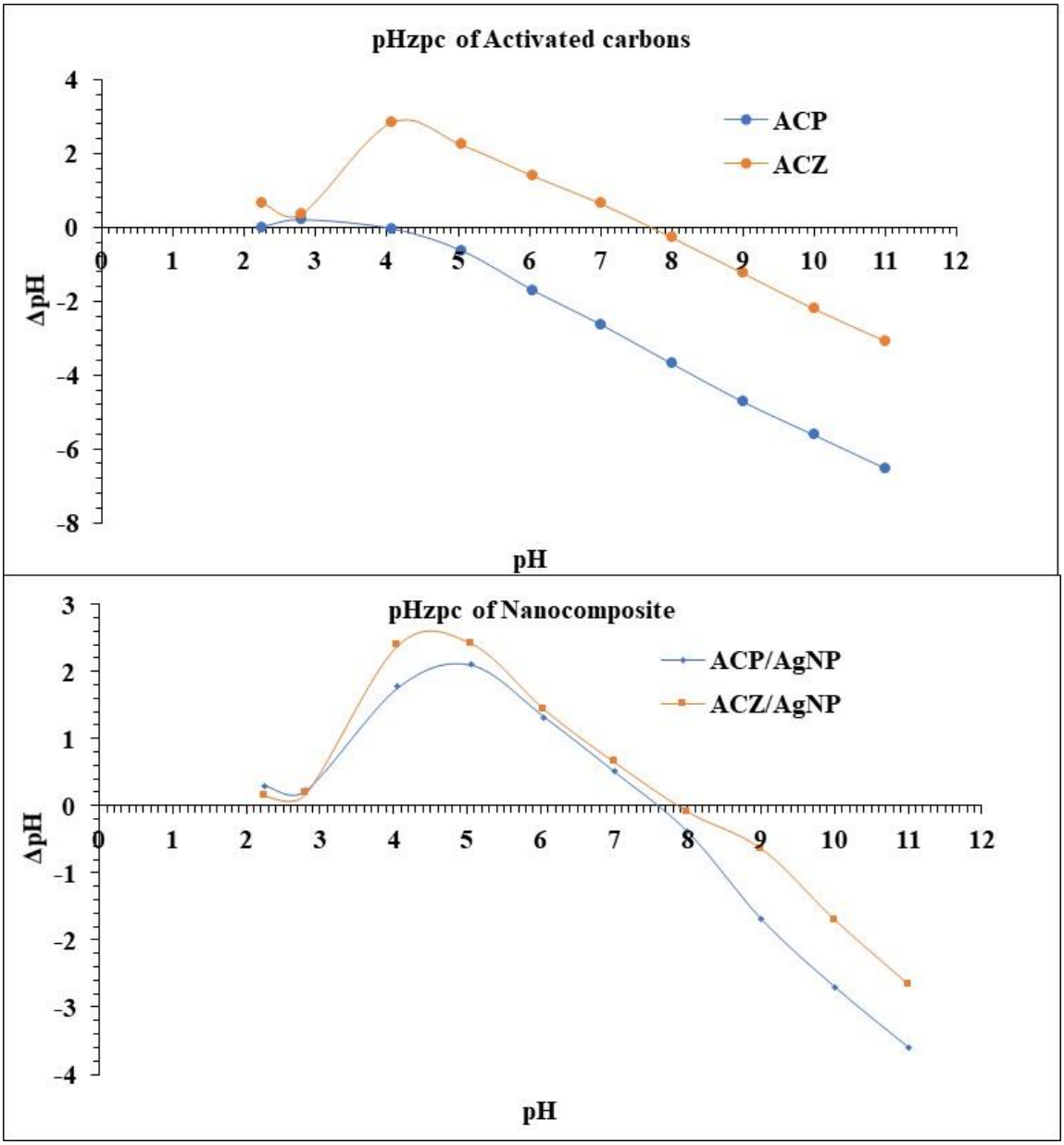

Figure 54: pH of point of zero charge (pH_{PZC}) for ACP, ACZ, ACP/AgNP and ACZ/AgNP

The pH and acid-base values of carbonaceous materials usually give a good indication of the surface of oxygen complexes and electrical surface undergone by them. The surface charge arises from the interaction between the carbon surface and the aqueous solution. The complexes on the surface are generally classified as acidic, basic and neutral. From Figure 52, the pH_{PZC} of the ACP, ACZ, ACP/AgNP and ACZ/AgNP were respectively 4.0, 7.7, 7.6 and 7.9. The above results of ACP has acidic surface nature, ie the surface of ACP contains mostly acidic functional groups. In the case of ACZ, ACP/AgNP and ACZ/AgNP, the pH_{PZC} values indicate that the three materials contain almost the same amount of acidic and basic functional

groups. This implies that below the respective pH_{PZC} values, the surface of the respective activated carbons and the composites are all charged positively while above these values their respective surfaces are positively charged. Also, at the pH_{PZC} values, the net charge on the surface of ACP, ACZ, ACP/AgNP and ACZ/AgNP materials is zero. It can also be observed that after precipitating the silver nanoparticle on the surfaces of ACP and ACZ to produce ACP/AgNP and ACZ/AgNP respectively, the drift in pH_{PZC} of ACP to ACP/AgNP is 3.6 while the drift in pH_{PZC} of ACZ to ACZ/AgNP is 0.02. This implies that during their respective conversions, more positive sites on the surface of ACP were netralised than that of the ACZ. This neutralisation may results either from the nanoparticles precipitated or from the nitrate ions evolving during the preparation of AgNPs from $AgNO_3$.

III.4.4. Scanning Electron Microscope (SEM) couple with Energy Dispersive X-Ray Crystallography (EDX) analysis

III.4.4.1. Scanning Electron Microscope (SEM)

The analysis of microscopic images obtained with a Phenom Pro X Scanning Electron Microscope operating at 15kV is given here. The surface morphologies of activated carbon and their composite samples produced were determined using Scanning Electron Microscope (SEM) coupled with Electron Dispersive X-ray crystallography to analyze the surface morphology and the elemental composition of the adsorbents. Figure 53 shows the SEM photograph of Samples ACP, ACZ, ACP/AgNP and ACP/AgNP 1000X magnification

a

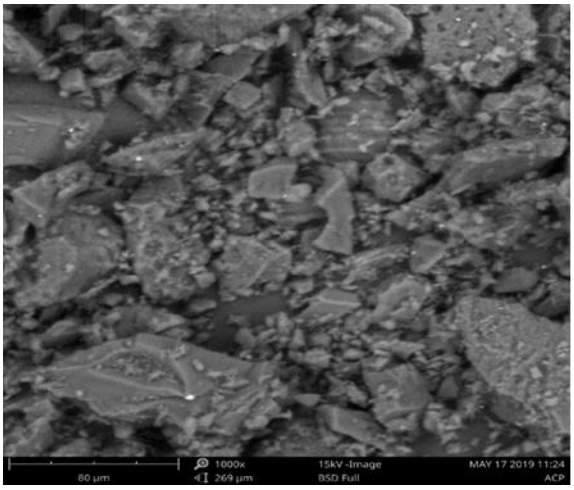

b

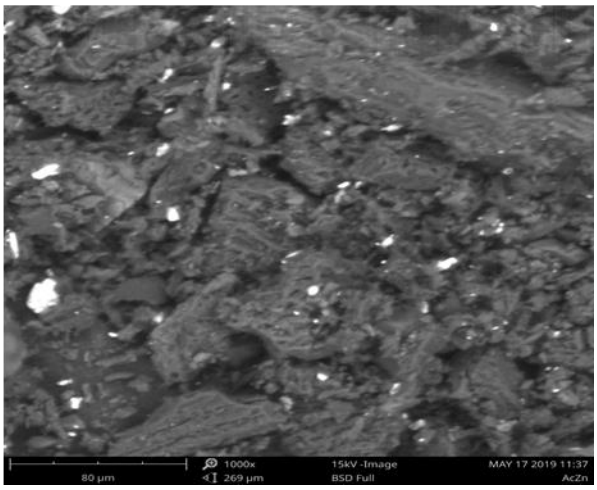

c 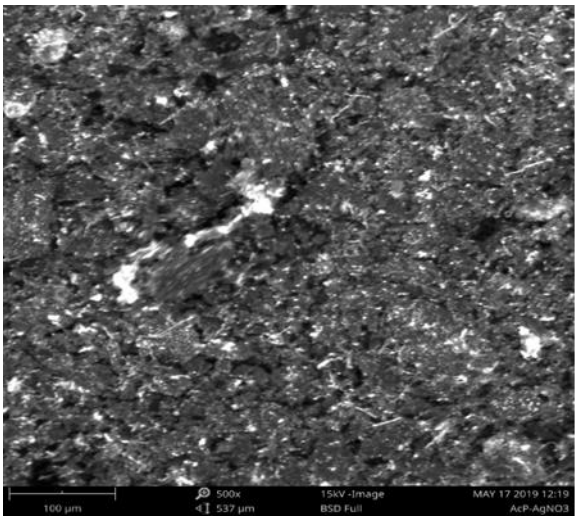

d 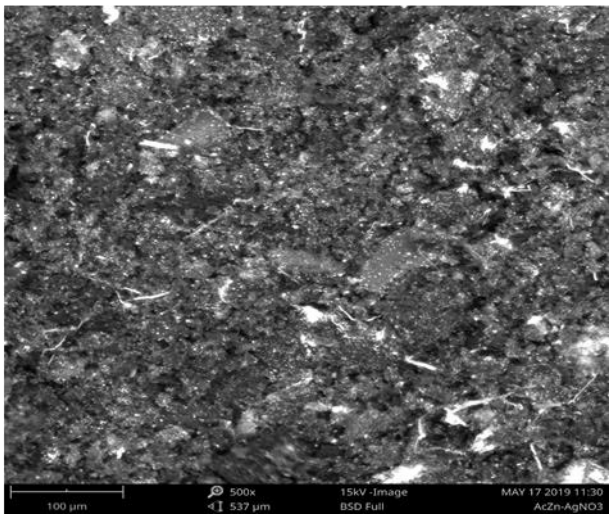

Figure 53: a) SEM-EDX Images of ACP, b) SEM-EDX images of ACZ, c) SEM-EDX images of ACP/AgNP, d) SEM-EDX images of ACZ/AgNP

The surfaces of Sample ACP and ACZ shows some rock like structures with the presence of some transport arteries with cracks and crevices with little sight of pore spaces. The ACP/AgNP and ACZ/AgNP Samples shows some transport pores and spongy surfaces with more visible micropores. All were observed to have some rock-like structures and more transport pores, serving as pathways for the adsorbates to enter the mesopores and micropores. The adsorbents have rough texture with heterogeneous surface and a variety of randomly distributed pore size. The samples also give a clearer pore structure, having more volume of pores and better pore structures with little agglomeration, making them more viable for adsorption and thus, the better the pore structure, the better its adsorption capability as compared to the RHS precursor. Hence the use of phosphoric acid and zinc chloride is tied to enhancement of the surface area and improvement of the pore structure. The pores seen in the Samples are as a result of the evaporation of the activating agents during carbonization and washing after activating, leaving empty spaces. In addition, the morphology of ACP is seen to be amorphous while the traces of ACZ, ACP/AgNP and ACZ/AgNP gives some crystallinity hence few transport pores and little agglomeration, which will not be very viable for adsorption. This might be due to the formation of Zincite (ZnO) after strong heating in the care of ACZ and the presence of silver in ACP/AgNP and ACZ/AgNP after doping with the AgNP respectively. Furthermore, Sample ACP gives a clearer pore structure, having more volume of pores and better pore structures with little agglomeration, making it more viable for adsorption and thus, the better the pore structure, the better its adsorption capability. Nevertheless, in all four cases,

well-developed porous surface was observed at higher magnification. The pores observed from SEM images are having diameter in micrometer (µm) range. These pores are considered as channels to the microporous network.

III.4.4.2. Energy Dispersive X-ray spectroscopy (EDX) of ACs and coposite samples

Natural adsorbents bear many oxygen surface groups such as carboxyl, carbonyl, ethers, quinines, lactones and phenols. To determine qualitatively and quantitatively the elemental composition of the carbons and the composites, EDX analysis was performed on the samples used for the SEM analysis and Figure 54 presents the results obtained.

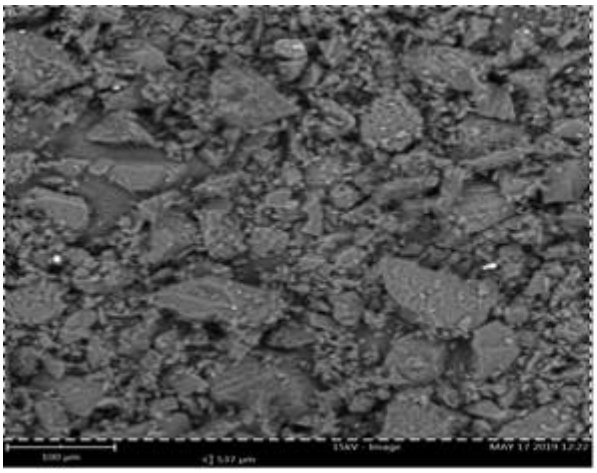

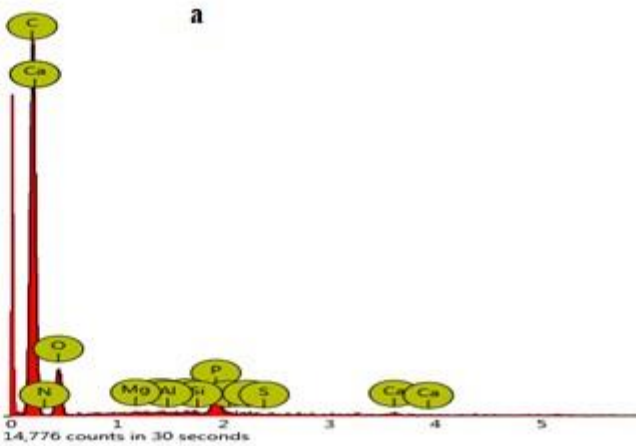

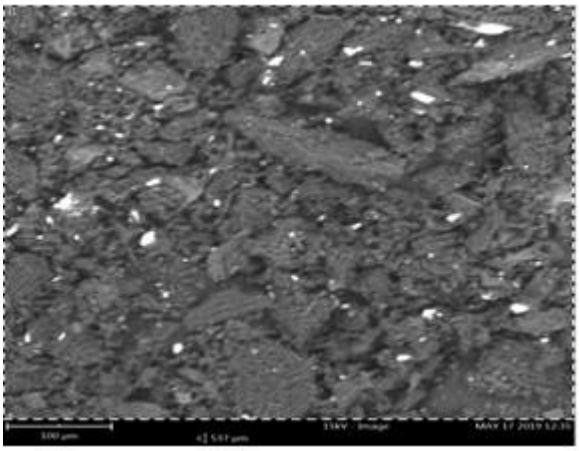

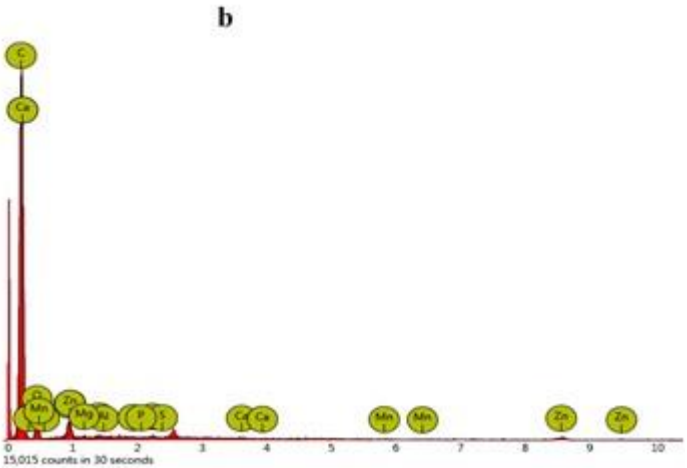

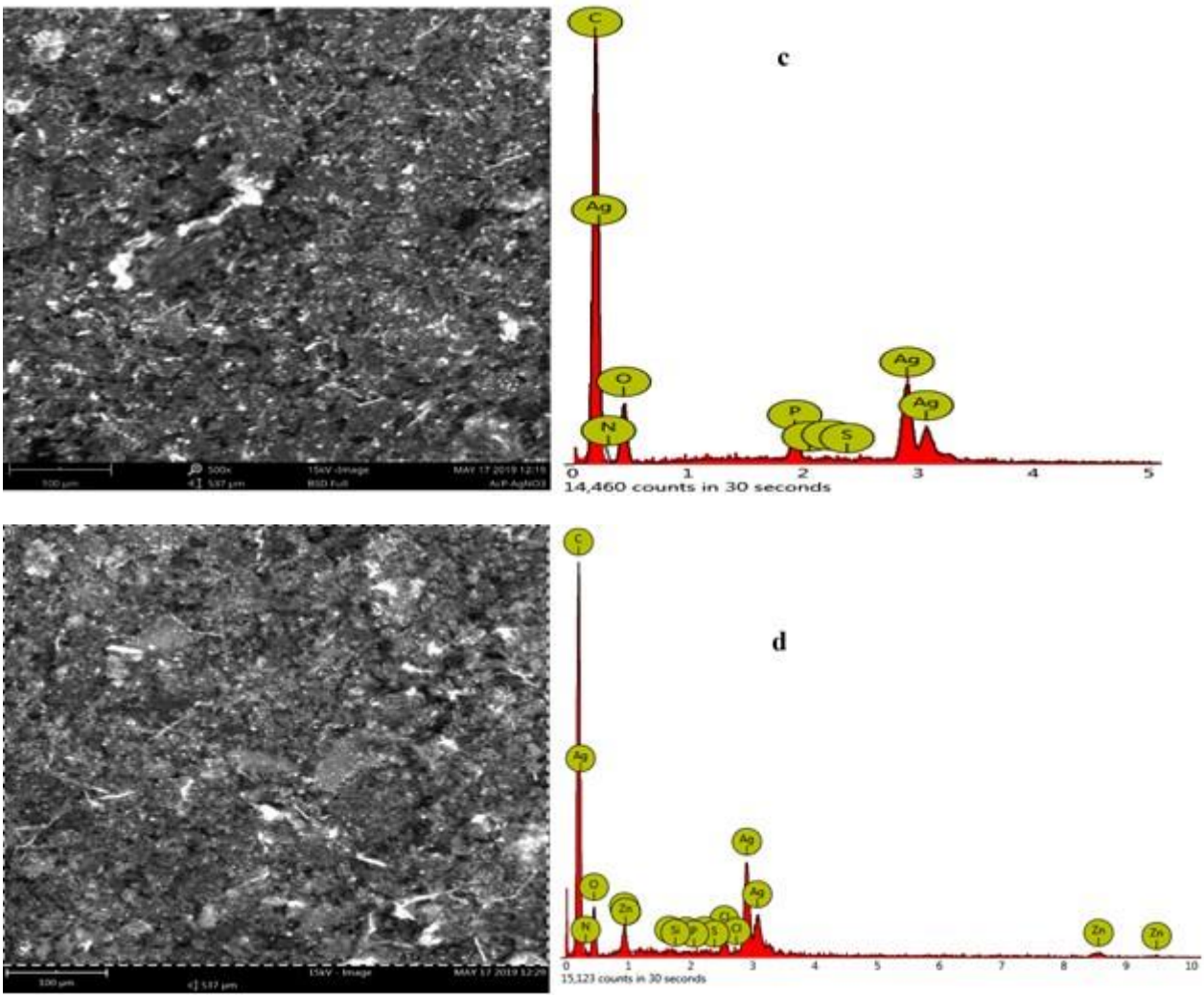

Figure 54: Scanning Electron Microscope-Energy Dispersive X-Ray crysallography (SEM/EDX) of a) ACP, b) ACZ, c) ACP/AgNP and d) ACZ/AgNP

As the prepared carbons are of highly microporous (pores having width in nanometers) in nature. ACs prepared at optimum conditions by different chemical activations were characterized by Energy Dispersive X-ray crystallography (EDX) is coupled with the SEM to observe mineralogic composition in the porous network. Figure 54 (experimental data found in appendix A, Table A-5 to Table A-8 pages 220 and 221) shows the EDX images of the chemically prepared ACs and their respective nanocomposite. From the figure, micropores of uniform pore size were observed clearly in all the cases. All the samples were found to be rich in carbon. The ACs (ACP and ACZ) samples were also rich in Ca than their respective composites (ACP/AgNP and ACZ/AgNP). ACP and ACZ samples were also found to contain significant amount of phosphorus (P) and zinc (Zn) respectively. These phosphorus (P) and zinc (Zn) were found to decrease significantly for the respective ACP/AgNP and ACZ/AgNP. This

could be as a results of the effect of the $AgNO_3$ facilitates the leaching of these elements with the help of the nitrate radical. Ag was the dominant elements in the nanocomposites (ACP/AgNP and ACZ/AgNP) after carbon. This was in accordance with the aim since its objective in the formation of the nanocomposite was to incorporate Ag into the AC skeleton. Also, the amount nitrogen and oxygen was found to significantly increase in the composites and was thought to come about from the NO_3^- radical of the $AgNO_3$ solution used to prepare the nanoparticles.

III.4.5. X – Ray Diffraction spectroscopy (XRD) of ACP, ACZ, ACP/AgNP and (d)ACZ/AgNP

The samples were characterized using X-ray Diffractometer (Philips X‘pert X-ray Diffractometer) employing 1.5046 Å copper source. The samples were scanned from $2\theta = 10 – 90°$. The value of the interplanar spacing between the atoms, d was calculated using the Bragg equation; $n\lambda=2d\sin\theta$. Where: $n=1$ is an integer, λ is the wavelength of the x-rays, d is the spacing of the planes of the atoms and θ is the angle of incidence of x-ray beam. The powder diffraction data for the 4 samples including the superposed graph comprising all 4 samples are given graphically. Figure 55 shows the XRD patterns of the prepared ACs and composite samples.

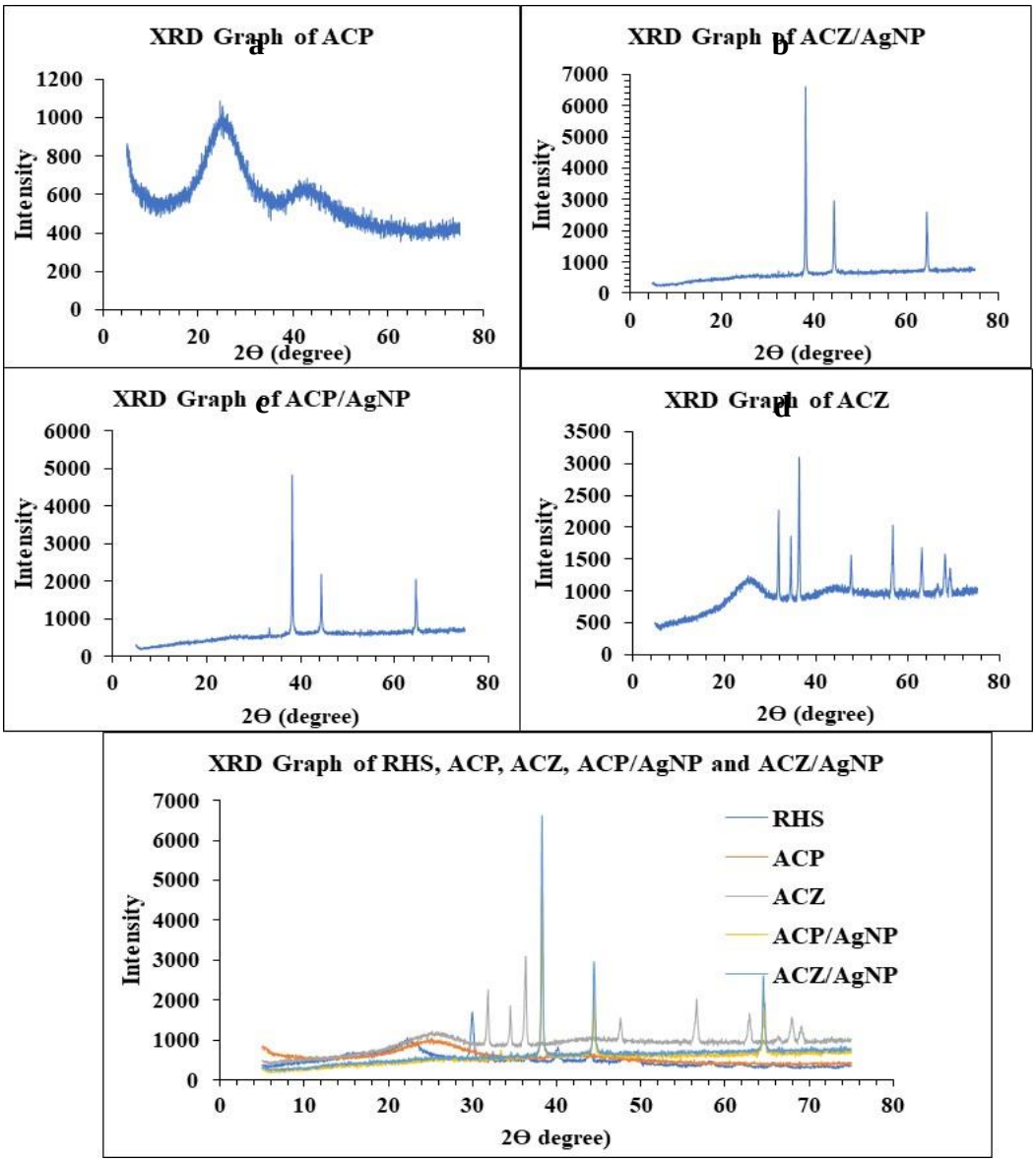

Figure 55: XRD results of (a) ACP, (b)ACZ, (c) ACP/AgNP and (d)ACZ/AgNP

Franklin, on the basis of XRD studies, classified activated carbons into two types, based on their graphitizing ability (Franklin, 1951). The non-graphitizing carbons are hard and show a well-developed microporous structure due to the formation of strong cross-linking between the neighbouring randomly oriented elementary crystallites. Whereas, graphitizing carbons has weak cross-linking and had a less developed porous structure (Bansal et al., 1988). Figure 55 shows the X-ray diffraction profiles of the ACs prepared at optimum conditions.

The RHS sample was found to contain a s strong diffraction peak at 29.9654 °C a series of weak diffraction peaks at 23.4856°, 36.5817°, 40.1731°, 43.9368°, 48.4898°, 49.4886°, 58.6167° and 65.7421° respectively was observed in Figure 33. These values correspond to reference code number 96-900-0575 (d_{hkl} = 5.40) and is attributed to the calcite. ACP sample

did not show any diffraction peaks and thus the diffused haloes (imperfect developing of photographs) appearing at 2θ values between 0 to 80 degrees, confirmed the absence of any ordered crystalline structure, and is an indication of the amorphous nature of material having some degree of non-arrangement in the molecular chain, which is an advantageous property for well-defined adsorbents. ACZ sample shows a mixture of strong and weak peaks at 2θ values between 0 to 80 degrees of respectively 31.8378°, 34.4838°, 36.3256°, 47.6036°, 56.6403°, 62.9018°, 66.4151°, 67.9504° and 69.0721°. This value corresponds to reference code number 96-900-4179 (d_{hkl} = 2.00) and is attributed to the zincite. Zincite is a rare minerale with high medicinal values. The XRD patterns of sample ACP/AgNP and ACZ/AgNP each possesses 4 crystalline peaks at 2Θ positions of 33.3774°, 38.2226°, 44.4013°, 64.5353°and 64.7265°; and 32.3547°, 34.5980°, 38.2457°, 44.4240°and 64.5517° respectively. These peaks are attributed to reference number d_{hkl} 4.00 corresponding to Ag. This shows that the doping process of AgNP on the two ACs was very effective.

Generally, broad peaks found at around 24º for all the samples confirm that the samples are non-graphitized and can have high microporous structure (Zhao *et al*., 2009) which was confirmed by the gas adsorption isotherms.

III.4.6. Determination of particle size of ACP. ACZ. ACP/AgNP. ACZ/AgNP materials

Carbon samples were crushed and sieved in the size less than 75 µm and 0.04-0.05 g of each sample was added into 5 mL of methanol. The sizes of the different Samples were measured by using MALVERN Zetasizer Nano ZS90 at 25 °C. The results are given in Figure 53.

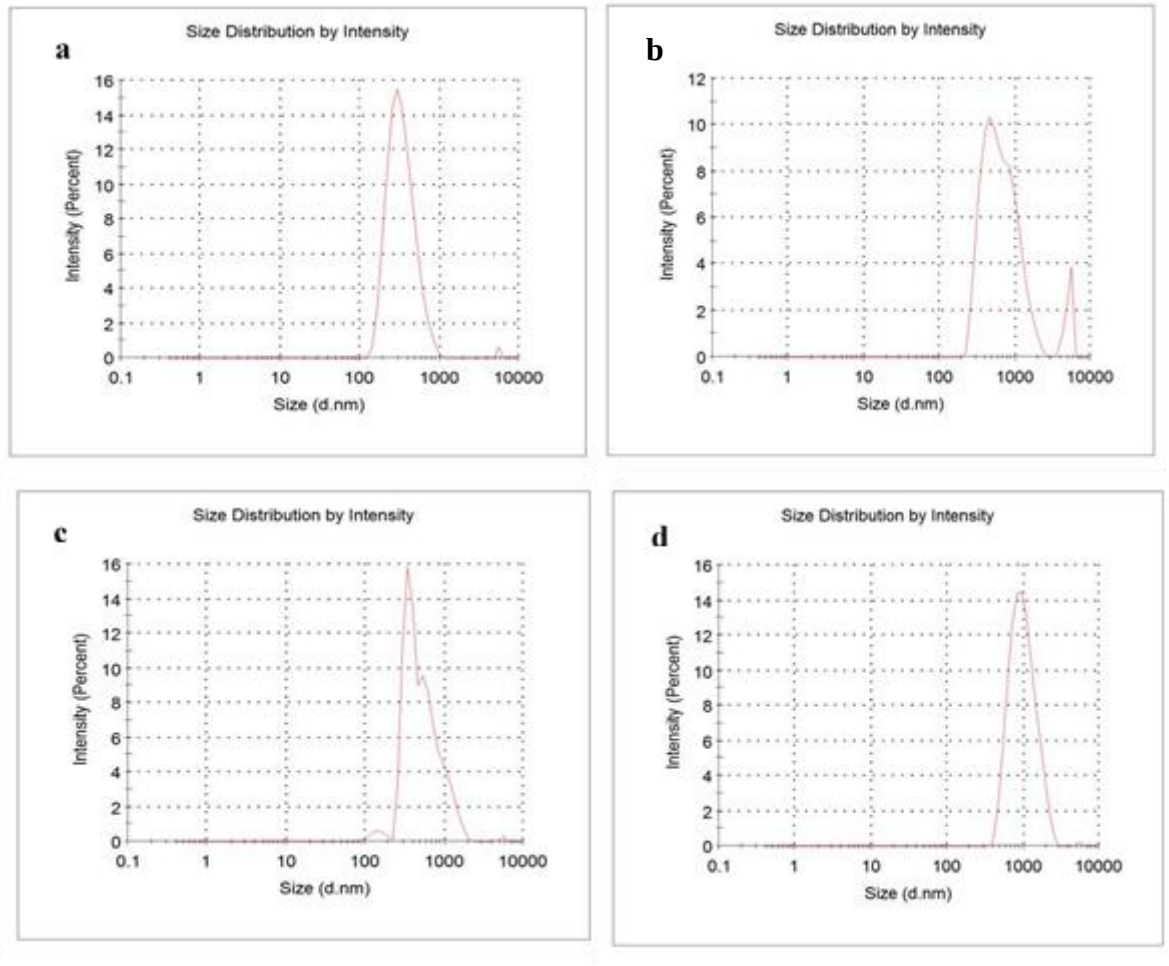

Figure 56: Particle size of (a) ACP, b) ACP, c) ACP/AgNP and (d) ACZ/AgNP materials biosynthesized

The size distribution of the ACP, ACZ, ACP/AgNP and ACZ/AgNP above were determined by Differential Light Scattering (Figures: 56a, 56b, 56c and 56d). Particle size distribution curve reveals that the ACZ and ACZ/AgNP obtained are polydispersed in nature, with average diameter of 459.5, 814.6, 638.6 and 1008 dnm for ACP, ACZ, ACP/AgNP and ACZ/AgNP respectively meaning all the AC and AC/AgNP samples are in the nano range. In addition, doping the ACP and ACZ samples with AgNPs increases the respective sizes by 179.1 and 193.4 dnm for ACP/AgNP and ACZ/AgNP. Also, the particles of ACP and ACZ/AgNP samples are divided into two different sizes of 380.6 dnm and 5890.0 dnm for ACP while for ACZ/AgNP, it is 1115 and 5484 dnm. That of ACZ and ACP/AgNP are divided into three different sizes of 438.3, 1054 and 5332 dnm; and 1231, 500.5 and 137.3 dnm respectively. It also results from the volume/size graph that the area of the peaks at 380.6, 1054, 500.5 and 1115.0 dnm for ACP, ACZ, ACP/AgNP and ACZ/AgNP respectively are higher than that of the other peaks with a % volume of respectively 97.4, 54.5, 76.9 and 99.7%. This implies that

there are more particles around that region than the others in the case of ACP, ACZ, ACP/AgNP while for ACZ/AgNP. This was evident as the Intensity size graph shows how these respective zones have the highest intensities meaning the more the particles in one zone, the more the turn to aggregates and hence scatter more light.

Furthermore, the 2nd Virial Coefficient (A2) which is a property describing the interaction strength between the particles and the solvent or appropriate dispersant medium. For samples where A2>0, the particles 'like' the solvent more than itself, and will tend to stay as a stable solution. When A2<0, the particle 'likes' itself more than the solvent, and therefore may aggregate. When A2=0, the particle-solvent interaction strength is equivalent to the molecule-molecule interaction strength – the solvent can then be described as being a theta solvent. The results above show the 2nd Virial Coefficient for ACP, ACZ, ACP/AgNP while for ACZ/AgNP are respectively 0.408, 0.359, 0.376 and 0.169 respectively. This implies that the particles like the solvent more than itself, and will tend to stay as a stable solution in a disperse manner. These particles therefore have stability, good colloidal nature and high dispersity of AgNPs due to negative-energative repulsion (Kumari *et al*., 2015) hence can interact with adsorbate molecules and this favors adsorption. Also, the intercept (corresponds to 1/M) is used to obtain the molecular weight of the samples a and are respectively 0.345, 0.344, 0.718 and 0.562 for ACP, ACZ, ACP/AgNP while for ACZ/AgNP.

III.4.7. Fourier Transformed Infra-red spectroscopy (FTIR)

Fourier transform infrared spectroscopy was used to determine the surface functional groups of the activated carbon obtained from RHS. The FTIR spectra of the activated carbons prepared by the respective activating agents and the ACs/AgNPs are shown in Figures 57 and 58.

III.4.7.1 Fourier Transform Infra-red spectroscopy for ACP and ACP/AgNP

The FTIR spectra measured within the range of 400 – 4000 cm^{-1} of the ACP and ACP/AgNP are shown in Figures 57.

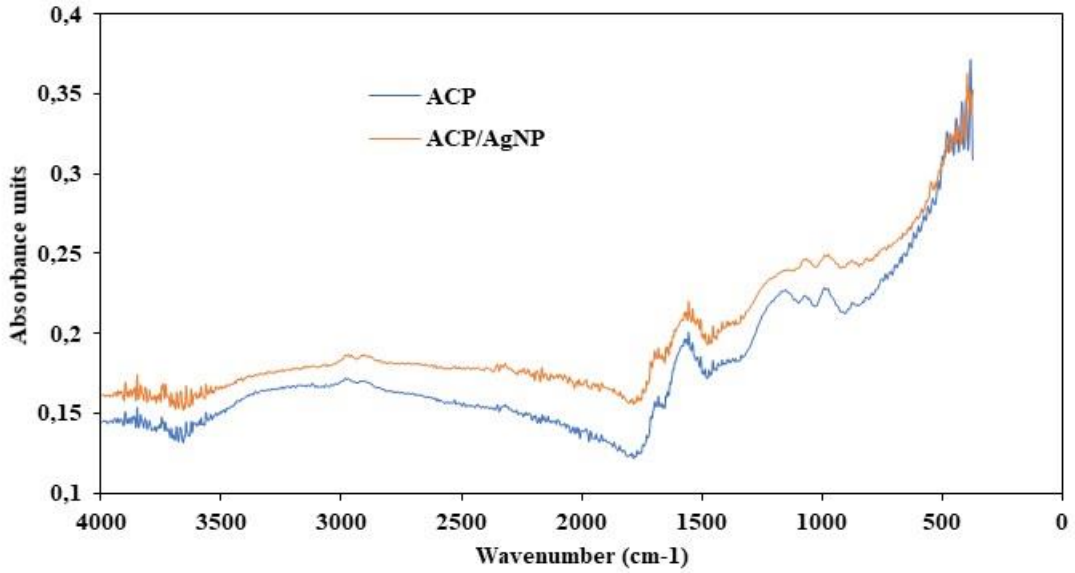

Figure 57: FTIR spectral of ACP and ACP/AgNP.

The FTIR spectral of ACP and ACP/AgNP are identical and from the FTIR spectrum of ACP, weak bands from 3800 to 3931 cm^{-1} can be attributed to –N-H stretching vibrations of amines and amide (II) band. Absorption bands due to aliphatic (2986 and 2855 cm^{-1}: C–H stretching in –CH– ; 1456 to 1488 cm-1 : –CH– deformation) were also observed (Abega *et al*., 2019). The bands at 885, 840, and 775 cm^{-1} are due to out-of-plane deformation mode of C–H for different substituted benzene rings. The small band at about 1700 cm^{-1} is usually assigned to C=O stretching vibrations of ketones, aldehydes, lactones or carboxyl groups. The spectra of the prepared activated carbons also show a strong band at 1600–1580 cm^{-1} due to C–C vibrations in aromatic rings. Also, the amide I band primarily consisted of the carbonyl (C=O) stretching of the peptide backbone at 1683 to 1697 cm^{-1} (Lekene *et al*., 2019). Broad band at 1075–1153 cm^{-1} (maxima at 1190–1200 cm^{-1}) is usually found with oxidized carbons and has been assigned to C–O stretching in acids, alcohols, phenols, ethers and/or esters groups; -C-N stretching groups in aromatic rings groups, aromatic rings and –N-O stretching groups respectively. Nevertheless, it is also a characteristic of phosphorous and phosphor carbonaceous compounds present in the phosphoric acid activated carbons usually assigned to O–C stretching vibrations in P–O–C (aromatic) linkage and to P,OOH. The shoulder at 1075 cm-1 was ascribed to ionized linkage P–O– in acid phosphate esters, and to symmetrical vibration in a P–O–P chain (Ankoro *et al*., 2016). The band at 1450 cm-1was assigned for N-H stretch vibration present in the amide linkages of the proteins. These functional groups have role in stability/capping of AgNP as reported in many studies (Kumari *et al*., 2015).

III.4.7.2 Fourier Transformed Infra-red spectroscopy for ACZ and ACZ/AgNP

The FTIR spectra measured within the range of 400 – 4000 cm^{-1} of the ACZand ACZ/AgNP are shown in Figures 58.

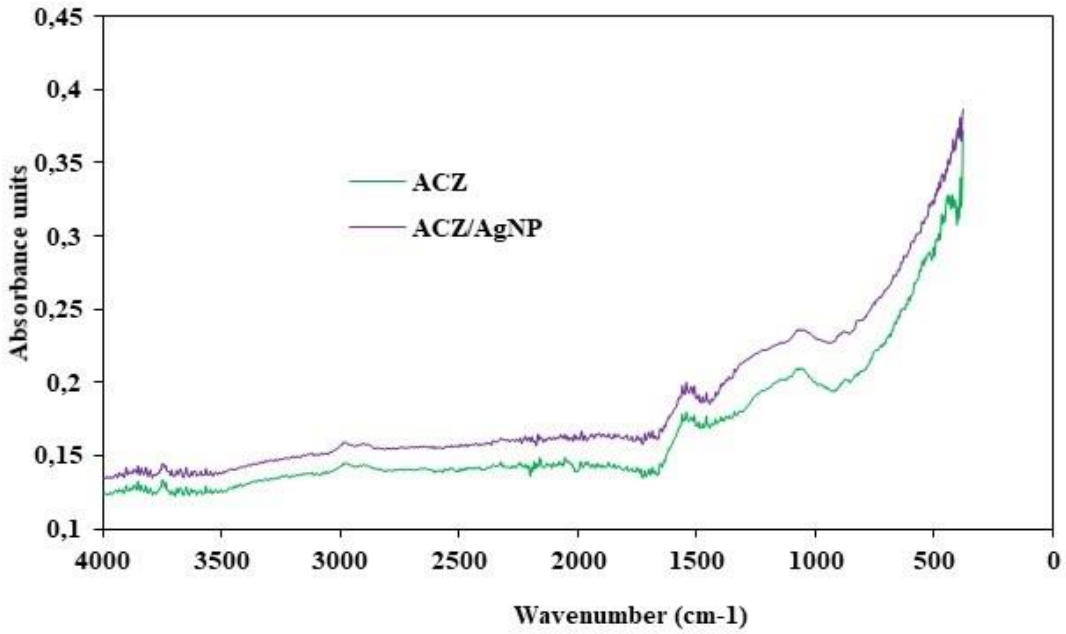

Figure 56: FTIR spectral of ACZ and ACZ/AgNP

The FTIR spectra were recorded to identify the different functional groups and the potential biomolecules that contributed to the reduction of the Ag^{+} ions and to the capping of the bio reduced AgNps (Visweswara *et al*., 2013). The FTIR spectrum was recorded 1 day following the formation of the AgNps. The bands observed around 3556 to 3931 cm^{-1} may be attributed to–N-H stretching vibrations of amines and amide (II) band groups. There were no peaks traces of –OH groups in all the materials, the peak at 2978 cm^{-1} may be attributed to C–H stretching vibrations (Abega *et al*., 2019), those around 1608 – 1716 cm^{-1} corresponds to the carbonyl groups in the α-helices present in the nut shell extract and C=O stretching vibration in the aldehydes, ketones esters, lactones and carboxylic groups on the surface of the ACs after activation. The amide I band primarily consisted of the carbonyl (C=O) stretching of the peptide backbone at 1684 and 1698 cm^{-1} (Lekene et al., 2019). It might also correspond to, C–C vibrations in aromatic rings. The observed peaks at 1418 – 1488 cm^{-1} denote –CH– deformation; which are associated with the in plane and out-of-plane aromatic ring deformation vibrations; it can also be attributed to CO_3^{2-} of calcite which can also be attributed to Ca-O formed when calcite is usually completely decomposed into CaO after the chemical activation. Vibrational frequency at 1066 cm^{-1} observed in both spectra could be ascribed to the -C–O stretching in

acids, alcohols, phenols, ethers and/or esters groups; O–C stretching vibrations; -C-N stretching groups in aromatic rings groups, aromatic rings and –N-O stretching groups respectively. The milled band around 409 – 546 cm^{-1}. could be assigned to -Zn-O of the zincite formed after activation and carbonisation.

Furthermore, the absence of peaks for Ag in ACP/AgNP and ACZ/AgNP spectral implies that the silver present in the nano-particles cluster precipitated is in the metallic form which could be originated to protein precipitation occurring during the reduction and stabilization of the AgNps (Visweswara *et al*., 2013). This observation indicated relatively interaction between the extract and Ag NPs. It also confirmed by the formation of Ag NPs which was materialised by a color change of synthesized Ag NPs solution.

III.4.8. Textural and Porous Characterisation of ACP, ACZ, ACP/AgNP and ACZ/AgNP materials

Various techniques exist for evaluating PSD of a micro-porous material such as the measurement of saturated amounts of probe molecules of various sizes, and by measurement of a single adsorption isotherm of gases at subcritical temperatures. The BET method was used to determine the surface area of the prepared carbons while the Barret Joyner Halender (BJH) adsorption desorption method was used o determine the pore volume and pore diameter. The N_2 adsorption-desorption isotherms of the prepare materials are given in Figures 59, 60, 61 and 62.

III.4.8.1. Nitrogen Gas Adsorption – Desorption Isotherms

Nitrogen (N2) gas adsorption-desorption isotherms of the activated carbons prepared with different chemical activating agents (H_3PO_4 and $ZnCl_2$) and the composites were carried out to investigate the respective porous characteristics.

a) Nitrogen Gas Adsorption – Desorption Isotherms for ACP

Figure 59, 60, 61 and 62 illustrates the volume of N_2 adsorbed on the activated carbon prepared by using H_3PO_4 and $ZnCl_2$ as activating agents.

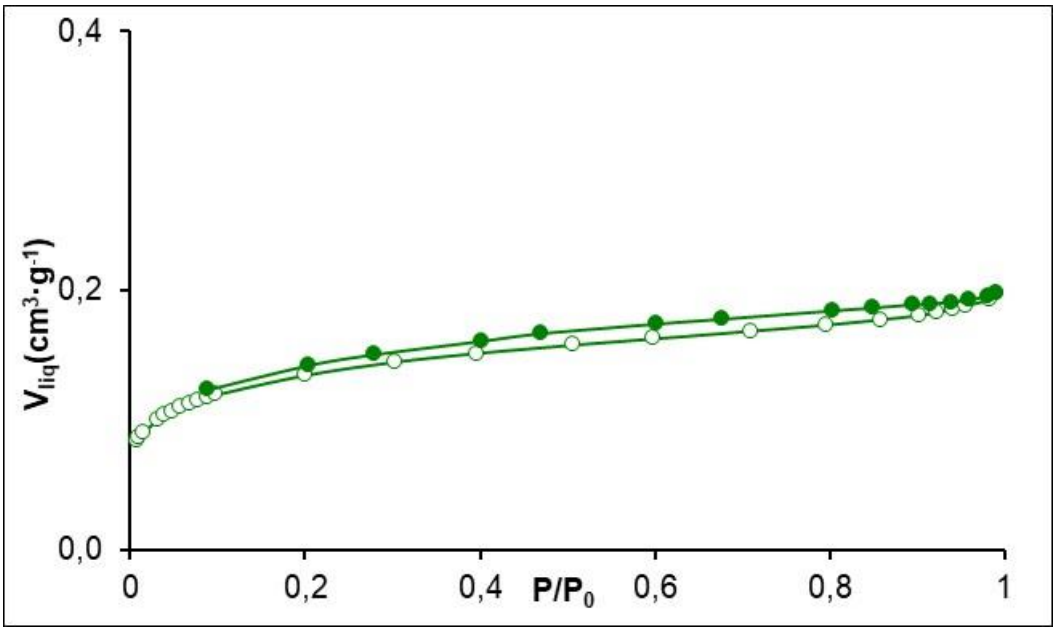

Figure 59: BET Nitrogen gas Adsorption-Desorption isotherm of ACP sample

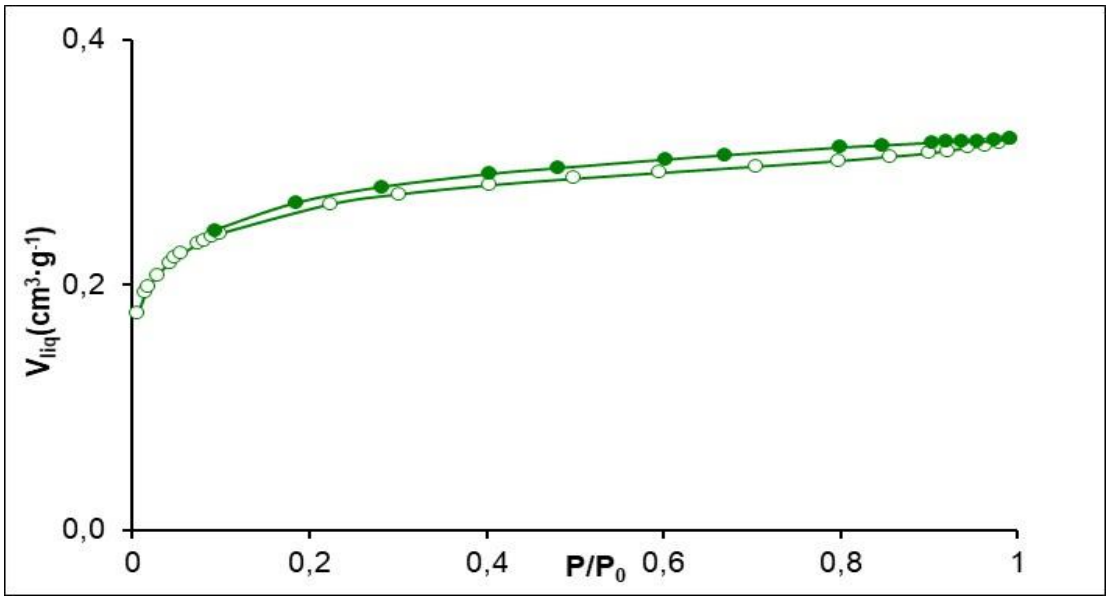

Figure 60: BET Nitrogen gas Adsorption-Desorption isotherm of ACZ sample

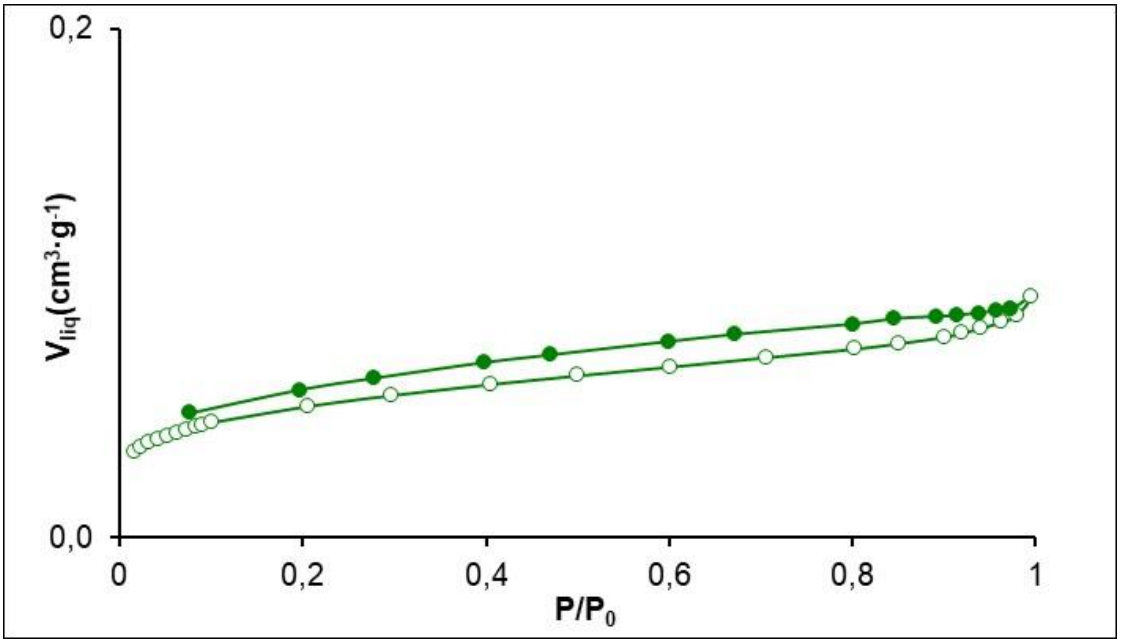

Figure 61: BET Nitrogen gas Adsorption-Desorption isotherm of ACP/AgNP composite

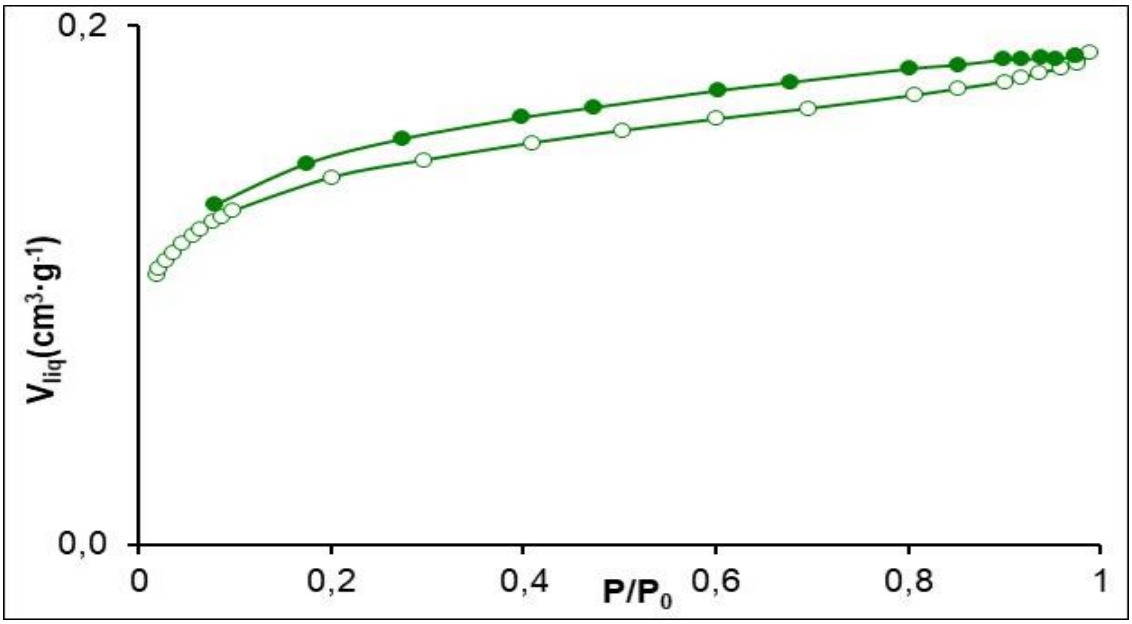

Figure 62: BET Nitrogen gas Adsorption-Desorption isotherm of ACZ/AgNP composite

Figure 59, 60, 61 and 62 depicts that the volume of N_2 adsorbed increases with the increase in relative pressure. This can result from the fact that the activating agent (H3PO4 and ZnCl2) would enhance the porosity development (Ramakrishna, 2012) and hence the increase in adsorption of N_2. All the materials exhibited Type IV isotherms which occur in adsorption on mesoporous materials. A characteristic property of this type of isotherm is its hysteresis loop. The exact shape of the hysteresis varies from one adsorption system to another. The

hysteresis formation is related to capillary condensation. The hysteresis formation is based on capillary condensation phenomena and hysteresis. Part of isotherms includes information about the mesopores. Because of condensation and evaporation phenomena, there exists a relationship between shape and position of isotherm and pore geometry. The complete pore filling causes a plateau in these isotherms and the limiting uptake value is reached. The low pressure hysteresis (LPH) tends to decrease with the decrease in relative presure denoting the distribution of micropores with uniform pore width. exhibited low pressure hysteresis (LPH) which occurs due to the swelling of non-rigid walls in pores with trapping of adsorbate molecules, and/or retention of molecules in pores similar in size to them. In addition, all the adsorbents also show H4 types of loops which also relates to slit-shaped pores but in the case of microporous materials. Furthermore, the size of the histeresis loop of the composites (ACP/AgNP and ACZ/AgNP) are large than those of their respective carbon (ACP and ACZ) implying the composite are more mesoporous than the presting carbon.

III.4.8.2. Pore Volume assesment and pore diameter measurement for ACP, ACZ, ACP/AgNP and ACZ/AgNP materials

Any porous material cannot be characterized by a single pore dimension; instead they exhibit an almost wide range of PSDs throughout the material matrix. Macroscopic or classical thermodynamic model such as BJH method which is based on the pore condensation phenomena can be applicable only in the meso-porous or macroporous region, but cannot be used for micro-pores or even v ery narrow meso-pores. Other methods, such as Dubinin-Radushkevich and DA methods can be used for micro-pore analysis (Ndi *et al.*, 2014).

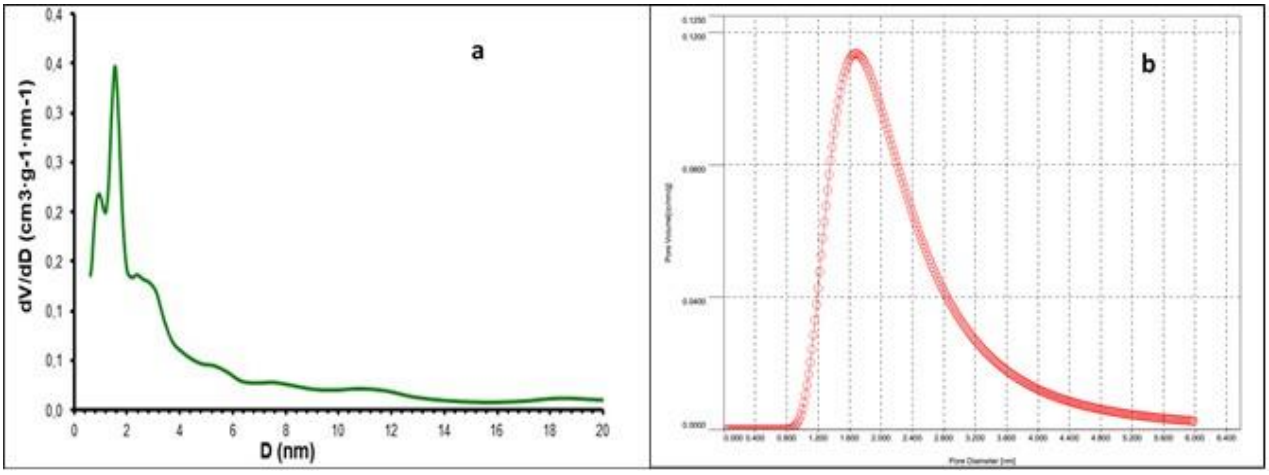

Figure 63: Barret Joyner Halenda (BJH) adsorption cumulative pore volume (a) and Dubinin-Astakhov (DA) pore size distribution (b) for ACP sample

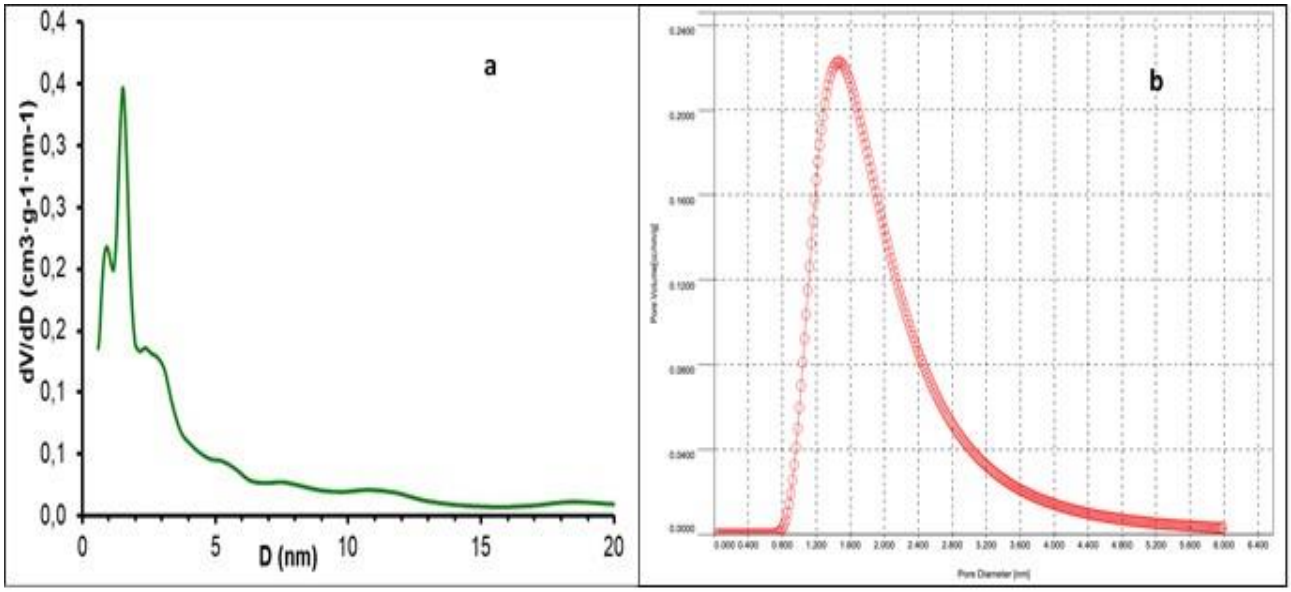

Figure 64: Barret Joyner Halenda (BJH) adsorption cumulative pore volume (a) and Dubinin-Astakhov (DA) pore size distribution (b) for ACZ sample

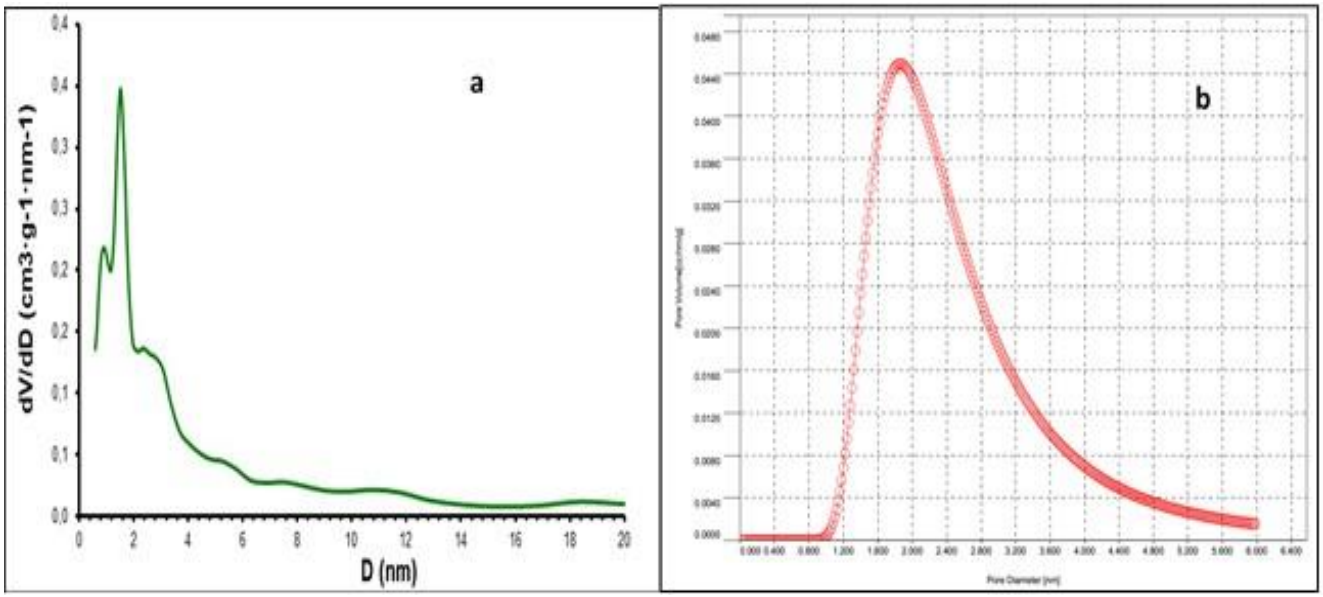

Figure 65: Barret Joyner Halenda (BJH) adsorption cumulative pore volume (a) and Dubinin-Astakhov (DA) pore size distribution (b) for ACP/AgNP composite

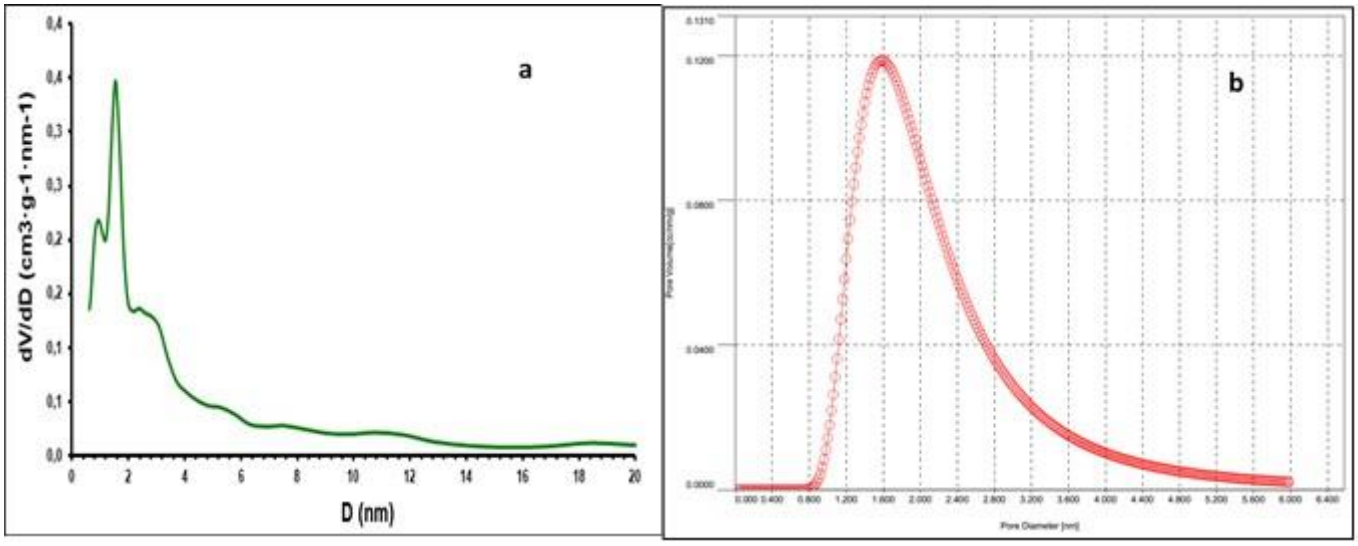

Figure 66: Barret Joyner Halenda (BJH) adsorption cumulative pore volume (a) and Dubinin-Astakhov (DA) pore size distribution (b) for ACZ/AgNP composite

From Figures 63, 64, 65 and 66 (a and b respectively), the BJH adsorption average pore diameter for ACP, ACZ, ACP/AgNP and ACZ/AgNP is of 3.649, 3.639, 3.652 and 3.681 nm respectively while that the DA miicropore diameter are respective 1.680, 1.460, 1.860 and 1.580 nm. This is an indication of meso-porous material (from IUPAC classification) while the DA values characterises that the material rich in micropores

The Summary Report of micromeritics analysis of ACP, ACZ, ACP/AgNP and ACZ/AgNP materials, the surface area mesurement (BET), the pore volume distribution (BJH) and the pore diameter distribution report for the carbons and their respective composites are summarised in Table XXXVII.

Table XXXVII: Summary Report of porousimetric analysis of ACP, ACZ, ACP/AgNP and ACZ/AgNP materials

Samples	ACP	ACZ	ACP/AgNP	ACZ/AgNP
Specific surface area (m^2/g)	386.613	615.400	367.400	335.100
Pore volume (cm^3/g) from BJH method	0.061	0.051	0.044	0.047
Pore diameter (nm) from BJH method	3.649	3.639	3.652	3.681
Pore diameter (nm) from DA method	1.680	1.460	1.860	1.580

From Table XXXVII, it can be seen that the specific surface area of the ACP, ACZ, ACP/AgNP and ACZ/AgNP from the BET method are respectively 336.613, 615.400, 367.400 and 335.100 m^2/g. The carbons (ACP and ACZ) were found to have a higher surface area than the composites (ACP/AgNP and ACZ/AgNP) which is as a result of the AgNP ocupying the pores thereby decreasing the specific surface area. Same trend was observed for the pore volumes and the resulting BJH cumulative pore volume for the four samples are 0.0605, 0.051, 0.044 and 0.047 cm^3/g for ACP, ACZ, ACP/AgNP and ACZ/AgNP respectively. Also, the Langmuir surface area and DR Method micropore area are higher than those of the the BET. These values can be confirmed by the maximum quantity adsorbed (Qm) (see appendix B, Table B-9 page 226). This difference in surface area and quantity absorbed can be explained by the fact that, during adsorption, the ratio of the number of the adsorbed particles with adsorption sites are less in multiple layer adsorption than in a single phase (monolayer) coverage. The BJH Cummulmative adsorption pore diameter (mesopores assessment) are 3.649, 3.639, 3.652 and 3.681 while that from the DA adsorption pore diameter method (micropores assessment) are 1.680, 1.460, 1.860 and1.580 for ACP, ACZ, ACP/AgNP and ACZ/AgNP respectively. Furthermore, the pore diameter for BJH method is higher than that from the DA. This implies that all the prepared samples are both microporous and mesoporous from IUPAC classification. Lekene *et al*., 2019 observed similar results. Furthermore, there was a general rise in the pores diameter still from the carbons to the respective composites and can be related complete filling of the micropores by the nanoparticles during the formation of the composite

III.5. Adsorption Studies of Indigo Carmine and Methyl Orange on ACP, ACZ, ACP/AgNP and ACZ/AgNP adsorbents

III.5.1. Variation of adsorption parameters of IC and MO adsorption on ACP, ACZ, ACP/AgNP and ACZ/AgNP

III.5.1.1. Influence of pH on IC and MO adsorption

pH measurement is an important parameter considered in the study of adsorption because it affects both the surface functional groups of the adsorbent and the adsorbate to be adsorbed. The adsorption of IC dye and MO in aqueous solution of initial concentration 100 mg/L was achieved by using a mass of 0.01 g each for the adsorbents ie, ACP, ACZ, ACP/AgNP and ACZ/AgNP. The pH was varied between 2 and 11 by either using NaOH or HCl both of concentrations 0.1 N. Figure 67 shows the variation of quantity adsorbed at different pH (Table B-1 and Table B-5 in appendix B for experimental data, page 223 and 224).

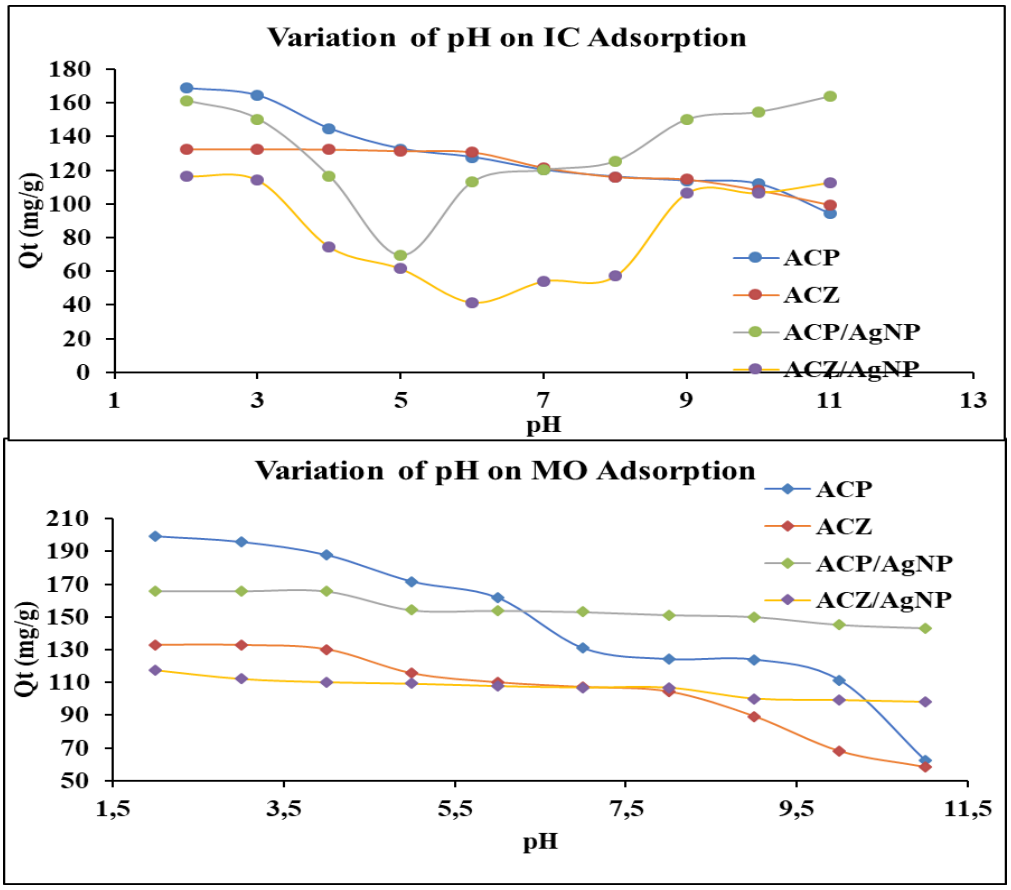

Figure 67: Variation of pH on IC and MO Adsorption on ACP, ACZ, ACP/AgNP and ACZ/AgNP

Figure 67 shows that the maximum adsorption of IC and MO dyes was at pH 2 for all the adsorbents. The maximum adsorption at pH 2 might be due to protonation of the surface of the adsorbents by the H^+ ions. This implies that at pH 2, the H^+ ions will neutralize all the

negative charges on the surface of the adsorbent leaving the surface positively charged thereby increasing the electrostatic force of attraction between the positively charged adsorbents and the negatively charged anionic dyes. Also, at pH lower than 4.0, 6.5, 7.6 and 7.7 (corresponding to pH_{PZC} for ACP, ACZ, ACP/AgNP and ACZ/AgNP respectively) the surface of the activated carbons and their respective composite becomes positively charged, and the electrostatic repulsion between the adsorbate and the adsorbents becomes weaker and the IC and MO may be easily transported to the surface of the adsorbents and become attached on the surface. It can also be due to the fact that at pH 2, there is protonation of the adsorbate, facilitating intra-particle diffusion and hence favors adsorption of IC and MO. A similar result was obtained by Alok *et al.,* (2007). But for pH greater than 2, the number of positively charged surface sites decreases, which did not favor adsorption due to electrostatic repulsion with negatively charged IC dye.

Also, at pH greater than the pH_{PZC} for the respective adsorbents, the excess OH^- ions which is very mobile increases the repulsion barrier on the surface of the negatively charged adsorbents which decreases the adsorption capacities of IC and MO respectively. They might also be a possibility of competition between the OH^- ions and the negative adsorbate (IC and MO) on the adsorbents. In both adsorption cases (IC and MO), the adsorption on the doped carbons was almost independent of pH. This can be attributed to the pH_{zpc} on the doped carbons which is almost 7. In both adsorption process on the ACP/AgNP and the ACZ/AgNP, the quantity of IC and MO dye adsorbed was found to increase significantly. The believed mechanisms is that, at pH greater than 7, there is the possibility of a redox reaction taking place which therefore facilitates the change in the form of the molecules and consequently its colour. The pH for further adsorption test was therefore taking as pH 2 in both cases.

III.5.1.2. Influence of contact time on IC and MO adsorption

With pH 2 and adsorbent mass of 0.01 g under agitation, the agitation time was varied between 5 and 60 min. The solutions were removed under their different agitation time and filtered. The filtrates were analyzed using UV-spectrometer. Figure 68 displayed the result obtained.

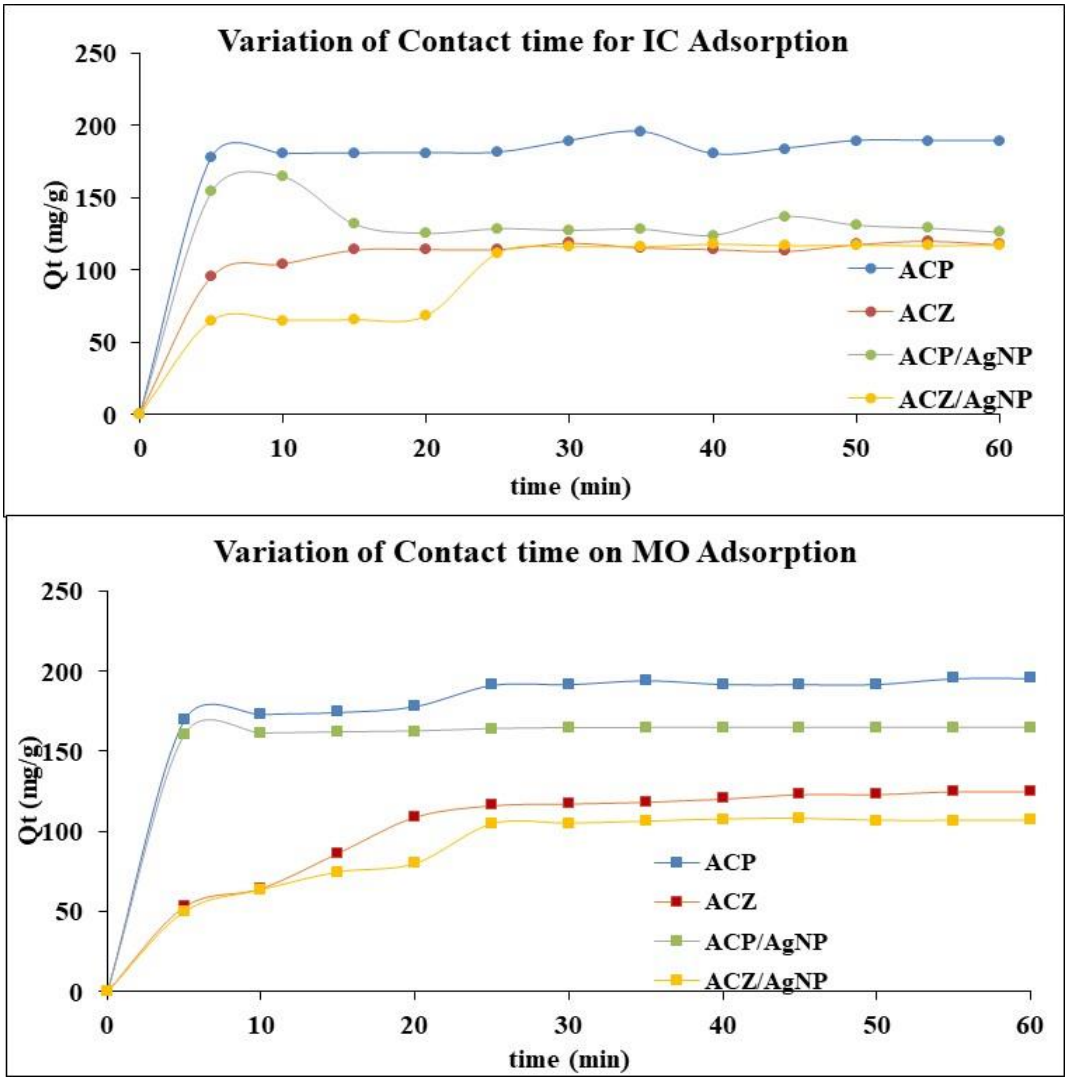

Figure 68: Variation of contact time on IC and MO Adsorption on ACP, ACZ, ACP/AgNP and ACZ/AgNP

The results for the four adsorbents indicate that, adsorption rate was rapid within the first five minute for all the adsorbents (Table B-2 and Table B-6 in appendix B for experimental data, page 223 and 224). It then slows down and come to equilibrium at 10 minutes for ACP and 20 min for both ACZ and ACP/AgNP adsorbents. In the case of ACZ/AgNP, it slows down up to 20 min and increased again from the 20th to the 25th min and finally slows down to attain equilibrium and 30 min beyond which there was no significant increase in the removal rate in the case of IC adsorption while in the case of MO, equilibrium was achieved at 10 minutes for ACP/AgNP and 25 min for ACP, ACZ and ACZ/AgNP adsorbents respectively. The speed is first rapid due to the availability of active sites for surface adsorption. It slows down due to saturation of adsorption site. The second increase may be due to Pore (intra-particle) diffusion from the bulk fluid onto the inner surface of the porous adsorbents through the film due to

continuous agitation. Similar results were obtained by Sumalatha *et al*., 2014. It later comes to equilibrium due to saturation of adsorption sites. It is though that the stages of sorption of IC and MO on activated carbon might be controlled by the diffusion process from bulk to the surface or the heterogeneous nature of the adsorbent.

III.5.1.3. Influence of Adsorbent dose on IC and MO adsorption

The study of the effect of adsorbent dosage for the removal of IC and MO dyes was done by varying the mass of the adsorbents, that is, ACP, ACZ, ACP/AgNP and ACZ/AgNP respectively from 0.01 to 0.06 g. After the respective consequent adsorption, the solutions as usual were filtered and the filtrate analyzed for the respective IC and MO residual concentrations (Table B-3 and Table B-7 in appendix B for experimental data, page 223 and 224), the graphs of Figure 69 demonstrate the quantity adsorbed versus the varied mass.

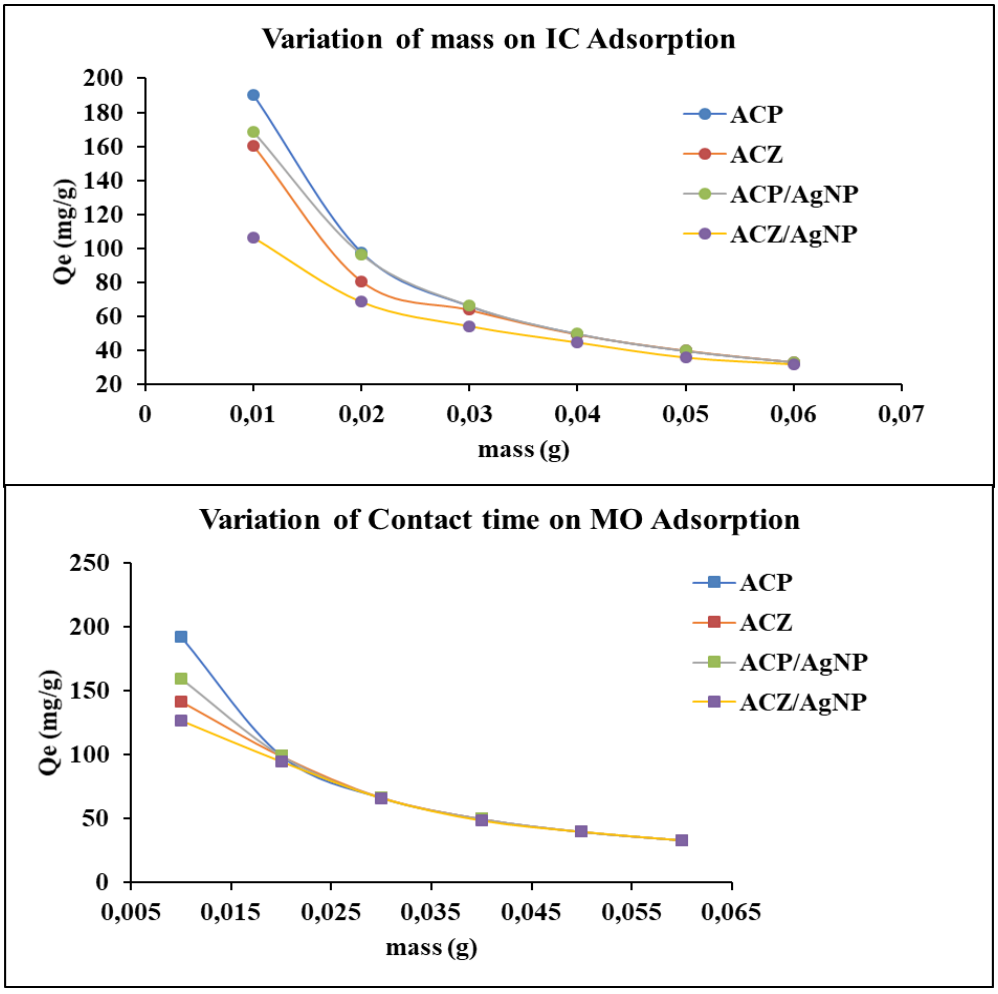

Figure 69: Variation of adsorbent dose on IC and MO Adsorption on ACP, ACZ, ACP/AgNP and ACZ/AgNP

From Figure 69, it shows that increasing the mass of the adsorbents, the quantity dyes adsorbed per gram showed a remarkable decrease for the four adsorbents. The decrease in adsorption capacity is basically due to masking of adsorption sites, that is, the available surface area for IC and MO adsorption respectively decreases due to aggregation of active sites for surface adsorption. Similar result was obtained by other researches precisely (Fungaro *et al.*, 2011; Ankoro *et al.*, 2016).

III.5.1.4. Influence of initial dye concentration on IC and MO adsorption

The concentration of IC and MO were respectively varied between 50 to 100 ppm for an adsorption pH of 2, adsorbent dose of 0.01 g and at their individual respective contact time obtained during the variation of contact time between the adsorbates and the carbonaceous materials. The analytical result obtained was plotted as shown Figure 70.

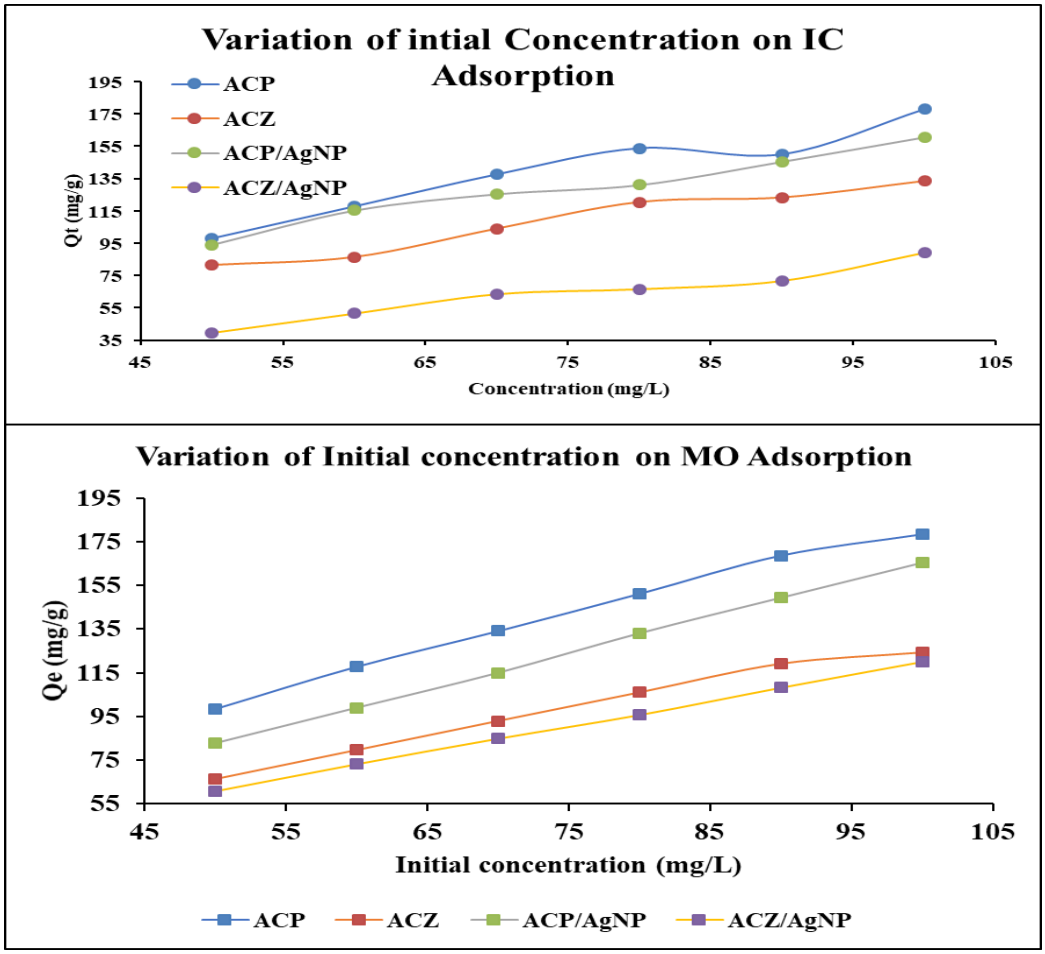

Figure 70: Variation of Initial Concntration of IC and MO Adsorption on ACP, ACZ, ACP/AgNP and ACZ/AgNP

It is observed (Figure 70) that as the initial dye concentration increase, the quantity adsorbed increase as a function of the initial dye concentration for the three adsorbents. This quantity increases from 98.801 to 177.801, 81.446 to 133.407, 94.108 to 160.678 and 39.638 to 89.181mg/g; 98.523 to 178.356, 66.351 to 124.204, 82.817 to 165.384 and 60.936 to 120.102 mg/g for respectively IC and MO adsorption on ACP, ACZ, ACP/AgNP and ACZ/AgNP adsorbents respectively (Table B-4 and Table B-8 in appendix B for experimental data, page 223 and 225). This increase is attributed to the fact that as the concentration of the adsorbates (IC and MO) increase, the distance between the dye molecules themselves and the adsorbents decreases. The number of effective collisions between the dye molecules and between the dye molecules and the adsorbents increases as a result of increase in the mobility of the molecules due to high collision between the molecules themselves. Ankoro et al 2016 observed similar phenomenon. These increase in effective collision helps to rupture the resistance force between the adsorbates and the adsorbents. Hence favoring adsorption which therefore leads to increase in the quantity adsorbed non the respective adsorbents. Furthermore, the adsorbents were found to have more affinity with IC than with MO. In addition, the adsorption capacity of ACP and ACP/AgNP was higher than ACZ and ACZ/AgNP. This could be as a result of ACP having an amorphous structure than ACZ while ACP/AgNP has a less crystalline structure than ACZ/AgNP. The undoped carbons had higher adsorption properties than the doped once confirming that some of the pores of the undoped once must have been blocked by the AgNPs during the doping process.

III.5.2. Adsorption Isotherm Studies

Adsorption isotherm which is the relationship between the adsorbate in the liquid phase and the adsorbate adsorbed on the surface of the adsorbent at equilibrium at constant temperature (Ndi *et al.*, 2014). In order to successfully represent the dynamic adsorptive behavior of any substances from the fluid to the solid phase, it is important to have a satisfactory description of the equilibrium state between the two phases comprising the adsorption system. Four Isotherms models were used to represent the adsorption behavior of the IC and MO dyes in the fluid phase to the solid phase. In this regard, the analyzed date was done under the four non-linear isotherms models of Langmuir, Freundlich, Tempkin and Dubinin-Kaganer-Raduskevich as presented Figure 71 and 72.

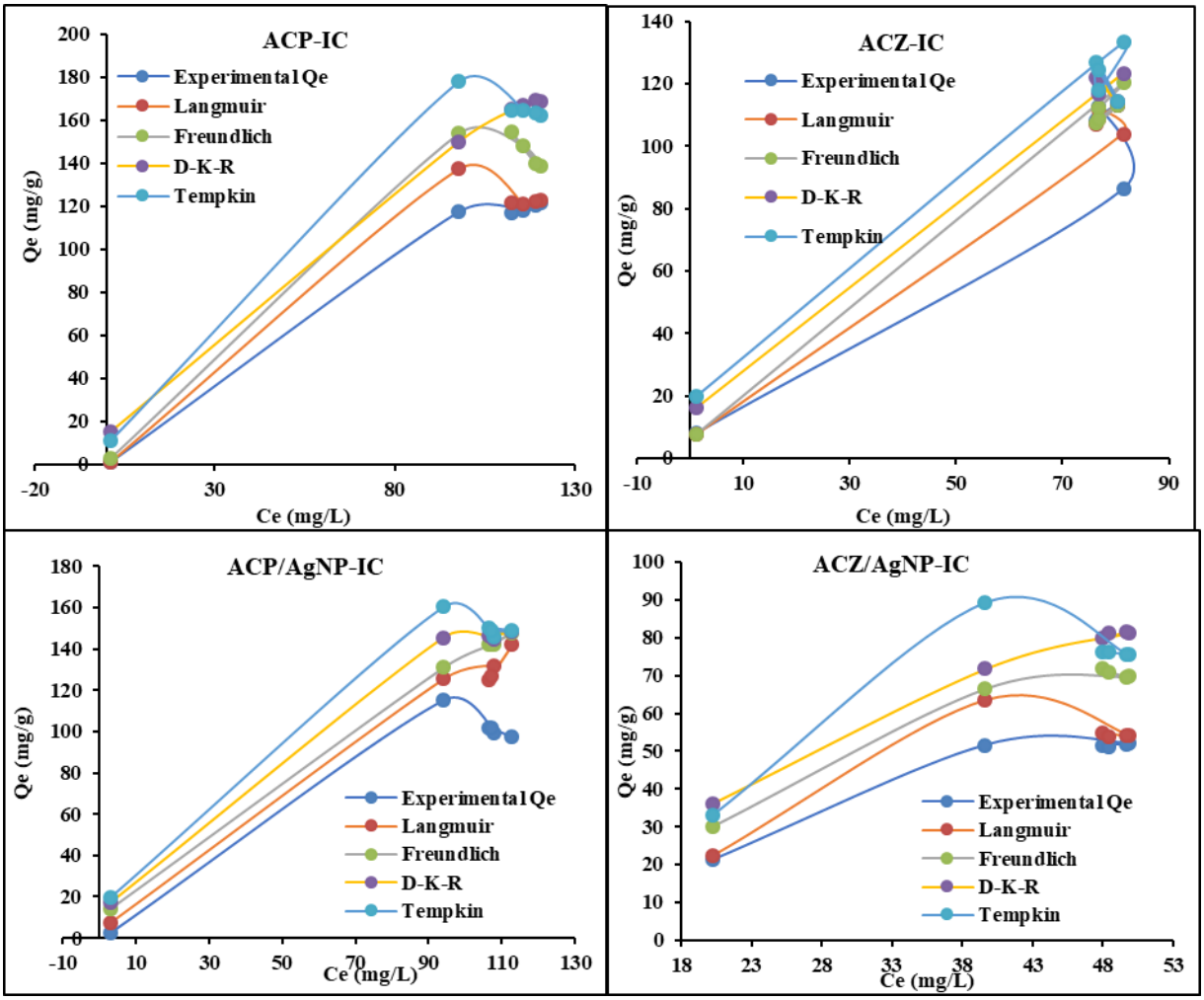

Figure 71: Non-Linear Adjustement of Langmuir. Freundlich. D-K-R and Tempkin Isotherm models on IC adsorption on ACP. ACZ. ACP/AgNP and ACZ/AgNP

A summary of the different relative isotherm constants and their respective determination coefficients (R^2, *RMSE* and χ^2) for the adsorption of IC on ACP, ACZ, ACP/AgNP and ACZ/AgNP are grouped in Table XXXVIII.

It should be noted that the smaller the *RMSE* and χ^2 values, ie the deviation of *RMSE* and χ^2 from the equilibrium quantity adsorbed (q_e) from the batch experiment, the better the results. It also indicates the better model fitting and the similarity of the model data with the experimental data respectively (Hossain *et al*., 2013).

Table XXXVIII: Summary of the different relative isotherm constants and their respective determination coefficients (R^2, *RMSE* and χ^2) for the adsorption of IC on ACP, ACZ, ACP/AgNP and ACZ/AgNP

Isotherm models	Parameters	Adsorbents			
		ACP	ACZ	ACP/AgNP	ACZ/AgNP
Langmuir	qe (exp) (mg g-1)	177.802	133.407	160.678	89.181
	q_m (mg g^{-1})	172.778	121.752	155.204	411.680
	K_L (L. g^{-1})	1.840	1.506	0.775	0.007
	R^2	1.000	0.999	1.000	0.999
	RMSE	16.345	16.750	14.463	10.879
	χ^2	7.880	9.956	7.048	7.344
	R_L	0.005	0.007	0.013	0.595
Freundlich	K_F (L. g^{-1})	119.050	74.673	87.491	3.769
	1/n	0.129	0.177	0.181	0.857
	R^2	0.607	0.672	0.791	0.669
	RMSE	19.812	13.480	11.882	10.956
	χ^2	11.388	6.766	4.803	7.432
D-K-R	q_s (mg. g^{-1})	165.447	114.674	150.000	101.544
	K_{ad} (mol^2. J^{-2})x10^{-7}	1.509	1.447	5.430	526.800
	E (kJ. mol^{-1})	1820.096	1859.119	959.589	97.426
	R^2	0.781	0.413	0.492	0.719
	RMSE	14.773	18.038	18.505	10.083
	χ^2	6.454	11.454	11.209	6.256
Tempkin	A_T (L. g^{-1})	467.595	88.647	43.947	0.115
	B_T (J. mol^{-1})	130.625	149.880	113.328	43.822
	R^2	0.631	0.640	0.771	0.694
	RMSE	9.190	14.137	12.412	10.523
	χ^2	10.681	7.303	5.205	6.817

ACP: Phosphoric acid activated carbon; ACZ: Zinc chloride activated carbon; ACP/AgNP: Phosphoric acid activated carbon doped with silver nanoparticles. ACZ/AgNP: Zinc chloride activated carbon doped with silver nanoparticles

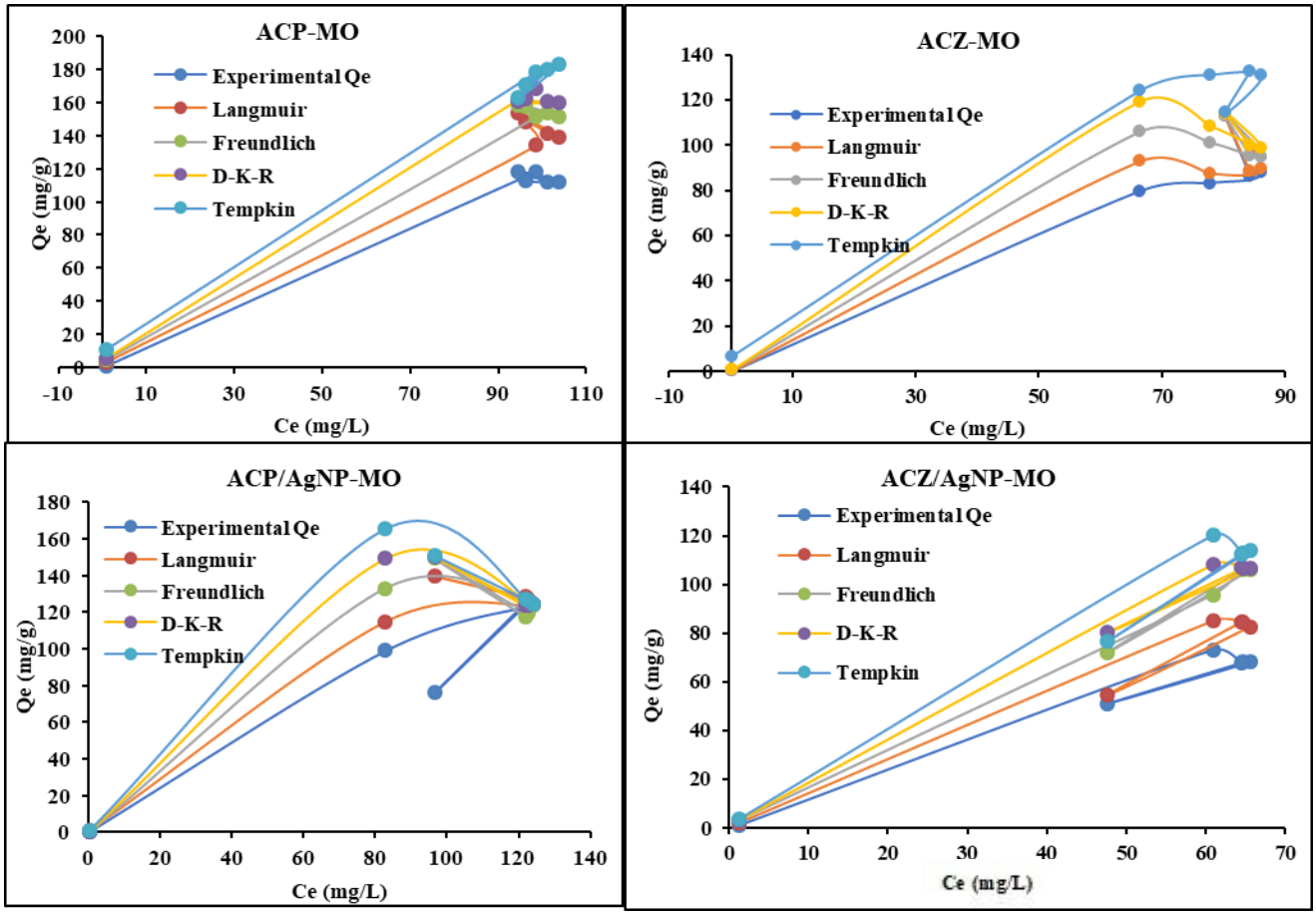

Figure 72: Non-Linear Adjustement of Langmuir, Freundlich, D-K-R and Tempkin Isotherm models on MO adsorption on ACP, ACZ, ACP/AgNP and ACZ/AgNP

A summary of the different relative isotherm constants and their respective determination coefficients (R^2, *RMSE* and χ^2) for the adsorption of MO on ACP, ACZ, ACP/AgNP and ACZ/AgNP are grouped in Table XXXIX.

Table XXXIX: Summary Table of the different relative isotherm constants and their respective determination coefficients (R^2. *RMSE* and χ^2) for the adsorption of MO on ACP. ACZ. ACP/AgNP and ACZ/AgNP.

Isotherm models	Parameters	Adsorbents			
		ACP	ACZ	ACP/AgNP	ACZ/AgNP
Langmuir	qe (exp) (mg g-1)	178.356	124.204	165.386	120.102
	q_m (mg g^{-1})	181.079	131.608	124.184	173.184
	K_L (L. g^{-1})	1.531	5.817	5808.395	0.474
	R^2	0.9999	0.9997	0.998	0.9998
	RMSE	9.655	9.543	34.778	7.337
	χ^2	2.506	3.874	38.975	2.233
	R_L	0.006	0.002	$1.721X10^{-6}$	0.021
Freundlich	K_F (L. g^{-1})	110.644	103.152	127.401	58.880
	1/n	0.211	0.124	0.032	0.485
	R^2	0.961	0.589	0.008	0.919
	RMSE	6.765	16.208	34.638	6.999
	χ^2	1.327	11.251	38.596	2.099
D-K-R	q_s (mg. g^{-1})	163.657	114.674	153	102.778
	K_{ad} (mol^2. J^{-2})$x10^{-7}$	1.218	1.447	8.790	539.600
	E (kJ. mol^{-1})	2026.216	1859.116	754.183	96.263
	R^2	0.836	0.413	0.182	0.720
	RMSE	13.791	18.038	23.484	10.075
	χ^2	4.898	11.454	24.838	6.218
Tempkin	A_T (L. g^{-1})	42.651	1458.425	$1220X10^{18}$	3.716
	B_T (J. mol^{-1})	85.150	172.897	450.726	59.242
	R^2	0.965	0.637	0.006	0.914
	RMSE	6.407	15.242	34.676	7.226
	χ^2	1.185	9.851	38.721	2.165

ACP: Phosphoric acid activated carbon; ACZ: Zinc chloride activated carbon; ACP/AgNP: Phosphoric acid activated carbon doped with silver nanoparticles. ACZ/AgNP: Zinc chloride activated carbon doped with silver nanoparticles

Langmuir adsorption isotherm is best known for its applicability to explain adsorption phenomenon on monolayer coverage hence predicting a chemisorption process with strong

forces between the adsorbate and the adsorbents. From Tables XXXVIII and XXXIX, the Langmuir for the four adsorbents and on both adsorbates was the most suitable and best to explain the adsorption phenomenon looking at its R^2 values which is unity or closer to unity with values of 1.000, 0.999, 1.000 and 0.999 for IC adsorption; and 1.000, 1.000, 0.998 and 1.000 for MO adsorption on ACP, ACZ ACP/AgNP and ACZ/AgNP respectively. Also, the maximum quantity adsorbed on the monolayer coverage (q_m) theoretically for both adsorbates on the respective adsorbents (except for ACZ/AgNP in both cases) is closer to the experimental quantities. This implies that most of the adsorbate molecules adsorbed at equilibrium is found on the monolayer coverage and this permits to presume a chemisorption phenomenon on the respective adsorbents. The high values of the Langmuir adsorption constant (K_L) on both adsorbates on the respective adsorbents (except for ACZ/AgNP for both adsorbates) implies the isotherm model is best applicable to explain the adsorption process taking place. This applicability was further substantiated by the low values of *RMSE* and χ^2 for both adsorbates (except for ACP/AgNP in the case of MO adsorption). Furthermore, the Langmuir separation constant R_L for all the adsorbents on the adsorption of both respective adsorbates being found between 0 and 1 (ie $0 < R_L < 1$) implies the adsorption of the two adsorbates on the respective adsorbents are favorable.

The Freundlich isotherm model which is best applies to adsorption on heterogeneous surfaces with interaction between the adsorbed molecules and the is no restriction to the formation of a multi-layer was not the best to explain the adsorption of IC on the four adsorbates but could be used to explain the adsorption of MO on ACP and ACZ/AgNP looking and the R^2 values which are respectively 0.961 and 0.919. Nevertheless, despite its non-satisfactory R^2 values in most cases, the high values the Freundlich constant (K_F) for adsorbates on all the adsorbents makes the model applicable to presume the possibilities of the formation of a multi-layer coverage on the surface of the respective adsorbents at higher dye concentrations. This possibility was further strengthened by the low values of *RMSE* and χ^2 for both adsorbates on all the respective adsorbents (except for ACP/AgNP in the case of MO adsorption). In addition, Freundlich heterogeneity factor *1/n* being lower that 1 implies the surface of the respective adsorbents is heterogenous vis-à-vis the adsorbates (IC and MO).

The information obtained from the Langmuir and Freundlich isotherms are generally insufficient to explain the physical and chemical characteristic of the adsorption phenomenon. Dubinin–Kaganer-Radushkevich isotherm is generally applied to express the adsorption mechanism with a Gaussian energy distribution onto a heterogeneous surface (Dada *et al.*,

2012; Mehrabi *et al.*, 2015). The model has often successfully fitted high solute activities and the intermediate range of concentrations data well. The approach was usually applied to distinguish the physical and chemical adsorption of adsorbate molecules with its mean free energy. E per molecule of adsorbate (for removing a molecule from its location in the sorption space to the infinity). From Tables XXXVIII and XXXIX the R^2 values of all the adsorbents were in sufficient to compromised the adsorption phenomenon but nevertheless, the theoretical quantities adsorbed at equilibrium is approximately the same as the experimental adsorbed quantities for all the adsorbates on the respective adsorbents studied. Also, despite the fact that the small values of the D-K-R adsorption isotherm constant K_{ad} could not be used to explain the adsorption process, the D-K-R energy constant (E) for all the adsorbents on the adsorption of IC and MO being far greater than 8 $kJmol^{-1}$, indicates that the adsorption processes of the adsorbents on the adsorbates is dominated by chemisorption with the formation of chemical bonds. This further confirms the strong interactive forces between the adsorbates and the adsorbents presumed by the Langmuir model.

The Tempkin Isotherm model is of used to explain adsorption phenomenon because it contains a factor that is explicitly taking into the account the adsorbent–adsorbate interactions by ignoring the extremely low and large value of concentrations, the model assumes that heat of adsorption (function of temperature) of all molecules in the layer would decrease linearly rather than the logarithmic with coverage (Mehrabi *et al.*, 2015). According to Tables XXXVIII and XXXIX, the Tempkin isotherm could be used to explain the adsorption of MO on ACP and ACZ/AgNP with R^2 values respectively 0.965 and 0.914; *RMSE* values of (6.407 and 7.226) and χ^2 values of (1.185 and 2.165). Nevertheless, despite the consequent low values of R^2 in some cases the high value of the Tempkin isotherm equilibrium binding energy constant A_T in all the adsorption process (both IC and MO on all four respective adsorbents) implies the bond energies of the adsorbents and the respective adsorbates is very high hence strong bond are formed between the adsorbates and the respective adsorbents. In addition, the high adsorption energies of the adsorption process of IC and MO on all the adsorbents further confirms the chemisorption process.

III.5.3. Adsorption Kinetics of IC and MO Adsorption

The adsorption kinetic study describes the speed at which the solute phase is retained on the surface of the adsorbents, the time necessary for the process to attained equilibrium and also predicts the limiting step of the adsorption process. It also permits one to determine the effectiveness of the adsorption process. The non-linear kinetic models of pseudo-first order, pseudo-second order, intra-particle diffusion and Elovich were studied in this our work with the aim of determining the type mechanism or type of adsorption put in place between the adsorbate and the adsorbent as well as the rate limiting step of the adsorption of IC and MO on ACP, ACZ, ACP/AgNP and ACZ/AgNP. In this regard, the graphs relative to the respective non-linear models (see chapter 1) is given by Figures 73 and 74 and Tables XL and XLI gives an over view summary of the kinetic parameters and their respective determination coefficients (R^2, *RMSE* and χ^2) for the adsorption process.

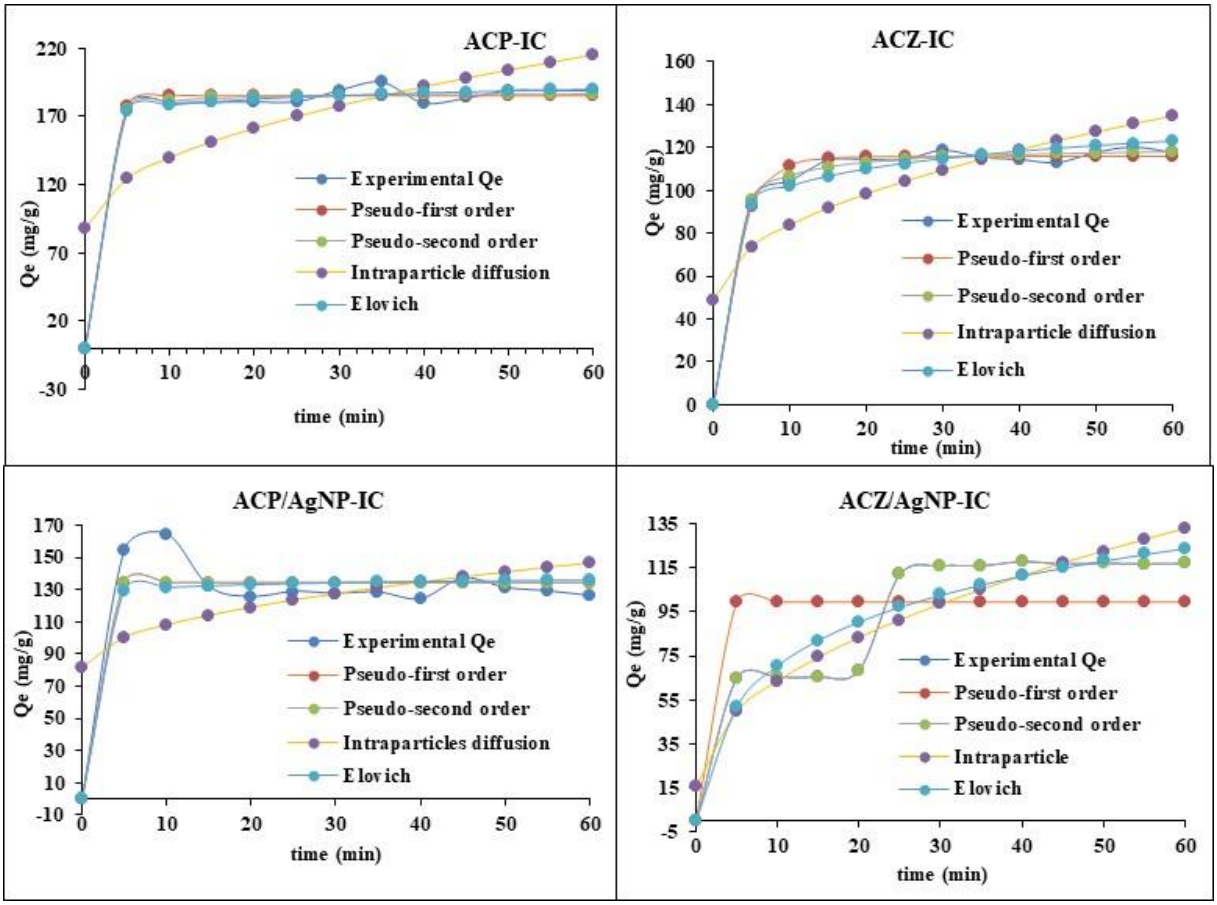

Figure 73: Non-Linear Adjustement of Pseudo-first order. Pseudo-second order. Intrapqrticle diffusion and Elovic kinetic models on IC adsorption on ACP. ACZ. ACP/AgNP and ACZ/AgNP

A summary of the different relative adsorption kinetic constants and their respective determination coefficients (R^2, *RMSE* and χ^2) for the adsorption of IC on ACP, ACZ, ACP/AgNP and ACZ/AgNP are grouped in Table XL.

Table XL: Summary table of Correlation coefficients and non-linear constants of kinetic models on the Adsorption Kinetics of IC

Kinetic models	Parameters	Adsorbents			
		ACP	ACZ	ACP/AgNP	ACZ/AgNP
Pseudo-first order	q_e (exp) (mg g^{-1})	180.186	114.473	176.532	115.876
	q_e (pred) (mg g^{-1})	185.505	115.755	133.967	99.455
	k_1 (min^{-1})	0.625	0.323	4.986	0.262
	R^2	0.991	0.992	0.896	0.262
	RMSE	5.015	3.087	12.490	24.758
	χ^2	1.492	0.940	12.809	67.794
Pseudo-second order	q_e (pred) (mg g^{-1})	188.209	120.613	133.966	125.000
	K_2 (mg $g^{-1}min^{-1}$)	0.015	0.006	2329.738	34.000
	R^2	0.993	0.995	0.896	1.000
	RMSE	4.397	2.268	12.490	0.000
	χ^2	1.145	0.494	12.810	0.000
Intra-particle diffusion	k_{id}	16.420	11.123	15.045	8.424
	C_i (mg. g^{-1})	87.972	48.703	16.114	81.279
	R^2	0.853	0.900	0.976	0.496
	RMSE	37.442	20.994	13.733	35.620
	χ^2	52.143	26.198	20.633	68.047
Elovich	α (mg $g^{-1}min^{-1}$)	26.433	$2.643x10^{21}$	6405.070	$5.225x10^{11}$
	β (g. min^{-1})	0.032	0.386	0.085	0.154
	R^2	0.894	0.870	0.984	0.994
	RMSE	11.832	13.989	4.305	4.262
	χ^2	17.991	16.363	1.802	1.077

ACP: Phosphoric acid activated carbon; ACZ: Zinc chloride activated carbon; ACP/AgNP: Phosphoric acid activated carbon doped with silver nanoparticles. ACZ/AgNP: Zinc chloride activated carbon doped with silver nanoparticles

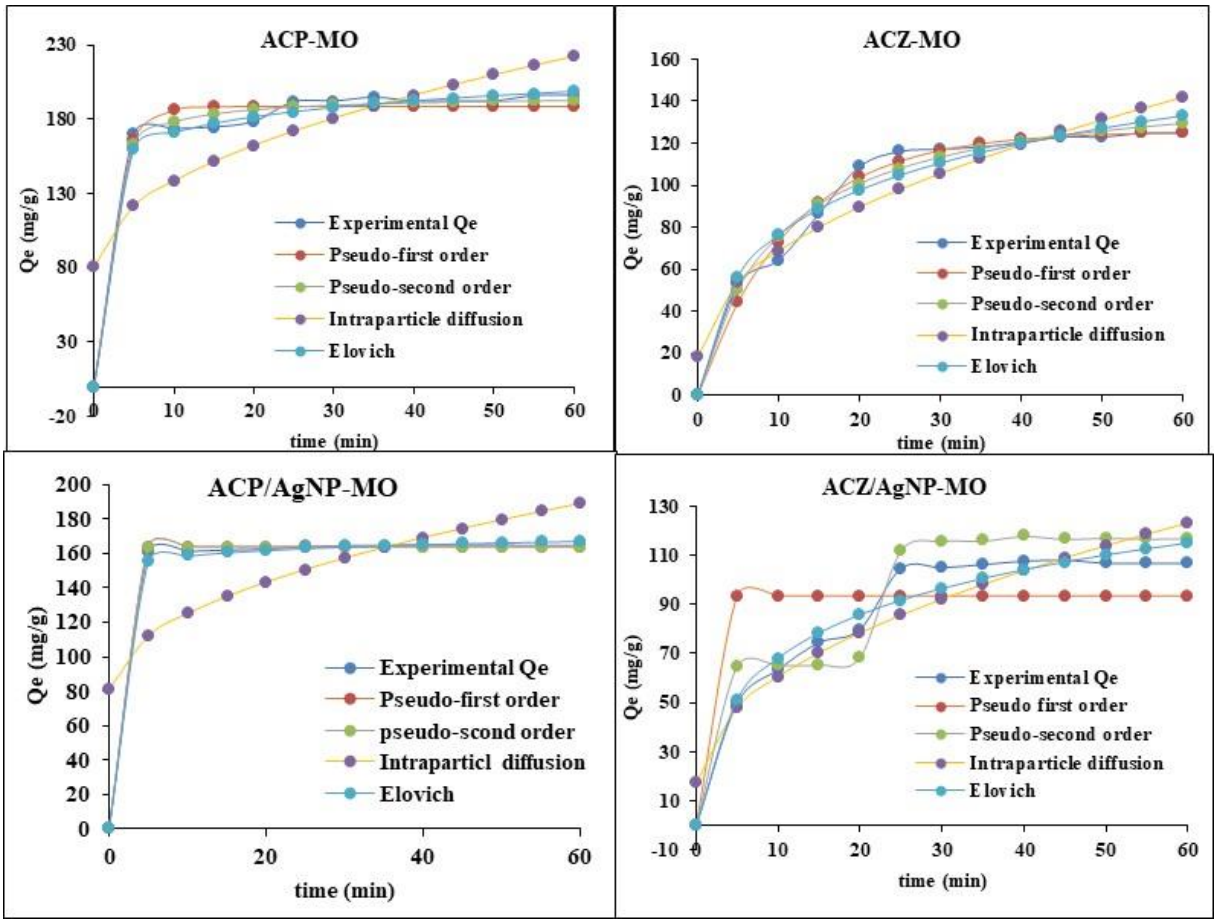

Figure 74: Non-Linear Adjustement of Pseudo-first order, Pseudo-second order, Intrapqrticle diffusion and Elovic kinetic models on MO adsorption on ACP, ACZ, ACP/AgNP and ACZ/AgNP

A summary of the different relative adsorption kinetic constants and their respective determination coefficients (R^2, *RMSE* and χ^2) for the adsorption of MO on ACP, ACZ, ACP/AgNP and ACZ/AgNP are grouped in TableXLI.

Table XLI: Summary table of Correlation coefficients and non-linear constants of kinetic models on the Adsorption Kinetics of MO

Kinetic models	Parameters	Adsorbents			
		ACP	ACZ	ACP/AgNP	ACZ/AgNP
Pseudo-first order	q_e (exp) (mg g^{-1})	191.452	116.273	161.174	104.697
	q_e (pred) (mg g^{-1})	188.849	125.827	163.586	93.358
	k_1 (min^{-1})	0.422	0.087	4.986	3.443
	R^2	0.980	0.987	0.999	0.413
	RMSE	7.754	4.594	1.628	20.716
	χ^2	3.528	3.498	0.178	50.566
Pseudo-second order	q_e (pred) (mg g^{-1})	196.000	150.616	163.586	125
	K_2 (mg $g^{-1}min^{-1}$)	0.005	0.001	2329.738	34
	R^2	0.992	0.980	0.999	0.927
	RMSE	4.983	5.553	1.628	10.414
	χ^2	1.505	3.728	0.178	13.157
Intra-particle diffusion	k_{id}	18.240	16.007	13.976	13.654
	C_i (mg. g^{-1})	80.568	18.078	80.689	17.482
	R^2	0.900	0.982	0.832	0.981
	RMSE	34.296	12.648	34.144	11.284
	χ^2	43.551	13.516	48.190	11.065
Elovich	α (mg $g^{-1}min^{-1}$)	93997.303	29.450	1.104 $X10^{14}$	30.299
	β (g. min^{-1})	0.065	0.030	0.208	0.037
	R^2	0.993	0.965	0.958	0.961
	RMSE	4.536	7.277	2.144	6.549
	χ^2	1.299	6.024	0.317	4.977

ACP: Phosphoric acid activated carbon; ACZ: Zinc chloride activated carbon; ACP/AgNP: Phosphoric acid activated carbon doped with silver nanoparticles. ACZ/AgNP: Zinc chloride activated carbon doped with silver nanoparticles

From the Tables XL and XLI, the pseudo-first kinetic model was most appropriate to explain the adsorption of IC on ACP and ACZ judging from its high R^2 values which is closer to unity and their experimental adsorbed quantity which is closed to the theoretical quantity adsorbed at equilibrium. Also, its low values of *RMSE* and χ^2 for ACP, ACZ and ACP/AgNP adsorbents makes the model suitable to explain the adsorption process. For MO adsorption, the pseudo-first kinetic model was most appropriate to explain the its adsorption on ACP, ACZ and

ACP/AgNP from its high R^2 values of respectively 0.980, 0.987 and 0.999 which is closer to unity. Also, their experimental quantity adsorbed which is closed to the theoretical quantity adsorbed at equilibrium confirms the validity of this model on the above respective adsorbent. Furthermore, the low values of *RMSE* and χ^2 for ACP, ACZ and ACP/AgNP adsorbents makes adds to the credibility of the model to explain the adsorption process.

The pseudo-second order kinetic model was most appropriate to explain the adsorption of IC on ACP, ACZ and ACZ/AgNP from its R^2 values which is closer to unity and their experimental adsorbed quantity which is closed to the theoretical quantity adsorbed at equilibrium. The reliability of this model to explain the adsorption mechanisms was further confirm by their respective low values of *RMSE* and χ^2 which are 4.397, 2.269, 12.490 and 0.000 and 1.145, 0.494, 12.810 and 0.000 (for *RMSE* and χ^2 respectively) for ACP, ACZ, ACP/AgNP and ACZ/AgNP respectively. For the adsorption of MO, the pseudo-second order kinetic model was best to explain the adsorption of MO on all the adsorbents from its R^2 values which is closer to unity and their experimental adsorbed quantity which is very closed to the theoretical quantity adsorbed at equilibrium. The low values of *RMSE* and χ^2 (4.983, 5.553, 1.628 and 10.414 for *RMSE;* and 1.505, 3.728, 0.178 and 13.157 for χ^2) further magnifies the model's validation of the adsorption mechanism of MO on the adsorbents. This model strongly described interaction between the surface of these adsorbents and the adsorbates, which indicates that the adsorption is might be with chemisorption with the formation of strong bonds between the adsorbents and the adsorbates.

With respect to R^2 values, the Intra-particle diffusion model is most suitable to explain the adsorption of IC on ACZ and ACP/AgNP with values of respectively 0.900 and 0.976 for IC adsorption while it was best for ACP, ACZ and ACZ/AgNP with values of 0.900, 0.982 and 0.981 respectively. However, the large values of the diffusion constant value K_{id} for all the adsorbents implies that diffusion rate of IC and MO is important in the adsorption process; but that's not withstanding, the high values of the constant C_i (which is the repulsion barrier between the adsorbate and the adsorbent) for all the adsorption processes (IC and MO) is an indication that the intra-particle diffusion step is not the rate limiting step in the adsorption mechanism. This therefore favors strong interaction between adsorbents and adsorbate molecules. This is further confirmed by the higher values of *RMSE* and χ^2 for all the adsorption process. This also indicates that the thickness of the boundry layer between adsorbents and the dyes (IC and MO) is high hence decrease the the chance of exthernal mass transfer but can increase the internal mass transfer (Ghaedi *et al*., 2015).

In the case of the Elovich model, all the R^2 values were significant but the best fitted interms of R^2 values was for ACP/AgNP and ACZ/AgNP composite materials with values of 0.984 and 0.994 respectively for IC adsorption. For MO adsorption all the R^2 values were very significant with values of 0.993, 0.965, 0.958 and 0.961 for ACP, ACZ, ACP/AgNP and ACZ/AgNP respectively. Also, the *RMSE* and χ^2 values which are respectively 4.305 and 1.802 for ACP/AgNP and 4.262 and 1.077 ACZ/AgNP for IC adsorption and the *RMSE* values (4.536, 7.277, 2.144 and 6.549); and the χ^2 values (1.299, 6.024, 0.317 and 4.977) throws further significance of this model to explain the adsorption of IC and MO on the above adsorbents. Nevertheless, The Elovich adsorption speed constant (α) for all four adsorbents is far greater than the desorption coefficient β for both the IC or MO adsorption processes which strongly declares without any doubt or fear of uncertainty that the adsorption process of IC on is the above respective adsorbents is chemisorption.

III.5.4. Characterisation of adsorbents by FTIR after adsorption of IC and MO on ACP, ACZ, ACP/AgNP and ACZ/AgNP adsorbents

The FTIR analysis of ACP, ACZ, ACP/AgNPand ACZ/AgNP after adsorption of IC and MOwas carried out to predict the role of surface groups in the adsorption process. The respective spectra were measured within 400 – 4000 cm^{-1}.

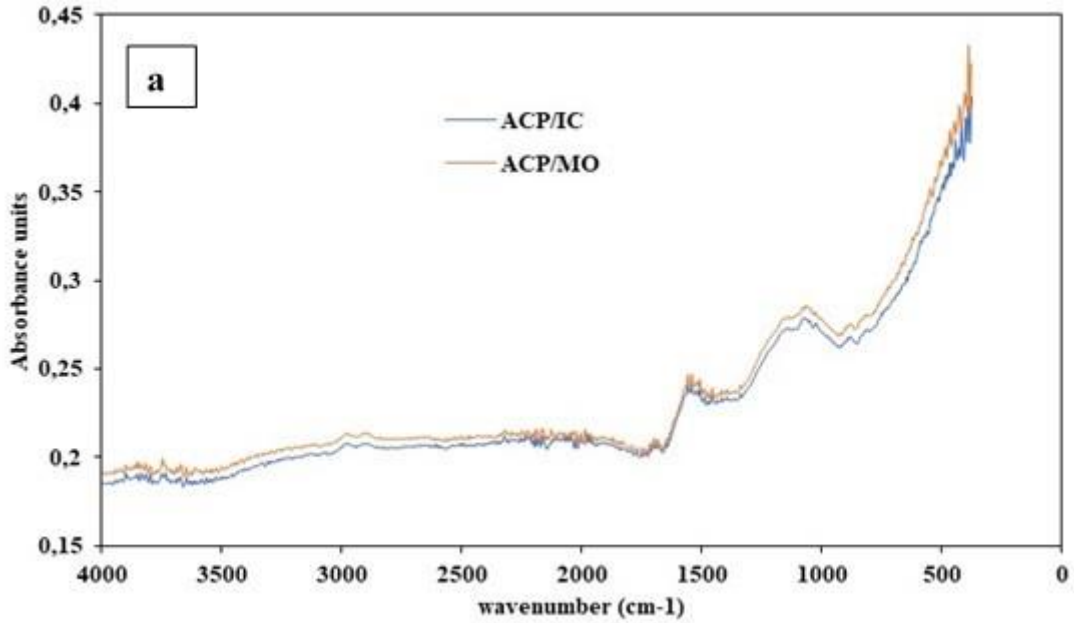

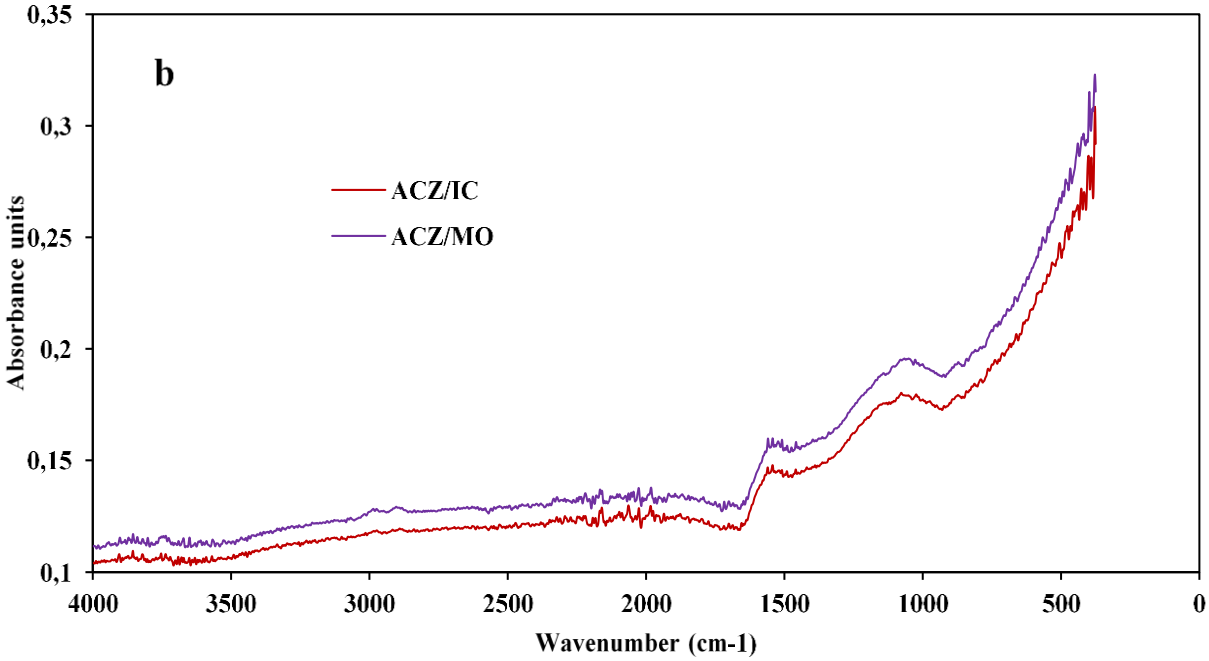
b
ACZ/IC
ACZ/MO
Absorbance units
0,35
0,3
0,25
0,2
0,15
0,1
4000
3500
3000
2500
2000
1500
1000
500
0
Wavenumber (cm-1)

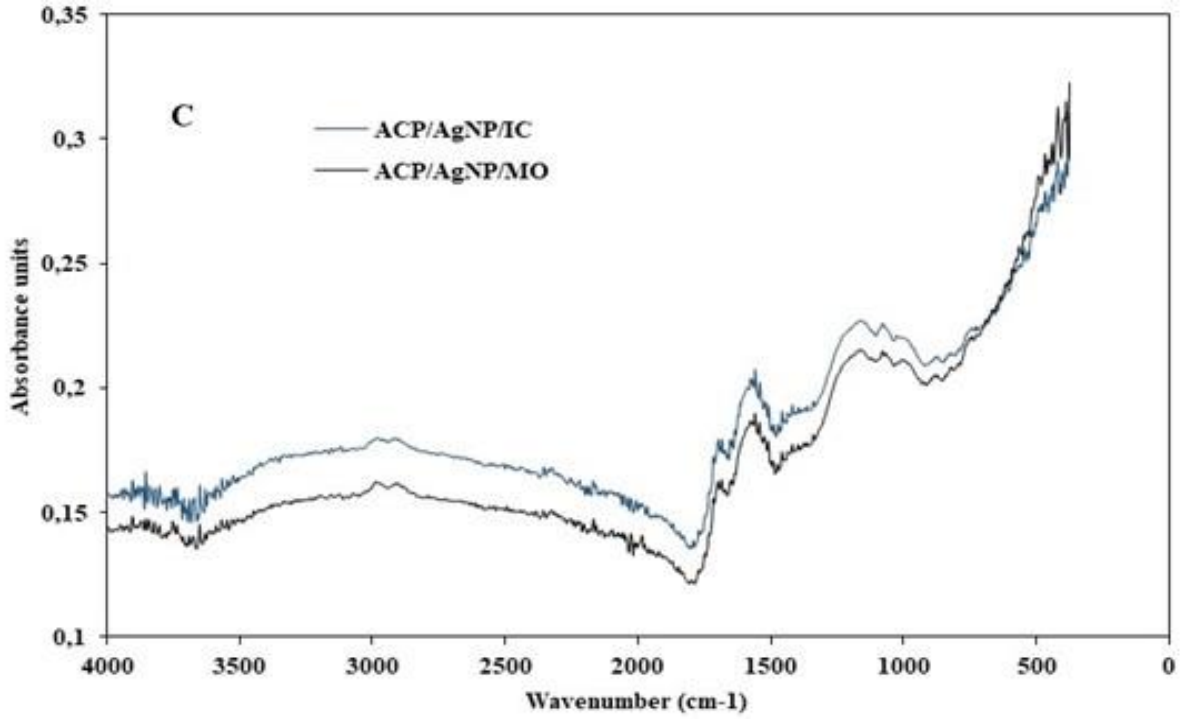
C
ACP/AgNP/IC
ACP/AgNP/MO
Absorbance units
0,35
0,3
0,25
0,2
0,15
0,1
4000
3500
3000
2500
2000
1500
1000
500
0
Wavenumber (cm-1)

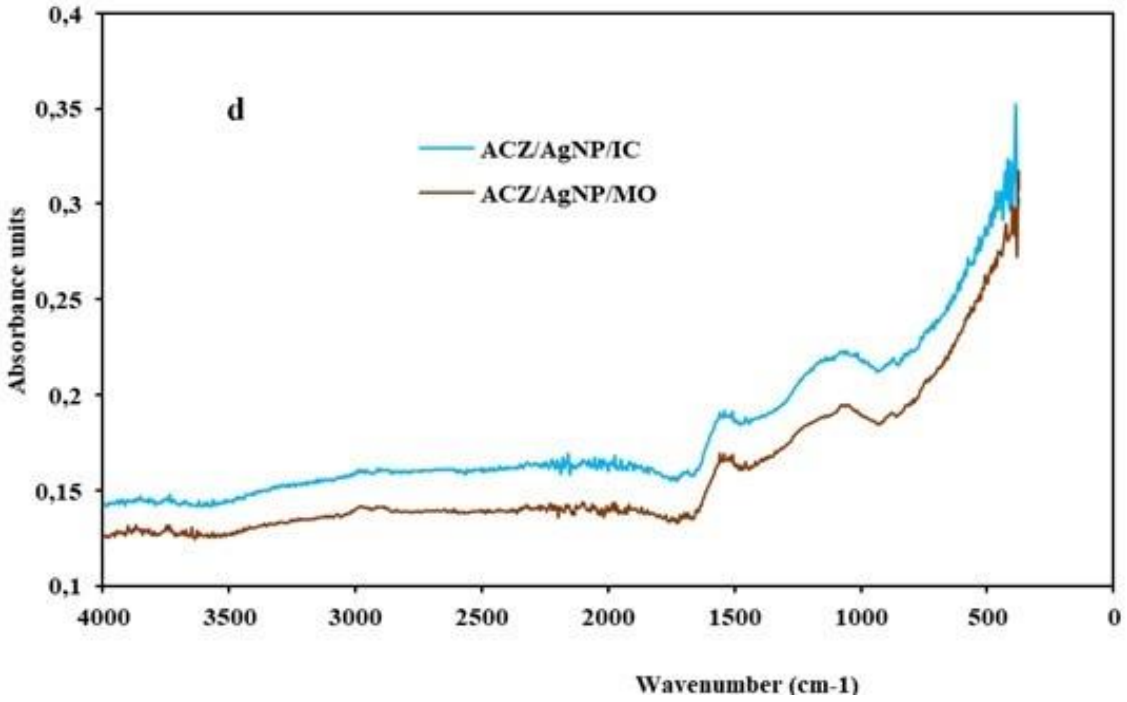

Figure 75: FTIR result after adsorption of IC and MO dyes on ACP, ACZ ACP/AgNP and ACZ/AgNP respectively

The FTIR spectra results of ACP, ACZ ACP/AgNP and ACZ/AgNP after adsorption of IC and MO are respectively as shown in Figure 75 (a, b, c and d). These results are identical to those of Figure 55 except that of ACP/IC and ACP/MO in which the bands around 3544 to 3758 and can be due to –OH stretching vibration in hydroxyl groups of alcohols, phenols, acids and adsorbed water of the ACP has diapered after adsorption. This may be due to the fact that the adsorption process that took place with the ACP involved the use of the –OH bonds during the process. Furthermore, the intensities of the peaks of the ACZ, ACP/AgNP and ACZ/AgNP of identical functional groups were found to decreased. This may be as a result of the adsorption process where the functions groups have been used up forming identical groups of other nature. Hence from the spectral after adsorption, we might say that the adsorption process involved in all the four material was dominated by chemisorption.

III.6. Antibacterial properties of RHS, RHS-NP, ACP, ACZ, ACP/AgNP and ACZ/AgNP Materials

The anti-bacteria properties of the RHS, RHS-NP, ACP, ACZ, ACP/AgNP and ACZ/AgNP materials were elucidated on seven different bacteria which are the typhoid-causing *Salmonella typhi (ST)*, food-poisoning *Staphylococcus aureus (SA)*, pneumonia-causing *Klebsiella pneumoniae* (KP) as well as the diarrheal-manifesting *Escherichia coli* (EC) and *Shigela flexneri (SF) and also on Salmonella enteritidis* (SE), *Salmonella typhimurium* (STM). This was achieved by first carrying out a screening test on the available bacteria species at our disposal. The results of the screening test are given in the Table XL.

III.6.1. Antibacterial preliminary screening profiles of RHS, RHS-NP, ACP, ACZ, ACP/AgNP and ACZ/AgNP Materials

The extracts were screened at a single concentration of 1 mg/mL against the aforementioned bacteria and the results of the screening effect are shown in the Table XLII.

Table XLII: Results of screening of the different samples from *Ricinodendron heudelotti* shells on the six enterobacteriaceae species

Sample	Microorganisms						
	SE	ST	STM	SA	KP	SF	EC
ACP	-	-	-	-	-	-	-
ACZ	-	-	-	-	-	-	-
ACP/AgNP(1 mM)	+	+	+	+	+	+	+
ACZ/AgNP(1 mM)	+	+	+	+	+	+	+
ACP/AgNP(5 mM)	+	+	+	+	+	+	+
ACZ/AgNP(5 mM)	+	+	+	+	+	+	+
RHSNP	+	+	+	+	+	+	+
RHSE	-	-	-	-	-	-	-

SE: S. enteritidis; ST: S. typhi; STM: S. typhimurium; SA: Staphylococcus aureus; KP:Klebsiella pneumoniae; SF:Shigella flexneri; EC:Escherichia coli; ACP: Phosphoric acid activated carbon; ACZ: Zinc chloride activated carbon; ACP/AgNP: Phosphoric acid activated carbon doped with silver nanoparticles; ACZ/AgNP: Zinc chloride activated carbon doped with silver nanoparticles; RHSE: Ricinodendron heudelotti shell extracts; RHSNP: Ricinodendron heudelotti shell nanoparticles; -: not active at 1 mg/mL; +: active at 1mg/mL

The results (Table XLII) shows that, at the tested concentration, the ACP, ACZ and the aqqueous extract of RHS were not active against any of the serovars and were therefore, not selected for the later part of the work. However, the composites materials (ACP/AgNP and ACZ/AgNP) at all concentrations and the RHSNPs were active on all the serovars.

III.6.2. Minimum Inhibitory Concentrations (MIC) and minimum Bacteria concentrations (MBC) of RHS, RHS-NP, ACP, ACZ, ACP/AgNP and ACZ/AgNP Materials

The microbial growth inhibition capacities of the RHS, RHS-NP, ACP, ACZ, ACP/AgNP and ACZ/AgNP materials from the screening test were assessed on the basis of minimum inhibitory concentration (MIC) and MBC. The MIC and MBC test was carried out on all the above prepared material in other to minimised any bias or experimental errors that might have arose during the screening process. The experimental MIC and MBC results are grouped in Table XLIII.

Table XLIII: Minimum inhibitory concentrations (MIC) and Minimum Bacteria concentrations of RHS, RHS-NP, ACP, ACZ, ACP/AgNP and ACZ/AgNP Materials

Sample	Parameter	Microorganism						
		SE	ST	STM	KP	SF	EC	SA
ACP	MIC	>1000	>1000	>1000	>1000	>1000	>1000	>1000
	MBC	>1000	>1000	>1000	>1000	>1000	>1000	>1000
ACZ	MIC	>1000	>1000	>1000	>1000	>1000	>1000	>1000
	MBC	>1000	>1000	>1000	>1000	>1000	>1000	>1000
ACP/AgNP(1 mM)	MIC	62.500	62.500	250.000	125.000	125.000	62.500	62.500
	MBC	>62.500	>62.500	>250.000	>125.000	>125.000	>62.500	>62.500
ACZ/AgNP(1 mM)	MIC	62.500	125.000	125.000	125.000	125.000	15.563	62.500
	MBC	>62.500	>125.000	>125.000	>125.000	>125.000	>15.563	>62.500
ACP/AgNP(5 mM)	MIC	31.125	125.000	125.000	62.500	62.500	31.125	7.782
	MBC	31.125	125.000	125.000	62.500	62.500	31.125	7.782
ACZ/AgNP(5 mM	MIC	15.563	31.125	31.125	62.500	31.125	7.782	7.782
	MBC	15.563	31.125	31.125	62.500	31.125	7.782	7.782
RHSE	MIC	>1000	>1000	>1000	>1000	>1000	>1000	>1000
	MBC	>1000	>1000	>1000	>1000	>1000	>1000	>1000
RHSNP	MIC	62.500	125	250	125	250	62.500	125
	MBC	>62.500	125	>250	125	>250	62.500	125
Ciprofloxacin	MIC	**0.156**	**0.039**	**0.078**	**0.156**	**0.078**	**0.078**	**0.078**

SE: *Salmonella enteritidis*; STM: *Salmonella typhimurium;* ST*: Salmonella typhi:* SA: *Staphylococcus aureus*; EC: *Escherichia coli*; KP: *Klebsiella pneumoniae*; SF: *S. flexneri ;* ACP: Phosphoric acid activated carbon; ACZ: Zinc chloride activated carbon; ACP/AgNP: Phosphoric acid activated carbon doped with silver nanoparticles.

ACZ/AgNP: Zinc chloride activated carbon doped with silver nanoparticles; RHSE: *Ricinodendron heudelotti shell extracts*; RHSNP: *Ricinodendron heudelotti shell nanoparticles.*

The MIC values range from 7.782µg/mL to 250µg/mL. The activated carbons doped with silver nanoparticles are generally more active than the simple nanoparticles alone (RHSNP). Equally, activated carbons with silver nanoparticles at a 5 mM $AgNO_3$ (ACP/AgNP and ACZ/AgNP) are more active than those doped at 1 mM $AgNO_3$ (ACP/AgNP and ACZ/AgNP). Also the carbons activated with $ZnCl_2$ (1 mM ACZ/AgNP and 5 mM ACZ/AgNP) are more active than those activated with H_3PO_4 acid (1 mM ACP/AgNP and 5 mM ACP/AgNP). ACZ/AgNP generally was the most active (with MIC ranging from (7.782- 62.5 µg/mL) and the RHSNP was the least active ranging from (62.5- 500 µg/mL). The results equally showed that *E. coli* and *S. aureus* were the most susceptible while *S. typhimurium* and *S. flexneri* were the most resistant. The un-doped activated carbons and the extracts showed no activity against any of the strains at the tested concentrations.

The MIC value of the samples varied from 7.782 to 250 µg/mL. The results show that doping generally increase the antibacterial properties of the extracts and the activated carbon, while the introduction of nanoparticles further increases this activity especially at the concentration of 5 mM $AgNO_3$. According to Tamokou *et al.,* in (2017), the antimicrobial activity of a plant extract is considered to be highly active if the MIC < 100 µg/mL; significantly active when 100 ≤MIC ≤512 µg/mL; moderately active when 512 <MIC ≤2048 µg/mL; weakly active if MIC > 2048 µg/mL and not active when MIC >10 000 µg/mL. However, to the best of our knowledge, no such classification exists for solid carbons, doped carbons and nanoparticles materials. Interestingly, these samples exhibited significant antibacterial activities (100 ≤ MIC ≤ 512 µg/mL) were obtained for the nanoparticles (RHSNP) as well as in cases of the doped activated carbon and highly active antimicrobial activities were obtained for most of the doped activated carbons. Compared with activities of the undoped particles, doping significantly increase the antibacterial potential of RHS. The RHS extract had no activity while sythesised nanoparticles have activities ranges between 62.5 for *Escherichia coli* to 250 for *Shigella flexneri*. Similar results were showed by Kumari *et al*., 2015. The difference in the antimicrobial activities from the RHSNP to the doped ACs can as a result of the increase in surface area as the nanoparticles are spread on the surface of the ACs.

In addition, the MBCs of the 1 mM $AgNNO_3$ and the nanoparticles (except for *Salmonella typhi, Staphylococcus aureus*, *Escherichia coli*, *Klebsiella pneumoniae*)are equal to that of MICs meaning these materials have a bacteriostatic effect vis a vis the studied bacteria.

The AgNP prepared using a 5 mM $AgNO_3$ solution was prepared and tested with different bacteria species with the aim of verify the effect of the $AgNO_3$ concentration on the bacterial inhibition mechanism. It results that, the MBCs of the AgNP prepared with 1 mM $AgNO_3$ solution on *Salmonella typhi*, *Staphylococcus aureus*, *Escherichia coli*, *Klebsiella pneumonia* and the composite prepared with the 5 mM $AgNO_3$ solution for all the different spectrum of bacteria studied were all equal to the MICs. These implies that these materials have a bactericidal effect with respect to the studied bacteria. It also implies increasing the $AgNO_3$ concentration increases its action from bacteriostatic to bactericidal. The mechanisms of the antimicrobial action can be illustrated in Figure 63.

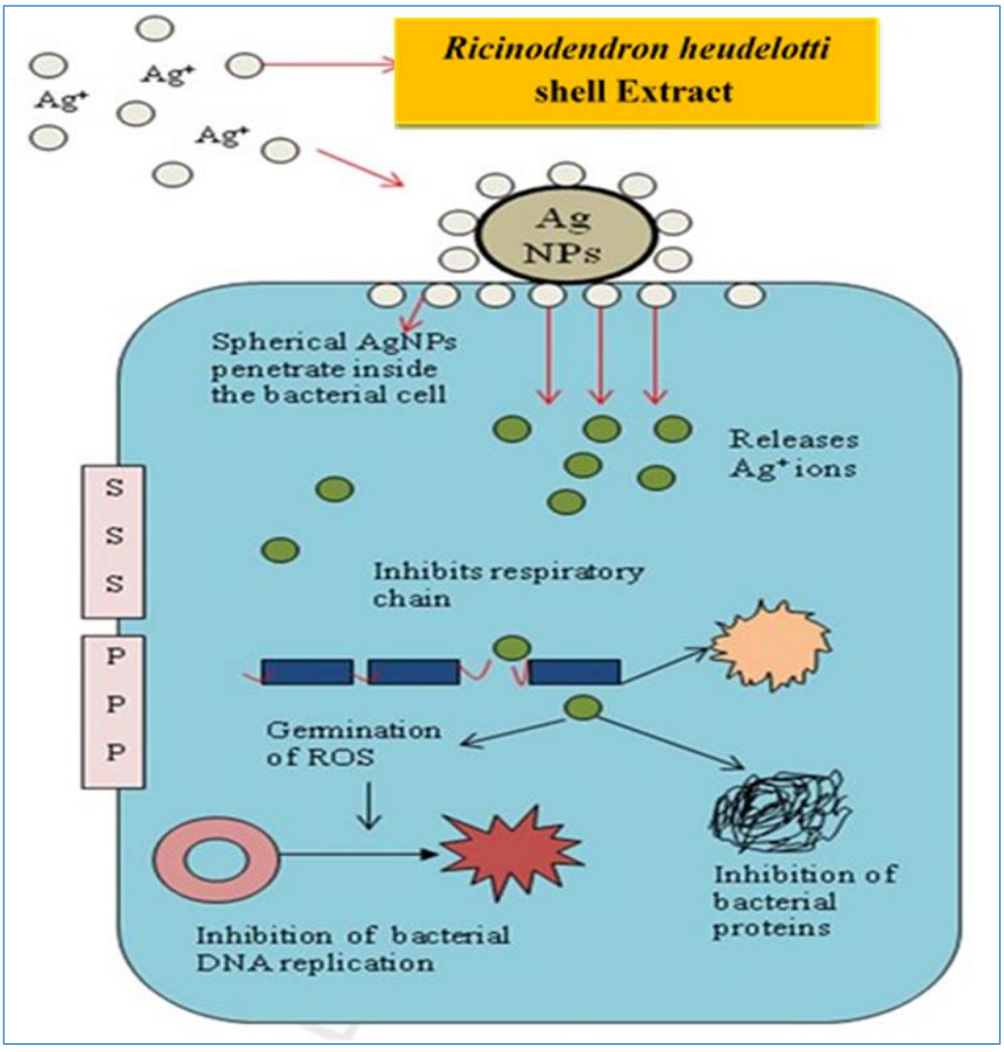

Figure 76: Proposed mechanisms of antibacterial activities exerted by *Ricinodendron heudelotti* shell extract capped AgNPs

The mechanism of the inhibitory action of the metal nanoparticles on micro organisms is not still clearly known. A hypothetical mechanism is therefore proposed for antibacterial

activities of photosynthesized AgNPs. The antibacterial effect could be explained on the basis of small sized AgNPs synthesized by RHS extract with extremely large surface area that provides better contact and interaction with the bacterial cell. This activity was further strengthened when the nanoparticles was spread on the surface of the ACs due to further in the surface area of the AgNPs as more contact between the bacterial and the nanoparticle was highly possible. Furthermore, on spreading the nanoparticles on the surface of the ACs, there is reduction of particle agglomeration effect hence preventing aggregation of the nanoparticles themselves which therefore increases its surface area for bacteria action. In addition, silver ions released from AgNPs may penetrate inside the cell membranes interacting with sulfur and phosphorus containing compounds such as proteins and DNA that may inhibit DNA replication, inhibits bacterial respiratory chain and inhibits bacterial protein hence resulting in loss of cell viability and ultimately leads to cell death (Al-Ansari *et al.,* 2019). It has also been proposed that the AgNPs can have a sustained release of silver ions once inside the bacterial cells (Feng *et al.,* 2001), and these ions can interact with thiol groups present in enzymes such as NADH dehydrogenases and disrupt the respiratory chain (Matsumura *et al*., 2003). The formation of free radicals by AgNPs induces oxidative stress which may be considered to be another mechanism of cell death (Kim *et al*., 2007).

Despite the fact that there are no limits for activities of solid carbon materials, it is particularly interesting to note that these nanoparticles are from products considered as waste (*Ricinodendron heudelotii* shells) and demonstrated herein to hold great perspectives in the development of complementary and/or alternative medicines to the use of synthetic antibiotic. The antibacterial activity of doped activated carbon from *Ricinodendron heudelotii* shells is therefore, presented herein for the first time. The significant activities recorded offers great perspective in the development of nanoparticle-base medication against. The significant activities recorded offers great perspective in the development of nanoparticle-base medication against the typhoid-causing *Salmonella typhi*, food-poisoning *Staphylococcus aureus*, pneumonia-causing *K. pneumoniae* as well as the diarrheal-manifesting *Escherichia coli* and *S. flexneri.*

III.7. Cytotoxicity test of ACP/AgNP and ACZ/AgNP of different concentration on vero cells Lining from the Kidneys of Monkeys

In general, the bactericidal properties of nanoparticles depend on their size, stability, and concentration added to growth medium, as this provides longer retention time for

interaction of nanoparticles and bacteria (Sizentsov *et al*., 2018). Bacterial cells are in the micron range. Most bacterial cells have cell membranes that contain pores in nanometer range. Potentially, synthesized nanoparticles can penetrate through such pores. Several studies have been carried out to determine the mechanism of bactericidal action of nanoparticles. For example, Tsao *et al.* suggested that, the treatment of Gram-positive bacteria with carboxyfullerene nanoparticles led to bacteria piercing and death (Tsao *et al*., 2002). Change in membrane lipid components is another proposed method by which it is possible to act on bacterial membrane.

However, it is difficult to distinguish bactericidal activity of nanoparticles from ions liberated by nanoparticles themselves (Yoon *et al*.2007). Earlier, Ruparelia *et al*. evaluated the concentration of released ions for 10 mg copper nanoparticles suspended in 100 mL nutrient media and distilled water (Ruparelia *et al*. 2008). They found that nutrient media can promote release of ions Cu^{2+} ions. Bioaccumulation ability of heavy metal cations (Cu^{2+}, Ag^{+} etc) by representatives of the microflora of the gastrointestinal tract, as it can be assumed that heavy metal cations in the form of nanoparticles in vivo are practically not absorbed in the intestine, but can pass through the gastrointestinal tract. Thus, microorganisms in the intestine can effectively adsorbed them on their surface (Sizentsov *et al*., 2018) which can lead to cell death. However, there are some other nanoparticles toxicity mechanisms discussed in the literature. For example, copper ions released by nanoparticles can be attached to a negatively charged bacterial cell wall and destroy it, thereby leading to protein denaturation and cell death surface (Sizentsov *et al*., 2018). In ddition, it was found that the absorption of copper ions by bacterial cells leads to disruption of important biochemical processes.

Therefore, cytotoxicity test in leaving cells is very important to evaluate bioaccumulation and biomagnification which can lead to death of importance cells of the body and also disrupte very important biochemical processes. In this light, cytotoxic assay of AgNPs which were produced using $AgNO_3$ solutions of two different concentrations (1 mM and 5 mM) and then spread on the ACs to obtained ACP/AgNP and ACZ/AgNP composite materials was performed on vero cell lining of the kidney of monkeys. The results are shown in Table XLII.

Table XLIV: Cytotoxicity test of ACP/AgNP and ACZ/AgNP at different concentrations

Name	CC50-1 (µg/mL)	CC50-2 (µg/mL)	Mean (CC50 /µg/mL)
ACP/AgNP(1 mM)	89,47	144,4	116,935 ± 38,84137549
ACZ/AgNP(1 mM)	48,84	65,39	57,115 ± 11,70261723
ACP/AgNP(5 mM)	110,9	93,87	102,385 ± 12,04202848
ACZ/AgNP(5 mM)	105,6	87,44	96,52 ± 12,84105915

ACP/AgNP: Phosphoric acid activated carbon doped with silver nanoparticles. ACZ/AgNP: Zinc chloride activated carbon doped with silver nanoparticles

Nanoparticles or nanocomposite materials targeted for clinical purposes must be reasonably non toxic and hence toxicity of different nanomaterials has been a subject of great interest. Earlier reports have shown that Ag, known to be safe and chemically inert in the nano-scale can be used in photothermal therapy and as imaging agents in living system. Since, the RHSNPs exhibits of antimicrobial activity, the toxicity studies were carried out on the vero cells lining of Monkeys. According to the National Institute for Cancer (NIC), a material is said to be toxic if the citotoxicity concentration at which 50 % (CC50) of the vero cells are killed is less than 20 µg/mL (Lunga *et al*., 2014). The non toxic nature of the materials are confirmed when the Ag nanoparticle composite materials is greater than 20 µg/mL. All the samples used in this experiment had CC50 greater than 20 µg/mL. Furthermore, the ACP/AgNP composite was found to be less toxic than the ACZ/AgNP composite material at all conentrations of the $AgNO_3$ solution use to prepare the nanoparticles for speading on the ACs. This may be due to their diffence in structure as the ACZ adsorbents used in the preparation of the ACZ/AgNP had crystalline peaks of zincite while ACP had amorphours structure. We believe that this zincite eventhough had some interesting medicinal value can be toxic at higher Zn concentration. In addition, the ACZ/AgNP (5 mM) is less toxic than the ACZ/AgNP (1 mM). This confirms our hypothetical reasoning, given that in the case of ACZ/AgNP (5 mM), there is the formation of more AgNPs which completely cover the surface of the ACZ thus preventing the Zn of the zincite to have access to the vero cells. Nevertheless, all the composite materials are still consider nontoxic and thus we can say that the composite materials formed cannot affect normal cells and can have possible medicinal applications, similar to our other systems without any fear or dought after verifying its toxicology test.

GENERAL CONCLUSION

In the quest for the search for novel materials and novel materials with antibacterial properties for wastewater and wastewater containing bacteria depollution by adsorption process. Novel approach for biosynthesis of AgNPs from aqueous *Ricinodendron heudelotii* shell extract was investigated and new approached for the production of composite materials was elucidated in this present work. These composite materials were produced by doping the produced AC with silver nanoparticles (AC/AgNP). This was acheived by successful precipitation loading of the synthesised silver nanoparticles of the *Recinodendron heudelotti* shells aqueous extract (RHSNPs) onto ACs.

This work therefore had as main objective to developed a new approach to prepare activated carbon with antibacterial properties from waste agricultural *Recinodendron heudelotti* shells. The first task was intended to use Designing of Experiments (DoE) by Central Composite Design (CCD) to modeled the preparation of the two AC samples (ACP and ACZ). From this step, the second task was to biologically sythesised silver nanoparticles (AgNPs) from aqueous extract of *Recinodendron heudelotti* shells. This new approached had as principal objective to eliminate or escape from the used of hazardous chemical capping agents reported from other works. The next phase was set to the successful loading of the bio-synthesised AgNPs onto the surface of the ACP and ACZ respectively and ACP/AgNP and ACZ/AgNP materials were respectively obtained. This approach permitted the even and homogenous dispersion of the AgNPs on the surface of the ACs. Results from FTIR from the doping samples shows the formation of two composite materials which were named ACP/AgNP and ACZ/AgNP respectively.

The UV-Visible analysis on the prepared AgNPs show the appearance of a strong and sharp peak at 453 nm which is related to the surface plasmon resonance (SPR) phenomenon confirming the synthesis of spherical nanoparticles of phenols. The Bohem titration carried out on the ACP, ACZ, ACP/AgNP and ACZ/AgNP samples shows higherr percentage of acidic groups.The XRD analysis of the samples reveals the amorphous nature of ACP sample, crystalline peaks of calcite and magnicite in RHS sample, zincite in in ACZ while peaks of silver were seen in ACP/AgNP and ACZ/AgNP carbon materials. This was also shown in their respective SEM-EDX images. Also, the presence of silver found in the XRD and SEM-EDX analysis but absent in the FTIR results shows that the silver present is in the metallic form (Ag^0). This therefore confirm the reduction of the Ag^+ to Ag^0 found in the nano-cluster of the

nanoparticle obtained during the preparation of the AgNPs. The presence of AgNPs (containing Ag^0) in the ACP/AgNP and ACZ/AgNP carbons has permitted to increase the antibacterial activities of ACP and ACZ on doping. The particle size analysis of the ACP, ACZ, ACP/AgNP and ACZ/AgNP gives an average particle size of 459.5, 814.6, 638.6 and 1008 dnm for ACP, ACZ, ACP/AgNP and ACZ/AgNP respectively (45.95, 81.46, 63.86 and 100.8 nm for ACP, ACZ, ACP/AgNP and ACZ/AgNP respectively) meaning all the ACs and AC/AgNPs samples are in the nano range. IN and MB number test carried out on ACP and ACZ and on their respective doped carbons ACP/AgNP and ACZ/AgNP was found to have percentage decrease from the doped carbons to the original carbons of 8.238 % and 16.835 for IN and 3.177 % and 7.827 % for MB number for ACP/AgNP and ACZ/AgNP respectively. The textural properties of the different materials (RHS, ACP, ACZ, ACP/AgNP and ACZ/AgNP) shows the increase in the specific surface area from the raw precursor (RHS) with BET value of 182 m^2/g to the prepared carbons with BET values of 386.613 m^2/g in ACP and 615.400 m^2/g in ACZ. This increase is tired to the effect of the different parameters which are activation temperature, holding time and activating agent employed during the preparation process. The composites ACP/AgNP and ACZ/AgNP were found to have lower specific surface area (367.400 m^2/g and 335.100 m^2/g in ACP/AgNP and ACZ/AgNP respectively) than their respective carbon. This is as a result of the doping of the carbon with AgNPs which occupying some of the pores resulting in decrease in the surface area. The composites were also found to have lower pore volumes than the carbons.

The efficiency of the ACP, ACZ, ACP/AgNP and ACZ/AgNP carbon materials were tested on the adsorption of IC and MO dyes in aqueous solutions. The adsorption capacities of ACP/AgNP and ACZ/AgNP were found to be slightly lower compared to that of the ACP and ACZ materials respectively. This could be as a result of the precipitated AgNPs occupying the active sites available for IC and MO adsorption. The equilibrium quantity adsorbed using the maximum equilibrium concentration was found to be 177.801 mg/g, 133.407 mg/g, 160.678 mg/g, and 89.181 mg/g for IC adsorption; 178.385 mg/g, 124.204 mg/g, 165.384 mg/g and 120.102 mg/g for MO adsorption on ACP, ACZ, ACP/AgNP and ACZ/AgNP respectively. This gives rise to a % decrease of 9.630 % and 33.151 % for IC adsorption; 7.273 % and 3.303 % for MO adsorption from ACP to ACP/AgNP and ACZ to ACZ/AgNP respectively.

The antibacterial activities of the four samples, the RHSNP and the RHS extract was done by the broth microdilution test method on the seven different bacteria of the typhoid-causing *Salmonella typhi*, food-poisoning *Staphylococcus aureus*, pneumonia-causing

Klebsiella pneumoniae as well as the diarrheal-manifesting *Escherichia coli* and *Singehla flexneri* species *and also on Salmonella enteritidis* (SE) and *Salmonella typhimurium* (STM). The synthesized RHSNPs and ACs/AgNPs have shown interesting antibacterial activityies ranging from 15.563 µg/mL in EC to 250 µg/mL in SF. These bacteria are a wide range of pathogenic bacteria which established their application in biomedicines. This was in accordance with the objectives of this work which was based on increases the antibacterial properties of the carbons without destroying their respective adsorption capacities.

Thus, it can be concluded that the prepared ACs and AgNPs synthesized using *Ricinodendron heudelotii* shell extract is a cost effective, simple and eco-friendly method that excludes the hazards arising out of the use of harmful reducing/capping agents. Therefore, the introduction of silver nanoparticles onto the activated carbon could be used in water filters and will attribute excellent antimicrobial property to the filters. This does not only prevent rapid blockage of filters, but also limits the possibilities of the spread of water borne diseases. Moreover, this process could be easily scaled up for the industrial applications to increase the yield of the nanoparticles significantly as the *Ricinodendron heudelotii* shells are considered as potential waste, which undoubtedly would establish its commercial viability in medicine.

PERSPECTIVES/RECOMMENDATIONS FOR FUTURE RESEARCH

In view amelioratng this present work, in the perspective of producing a more efficient and/or less toxic ACs and composites, we envisage to carry out the following investigations in the near future;

- ✓ Optimised the preparation of different ACs using different methods (Physical activation method, Hydrothermal activation methods etc)
- ✓ Investigate and give clear definition of the legal boundary conditions for indirect potable reuse. Based on a scientific environmental and public health approach, threshold values should bedefined to avoid over-engineered systems for "complete" removal of trace contaminants, mainly driven by analytical capacities and less by sound science.
- ✓ Improved spectroscopic analysis of ACP, ACZ, ACP/AgNP, ACZ/AgNP and AgNPs is warranted to understand their nano-structure.
- ✓ Evaluate the adsorption capacities of the prepared ACP, ACZ, ACP/AgNP, ACZ/AgNP using batch and continuous system other dyes and heavy metals pollutants.
- ✓ Study the Photocatalytic effect of the ACP, ACZ, ACP/AgNP, ACZ/AgNP and AgNPs on dyes.

- ✓ Give a clear boundry conditions for MIC values for solid materials such as ACs and ACs/AgNPs
- ✓ Performing the acute toxicity and in-vivo toxicology study of the ACP, ACZ, ACP/AgNP, ACZ/AgNP and AgNPs samples.
- ✓ Evaluate the preparation of AgNPs using the extracts of other solvents such as methanol, ethanol etc.
- ✓ Test the effect of ACP/AgNP, ACZ/AgNP and AgNPs composites on cancenogenic cells.

REFERENCES

Abdul H., Anuar K., Zainal Z., Mohd Z., Kuang D., Faujan A. and Ong S., (2001), "Preparation and characterization of activated carbon from Gelan Wood Bark (MelalencaCajupiti)", *Malaysian Journal of Analytical Science*, **7**, 65-68.

Abega A. V., Ngomo H. M., Nongwe I., Mukaya H. E., Kouoh S. P. M. A. and Mbianda X. Y., (2019), "Easy and convenient synthesis of CNT/TiO_2 nanohybrid by in-surface oxidation of Ti^{3+} ions and application in the photocatalytic degradation of organic contaminants in water", *Synthetic Metals*, **251,** 1–14.

Aber S., Khataee A. and Sheydaei M., (2014), "Optimization of Activated Carbon fiber preparation from Kenaf using K2HPO4 as chemical activator for Adsorption of phenolic compounds", *Bioresource Technology*, **100**, 6586-6591.

Adewumi I. K. and Ogedengbe M. O., (2005), "Optimising for Activated Charcoal production from Palm Kernel Shells", *Journal of Applied Sciences*, **5(6)**, 9434-9445.

Ahmad A. A., Hameed B.H. and Ahmad A. L., (2009), "Removal of disperse dye from aqueous solution using waste-derived activated carbon: Optimization study", *Journal of Hazardous Materials*, **170**, 612–619.

Ahmad A. M. and Alrozi R., (2010), "Optimization of prepartion conditions for Mangosteen peel-based Activated Carbons for the removal of Remazol Brilliant Blue R using response surface methodology", *Chemical Engineering Journal*, **165**, 883-890.

Ahmed M.A., Brick A.A. and Mohamed A.A., (2017), "An efficient adsorption of indigo carmine dye from aqueous solution on mesoporous Mg/Fe layered double hydroxide nanoparticles prepared by controlled sol-gel route", *Chemosphere*, **174**, 280-288.

Aksa H., (2012), "Étude Cinétique et Thermodynamique de l'Adsorption des Métaux Lourds par l'Utilisation des Adsorbants Naturels", *Thèse de Doctorat en Génie des Procédés et de l'Environnement*, Université M'Hamed Bougara-Boumerdes, Boumerdes-Algérie, 70.

Al-Ansari M., Alkubaisi N., Gopinath K., Karthika V., Arumugam A. and Govindarajan M., (2019), "Parameters optimization for nitrate removal from water using activated carbon and composite of activated carbon and Fe_2O_3 nanoparticles", *Journal of Cluster Science*, **30,**1081–1089.

Al-Ansari M., Alkubaisi N., Gopinath K., Karthika V., Arumugam A. and Govindarajan M., (2019), "Facile and Cost-Effective Ag Nanoparticles Fabricated by *Lilium lancifolium* Leaf Extract: Antibacterial and Antibiofilm Potential", *Journal of Cluster Science*, **30**, 1081–1089.

Al-Degs Y. S., Khraished M. A. M. Allen S. J. and Ahmad M. N., (2009), "Adsorption characteristics of reactive dyes in columns of Activated Carbon", *Journal of Hazardous Materials*, **165**, 944-949.

Alison L. H., (2007), "The use of Non-Timber Forest Products in the Congo Basin: Constraints and Opportunities", 56.

Alkhatib M. F., Mamun A. A. and Akbar I., (2014), "Application of Response surface methodology (RSM) for Optimization of color removal from Pome by granular Activated Carbon", *International Journal of Environmental Sciences and Technology*, 1-8.

Alok M., Jyoti M. and Lisha K., (2007), "Utilization of Hen Feathers for the Adsorption of Indigo Carmine from Simulated Effluents", *Journal of Environmental Protection science*, **1**, 92-100.

AlOthman Z. A., Habila M.A. and Ali R., (2011), "Preparation of Activated Carbon Using the Copyrolysis of Agricultural and Municipal Solid Wastes at a Low Carbonization Temperature", *International Conference on Biology, Environment and Chemistry*, **24,** 67-72.

Al-Qodah Z. and Shawabkah R., (2009), "Production and Characterization of Granular Activated Carbon from Activated Sludge", *Brazilian Journal of Chemical Engineering*, **26(01)**, 127 – 136.

Alzaydien A. S., (2015), "Adsorption Behavior of Methyl Orange onto Wheat Bran: Role of Surface and pH", *Oriental Journal of Chemistry*, **31(2),** 643-651.

Amir S., (2012), "Production of activated carbon within the indirect gasification process", *Master Thesis* within the sustainable Energy system program, Chalmers University of Technology Gothenburg, Gothenburg –Sweden, 56.

Anagho S.G., Ketcha J.M., Tchuifon T. D. and Ndi J. N., (2013), "Kinetic and equilibrium studies of the adsorption of Mercury (II) ions from aqueous solution using Kaolinite and Metakaolinite clays from southern Cameroon", *International Journal of Research and chemical Environment*, **3**, 1-11.

Anagho S.G., Tchuifon T. D., Nche G., Ndi J. N., Ketcha J.M. and Mouminou N., **(**2013**),** "Nickel adsorption from aqueous solution onto kaolinite and metakaoline kinetic and equilibrium studies", *International Journal of Chemistry*, **4**, 1-14.

Andel T. V., (2006), "Les produits forestiers autres que le bois d'oeuvre", Fondation Agromisa et CTA, Wageningen, Pays Bas, 80.

Angus S., Chih-Ming M., Ri-Tian R. and Chang-Tang C., (2012), "Adsorption kinetics and and Isotherm for the removal of Methyl Orange from wastewaters using copper oxide catalyst prepared by the waste printed circuit boards", *Sustain Environmental Research*, **22**, 209-215.

Ankoro N. O**.**, Kouotou D., Belibi Belibi P. D., Ndi J. N. and Ketcha J. M., (2016), "Removal of Indigo Carmine Dye (IC) by Batch Adsorption method onto dried Cola Nut Shells and its Active Carbon from Aqueous Medium", *International Journal of Engineering Sciences & Research Technology*, **5(3),** 874-887.

Anneliese T., (2011), "Adsorption of Methylene blue onto Carbon/Cobalt Ferrite/Alginate Beads and Acid Modified Rice Husks", 24.

Assano T., Burton F. L., Leverenz H. L., Tsuchihashi R. and Tchobanoglous G., (2007), "Water reuse - issues, technologies, and applications", Mc Graw Hill, New York, 435.

Assanvo E. F., Gogoib P., Doluib S. K. and Baruah S D., (2015), "Synthesis, characterization, and performance characteristics of alkyl resins based on Ricinodendron heudelotii oil and their blending with epoxy resins", *Industrial Crops and Products*, 65, 293–302.

Asuquo E. D. and Alastair D. M., (2016), "Sorption of cadmium (II) ion from aqueous solution onto sweet potato (Ipomoea batatas L.) peel adsorbent: characterisation, kinetic and isotherm studies", *Journal of Environmental Chemical Engineering*, 1-67.

Babayemi A. K., (2016), "Thermodynamics, Non-Linear Isotherms, Statistical Modeling and Optimization of Phosphorus Adsorption from Wastewater", *American Journal of Engineering and Applied Sciences*, **9 (4)**, 1019-1026.

Babweteera F. and Brown N., (2010), "Spatial patterns of tree recruitment in East African tropical forests that have lost their vertebrate seed dispersers", *Journal of Tropical Ecology.*, **(26),** 193–203.

Baccar R., Bouzid J., Feki M. and Montiel A., (2009), "Preparation of Activated Carbon from Tunisian olive-waste cakes and its application for adsorption of heavy metal ions", *Journal of Hazardous Materials*, **162**, 1522-1529.

Bansal R. C., Donnet J. B. and Stoeckli, H. F., (1988), "Active carbon", *Marcel Dekker*, New York, 502.

Berg J. M., Tymoczko J. L. and Stryer L., (2002), "Molecular Cell Biology", *WH Freeman*, 5th ed, 1050.

Beros M., Ventresque C., Bablon G., Tanghe N. and Chagneau G., (2003), "Operational experiences with a NF full-scale plant for drinking water treatment", Proceedings of the 4th ATSV Conference, Aachen,1-2.

Biagini E., Barontini F. and Tognotti L., (2006), "Devolatilization of Biomass Fuels and Biomass Components studied by TG/FTIR Technique", *Industral and Engineering Chemical Research*, **45**,4486-4493.

Binti N., (2007), "The production and Characterization of Activated carbon using local Agricultural waste through chemical activation process", Thesis for Master of Science, **43**.

Bixio D. and Wintgens T., (2006), "Water reuse system management manual-AQUAREC", Office for Official Publications of the European Communities, Luxembourg, 411.

Boehm H. P., (1994), "Some aspects of the surface chemistry of carbon blacks and other carbons", *Carbon*, **32(5)**, 759-769.

Brayner R., Ferrari-Iliou R., Brivois N., Djediat S., Benedetti M. and Fiévet F., (2006), "Toxicological impact studies based on Escherichia coli bacteria in ultrafine ZnO nanoparticles colloidal medium", *Nanotechnology Letters,* **6(4)**, 866-870.

Cabeen M. T and Jacobs-Wagner C., (2005), "Bacterial cell shape", *Nature Reviews Microbiology*, **3(8),** 601-10.

Canteli A. M. D., Carpiné D., Scheer A. P., Mafra M. R. and Igarashi-Mafra L., (2014), "Fixed-bed column adsorption of the coffee aroma compound benzaldehyde from aqueous solution onto granular Activated Carbon from coconut husk", *LWT-Food Science and Technology*, **59**, 1025-1032.

Caspa R. G., Tchouamo I. R., Mweru J. P. M., and Mbang J. A., (2018), "M arketing Ricinod endron heudelotii Kernels and Gnetum spp. Leaves Around Lobeke National Park, Eas t Cameroon", *Tropicultura*, **36(3**), 565-577.

CE-FAO, (1999), "Données statistiques des produits forestiers non-ligneux du Cameroun", PROJET GCP/INT/679/EC, Yaounde, Cameroon.

Centers for Disease Control and Prevention, (2007), "Bacterial Foodborne and Diarrheal Disease National Case Surveillance", Annual Report, 2004. Atlanta: U.S. Department of Health and Human Services, 55.

Chakkrit U. and Songsak S., (2013), "Removal of methyl orange from aqueous solutions by adsorption using Chitosan Intercalated Montmorillonite", *Songklankarin Journal of Scientific Technology*, **35**, 451-459.

Cho E. J., Holback H., Liu K. C., Abouelmagd S. A., Park J. and Yeo Y., (2013), "Nanoparticle characterization: State of the art, challenges, and emerging technologies", *Molecular pharmacology*, **10(6)**, 2093-2110.

Chow Q. W., (2010), "predicting Adsorption Isotherms in Natural water using Polyparameter linear free energy relationships", PhD Thesis, Environmental Science in Civil Engineering, University of Illinois at Urbana-Champaign, Urbana, Illinois, 115.

CIFOR Central Africa C/o IITA, (2008), "Humid Forest Eco regional Centre", Yaoundé, Cameroon, 1-7.

Çiğdem Ç., (2005), "Production and Characterization of Activated Carbon from Hazelnut Shell and Hazelnut Husk", Master Thesis in Chemical Engineering, of Middle East Technical University, Middle East.

Cosyns H. P., Damme V., De Wulf R. and Degrande A., (2013), "Can Rural Development Projects Generate Social Capital? A Case Study of *Ricinodendron heudelotii* Kernel Marketing in Cameroon", *Small-scale Forestry*, 1-20.

Crump J. A., Sjölund-Karlsson M., Gordon M.A., and Parry C.M., (2015), "Epidemiology, Clinical Presentation, Laboratory Diagnosis, Antimicrobial Diagnosis and Antimicrobial Management of Invasive Salmonella Infections", *Clinical Microbiology Reviews*, **28**, 901-937.

Dada A., Olalekan A., Olatunya M. and DADA O., (2012), "Langmuir, Freundlich, Temkin and Dubinin–Radushkevich Isotherms Studies of Equilibrium Sorption of Zn^{2+} Unto Phosphoric Acid Modified Rice Husk" *Journal of Applied Chemistry*, **3**, 38-45.

Daniel R., Shara L., Deanna T., Charlotte R., Irving A. and Dean A., (2007), "Certain activated carbon from China", United State International Trade Commission, 126.

Danish M. and Ahmad T., (2018), "A review on utilization of wood biomass as a sustainable precursor for activated carbon production and application", *Renewable and Sustainable Energy Reviews*, **87**, 1-21.

Das D., Samal D. P. and Meikap B. C., 2015, "Preparation of Activated Carbon from Green Coconut Shell and its Characterization" *Journal of Chemical Engineering Process and Technology*, **6 (5),** 2157-7048.

Das S., (2014), "Characterization of Activated Carbon of Coconut Shell, Rice Husk and Karanja Oil cake", Bachelor of Technology Thesis of Department of Chemical Engineering, National Institute of Technology of Rourkela, Rourkela, India, 42.

David G. E. M., (2017), "Global burden of bacterial infections: The role of vaccines in reducing AMR", *Lecture notes of the Faculty of Medicine of the Imperial College, London*, UK, **552**, 163-167.

Deen J., von Seidlein L., Andersen F., Elle N., White NJ. and Lubell Y., (2012), "Community-acquired bacterial bloodstream infections in developing countries in south and southeast Asia: a systematic review", *Lancet Infectious Diseases*, **12**, 480-487.

Dias-Júnior A. F., Andrade C. R., Protásio T. P., Brito J. O., Trugilho P. F., Oliveira M. P and Dambroz G. B. V., (2019), "Thermal profile of wood species from the brazilian semi-arid region submitted to pyrolysis", *Cerne*, 25(1), 44-53.

Dina J. D. D., Abdul R. N., Ndi J. N., and Ketcha J.M., (2012), "Adsorption of Acetic Acid onto Activated Carbons Obtained from Maize Cobs by Chemical Activation with Zinc Chloride ($ZnCl_2$)", *Research Journal of Chemical Sciences*, **2**, 42-49.

Djague F., (2019), "Antimicrobial and Biocontrol Agents", Dissertation for Master of Science in Biochemistry, Laboratory for Phytobiochemistry and Medicinal Plants study of the Univesity of Yaoundé I, Cameroon, 78.

Dong M., Wu Z., Min L., Zhi W. and Li Z., (2012), "Combining the physical adsorption approach and covalent Attachment method to prepare a Bifunction Bioreaction", *International Journal of Molecular Sciences*, **13**, 11443-11454.

Dong S., Feng J., Maohong F., Yunqing P., Limin H., Xiao H., Menglin L., Jingyu S. and Jianhui S., (2015), "Recent developments in heterogeneous photocatalytic water treatment

using visible lightresponsive photocatalysts: a review", *The Royal Society of Chemistry*, **5**, 14610–14630.

Doolittle, R.F., Feng D.F., Tsang S., Cho G. and Little E., (1996), "Determining divergence times of the major kingdoms of living organisms with a protein clock", *Science,* **271(5248),** 470–477.

Douglas C., (1997), "Design and Analysis of Experiments" 4th edition, New York, John Wiley & Sons, 34.

Doying E. G., (1966), "Activatable Coke from Carbonaceous Residues", *United States Patent Office*, **364,270**, 204-8.

Dusenbery D. B., (2009), "Living at Micro Scale", *Harvard University Press*, 416.

Egbe E.A., Tabot P.T. and Fonge B.A., (2012), "Ethnobotany and Prioritization of Some Selected Tree Species in South-western Cameroon", *Master Thesis* of Department of Plant and Animal Sciences, University of Buea, Buea, Cameroon, 85.

Egila E. F., (2015), "Characterization of Microwave Activated Carbon derived from the mixture of Palm Kernel and Coconut shells", *Master Thesis* of the Department of Physics, Faculty of Science, Ahmadu Bello University, Zaria, Nigeria, 95.

Elhussien M. H., Hussein R. M., Nimir S. A. and Elsaim M. H., (2017), "Preparation and Characterization of Activated Carbon from Palm Tree Leaves Impregnated with Zinc Chloride for the Removal of Lead (II) from Aqueous Solutions", *American Journal of Physical Chemistry*, **6(4)**, 59-69.

Elkady M. F., Hussein M. M. and Atiaa H. M., (2015), "Preparation of nano-activated carbon from carbon based material for copper decontamination from wastewater", *American Journal of Applied Chemistry*, **3(3-1)**, 31-37.

El-Shafey E. I., Syeda N.F.A., Al-Busafi S. and Al-Lawati H. A. J., (2016), "Preparation and characterization of surface functionalized activated carbons from date palm leaflets and application for methylene blue removal", *Journal of Environmental Chemical Engineering*, **4(3),** 2713-2724.

Elyounssi K., Collard F. X., Mateke N. J. A. and Blin J., (2012), "Improvement of charcoal yield by two-step pyrolysis on Eucalyptus wood: A thermogravimetric study", *Fuel*, 96, 161–167.

Ernst M., (2000), "Separation of organic compounds from municipal wastewater treatment plant effluents by means of ultra- and nanofiltration membranes for artificial groundwater recharge", VDI series 15, Environmental Engineering, VDI Verlag, Dusseldorf, 221.

Essa M. A., Al-Zahrani M. A. and Nesaratnam S., (2013), "Optimisation of activated carbon production from date pits", *International Journal of Environmental Engineering*, **5(3)**, 325-338.

European Centre for Disease Prevention and Control (2016) “Laboratory standard operating procedure for multiplelocus variable-number tandem repeat analysis of Salmonella enterica serotype Enteritidis”, Stockholm: ECDC.

European Centre for Disease Prevention and Control and European Food Safety, (2017), “Authority. Multi-country outbreak of Salmonella Enteritidis infections linked to Polish eggs”, ECDC and EFSA, Stockholm and Parma.

Fabien J., Fuche., Ousmane S., Raphael S., Sharon M and Tennant, (2016), “Salmonella Serogroup C: Current Status of Vaccines and Why They Are Needed”, *Clinical and Vaccine Immunology*, **23**, 737–745.

Farombi E. O., Britton G. and Emerole G. O. (2000), “Evaluation of the antioxidant and partial characterisation of extracts from browned yam flour”, *Food Research International*, **33**, 493-499.

Fazal-ur-Rehman M., (2018), “Methodological trends in preparation of Activated Carbon from local sources and their impacts on production: A review”, *Chemistry International,* **4(2),** 109-119.

FDA, (2012), Bad bug book: “Foodborne pathogenic microorganisms and natural toxins handbook”, 2nd ed., US Food and Drug Administration, *Silver Spring*, 87–92.

Feng Q. L., Wu J., Chen G. Q., Cui F. Z., Kim T. N. and Kim, J. O., (2001), “A mechanistic study of the antibacterial effect of silver ions on Escherichia coliandStaphylococcus aureus”, *Journal of Biomedical Materials Research*, **52**, 662-668.

Feng, Q.L, J. Wu, G.Q, Chen, F.Z. Cui, T.N. Kim and Kim, J.O. A mechanistic study of the antibacterial effect of silver ions on Escherichia coli and Staphylococcus aureus. *J. Biomedi.Mat.Res. Part A.*52(4): 662668, 2000.

Firdhouse M. J. and Lalitha P., (2015), “Biosynthesis of silver nanoparticles and its applications-A Review”, Journal *of Nanotechnology,* 1-18.

Fondoun J. M., Tiki Manga T. and Kengue, J. (1998), “*Ricinodendron heudelotii* (Djansang): Ethnobotany and importance for forest dwellers in Southern Cameroon”, In: Second International Workshop on African Pear Improvement and other New Sources of Vegetable Oils, Edited by Kapseu, C. and Kayem, G. J. Presses, Universitaires de Yaoundé, Yaoundé, 247-259.

Foo K. Y., and Hameed B.H., (2011), “Utilization of Rice Husks as a feedstock for preparation of Activated Carbon by Microwave induced KOH and K_2CO_3 activation”, *Bioresource Technology,* **102**, 9814–9817.

Franklin R. E., (1951), “Crystalline growth in graphitizing and non-graphitizing carbons”, *Proceedings of The Royal Society A,* **209**, 196-218.

Fredrickson J. K., Zachara J. M., Balkwill D. L., Kennedy D. and Li S. M., (2004), "Geomicrobiology of high-level nuclear waste-contaminated vadose sediments at the Hanford site", Washington State, *Applied and Environmental Microbiology,* **70(7),** 4230-4245.

Fulazzaky M. A., (2011), "Determining the resistance of mass transfer for adsorption of the surfactants onto granular Activated Carbons from hydrodynamic column", *Chemical Engineering Journal,* **166**, 832-840.

Fumba G., Essomba J. S., Tagne G. M., Ndi Nsami J., Belibi Belibi P. D. and Ketcha Mbadcam J., (2014), "Equilibrium and Kinetic Adsorption Studies of Methyl Orange from Aqueous Solutions Using Kaolinite, Metakaoloinite and Activated Geopolymer as Low Cost Adsorbents", *Journal of Academia and Industrial Research*, **3**, 156-163.

Fungaro D., Yamaura M. and Carvalho T., (2011), "Adsorption of anionic dyes from aqueous solution on Zeolite from fly ash-iron oxide magnetic nanocomposite", *Chemical and Environmental Technology Center, Nuclear and Energy Research Institute*, **2**, 305-316.

Futselaar H., Schonewille H., and van der Meer W., (2002), "Direct capillary nanofiltration - a new high-grade purification concept", *Desalination,* **145**, 75-80.

Fylstra D., Lasdon L., Watson J. and Waren A., (1998), "Design and Use of the Microsoft Excel Solver", *Interfaces,* **28(5),** 29-55.

Gal-Mor O., Boyle E. C and Grassl G. A., (2014), "Same species, different diseases: how and why typhoidal and non-typhoidal Salmonella enterica serovars differ", *Frontiers in Microbiology*, **5,** 391.

Gao Y., Shiping X., Yue Q., Yuwei W. and Baoyu G., 2016, "Chemical preparation of crab shell-based activated carbon with superior adsorption performance for dye removal from wastewater", *Journal of the Taiwan Institute of Chemical Engineers*, **000**, 1–9.

Gh G. and Ehrampoush M., (2010), "application of Iron impregnated Activated Carbon for removal of Arsenic from water", *Tranian Journal of Health Science and Engineering*, **1**, 145-156.

Ghaedi M., Shojaeipour E., Ghaedi A. M. And Sahraei R., (2015), "Isotherm and Kinetics study of Malachite green adsorption onto copper nanowires loaded on Activated Carbon: Artificial neural network modeling and genetic algorithm optimization", *Molecular and Biomolecular Spectroscopy*, **142,** 135-149.

Ghaedia M., Ghaedi A. M., Abdi F., Roosta M., Vafaei A. and Asghari A., (2013), "Principal component analysis- adaptive neuro-fuzzy inference system modeling and genetic algorithm optimization of adsorption of methylene blue by activated carbon derived from Pistacia khinjuk", *Ecotoxicology and Environmental Safety*, **96**, 110–117.

Ghasemi M., Khosroshahy M. Z., Abbasabadi A. B., Ghasemi N., Javadian H., And Fattahi M., (2015), "Microwave-assisted functionalization of Rosa Canina-L Fruits Activated Carbon with

tetraethylenepentamine and its adsorption behavoir toward Ni(II) in aqueous solution: Kinetic, equilibrium and thermodynamic studies", *Power Technology*, **274**, 363-371.

Global Burden of Disease, (2018), "Global Burden of Disease Results Tool. GBD Results Tool GHD", Available at: http://ghdx. Healthdata.org/gbd-results-tool.

Goel J., Kadirvelu K., Rajagopal C., and Garg V. K., (2005), "Removal of lead (II) by adsorption using treated granular Activated Carbon: Batch and column studies", *Journal of Hazardous Materials*, **125**, 211-220.

Gonzàlez P. G., Hernàndez-Quiroz and Garcia-Gonzàlez., (2014), "The use of experimental design and response surface methodologies for the synthesis of chemically activated carbons produced from bamboo", *Fuel Processing Technology*, **127**, 133-139.

Goupy J. and Creighton L., (2006), "Introduction aux Plans d'Expériences", 336.

Govindarajan M., Khater H. F., Panneerselvam C. and Benelli G., (2016), "Natural remedies in the fight against parasites", *Research in Veterinary Science*. **107,** 95-101.

Gratuito M. K. B., Panyathanmaporn T., Chumnanklang R. A., Sirinuntawittaya and Dutta A., (2008), "Production of activated carbons from coconut shell: Optimization using response surface methodology", *Bioresource Technology*, **99**, 4887-4895.

Gray J. T. and Fedorka-Cray P. J., (2002), "Salmonella in Foodborne Diseases", 2nd ed., Cliver, D. O. and Riemann, H. P. (Eds). Academic Press, San Diego, 55-68.

Guimarães D. O., Momesso L. S. and Pupo M. T., (2010), "Antibióticos: importância terapêutica e perspectivas para a descoberta e desenvolvimento de novos agentes", *Quim Nova*. **33(3),** 667-679.

Gunn J. S., Marshall, J. M., Baker, S., Dongol, S., Charles, R. C., and Ryan, E. T., (2014), "Salmonella chronic carriage: Epidemiology, diagnosis, and gallbladder persistence", *Trends in Microbiology*, **22**, 648–655.

Guo S., Xu J., Wei Y., JunHong X., Yi L. and Xue R., (2016), "Clinical and molecular characteristics of Klebsiella pneumoniaeventilator-associated pneumonia in mainland China", *BMC Infectious Diseases*, **16(60)**, 1-7.

Harrache Z., Abbas M., Aksil T. and Mohamed T., (2019), "Thermodynamic and Kinetics Studies on Adsorption of Indigo Carmine from Aqueous Solution by Activated Carbon", *Microchemical Journal*, **144**, 180-189.

He J., (2013), "Des (bio)nano-composites utilisés dans le traitement d'eaux contaminées par de l'arsenic/gentamicine ou pour des applications médicales", Thèse de Doctorat De L'Université de Grenoble, France, 164.

Himanshu P. and Vashi R., (2010), "Decolonization of Dyeing Mill waste water by adsorption and Coagulation", *E-Journal of chemistry*, **7**, 1468-1476.

Hogan M. C. (2011), "Bacteria. Encyclopedia of Earth. eds. Sidney Draggan and Cleve land Chemical Journal of National council for Science and the Environment, Washington, DC.
Hossain M. A., Ngo H. H. and Guo W., (2013), "Introduction of Microsoft Excel SOLVER Function – Spreadsheet Method for Isotherm and Kinetics Modeling of Metals Biosorption in water and wastewater", *Journal of Water Sustainability*, **3(4),** 223-237.

Hsiao M. S., Chen D. S. and Yeh C., (2006), "One-pot synthesis of hollow Au3Cu1 spherical-like and biomineral botallackite $Cu_2(OH)_3Cl$ flowerlike architectures exhibiting antimicrobial activity", *Journal of Physical Chemistry and Biominerals*, **110**,205-210.

Hu Y-N., Wang H-Y., Gao G-P., Meng C. and Yuan W-K, (2011), "The Adsorption of touenediamine from the wastewater by Activated Carbon in batch and fixed bed systems", *Desalination*, **279**, 54-60.

Hulteen J. C., Treichel D. A., Smith M. T., Duval M. L., Jensen T. R. and Duyne R. P., (1999), "Nanosphere Lithography: Size-Tunable Silver Nanoparticle and Surface Cluster Arrays", *Journal of physical chemistry and biosynthesis*, **103**, 3854-3863.

Jorge L. and Simon Y., (1992), "Effect of the Preparation Method on the Pore size distribution of Activated carbon from Coconut shell", *Printed in Great Britain*, **30**, 601-604.

Karacan F., Ozeden U. and Karacan S., (2007), "OptimiZation of manufacturing conditions for Activated Carbon from Turkish lignite by chemical activation using response surface methodology", *Applied Thermal Engineering*, **27**, 1212-1218.

Karthik C and Radha K. V., (2016), "Silver nanoparticle loaded activated carbon: An escalated nanocomposite with antimicrobial property", *Orientation Journal of Chemistry*, **32(1),** 735-741**.**
Keestra-Gounder A. M., Tsolis R. M. and Bäumler A. J., (2015), "Now you see me, now you don't: the interaction of Salmonella with innate immune receptors" *Nature Reviews Microbiology*, **13**, 206–216.

Keijzer M., Van Bommel M. R., Hofmann-de Keijzer R., Knaller R., Oberhumer E., (2015), "Indigo Carmine: understanding a problematic Blue dye", Contributions to the Vienna Congress, S87-S95.

Keith K. H. C., Porter J. F. and Mckay G., (2000), "Langmuir Isotherm Models Applied to the Multicomponent Sorption of acid dyes from effluent onto Activated Carbon", *Journal of Chemical Engineering Data*, **45**, 575-584.

Ketaona A. D. A., Tchiégang C. and Noumi G. B., (2013), "Quality of *Ricinodendron Heudelotii* (Bail.) Pierre Ex Pax Seeds Oil as affected by heating", *International Journal of Engineering Research and Science and Technology*, **2(4),** 1-9.

Ketcha J. M., Dongmo S. and Dinka'a N. D., (2012), "Kinetic and Thermodynamic studies of the adsorption of Nickel (II) Ions from aqueous solutions by Smectite Clay from Sabga-Cameroon", *International Journal of Current Research*, **4,** 162-167.

Ketcha J. M., Ngomo H. M., Tcheka C., Abdul R. N., Djoyo H. and Kouotou D., (2009), "Batch Equilibrium Adsorption of Cyanides from Aqueous Solution onto Copper- and Nickel-Impregnated Powder Activated Carbon and Clay", *Journal of Environmental Protection Science,* **3**, 53-57.

Khan S. A., Khan S. B., Kamal T., Yasir M. and Asiri A. M., (2016), "Antibacterial nanocomposites based on Chitosan/Co-MCM as a selective and efficient adsorbent for Organic dyes", *International Journal of Biological Macromolecules*, **91**, 744–751.

Kilpimaa, S., Runtti, H., Kangas, T., Lassi, U., Kuokkanen, T., (2014), "Removal of phosphate and nitrate over a modified Carbon residue from Biomass gasification", *Chemical Engineering Research and Design***, 92(10)**, 1923-1933.

Kim J. S., Kuk E., Yu K., Kim J. H., Park S. J. and Lee, H. J., (2007), "Antimicrobial effects of silver nanoparticles", *Nanomedicine*, **3**,95-101.

Kouotou D., (2014), "Optimisation des Conditions de preparation des Charbons Actifs a Base des dechets de Coques de Noix de Palme par la Methode des Plans d'Expériences: Application a l'Elimination des Polluants des Eaux", Doctorate thesis in physical Chemistry, University of Yaoundé I, Yaoundé, Cameroon, 219.

Kouotou D., Manga H. N., Baçaoui A., Yaacoubi A., and Ketcha J. M., (2013), "Optimization of Activated Carbons prepared hy H_3PO_4 and steam activation of Oil Palm Shells", *Journal of Chemistry*, 1-10.

Kristina P., (1997), "*Ricinodendron Heudelotii*", Oxford Forestry Institute Department of Plant Sciences, University of Oxford, United Kingdom, 45.

Kumar A. and Jena H. M., (2016), "Preparation and characterisation of high surface area Activated Carbon fom Fox nut (Euryale ferox) shell by chemical activation with H_3PO_4", *Results in Physics*, **6**, 651-658.

Kumari J., Mamta B. and Ajeet S., (2015), "Characterization of silver nanoparticles synthesized usingUrtica dioicaLinn. leaves and their synergistic effects with antibiotics", *Journal of Radiation Research and Applied Sciences*, 1-11.

Kundu A., Gupta B. S., Hashim M. A., Sahu J. N., Mujawar M. and Redzwan G., (2015), "Optimisation of the process variables in production of Activated Carbon by Microwave heating", *The Royal Society of Chemistry*, **5**, 35899–35908.

Kundu A., Gupta B. S., Hasim M. A. and Ghufran R., (2014), "Taguchi optimization approach for production of Activated Carbon from phosphoric acid impregnated Palm Kernel shell by microwave heating", *Journal of Cleaner Production*, 1-8.

Kwaghger A. and Ibrahim J., (2O13), "Optimization of Conditions for The Preparation of Activated Carbon from Mango Ntus using HCl", *American Journal of Engineering Research*, **2**, 74-85.

Langridge G. C., Nair S and Wain J., (2009), "Nontyphoidal Salmonella serovars cause different degrees of invasive disease globally", *The Journal of infectious diseases*, **199**, 602-603.

Le Loir Y., Baron F. and Gautier M., (2003), "Staphylococcus aureus and food poisoning", *Genetic and Molecular Research*, **2(1)**, 63-76.

Leakey R. R. B., (1999), "Potential for novel food from Agroforestry trees: A Review", *Food chemistry*, **66,** 1-14.

Leimkuehler E. P., (2010), "Production, Characterization, and Applications of Activated Carbon", *Master thesis* of the Faculty of the Graduate School University of Missouri, Missouri, USA, 66.

Lekene N. R. B., (2013), "Kinetic and Equilibrium Adsorption studies of Phenol and Methylene Blue in Aqueous Solution by Activated Carbon", Master of physical chemistry, University of Yaoundé I, Yaoundé Cameroon, 72.

Lékéné N. R. B., Ndi J. N., Asma R., Kouotou D., Belibi B. P. D., Muhammad I. B. and Ketcha J. M., 2019, "Optimization Conditions of the Preparation of Activated Carbon Based Egusi (*Cucumeropsis mannii* Naudin) Seed Shells for Nitrate Ions Removal from Wastewaterl", *American Journal of Analytical Chemistry*, **9**, 439-463.

Lemaro F.A. and Rotich B. K., (2012), "Preparation and Characterisation of Activated Carbon from Locally available materials, viz. Coconut Shells", Thesis of Department of Mechanical & Manufacturing Engineering, University of Nairobi, Kenya, 120.

Li B., Dai F., Xiao Q., Yang L., Shen J., Zhang C. and Cai M., (2016), "Activated Carbon from Biomass Transfer for High-Energy Density Lithium-Ion Super capacitors", *Advanced Energy Materials*, **6**, 1-6.

Lönnermark E., Lappas G., Friman V., Wold A. E. and Backhaus E., (2015), "Effects of probiotic intake and gender on nontyphoid Salmonella infection", *Journal of Clinical Gastroenterology*, **49,** 116–123.

Lunga P. K., Tamokou J. D., Fodouop P. C. S., Kuiate J. R., Tchoumboue J. and Gatsing D., (2014), "Antityphoid and radical scavenging properties of the methanol extracts and compounds from the aerial part of *Paullinia pinnata*", *SpringerPlus*, **3(302)**, 1-9.

Machado S., Pacheco J. G., Nouws H. P. A., Albergaria J. T. and Delerue-Matos C., (2015), "Characterization of green zero-valent iron nanoparticles produced with tree leaf extracts", *Science Total Environement*, **533,** 76-81.

Maeva F. E., Segnou M. L., Ebongue C. O., Deli V., Nyobe J.C. N. and Mpondo E. M., (2015), "Synthesis, optimization and effect of condition reactions studies of seed kernel aqueous extract mediated silver nanoparticles from Ricinodendron heudelotii (Baill) Pierre Pax", *International Journal of Biosciences*, **7(4),** 47-56.

Mahmood T., Ali R., Naeem A., Hamayun M. and Aslam M., (2017), "Potential of used Camellia sinensisleaves as precursor for activated carbon preparation by chemical activation with H_3PO_4; optimization using response surface methodology", *Process Safety and Environment Protection,* **109,** 548-563.

Malarvizhi R. and Sulochana N., (2008), "Sorption isotherm and kinetic studies of Methylene blue uptake onto activated carbon prepared from wood apple shell" *Journal of Environmental Protection Science*, **2**, 40-60.

Maleki A., Hamesadeghi U., Daraei H., Hayati B., Najafi F., McKay G. and Rezaee R., 2017, "Amine functionalized multi-walled carbon nanotubes: Single and binarysystems for high capacity dye removal", *Chemical Engineering Journal*, **313**, 826-835.

Manirakiza D., (2007), "Etude de la Consommation D'*Irvingia* Spp. (Mangue Sauvage) et *Ricinodendron Heudelotii* (Njansang) a Yaounde et Libreville", CIFOR/ Afrique Centrale, 29.

Matsumura Y., Yoshikata K., Kunisaki S., and Tsuchido T., (2003), "Mode of bactericidal action of silver zeolite and its comparison with that of silver nitrate", *Applied and Environmental Microbiology*, **69**, 4278-4281.

Matthew F., (2004), "Activation and uses of Powder Activation Carbon for removing 2-Methylisoborneol in water utilities", Master Dissertation of physical Chemistry, University of Florida, Florida-USA, 42.

Mehrabi N., Soleimani M., Yeganeh M. M. and Sharififard H, 2015, "Parameters optimization for nitrate removal from water using activated carbon and composite of activated carbon and Fe_2O_3 nanoparticles", *The Royal Society of Chemistry*, **5(64)**, 51470-51482.

Meier J. (2008) "Effect of powdered Activated Carbon on the nanofiltration of sewage plant effluent", PhD Thesis, Department of Chemical Engineering, RWTH Aachen University, Aachen, Germany, 205.

Meier J. and Melin T., (2005), "Wastewater reclamation by the PAC/NF process", *Desalination,* **178**, 27-40.

Meier J., Melin T. and Eilers L., (2002), "Nanofiltration and adsorption on powdered adsorbent as process combination for the treatment of severly contaminated waste water", *Desalination,* **146**, 361-366.

Menéndez-Diaz J. A. and Martin-Gullón I., (2006), "Types of Carbon adsorbents and their production", *Activated Carbon Surfaces in Environmental Remediation*, 1-45.

Metzger, S., (2010) "Einsatz von Pulveraktivkohle zur weitergehenden Reinigung von kommunalem Abwasser (Application of activated carbon for the advanced treatment of municipal wastewater)", PhD thesis, Technical University of Berlin, Oldenbourg Industrieverlag, Munich, 145.

Micheal D., (1999), "The Regeneration of granular activated carbon using Hydrothermal Ghanizadeh Technology*",* Master's thesis University of Texas, Texas-USA, 85.

Middea A., Spinelli L. S., Souza Jr F. G., Neumann R., Thais L.A.P. F., Otavio da F.M. G., (2017), "Preparation and characterization of an organo-palygorskite-Fe3O4 nanomaterial for removal of anionic dyes from wastewater", *Applied Clay Science*, **139**, 45–53.

Min-Shen C., Pang-Yen H. and Hasing-Ya L., (2003), "Adsorption behavior of dye AAVN and iRB4 in acid solutions on chemically cross-linked Chitosan Beads", *J. Chinise Institue of Chemical Engeering Sciences*, **34**, 625-634.

Miriam B., Ramero R., Gabriela R., Carlose B., Teresa T. and Reyna N., (2013), "Ozonation of Indigo Carmine catalyzed with Fe-Pillard clay", *International Journal of photo enrgy*, **7**, 1-8.

Mittal A., Malviya A., Kaur D., Mittal J. and Kurup L., (2007), "Studies on the adsorption kinetics and isotherms for the removal and recovery of Methyl Orange from wastewaters using waste materials", *Journal of Hazardous Materials*, **148**, 229–240.

Mohammed A. and Gemal O., (2014), "Adsorption of Tatrazine on medical Activated Charcoal tablets under control condition", *Journal of Environmental Analytical Chemistry*, **1,** 1-7.
Mohammed S., Wan M., Amirhossein H. and Ahmad S., (2010), "A review on the surface modification of activated carbon from carbondioxide adsorption", *Journal of Analytical and Applied Pyrolysis*, **89**, 143-151.

Mona A., Soheir A. and Amina A., (2012), "Basic Dye adsorption on Low Cost Biopolymer: Kinetic and Equilibrium Studies", *Journal of Applied Chemistry*, **2**, 27-36.
Morgana T., (2007), "Impact of surface chemistry on Adsorption: Tailoring of activated carbon", *Master Thesis* in Chemistry, University of Florida, USA, 30.

Mosmann T., (1983), "Rapid Colorimetric Assay for Cellular Growth and Survival: Application to Proliferation and Cytotoxicity Assays", *Journal of lmmunological Methods*, **65**, 55-63.

Moumenine S., (2011), ''Élimination de Polluants des Eaux d'Usines par Adsorption sur le Charbon Chêne en Combinaison avec un Désinfectant'', Mémoire de Génie des Procédés. Université Abou Bekr Belkaid-Tlemcen, Tlemcen-Algérie, 57.

Mukherjee P A., Ahmad D., Mandal S., Senapati S., Sainkar R., Khan M. I., Parishcha R., Ajaykumar P. V., Alam M., Kumar R. and Sastry M., (2001), "Fungus-Mediated synthesis of silver Nanoparticles and their Immobilizaton in the mycelial Matrix: A Novel Biological Approach to Nanoparticles synthesis", *Nano Letters*, **1**, 515-519.

N'guessan J., (2010), ''Étude Expérimentale et Modélisation d'un Procédé Séquentiel AD-OX d'Élimination de Polluants Organiques'', Thèse de Génie des Procédés et de l'Environnement. France: École Doctorale de MEGEP, 208.

Nahil M. A. and Williams P. T., (2011), "Recycling of carbon fibre reinforced polymeric waste for the production of Activated Carbon Fibres", *Journal of Analytical and Applied Pyrolysis*, **91**, 67–75.

Naparat J., (2010), "A study of the adsorption of Indigo and derivatives onto silk", Thesis for Doctorate degree in the University of Technology, Suranaree University of Technology, 255.

Nasehir K., Muhamed F., Ismail A., Olugbenga S. and Mohld A., (2010), "Effect of preparation condition of Activated Carbon prepared from Rice Husk by CO_2 Activation for removal of Cu (II) from aqueous solution", *International Journal of Engineering and Technology*, **10,** 45-49.
Nauciel C. and Vildé J. L., (2005), "Bactériologie Médicale", 2nd edn. *Elsevier Masson, France,* 257.

Ndi J. N. and Ketcha J. M., (2013), "The Adsorption Efficiency of Chemically Prepared Activated Carbon from Cola Nut Shells by $ZnCl_2$ on Methylene Blue", *Journal of Chemistry*, **201**, 1-7.

Ndi J. N., Ketcha J. M., Anagho G. S., Ghogomu N. J. and Belibi B. P. D., (2014), "Physical and chemical characteristics of activated carbon prepared by pyrolysis of chemically treated Cola nut (cola acuminata) Shells wastes and its ability to adsorb organics", *International Journal of Advance Chemical Technology*, **3**, 1-12.

Ndi Nsami J., (2014), "The Textural properties and adsorption Characteristics of prepared Activated carbon from Cola nut shells wastes: Application for the Elimination of Dye stuff from aqueous solution", Doctorate thesis in physical Chemistry, University of Yaoundé I, Yaoundé-Cameroon, 200.

Ndumbe L. N., Ingram V., Tchamba M. and Nya S., (2018), "From trees to money: the contribution of Njansang (*Ricinodendron heudelotii*) products to value chain stakeholders' financial assets in the South West Region of Cameroon", *Forests, Trees and Livelihoods*, 2164-3075.

Nezih U. Y., (2004), "Production and Characterization of Activated Carbon from Apricot Stones", *Master Thesis* of the Department of Chemical Engineering, The Middle East Technical University, 135.
Ngakou C. S., Anagho G. S. and Ngomo H. M., (2019), "Non-linear Regression Analysis for the Adsorption Kinetics and Equilibrium Isotherm of Phenacetin onto Activated Carbons", *Current Journal of Applied Science and Technology*, **36(4)**, 1-18.

Ngo Mpeck M. L., Asaah E., Tchoundjeu Z. and Atangana A.R., (2003), "Strategies for the domestication of Ricinodendron heudelotii: Evaluation of variability in natural populations from Cameroon", *Food, Agriculture & Environment,* **1(3&4)**, 257-262.

Ngulube T., Gumbo J. R., Masindi V. and Maity A., (2017), "An update on synthetic dyes adsorption onto Clay based minerals: A state-of-art review", *Journal of Environmental Management,* **191**, 35-57.

Nkwaju Y., (2013), "Adsorption of Manganese (II) in aqueous solutions onto Granular Activated carbon and modified Activated carbon by the Iron oxide*", Master Thesis* in physical chemistry University of Yaoundé I, Yaoundé-Cameroon, 40.

Nouri M., Khodaiyan F., Razavi S. H. and Mousavi M., (2016), "Improvement of Chitosan production from persian Gulf shrimp waste by response surface methodology", *Food Hydrocolloids,* **59**, 50-58.

Nourozi M., Chuah T. and Thomas S., (2009), "Adsorption of reactive dyes by palm kernel shell activated carbon: Application of film surface and film pore models", *E-Journal of Chemistry*, **6,** 949-954.

Nuran B., (2007), "The Response Surface Methodology", Master Thesis of Department of Mathematical Sciences, Indiana University South Bend, Indiana, India, 84.

Oh W-C. and Jang W-C., (2003), "Physical properties and biological effects of Activated Carbon fibers treated with the herbs", Carbon, **41**, 1737-1742.

Okoro C. K., Kingsley R. A., Connor T. R., Harris S. R., Parry C. M., Al-Mashhadani M. N. and Kariuki S, (2012), "Intra-continental spread of human invasive Salmonella typhimurium pathovariants in sub-Saharan Africa", *Nature Genetics,* **44(11)**, 1215–1221.

Olasehinde G.I., Akinlabu D.K., Owoeye F.T., Owolabi E.F., Audu O.Y. and Mordi R.C., (2016), "Phytochemical and Antimicrobial Properties of Oil Extracts from the Seeds of Ricinodendron heudelotii", *Research Journal of Medicinal Plants,* 1-4.

Olushola S., Oladayo A., Bolanle D. and Oladunni O., (2012), "Adsorption and Intraparticulate Diffusivities of Congo Red onto Kola Nut Pod Carbon", *Pollution Journal of Environmental Studies*, **21**, 1147-1152.

OYA A., Wakahara T. and Yoshida S., (1993), "Preparation of pitch-based Antibacterial Activated Carbon Fiber", *Carbon*, 31(8), 1243-1247.

Panahi R., Vasheghani E. and Shojosadati S., (2008), "Determination of Isotherm for L-lysine imprinted polymer", *Iranian Journal of Chemical Engineering*, **5,** 49-55.

Pantidos N. and Horsfall L. E., (2014), "Biological synthesis of mmetallic nanoparticles by Bacteria, Fungi and Plants", *Journal of Nanomedicine and Nanotechnology,* **5(5)**, 1–10.
Parys V. J., (2012), " Impact van geleide Njangsang-commercialisering op de extractie en het voorkomen van *Ricinodendron heudelotii* (Baill.) Pierre ex Pax", Master in de bio-ingenieurswetenschappen: Bos en Natuur, University of Gent, Holland, 137.

Philpott D. J., Edgeworth J. D. and Sansonetti P. J., (2000), "The pathogenesis of *Shigella flexneri* infection: lessons from in vitro and in vivo studies", *The Royal Society*, **355**, 575-586.
Pommerville J. C., (2013), "Fundamentals of Microbiology", 10th ed., Sudbury M. A: Jones &Bartlett, 106.

Popoff M. Y., Bockemuhl J. and Gheesling L. L., (2004), "Supplement 2002 (no. 46) to the Kauffmann-White scheme", *Research in Microbiology*, **155**, 568–570.

Priester J. P., Stoimenov R., Mielke S., Webb C., Ehrhardt J., Zhang G. S. and Holden P., (2009), "Effects of soluble cadmium salts versus Cd Se quantum dots on the growth of planktonic Pseudomonas aeruginosa", *Environmental Science and Technology*, **43**, 2589-2594.

Pui C. F., Wong W. C., Chai L. C., Nillian E., Ghazali F. M., Cheah Y. K., Nakaguchi Y., Nishibuchi M and Radu S., (2011), "Simultaneous detection of Salmonella spp, Salmonella typhi and Salmonella typhimurium in sliced fru its using Multiplex PCR", *Food Control*, **22**, 337-342.

Qui P., Cui M., Kang K., Park B., Son Y., Khim E., Jang M. and Khim J., (2014), "Application of Box-Behnken design with response surface methodology for modeling and optimizing ultrasonic oxidation of arsenite with H_2O_2", *Central European Journal of Chemistry*, **12(2)**, 164-172.

Rahman B. A., Wasfy M. O., M. Maksoud A., Hanna N., Dueger E., and House B., (2014), "Multi-drug resistance and reduced susceptibility to ciprofloxacin among *Salmonella enterica serovar typhi* isolates from the Middle East and Central Asia", *New Microbes and New Infections*. **2(4)**, 88-92.

Rahmaniyan, F., Shamel A. and Shafaghatlonbar A., (2015), "Evaluation of biologically synthesized silver nanoparticles by the bioreduction method", *Synthesis and React*ivity *in Inorganic Metal-organic and nano-metal chemistry*, **45(10)**, 1495-1500.

Ramakrishna Gottipati, (2012), "Preparation and Characterization of Microporous Activated Carbon from Biomass and its Application in the Removal of Chromium(VI) from Aqueous Phase", PhD Thesis of the Department of Chemical Engineering National Institute of Technology, Rourkela Odisha, India, 242.

Ramesh T. N., and Sreenivasa V. P., (2015), "Removal of Indigo Carmine Dye from Aqueous Solution Using Magnesium Hydroxide as an Adsorbent", *Journal of Materials*, **753057**,10.

Ramin A., (2009), "Production of Activated Carbon and its Catalytic Application for Oxidation of Hydrogen Sulphide", PhD Thesis of the Department of Chemical Engineering, University of Saskatchewan, Saskatoon, Saskatchewan, 269.

Rastaldo R., Pagliaro P., Cappello S., Penna C., Mancardi D., Westerhof N., and Losano G., (2007), "Nitric oxide and cardiac function", *Life Sciences*, **81**, 779-793.

Ravikumar K., Ramalingam S., Krishnan and Balu K., (2006), "Application of response surface methodology to optimize the process variables for Reactive Red and Acid Brown dye removal using a novel adsorbent", *Dyes and Pigments*, **70**, 18-26.
Regina K., (2010), "Indigo Carmine favored but fading", 40.

Richard A. H., Pamela C. C., and Bruce D. F. (2006), "Microbiology-Lippincott's Illustrated Reviews", 2nd eddtion, Lippincott Williams & Wilkins.

Richard C., (2003), "Activated Charcoal-Universal antidote and Detoxifier", *Journal of the Megahealth Society*, **5,** 1-4.

Ríos-Hurtado J. C., Múzquiz –Ramos E. M., Zugasti-Cruz and Cortés-Harnándezd. A., (2016), "Mechanosynthesis as a simple method to obtain a Magnetic Composite (Activated Carbon/Fe_3O_4) for Hyperthermia treatment", *Journal of Biomaterials and Nanobiotechnology*, **7**, 19-28.

Roop C. B. and Meenakshi G., (2005), "Activated Carbon Adsorption", *Taylor & Francis Group, LLC*, New York, USA, 487.

Rosas J. M., Bedia J., Rodríguez-Mirasol J. and Cordero T., (2009), "HEMP-derived Activated Carbon Fibers by chemical activation with phosphoric acid", *Fuel*, **88**, 19-26.

Ruparelia J. P., Chatterjee A. K., Duttagupta S. P. and Mukherji S., (2008), "Strain specificity in antimicrobial activity of silver and copper nanoparticles", *Acta Biomater*, **4(3)**:707–716.

Saklani V., Suman V. K., and Jain K., (2012), "Microbial synthesis of silver nanoparticles; a review", *Journal of Biotechnology and Biomaterials*, **13**, 1-3.

Salavati-Niasari M., Davar F. and Mir N., (2008), "Synthesis and characterization of metallic copper nanoparticles via thermal decomposition", *Polyhedron,* **27(17)**, 351-3518.

Samarghandi M., Hadi M., Moayedi S. and Barjasteh A., (2009), "Two-Parameter Isotherms of Methyl Orange Sorption by Pinecone Derived Activated Carbon*", Iranian Journal of Environmental Health and Scientific Engineering*, **6,** 285-294.

Sánchez-Rodríguez S., Trujillo-Reyes J., Gutiérrez-Segura E., Solache-Ríos M. and Colín-Cruz A., (2015), "Removal of Indigo Carmine by a Ni Nanoscale Oxides/Schoenoplectus acutus Composite in Batch and Fixed Bed Column systems", *Separation Science and Technology*, **50(11)**, 1602-1610.

Sathishkumar P., Arulkumar M. and Palvannan T., (2012), "Utilization of agro-industrial wasteJatropha curcaspods as an activated carbon for the adsorption of reactive dye Remazol Brilliant Blue R (RBBR)", *Journal of Cleaner Production*, **22**, 67-75.

Schulz H. and Jorgensen B., (200), "Big bacteria. Annual Review of Microbiology", **55**, 105-137.

Sharma P., Dahiya1 S., Balaji V., Kanga A., Panda P. and Das R., (2016), "Typhoidal Salmonellae: Use of Multi-Locus Sequence Typing to Determine PopulationStructure", *PLoS ONE*. 11(9), 0162530.

Silvestry-Rodriguez N, K.R. Bright, D.C. Slack, D.R. Uhlmann .and Gerba, C. P. Inactivation of Pseudomonas aeruginosa and Aeromonas hydrophila by silver in tap water. *Journal of Environmental Science and Health*. 42(11):1579-1584, 2007.

Siti R., (2010), "Production of activated carbon using local Agricultural waste for Ground water treatment in university Malaysia pattang", Thesis for Bachelor of Civil Engineering University of Malaysia, 24.

Sivakumav B., Kannan C. and Karthikeyan S., (2012), "Preparation and characteriization of Activated Carbon prepared from Balsamodenn Candatum Wood Waste through Various Activation Processes", **5**, 321-327;

Sizentsov A. N., Kvan O. V., Miroshnikova E. P., Gavrish I. A., Serdaeva V. A. and Bykov A. V., (2018), "Assessment of biotoxicity of Cu nanoparticles with respect to probiotic strains of microorganisms and representatives of the normal flora of the intestine of broiler chickens", Environmental Science and *Pollution Research, Sizentsov*, **25(16)**, 15765–15773.

Snyder S.A., Adham S., Redding A.M., Cannon F.S., DeCarolis J., Oppenheimer J., Wert E.C. and Yoon Y., (2007), "Role of membranes and activated carbon in the removal of endocrine disruptors and pharmaceuticals", *Desalination*, **202**, 156-181.

Sodeinde O., (2012), "Preparation of a locally produce Activated Carbon from coconut shells and it no in reducing Hexamine cobalt (III)", *International journal of chemical engineering and Application*, **3(1),** 67-71.

Stewart C. M., (2003), "Staphylococcus aureus and staphylococcal enterotoxins", Ch 12 In: Hocking AD (ed) Foodborne microorganisms of public health significance, 6th ed, Australian Institute of Food Science and Technology (NSW Branch), Sydney, 359–380.

Sugumaran P., Priya V., Ravichandran P. and Seshadri S., (2012), "Production and Characterization of Activated Carbon from Banana Empty Fruit Bunch and Delorixregia fruit pod", *Journal of Sustainable Energy and Environment*, **3**, 128-132.

Sumalatha B., Kumar Y., Kiran K., Babu J., Venkata N., Maria D. and Venkateswarulu T., (2014), "Removal of Indigo Carmine from aqueous solution by using Activated Carbon", *Research Journal Pharmaceutical, Biological and chemical science*, **5**, 912.

Sunderland T. C. H. and Obama C., (1999), "A preliminary survey of non-wood forest products of Equatorial Guinea", In: Non-Wood Forest Products ofCentral Africa: Current Research Issues and Prospects for Conservation and Development. Edited by Sunderland, T. C. H., Clark, L. E. and Vantomme, P. FAO, Rome, 211-220.

Suzan S., (2013), "A Comparative Optimisation Study of Activated Carbon Production from Hazelnut Shells by Thermal and Microwave Heating Methods", PhD Thesis of the Department of Civil and Environmental Engineering, Imperial College, London, 349.

Sze M. F. F. and McKay G., (2012), "Enhance mitigation of para-chlorophenol using stratified Activated Carbon adsorption columns", *Water Research*, **46**, 700-710.

Sze M. F. F., Lee V. K. C. and McKay G., (2008), "Simplified fixed bed column model for adsorption of organic pollutants using tapered Activated Carbon columns", *Desalination*, **218**, 323-333.

Tabuna H., (1999), "The markets for Central African non-wood forest products in Europe", In: Non-Wood Forest Products of Central Africa: Current Research Issues and Prospects for Conservation and Development Edited by Sunderland, T. C. H., Clark, L. E. and Vantomme, P. FAO, Rome, 251-263.

Tagne G. M., Ndi Nsami J. and Ketcha Mbadcam J., (2013), "Adsorption of Copper (II) Ions from aqueous Solution onto Synthetic Goethite and Two Naturally available Red Soils from Yaoundé-Cameroun", *British Biotechnology Journal*, **2**, 221-235.

Tai C. Y., Chang M. and Liu H., (2007), "Synthesis of Magnesium Hydroxide and Oxide Nanoparticles Using a Spinning Disk Reactor", *Industriiial and engineering chemistry research,* **46(17)**, 5536-5541.

Tamokou J. D., Mbaveng T. A. and Kuete V., (2017), "Antimicrobial activities of African medicinal spices and vegetables, in Medicinal spices and vegetables from Africa: therapeutic potential against metabolic inflammatory infectious and systemic diseases", 1st edition, *Elsevier*, 207-237.

Tan I. A. W., Ahmed A. L., and Hameed B. H., (2008), "Optimization of the preparation conditions for Activated Carbons from Coconut Husk using Response surface methodology", *Chemical Engineering Journal*, **137,** 462-470.

Taro and Kathleen, (2007), "Foundations in Microbiology", 6th international ed., *McGraw-Hill*, 108-109.

Tchoundjeu Z. and Atangana A. R., (2006), "*Ricinodendron heudelotii*", Research project funded by the United Kingdom Department for International Development (DFID) for the benefit of developing countries, Southampton Centre for Underutilised Crops, University of Southampton, Southampton, UK, 85.

Teh L. C., Rozilawati A. G., Fadzilah A. A. M., Mohammad R. S., (2013), "Herbal Extract Decolourization Device Using Activated Carbon", *Jurnal Teknologi, Sciences* & *Engineering*, **61(1),** 73-79.

Thanh D. P., Karkey A. and Dongol S A., (2016), "Novel ciprofloxacin resistant subclade of h58. *Salmonella typhi* is associated with fluoroquinolone treatment failure", **5**, 14003.

Thomas B., (2012), "Remadiating Petroleum Contaminants with Activated Carbon Injectetes", Thesis of Chemical Engineering, University of Colorado, Colorado, USA, 120.

Thomas B., Vithiya S. M. B. and Prasad T A. A., (2018), "Removal of Indigo Carmine Dye from Aqueous Solution Using Magnesium Hydroxide as an Adsorbent", *The Pharma Innovation Journal*, **7(4)**, 42-46.

Thuan T. V., Quynh B. T. P., Nguyen T. D., Ho V. T. T. and Bach L. G., (2016), "Response surface methodology approach for optimization of Cu^{2+}, Ni^{2+} and Pb^{2+} adsorption using KOH-activated carbon from banana peel", *Surfaces and Interfaces*, **000**, 1-9.

Tiwari D. K., Behari J. and Sen P., (2008), "Application of Nanoparticles in Waste Water Treatment, *World Applied Science Journal*, **3(3)**, 417-33.

Tsao N., Luh T. Y., Chou C. K., Chang T. Y., Wu J. J., Liu C. C. and Lei H. Y., "(2002) In vitroaction of carboxyfullerene", *Journal of Antimicrob Chemother*, **49(4)**, 641–649.

Üner O., Ünal G. and Bayrak Y., (2015), "Preparation and characterization of mesoporous activated carbons from waste watermelon rind by using the chemical activation method with zinc chloride", *Arabian Journal of Chemistry*, http://dx.doi.org/10.1016/j.arabjc.2015.12.004.

Veerasamy R., ZiXin T., Gunasagaran S., Wei T. F. X., Yang E. F. C., Kumar N. J. and Dhanaraj S. A., (2011), "Biosynthesis of silver nanoparticles using mangosteen leaf extract and evaluation of their antimicrobial activities", *Journal of Saudi Chemistry Society,* 15, 113-120.

Villota E., Lei H., Qian M., Yang Z., Villota S. M., Yadavalli G., and Zhang Y., (2017), "Thermodynamics, Non-Linear Isotherms, Statistical Modeling and Optimization of Phosphorus Adsorption from Wastewater", *ACS Sustainable Chemistry & Engineering*, 1-26.

Vincenzo T., Giordano U., Massimo R., Sabrina C., Paolo V., Antonella L. and Giuseppe M., (2013), "Effect of powdered Activated Carbon to Reduce Fouling in Membrane Bioreaction: A sustainable solution case study", *Sustamability Journal*, **5**, 1501-1509.

Visweswara R. P., Tnvkv P., Rayees A. S., Satheesh K., B., Ganapathi N., Cirandur S. R., Ismail A. R., Siew H. G., (2013), "Biogenic silver nanoparticles using *Rhinacanthus nasutus* leaf extract: synthesis, spectral analysis, and antimicrobial studies", *International Journal of Nanomedicine***, 8(3),** 3355–3364.

Vivien J. and Faure J. J., (1985), "Arbres des Forêts Denses d'Afrique Centrale", Ministère des Relations Extérieures, Coopération et Développement, ACCT, Paris.

Vorgelegt Von Christian Kazner, (2011), "Advanced Wastewater Treatment by Nanofiltration and Activated Carbon for High Quality Water Reuse", PhD Thesis, Technical University of Berlin, Oldenbourg Industrieverlag, Munich, Germany, 206.

Wanjun W., Guocheng H., Jimmy C. Y., Po K. W., (2015), "Advances in photocatalytic disinfection of bacteria: Development of photocatalysts and mechanisms", *Journal of Environmental Sciences,* **34,** 232–247.

Westerhoff P., Karanfil T. and Crittenden J, (2006), "Aerogel and Iron-Oxide Impregnated Granular Activated Carbon Media for Arsenic removal", Research funded by Awwa Research Foundation (AwwaRF) and U.S. Department of Energy, Washington, USA, 98.

Wimonrat T., Manop S., Phunsiri H., Saksit C. and Chalerm R., (2010), "Preparation of activated carbon derived from Jatropha curcas fruit shell by simple thermo-chemical and characterization of their physic-chemical properties", *Chemical Engineering Research and Design*, **89**, 335-340.

Wong V. K., Baker S., and Pickard D. J., (2015), "Phylogeographical analysis of the dominant multidrug-resistant H58 clade of *Salmonella typhi* identifies inter-and intracontinental transmission events", *Nature Genetics*. **47(6)**, 632–639.

Worch E, (2012), "Adsorption Technology in Water Treatment", Printing: Hubert & Co. GmbH & Co. KG, Göttingen, Dresden, Germany, 345.

Yakout S.M., El-Deen S. G., (2016), "Characterization of activated carbon prepared by phosphoric acid activation of olive stones", *Arabian Journal of Chemistry*, **9**, 1155–1162.
Yang H.,

Yang R., Chen H., Zheng C., Lee D. H. and Liang D. T., (2006), "In-Depth investigation of Biomass Pyrolysis based on three Major Components: Hemicellulose, Cellulose and Lignin", *Energy & Fuels*, **20**,388-393.

Yirankinyuki F. F., Lamayi D. W., Muhammad U. A. and Musa B., (2018), "Assessing the Suitability of *Ricinodendron Heudelotii* Seed Oil for Paint Formulation"*, Journal of Applied Chemistry*, **11(7)**, 37-42.

Yoon K., Hoon B. J., Park J. H., Hwang J., (2007), "Susceptibility constants of *Escherichia coli* and Bacillus subtilis to silver and copper nanoparticles", *Science Total Environment*, **373(2–3)**,572–575.

Yu M. K., Park J. and Jon S., (2012), "Targeting strategies for multifunctional nanoparticles in cancer imaging and therapy", *Theranostics*, **2**, 3-44.

Yuhui M., (2016), "Comparison of Activated Carbons Prepared from Wheat Straw via $ZnCl_2$ and KOH Activation", *Waste Biomass Valor*, 1-11.

Yusufu M. I., Ariahu C. C. and Igbabul B. D., (2012), "Production and characterization of activated carbon from selected local raw materials", *African Journal of Pure and Applied Chemistry*, **6(9),** 123-131.

Zhang L., Wan L., Chang N., Lui J., Duan C., Zhou Q., Li X. and Wang X., (2011), "Removal of phosphate from water by Activated Carbon fiber loaded with lanthanum oxide", *Journal of Hazardous Materials*, **190**, 848-855.

Zhao J., Yang L., Li F., Yu, R. and Jin, C., (2009), "Structural evolution in the graphitization process of Activated Carbon by high-pressure sintering", *Carbon*, **47**, 744-751.

Zige D. V., Ohimain E. I., and Sridhar M. K., (2013), "A community based screening of asymptomatic typhoid carriers in Wilberforce Island, Bayelsa State", *Nigeria International Journal of Health Sciences and Research*, **3**, 119-126.

Zwickenpflug B., Böhler M., Sterkele B., Joss A., Siegrist H., Traber J., Gujer W., Behl M., Dorusch F., Hollender J., Ternes T. and Fink G., (2010), "Use of powdered Activated Carbon for the removal of Micropollutants from municipal wastewater", Final report of the MicroPoll

project, EAWAG on behalf of the Swiss Federal Office for the Environment, Dübendorf. Hasan S. Review on nanoparticles; their synthesis and type; *mechanism* 4: 9-11, 2015.

APPENDICES

Appendix A: Analytical data for Characterisation of RHS precursor ACs and ACs/AgNPs

Table A-1: Data for proximate analysis of RHS

Parameters	%composistion
Ash Content	4.833
Moisture Content	5.280
Volatile Matter Content	62.571
Fixed Carbon Content	27.266

Table A-2: Data for X-Ray Fluorescence data of RHS

oxides	SiO_2	TiO_2	Al_2O_3	Fe_2O_3	MnO	MgO	CaO	K_2O	P_2O_5	LOI	SOMME
%composition	0.09	0.01	0.09	0.11	0.17	1.65	12.1	0.02	0.03	83.65	97.91

Table A-3: Data for pH of Zero-point charge

pH	**ACP**	**ACZ**	**ACP/AgNP**	**ACZ/AgNP**
	ΔpH	ΔpH	ΔpH	ΔpH
2.24	0.01	0.67	0.30	0.14
2.80	0.20	0.38	0.23	0.18
4.06	-0.04	2.85	1.77	2.40
5.05	-0.64	2.24	2.10	2.42
6.05	-1.71	1.40	1.32	1.43
7.00	-2.63	0.65	0.51	0.65
8.00	-3.69	-0.27	-0.39	-0.09
9.00	-4.72	-1.24	-1.69	-0.64
10.00	-5.62	-2.21	-2.70	-1.70
11.00	-6.52	-3.08	-3.60	-2.66

Table A-4 Data for IN and MB number test on ACP/AgNP and ACZ/AgNP

Concentration	**IN**		**MB**	
	ACP/AgNP	**ACZ/AgNP**	**ACP/AgNP**	**ACZ/AgNP**
0.001	555.821	545.374	96.3	91.325
0.002	552.989	532.049	94.804	90.019
0.003	542.189	517.772	93.77	88.895

Table A-5: Data for SEM-EDX Elemental composition on ACP

Element Number	Element Symbol	Element Name	Atomic Conc.	Weight Conc.
6	C	Carbon	79.04	73.09
8	O	Oxygen	17.36	21.39
7	N	Nitrogen	2.35	2.53
15	P	Phosphorus	0.90	2.14
20	Ca	Calcium	0.09	0.29
13	Al	Aluminium	0.08	0.16
14	Si	Silicon	0.07	0.15
16	S	Sulfur	0.06	0.14
12	Mg	Magnesium	0.05	0.10

Table A-6: Data for SEM-EDX Elemental composition on ACZ

Element Number	Element Symbol	Element Name	Atomic Conc.	Weight Conc.
6	C	Carbon	85.49	77.59
8	O	Oxygen	8.58	10.38
30	Zn	Zinc	1.13	5.57
7	N	Nitrogen	3.14	3.32
11	Na	Sodium	1.20	2.09
13	Al	Aluminium	0.15	0.31
12	Mg	Magnesium	0.15	0.27
25	Mn	Manganese	0.05	0.19
16	S	Sulfur	0.06	0.14
20	Ca	Calcium	0.04	0.11
15	P	Phosphorus	0.02	0.04

Table A-7: Data for SEM-EDX Elemental composition on ACP/AgNP

Element Number	Element Symbol	Element Name	Atomic Conc.	Weight Conc.
6	C	Carbon	73.42	52.60
47	Ag	Silver	3.92	25.21
8	O	Oxygen	19.53	18.64
7	N	Nitrogen	2.21	1.84
15	P	Phosphorus	0.83	1.53
16	S	Sulfur	0.09	0.18

Table A-8: Data for SEM-EDX Elemental composition on ACZ/AgNP

Element Number	Element Symbol	Element Name	Atomic Conc.	Weight Conc.
6	C	Carbon	72.67	47.27
47	Ag	Silver	4.76	27.83
8	O	Oxygen	14.18	12.29
30	Zn	Zinc	1.69	5.98
7	N	Nitrogen	4.41	3.35
11	Na	Sodium	1.47	1.83
17	Cl	Chlorine	0.43	0.82
16	S	Sulfur	0.15	0.25
15	P	Phosphorus	0.12	0.20
14	Si	Silicon	0.11	0.17

Appendix B: Titration curve for IC and MO dyes and data for adsorption measurement

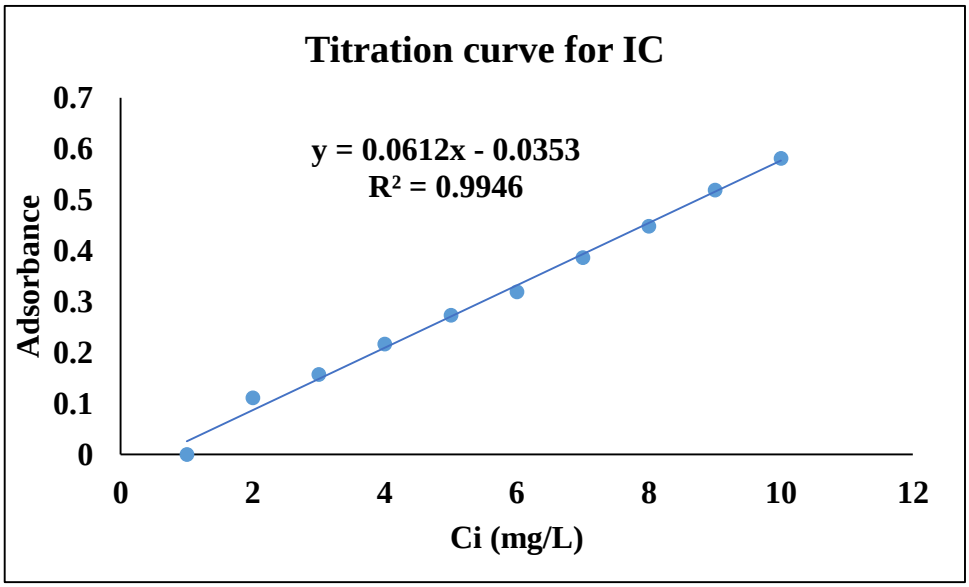

Figure B-1: Titration curve of IC

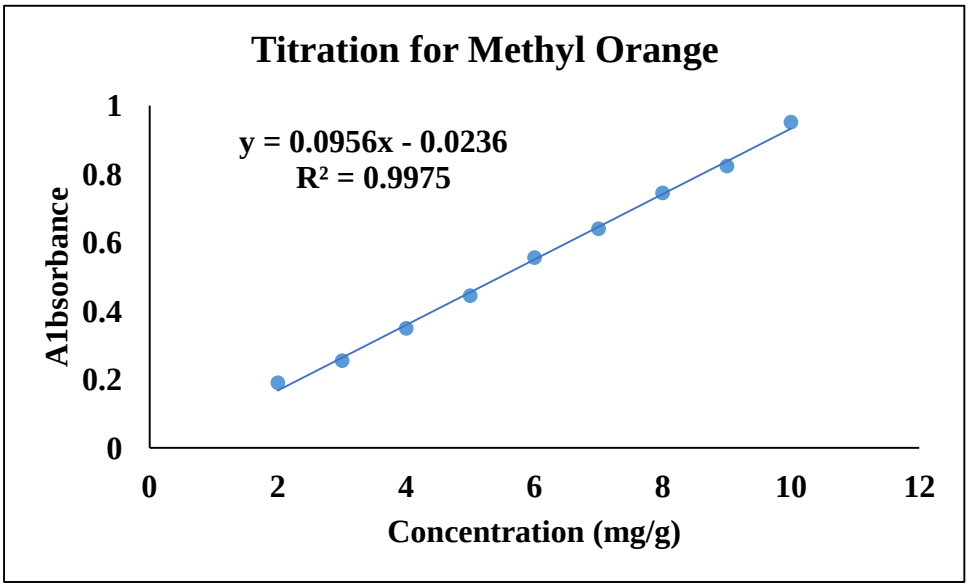

Figure B-2: Titration curve of MO

Table B-1. Data for the variation of of pH of IC adsorption on ACP, ACZ, ACP/AgNP and ACZ/AgNP

pH	ACP	ACZ	ACP/AgNP	ACZ/AgNP
	Qt	Qt	Qt	Qt
2	168.673	132.38	161.266	116.595
3	164.229	132.346	150.346	114.024
4	144.621	132.281	116.386	74.425
5	132.66	131.301	69.592	61.503
6	127.716	130.625	113.211	41.556
7	120.136	121.497	120.136	54.192
8	116.049	115.985	125.365	57.242
9	113.696	114.569	150.101	106.508
10	111.735	108.163	154.458	106.595
11	94.069	99.536	163.695	112.826

Table B-2. Data for the variation contact time of IC adsorption on ACP, ACZ, ACP/AgNP and ACZ/AgNP

time	ACP	ACZ	ACP/AgNP	ACZ/AgNP
0	00.000	00.000	00.000	00.000
5	177.801	95.571	154.098	64.882
10	180.186	104.329	164.490	65.275
15	180.67	114.068	131.737	65.471
20	180.971	114.48	125.528	68.412
25	181.199	114.473	128.633	111.976
30	189.271	118.839	127.544	115.876
35	195.546	115.527	128.306	115.985
40	180.186	114.481	124.058	117.858
45	183.781	113.044	136.966	116.747
50	189.304	117.858	131.084	117.161
55	189.304	120.19	129.014	116.747
60	189.304	117.728	126.144	117.074

Table B-3. Data for the variation of mass of ICadsorption on ACP, ACZ, ACP/AgNP and ACZ/AgNP

m (g)	ACP	ACZ	ACP/AgNP	ACZ/AgNP
0.01	190.219	160.186	168.542	106.582
0.02	97.708	80.649	96.515	68.552
0.03	66.097	63.798	66.239	54.234
0.04	49.687	49.434	49.695	44.621
0.05	39.75	39.991	39.763	35.737
0.06	33.136	33.174	33.136	31.73

Table B-4. Data for the variation of Initial concentration of IC adsorption on ACP, ACZ, ACP/AgNP and ACZ/AgNP

Concentration	ACP	ACZ	ACP/AgNP	ACZ/AgNP
50	97.801	81.446	94.108	39.638
60	117.637	86.403	115.382	51.577
70	137.441	103.94	125.48	63.516
80	153.62	120.362	131.134	66.61
90	149.89	123.222	145.546	71.752
100	177.801	133.407	160.678	89.181

Table B-5. Data for the variation of pH of MO adsorption on ACP, ACZ, ACP/AgNP and ACZ/AgNP

pH	ACP	ACZ	ACP/AgNP	ACZ/AgNP
2	199.151	132.865	165.889	117.64
3	195.72	132.739	165.802	112.262
4	187.791	130.159	165.715	110.207
5	171.523	115.548	153.93	109.284
6	161.69	110.053	153.09	107.844
7	130.895	107.18	150.078	106.995
8	124.243	104.446	153.058	106.906
9	123.992	89.375	154.209	106.995
10	111.331	68.162	154.243	107.844
11	62.389	58.497	154.261	109.284

Table B-6. Data for the variation of contact time of MO adsorption on ACP, ACZ, ACP/AgNP and ACZ/AgNP

time	ACP	ACZ	ACP/AgNP	ACZ/AgNP
0	00.000	00.000	00.000	00.000
5	169.757	52.909	160.380	49.877
10	173.146	64.396	161.174	63.476
15	174.444	86.538	161.949	74.564
20	178.146	109.049	162.49	79.919
25	191.452	116.273	164.041	104.697
30	191.891	117.389	164.547	105.075
35	194.360	118.457	164.669	106.306
40	191.954	120.368	164.843	107.684
45	191.912	123.213	164.843	108.115
50	191.933	123.227	164.791	106.835
55	195.573	125.04	164.651	106.847
60	195.782	125.054	164.651	106.896

Table B-7. Data for the variation of mass of MO adsorption on ACP, ACZ, ACP/AgNP and ACZ/AgNP

mass	ACP	ACZ	ACP/AgNP	ACZ/AgNP
0.01	192.406	141.9	159.735	126.418
0.02	99.46	99.084	99.408	94.575
0.03	66.467	66.63	66.321	66.077
0.04	49.861	49.803	49.84	48.626
0.05	39.901	39.868	39.897	39.88
0.06	33.324	33.241	33.248	33.244

Table B-8. Data for the variation of Initial concentration of MO adsorption on ACP, ACZ, ACP/AgNP and ACZ/AgNP

conc	ACP		ACZ	ACP/AgNP	ACZ/AgNP
50	98.523		66.351	82.817	60.936
60	117.854		79.629	99.031	73.305
70	134.109		92.907	115.017	84.982
80	151.159		105.975	133.114	95.795
90	168.628		119.058	149.344	108.256
100	178.356		124.204	165.384	120.102

Table B-9: Summary Report of micromeritics analysis of ACP, ACZ, ACP/AgNP and ACZ/AgNP materials

Materials		ACP	ACZ	ACP/ AgNP	ACZ/ AgNP
Surface Area (m^2/g)	Single Point BET	386.613	615.4	217.3	335.100
	Multipoint Point BET	22.280	38.77	367.4	23.860
	Langmuir surface area	548.300	893.9	2590	531.300
	BJH Cum. Adsorption surface area	30.036	27.35	403.9	24.670
	DH Cum. Adsorption surface area	31.820	28.06	430.1	25.790
	t-method external surface area	22.280	38.77	367.4	23.860
	DR Method micropore area	479.000	834.2	384.5	485.400
	DFT Cum. Surface area	270	472.4	84.19	238.800
Pore Volume (cc/g)	BJH Cum. adsorption pore volume	0.061	0.051	0.044	0.047
	DH Cum. adsorption surface pore volume	0.060	0.051	0.043	0.047
	DR method micropore pore volume	0.170	0.296	0.075	0.173
	DFT method micropore volume	0.175	0.283	0.081	0.168
Pore Size (nm)	BJH Cum. adsorption pore diameter	3.649	3.639	3.652	3.681
	DH Cum. adsorption pore diameter	3.649	3.639	3.652	3.681
	DR method adsorption pore diameter	2.654	2.169	3.407	2.676
	DA method adsorption pore diameter	1.680	1.460	1.860	1.580
	DFT method adsorption pore diameter	1.847	1.178	1.847	1.847

Appendix C: Characterisation Equipment

Figure C-5. XRD machine

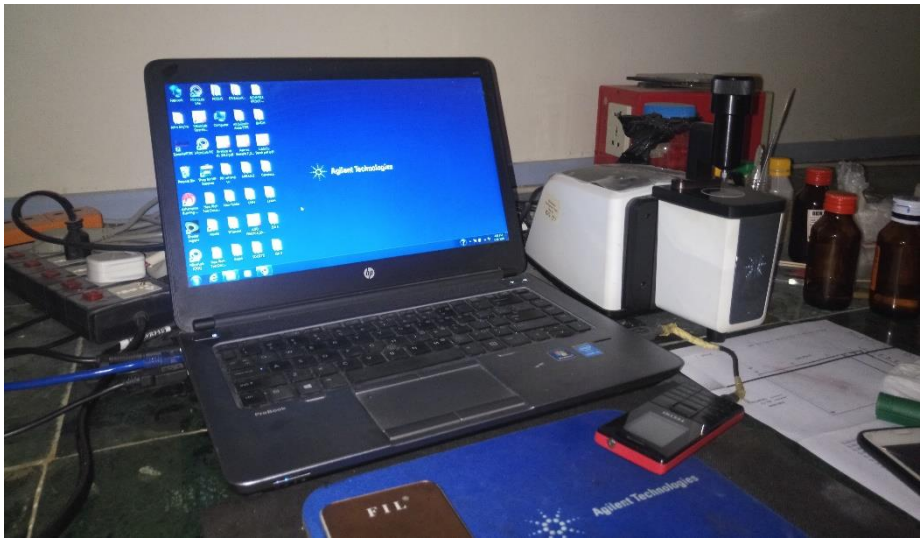

Figure C-6. FTIR Machine

Figure C-7. TGA Machine

LIST OF PUBLISHED ARTICLES

Ankoro N. O., Kouotou D., Lunga P. K., Agbor G. T., Lekene N. R., Ndi J. N. and Ketcha J. M., (2020), "Effect of Doping Activated Carbon Based Ricinodendron Heudelotti Shells with AgNPs on the Adsorption of Indigo Carmine and its Antibacterial Properties", *Arabian Journal of Chemistry*, **13**, 5241–5253.

REPRINT OF ARTICLE REALISED WITHIN THE SCOPE OF THIS THESIS